Studying roles of the kinetochore component Ndc80 in spindle assembly checkpoint

Aldona Chmielewska

University College London

and

Cancer Research UK London Research Institute

PhD Supervisor: Takashi Toda

A thesis submitted for the degree of

Doctor of Philosophy

University College London

September 2015

To my Husband, Mother and Brother

Declaration

I, Aldona Chmielewska confirm that the work presented in this thesis is my own. Where information has been derived from other sources, I confirm that this has been indicated in the thesis.

Abstract

Faithful chromosome segregation is facilitated by the establishment of proper kinetochore-microtubule attachment. Incorrect attachments activate the spindle assembly checkpoint (SAC), which blocks anaphase onset by recruitment of a cohort of SAC components (Mph1, Mad1, Mad2, Mad3, Bub1 and Bub3) to the kinetochores. Spc7/KNL-1, a component of the outer kinetochore KMN network (KNL-1/Mis12 complex/Ndc80 complex), acts as a platform for Bub1 and Bub3 localisation upon phosphorylation by Mph1/MPS1. The Ndc80 protein, a major microtubule-binding site, was shown to be important for Mph1/MPS1 localisation to kinetochores in humans; however, the precise mechanism remains largely elusive.

In this study, I show isolation and characterisation of an *ndc80* mutant (*ndc80-AK01*). This mutant was isolated using a PCR-based random mutagenesis method. The *ndc80-AK01* mutant contains a single point mutation within an uncharacterised linker region that connects a calponin-homology domain and a coiled-coil domain. This mutant is hypersensitive to microtubule poisons with no apparent growth defects in the absence of drugs. Subsequent analysis indicates that *ndc80-AK01* is defective in SAC signalling, as this mutant does not arrest in mitosis; instead mutant cells proceed into lethal cell division in the absence of microtubules. Localisation studies of SAC components have shown the absence of GFP-tagged Ark1, Mph1, Bub1, Bub3, Mad3, Mad2 and Mad1 from kinetochores under mitotic arrest conditions. Genetic and cell biological data indicate that the Ndc80 linker region may act as a structural platform for kinetochore recruitment of Mph1, which is one of the most upstream SAC components. Intriguingly, artificial tethering of Mph1 to the kinetochore restores checkpoint signalling, further confirming the function of Ndc80 as a kinetochore platform for Mph1. These data have unveiled a hitherto unknown function of the Ndc80 linker region in the SAC. The significance of these findings and the evolutionary conservation and diversification of roles for Ndc80 in SAC signalling will contribute to the elucidation of the molecular mechanisms of chromosome segregation.

Acknowledgement

First and foremost, I would like to express my sincere gratitude to my PhD supervisor Takashi Toda for all the support, supervision and guidance. I thank him for the discussions we had and I am grateful for his understanding and patience.

I would like to thank my lab, past and present members: Corinne, Hiro, Ngang Heok, Kuo-Shun, Risa, Akiko, Takayuki, Masashi, Yuzy, Hirofumi and Agathe. Thank you for all the technical help, scientific advice and fun moments we shared throughout the last four years. In particular thanks go to Hiro, Ngang Heok and Corinne for being extremely supportive scientifically and socially, as well as for reading the manuscript.

Special thanks also go out to my thesis committee members, Jacqueline Hayles and Frank Uhlmann for discussions on my project, all advices and suggestions.

The yeast groups on the third floor (Jacky's, Julie's, Paul's and Frank's lab) also deserve special acknowledgement for the amazing collaborative and friendly atmosphere and constant support in the most difficult moments of the project. Another big thanks go to my great friends from my PhD year group for making London Research Institute one big supportive family. I would like to mention in particular my good friends Corinne, Ainhoa, Molly, Sakshi, Meghna, Martina and Alfonso who were the most supportive people I know and helped me throughout PhD from the very beginning.

I would like to thank all my friends that supported me in the difficult moments, especially friends from Edinburgh -Mari, Anhad, Sophie, Bota, Chisato, Sarah and Marta; and friends from high school - Janek, Robert, Wojtek, Ola, Aga, Dorota, Kasia and Justyna; also all friends from London who made the city my home.

Deepest thanks with love to my mum, brother and husband and my entire family for unlimited support, care and encouragement. I would not be able to do it without you. Thank you for believing in me.

Table of Contents

Table of figures

List of tables

Abbreviations

Δ	gene deletion
aa	amino acid
APC/C	anaphase-promoting complex/cyclosome
Ark1	Aurora related kinase 1
bp	base pair
BSA	bovine serum albumin
CBB	coomassie brilliant blue
CBZ	carbendazim, methyl-2-benzizimidazole carbamate (MBC)
CCAN	constitutive centromere-associated network
CFP	cyan fluorescent protein
CH	calponin homology
CPC	chromosomal passenger complex
cut	cell untimely torn
DAPI	4',6-diamidino-2-phenylidole
dNTP	deoxynucleoside triphosphate
DTT	dithiothreitol
ECL	enhanced chemiluminescence
EMM	Edinburgh minimal medium
GFP	green fluorescent protein
H_2O	water
HA	hemagglutinin epitope
hph^r	hygromycin B resistance
HU	hydroxyurea
IgG	immunoglobulin G
IP	immunoprecipitation
IPTG	isopropyl β-D-1-thiogalactopyranoside
kan^r	kanamycin resistance
KT	kinetochore
LB	Luria-Bertani
mCherry	monomeric red fluorescent protein

mRFP	monomeric red fluorescent protein
Mps1	Monopolar spindle 1
MT	microtubule
NaOH	sodium hydroxide
nat^r	nourseothricin resistance
NE	nuclear envelope
OD_{600}	optical density at 600 nm
PBS	phosphate buffered saline
PCR	polymerase chain reaction
PEG	polyethylene glycol
PMSF	phenylmethylsulphonyl fluoride
PNPP	ρ-nitrophenyl phosphate
PVDF	polyvinylidene Difluoride
rpm	rotations per minute
RT	room temperature
SAC	spindle assembly checkpoint
SDS-PAGE	sodium dodecyl suphate polyacrylamide gel electrophoresis
SPB	spindle pole boy
TBZ	thiabendazole
ts	temperature sensitive
WCE	whole cell extract
YE5S	yeast extract with supplements
YFP	yellow fluorescent protein

Chapter 1. Introduction

1.1 Cell cycle and mitosis

In 1855, Rudolph Virchow formed his famous cell theory *'omnis cellula e cellula'*[1] where he stated that each cell arises from a pre-existing cell. Tremendous progress has been achieved, especially in the 1970s and 1980s, in our understanding of the cell cycle - mainly obtained from genetic analysis in yeasts (Nurse et al., 1998, Nurse, 2000, Hartwell et al., 1974, Hartwell et al., 1973). All living organisms go through the cell cycle; a repetitive series of distinct events proceeding in a specific order for cell reproduction. In unicellular organisms, an entirely new organism is generated, whereas multicellular organisms, such as humans, require cell division for multiple stages of life – embryonic growth, tissue regeneration, organ development and cell replacement. This process needs to be tightly regulated as abnormalities can lead to cell death or uncontrolled cell proliferation and hence tumour formation (Hanahan and Weinberg, 2011).

1.1.1 Cell cycle

The cell cycle is divided into four continuous, yet distinct phases - a gap phase (G1), DNA replication (S phase), a second gap phase (G2) and mitosis (M). However, depending on the environmental conditions, cells can stop proliferating and enter a quiescent state (G0 phase). In short, G1 and G2 phases are periods where a cell takes up nutrients, increases in size and synthesises proteins required for S or M phases. During S phase, chromosomes and centrosomes (spindle pole bodies, SPBs, in yeast) are duplicated for equal division. G1, S and G2 phases are collectively referred to as interphase, a period of preparation for cell division. In mitosis, duplicated chromosomes are divided equally into two new identical daughter cells, which are physically separated during a process called cytokinesis (Figure 1.1).

The order and timing of the cell cycle phases is tightly controlled, primarily by cyclin-dependent kinases (Cdks) and cyclins (Cdk activators). There are several cyclins in the

[1] Each cell stems from another cell

cell cycle whose level fluctuates between different phases. These fluctuations are linked with Cdk activity that also oscillates during the cell cycle – activity is low upon entry to G1, high from S to M phase then drops at the end of M phase. In addition to tight control of cell cycle progression, there are several transition points known as checkpoints - surveillance mechanisms by which cells enter the next phase in the cell cycle only after completing the previous one.

1.1.2 Mitosis

During the cell cycle, mitosis is the shortest phase with the most profound changes leading to the separation of genetic material into two daughter cells. Mitosis consists of prophase, prometaphase, metaphase, anaphase and telophase (Figure 1.1), proceeding in this order (Pines and Rieder, 2001). At the beginning of prophase, chromosomes condense, centrosomes move to opposite poles and the spindle begins to form. This is followed by the complete breakdown of the nuclear envelope. In prometaphase, spindle microtubules grow from each centrosome and 'search and capture' sister chromatids via their kinetochore regions. During metaphase, all sister chromatid pairs are bioriented and aligned at equator of the cell or metaphase plate. Subsequently, kinetochore microtubules firstly shorten and pull sister chromatids apart to opposite poles (anaphase A), and then interpolar (pole-to-pole) microtubules progressively elongate to push spindle poles further away from each other (anaphase B). Sister chromatid separation occurs when the cohesion complexes, which hold sister chromatids together, are cleaved by the protease separase. Separase only becomes activated by the ubiquitylation and subsequent degradation of its binding partner securin through an ubiquitin ligase complex known as a anaphase-promoting complex/cyclosome (APC/C). Anaphase is triggered by, in addition to securin destruction, that of cyclin B, a regulatory subunit of Cdk1, whose destruction leads to mitotic exit. Telophase then sees chromosomes decondense and the actomyosin-based contractile ring forms and also the nuclear envelope reforms. Lastly, in cytokinesis, the contractile ring constricts at the cleavage furrow leading to the formation of two daughter cells.

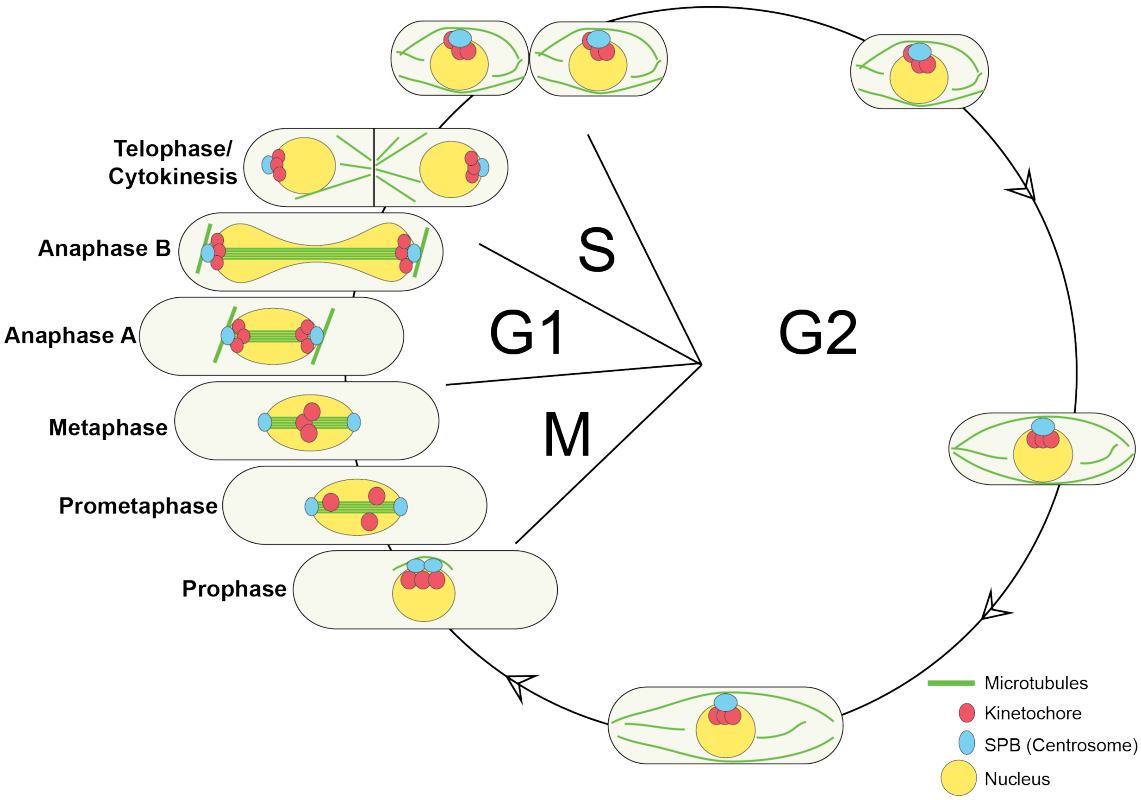

Figure 1.1. Fission yeast cell cycle and mitosis

The phases of the cell cycle are very well conserved in between the species. The cell progresses from G1 to S and then in G2 phase accumulates nutrients for growth before finally entering mitosis (M phase).

1.1.3 Microtubules and MAPs during cell division

Microtubules (MTs) are one of the elements of the cytoskeletons that have roles in intracellular trafficking, cell polarity, cell migration as well as mitosis. Microtubule protofilaments are composed of heterodimers of α- and β-tubulin, arranged in an unidirectional head-to-tail configuration, where α-tubulin is at the minus end (less dynamic) and β-tubulin faces towards the dynamic plus end (Nogales, 1999). Thirteen protofilaments form a hollow cylindrical structure (about 24 nm in diameter) that is highly dynamic – it undergoes constant addition and loss of tubulin dimers, driven by the hydrolysis of GTP (Figure 1.2a). The plus end of microtubules polymerises rapidly by the incorporation of GTP-bound αβ-tubulin – a straight, stable GTP cap forms if this addition dominates. Microtubules depolymerise when GTP is hydrolysed to GDP from β-tubulin at the tip – the cap is lost from the plus end if hydrolysis occurs faster than addition (Nogales et al., 1998, Desai and Mitchison, 1997). This is because GDP-bound

tubulin dimers confer a more bent conformation to the microtubule tip, causing it to become unstable as less precise tubulin contacts are formed. GDP-bound dimers then peel away and hence the microtubule shortens. Intrinsic, dynamic cycling of polymerisation and depolymerisation referred to as 'dynamic instability', is proposed to underlie various microtubule-based activities, such as intracellular trafficking, cell motility and chromosome segregation (Mitchison and Kirschner, 1984).

During mitosis, there are three types of microtubules, which are nucleated from SPBs/centrosomes (Figure 1.2b); astral microtubules, inter-polar microtubules and kinetochore microtubules. As in metazoans, fission yeast astral microtubules, despite being non-essential (Khodjakov et al., 2000), were originally proposed to play a critical role in nuclear positioning in the cells and regulate spindle alignment during mitosis in fission yeast (Oliferenko and Balasubramanian, 2002, Gachet et al., 2004, Gachet et al., 2001, Tournier et al., 2004). However, recent studies contradict this proposition. It has been proposed that the function of astral microtubules is due to their nuclear localisation in early mitosis, rather than the cytoplasm as previously assigned (Zimmerman et al., 2004, Daga and Nurse, 2008). Inter-polar microtubules together with motor proteins, microtubule associated proteins (MAPs) and cross-linkers, play a role in organising the spindle midzone and spindle elongation (Glotzer, 2009, Fu et al., 2009, Loiodice et al., 2005), as well as positioning of the actomyosin ring for cytokinesis (Hagan and Yanagida, 1992, Ding et al., 1993, Glotzer, 2009). Among these three microtubule populations, the key players are kinetochore microtubules that bind chromosomes at the kinetochore region, enabling their proper segregation. In mammalian cells, 20-40 microtubules bind each kinetochore (Rieder, 1981), whereas in budding yeast there is a 1 to 1 ratio (King et al., 1982) and in fission yeast there are 2-4 microtubules per kinetochore (Ding et al., 1993).

MAPs play multiple critical roles in mitosis, one being their regulation of microtubule dynamics. The main players belong to the TACC and TOG proteins and kinesin families of proteins that are conserved across species. In general, TOG proteins are microtubule polymerases that can catalyse microtubule growth by the addition of αβ-tubulin at the plus end of microtubules (Brouhard et al., 2008). Alp7/TACC and

Alp14/TOGG, in yeast, form a complex that shuttles between the nucleus and cytoplasm, accumulating in the nucleus and SPBs and subsequently localising to kinetochores during mitosis (Sato and Toda, 2007, Sato and Toda, 2010, Okada et al., 2014). Alp7-Alp14 were shown to bind microtubules, the Ndc80 loop region (Tang et al., 2013) and the Klp5-Klp6 complex (Tang and Toda, 2015a). *alp7* or *alp14* deletion is synthetic lethal with deletions of *dis1*, *klp5* and *klp6* suggesting overlapping roles between them (Garcia et al., 2001, Garcia et al., 2002)(Corinne Pinder in our group, unpublished data). Dis1, another TOG protein, binds microtubules and also localises to the loop region of Ndc80 (Hsu and Toda, 2011). Klp5-Klp6, members of the kinesin-8 family, are predicted to destabilise microtubules and to also bring PP1 (protein phosphatase 1), a key component of checkpoint silencing, to the kinetochore for mitotic progression into anaphase (Meadows et al., 2011, Zhu et al., 2005, Tang and Toda, 2015a, Vanoosthuyse and Hardwick, 2009). The better understanding of motor proteins will provide more critical information on kinetochore-microtubule attachments.

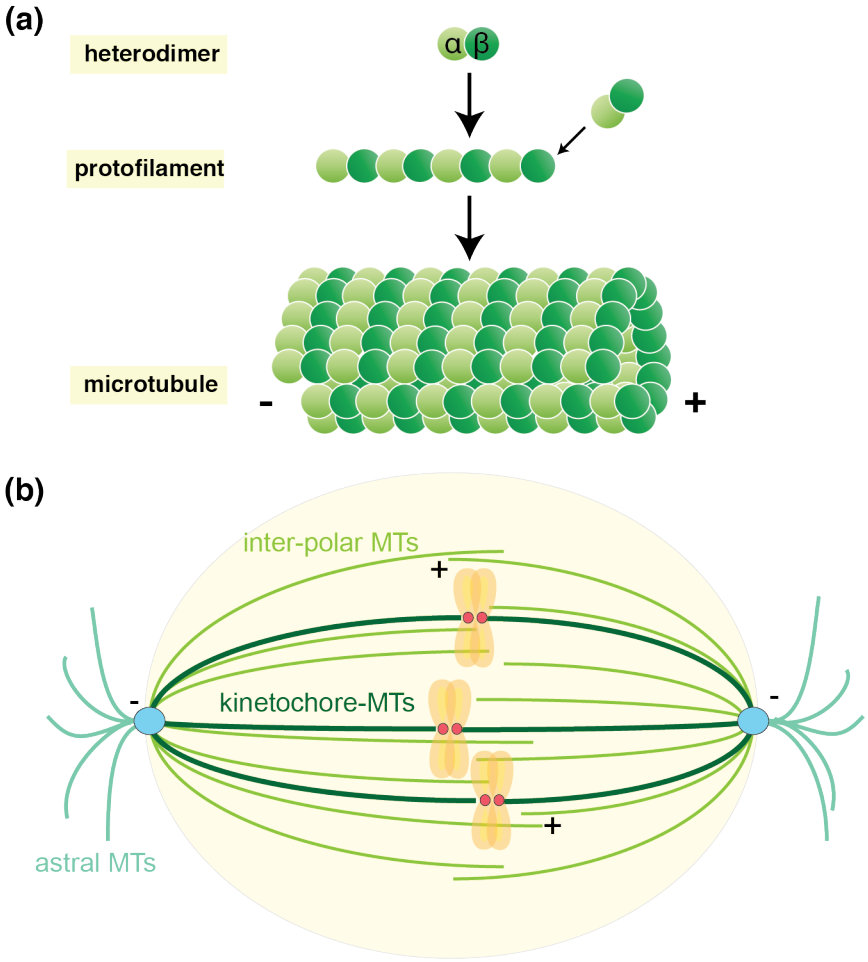

Figure 1.2. Microtubule structure and types of microtubules in mitosis.

(a) α- and β-tubulin proteins form a heterodimer, which assembles into protofilaments in a head-to-tail configuration, with α-tubulin always facing the minus end. Assembly of thirteen protofilaments forms a polar microtubule in a unidirectional manner. (b) The major types of mitotic microtubules emanating from SPBs/centrosomes. Kinetochore microtubules bind to kinetochores at the centromeric regions of chromosomes. Inter-polar microtubules interact with each other in an antiparallel manner, whereas astral microtubules interact with the cell cortex.

1.2 Fission yeast as a model organism

In the current study, fission yeast was used as a model system. *Schizosaccharomyces pombe* is a unicellular, rod-shaped fungus. Its whole genome contains 5144 genes located on three chromosomes of 5.7, 4.7 and 3.5 Mb in size (Wood et al., 2002, Rhind et al., 2011, Bitton et al., 2011). These genes and the cellular processes they control are highly conserved, in particular the cell cycle (for example Table 1.1 and Table 1.2). The cell cycle in yeast is very similar to higher eukaryotes, but there are major differences.

Firstly, the proportion of time spent in each of the G1, S, G2 and M phases is different (Figure 1.1). Fission yeast spends 70% of the time in G2 phase and mitosis at 27˚C lasts less than 30 minutes. Secondly, fission yeast undergoes a closed mitosis, wherein the nuclear envelope is not broken down during cell division, in contrary to an open mitosis seen in higher eukaryotes (Forsburg and Nurse, 1991). During this process, the centrosome equivalent – spindle pole body (SPB) is inserted into the nuclear envelope, duplicated and there conducts cell division, eventually returning to the cytoplasmic surface of the nucleus (Ding et al., 1997).

Similar to metazoan kinetochores that bind multiple microtubules, the fission yeast kinetochore can bind 2-4 microtubules, strongly resembling those of metazoan mitosis (Winey et al., 1995, Ding et al., 1993).

The major advantage of using fission yeast, as a model organism, is the ease of maintenance and their fast growth rate (3 hours per cell cycle in rich medium at 27˚C). *S. pombe* cells normally grow as haploid and upon starvation they are able to mate (h^+ and h^-) forming a diploid zygote which undergoes meiosis and sporulation. This life cycle enables isolation of the haploid offspring with required genotype. Another strong point is that genetic manipulation is relatively easy, a high rate of homologous recombination on chromosomes enables successful integrations for gene tags, fusions, deletions or replacements. Additionally, sequencing of the whole genome led to the creation of very comprehensive database (PomBase) (Wood et al., 2002) and various tools, such as deletion libraries (covering 99% of the genome)(Kim et al., 2010, Spirek et al., 2010), comparative functional genomics (Rhind et al., 2011) and ORFeomes (open reading frame) with detailed protein localisation (Hayashi et al., 2009, Matsuyama et al., 2006).

1.3 Kinetochore complex

1.3.1 Structure overview

The kinetochore is a specialised region of the chromosomes that is responsible for the direct binding of DNA to microtubules for accurate chromosome segregation. It consists of more than 100 hierarchically arranged proteins that assemble on centromeric DNA of chromosomes (Foley and Kapoor, 2013, Cheeseman, 2014). Initial electron microscopy observations of the kinetochore in the 1960s and 1970s have distinguished a three-layered structure dependent on the composition of the kinetochore and its proximity to centromeric chromatin. These layers constitute inner, middle and outer regions, covered by a fibrous 'corona' (Jokelainen, 1967, Brinkley and Stubblefield, 1966, Comings and Okada, 1971).

The inner kinetochore localises to a centromeric stretch of DNA, demarcate by CENP-A, variant of histone H3 enriched at the centromere, and is composed of the constitutive centromere-associated network (CCAN) (Westhorpe and Straight, 2013). The middle region with no definite structure is followed by the outer kinetochore that binds the microtubules via the KMN network (KNL1/Spc7, the MIS12 complex and the NDC80 complex (discussed in detail in chapters 1.3.3, 1.3.3.1 and 1.3.3.3)(Foley and Kapoor, 2013, Deluca and Musacchio, 2011, DeLuca and Musacchio, 2012). The fibrous 'corona' stretches 100-150 nm from the outer kinetochore with microtubule-associated proteins (MAPs) and motors including CENP-E, dynein and CENP-F (Varma et al., 2013, Wan et al., 2009, Pfarr et al., 1990).

Since the first identification of the kinetochore in the 1960s, major progress has been made in the field. I will provide a summary of the current understanding of kinetochore structure and function in mitosis, including recognition of the specific chromosomal site upon which the kinetochore is built, formation of kinetochore-microtubule connections and the forces driving the chromosome segregation as well as interacting proteins.

1.3.2 Assembly of the kinetochore structure

Kinetochore assembly occurs at a specialised chromatin domain called the centromere, which is marked by histone H3 variant – CENP-A (Cnp1 in *S. pombe*, Cse4 in *S. cerevisiae*) (Blower et al., 2002, Earnshaw, 2015). The simplest point centromere, in budding yeast, is only 125 bp long and is divided into three regions CDEI, CDEII (containing CENP-A/Cse4) and CDEIII (Saunders et al., 1988, Meraldi et al., 2006). In contrast, fission yeast has the regional centromeres, spanning 35-110 kb in length, where the middle CENP-A/Cnp1-containing region is flanked by pericentric heterochromatin. In vertebrates, the centromere is 1-2.5 Mb long and both the centromeric and pericentromeric regions of heterochromatin are occupied by non-coding tandem repeats of satellite sequences, e.g. α-satellite (Cleveland et al., 2003, Steiner and Henikoff, 2015). In budding yeast, assembly of the kinetochore is sequence-dependent on a specified point of centromere region. Conversely, in vertebrates and fission yeast, kinetochore localisation to 'regional' centromere DNA is nucleotide sequence-independent and thought to be specified by epigenetic regulation (Pidoux and Allshire, 2004, Earnshaw, 2015). The third type of the centromere is a holocentromere that is found in nematodes and spans the entire length of chromosomes (Maddox et al., 2004, Steiner and Henikoff, 2015, Yamagishi et al., 2014).

Although CENP-A is a universal hallmark of the centromere, localisation of CENP-A to non-centromeric sites was insufficient to reassemble the kinetochore *de novo* at these sites (Van Hooser et al., 2001). Another 15 CCAN components work together with CENP-A to create a kinetochore interface (Cheeseman, 2014, Cheeseman and Desai, 2008). The first *in vitro* reconstitution of the budding yeast kinetochore-microtubule interface resulted in the identification of key elements of the kinetochore required for its function (Akiyoshi et al., 2010). First to be identified (Earnshaw and Migeon, 1985), CENP-A and CENP-C are essential for kinetochore assembly, with CENP-A functioning as a kinetochore landmark (Akiyoshi et al., 2010, Takeuchi and Fukagawa, 2012). CENP-C localisation is dependent on CENP-A - once localised it acts as a structural hub for kinetochore assembly and integrity. The N-terminus of CENP-C binds the Mis12 complex where it interacts with Nsl1 and Nnf1 (Gascoigne et al., 2011), while the PEST domain of CENP-C interacts with the CENP-H/I/K/M subcomplex

(Klare et al., 2015, Basilico et al., 2014). In turn, the localisation of CENP-C depends on CENP-H and CENP-I (Fukagawa et al., 2001, Nishihashi et al., 2002). siRNA knockdown of CENP-H, CENP-I and CENP-K all cause the same chromosome alignment defects, suggesting the proteins to form complex (Okada et al., 2006, McClelland et al., 2007, Cheeseman and Desai, 2008). This complex was later shown to be a tetramer of the above in addition to its regulator CENP-M, forming the CENP-H/I/K/M complex (Basilico et al., 2014). Other components whose roles have not been fully elucidated include CENP-B, CENP-R, CENP-L/U and the CENP-O/P/Q/U complex. CENP-B localises to α-satellite DNA but its depletion does not impact the recruitment of other kinetochore components (Masumoto et al., 1989, Earnshaw and Migeon, 1985). CENP-N/L bind directly to CENP-A (Carroll et al., 2009, Hinshaw and Harrison, 2013), whereas CENP-O/P/Q/U (known as the COMA complex in budding yeast) may play a role in microtubule binding (Perpelescu and Fukagawa, 2011, Amaro et al., 2010) and interacts with the uncharacterised CENP-R (Hori et al., 2008) The scheme of kinetochore assembly is shown in Figure 1.3.

Another key complex is CENP-T/W/S/X, which forms a nucleosome-like structure (Nishino et al., 2012) and data suggests that it can bind DNA of the centromeric region. However, CENP-T/W/S/X localisation is dependent on CENP-A (Basilico et al., 2014), among other factors (Hori et al., 2008, Gascoigne et al., 2011). In addition, the flexible N-terminus of CENP-T interacts with the Ndc80 complex through the globular domains of Spc25 and Spc24 (Suzuki et al., 2011, Gascoigne et al., 2011). Artificial targeting of CENP-T or CENP-C to ectopic site is sufficient to recruit a functional kinetochore-like structure (Hori et al., 2013, Gascoigne et al., 2011).

CENP-C and CENP-T/W/S/X complexes act as a bridge between inner and outer kinetochore components. The majority of CCAN components are conserved in yeasts (as shown in Table 1.1). Fission yeast kinetochore proteins were also studied and a number of metazoan homologs with similar functions were identified, e.g. Cnp3/CENP-C (Holland et al., 2005).

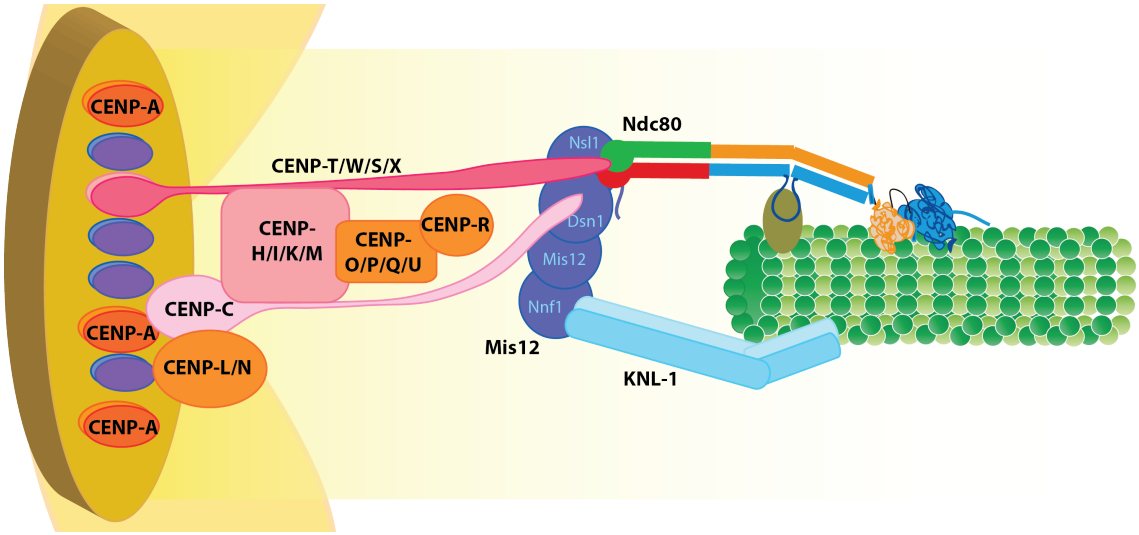

Figure 1.3. Assembly of the kinetochore structure.

The constitutive centromere-associated network (CCAN) is a network of the proteins localising to the kinetochore and acts as a scaffold enabling the attachment to microtubules. CENP-A is localised to the inner kinetochore, where it directly binds to CENP-C and CENP-L/N. The CENP-T/W/S/X complex has a histone fold and also localises to the inner kinetochore. The tails of CENP-C and CENP-T protrude to the outer kinetochore acting as the bridge to the KMN network and potentially a supporting scaffold to other CENPs (the CENP-H/I/K/M complex, the CENP-O/P/Q/U complex and CENP-R). The KMN network consists of the Mis12 complex (Mis12, Dsn1, Nsf1 and Nnl1), the Ndc80 complex (Ndc80, Nuf2, Spc24 and Spc25) and the Knl1 complex.

Complex	*S. pombe*	*S. cerevisiae*	*H. sapiens*
KMN network	Ndc80 complex		
	Ndc80	Ndc80	NDC80/HEC1
	Nuf2	Nuf2	NUF2
	Spc25	Spc25	SPC25
	Spc24	Spc24	SPC24
	Mis12/Mtw1/MIND complex		
	Mis12	Mtw1	MIS12
	Mis13/Dsn1	Dsn1	DSN1
	Nnf1	Nnf1	NNF1
	Mis14/Nsl1	Nns1	NSL1
	Knl1/Spc7/Spc105 complex		
	Spc7	Spc105	Knl1/Blinkin
	Sos7	YDR532C/Kre28	Zwint
Constitutive centromere associated network (CCAN)	Cnp3	Mif2	CENP-C
	Fta1	Mcm19	CENP-L
	Mis15	Chl4	CENP-N
	Mal2	Mcm21	CENP-O
	Fta2	Ctf19	CENP-P
	Fta7	Okp1	CENP-Q
			CENP-R
	Fta4		CENP-U
	CENP-TWSX		
	Mhf1/SPBC2D10.16	YOL86-A	CENP-S
	Mhf2/SPCC576.12C	YDL160C-A	CENP-X
	Cnp20/SPBC800.13	Cnn1	CENP-T
	New1/SPAC17G8.15	YDR374W-A	CENP-W
	CENP-HIKM		
	Fta3	Mcm16	CENP-H
	Mis6	Ctf3	CENP-I
	Sim4	Mcm22	CENP-K
	Mis17	Iml3	CENP-M
CENP-A nucleosome	Cnp1	Cse4	CENP-A
	Abh1, Cbh1, Cbh2	-	CENP-B

Table 1.1. Kinetochore components are conserved from yeasts to humans.

Kinetochore proteins in fission yeast (*S. pombe*), budding yeast (*S. cerevisiae*) and human (*H. sapiens*) are shown. Adapted and modified from (Perpelescu and Fukagawa, 2011).

1.3.3 Attachment of kinetochore to spindle microtubules

During mitosis, the kinetochore must form an attachment to microtubules to enable proper chromosome segregation via widely conserved outer kinetochore components. From yeast to higher vertebrates the KMN network (called the NMS – Ndc80-MIND-Spc7/Spc105 in yeast) consists of the Knl1/Spc105/Spc7/Blinkin complex, the Mis12/MIND complex and the Ndc80 complex (Figure 1.3). The KMN network functions as a platform the recruitment of another microtubule-associated proteins and spindle assembly checkpoint components (discussed extensively below) (Cheeseman et al., 2006, Cheeseman, 2014, Martin-Lluesma et al., 2002, Liu et al., 2005).

1.3.3.1 The Mis12 complex

The Mis12 protein, identified and named in a mutant screen based on its phenotype – minichromosome loss 12 (Takahashi et al., 1994), plays an essential role in chromosome segregation (Goshima et al., 1999). Increased frequency of chromosome missegregation and longer spindles were observed in budding yeast and humans in *mis12* (Mtw1 in budding yeast) mutants or depletion, respectively (Goshima et al., 1999, Goshima and Yanagida, 2000, Kline et al., 2006). Mis12, together with Mis13 (Dsn1 in budding yeast), Mis14 (Nsl1 in budding yeast) and Nnf1, forms the Mis12 complex (also called MIND in budding yeast). The primary role of the Mis12 complex is to link the inner and outer kinetochore and to stabilise KMN-microtubule interactions. The N-terminal region of CENP-C interacts with Nsl1 and Nnf1 components (Gascoigne et al., 2011, Screpanti et al., 2011), whereas Nsl1 and Dsn1 bind the globular heads of Spc24 and Spc25 of the Ndc80 complex (Hornung et al., 2011). Furthermore, the Mis12 complex also binds KNL1. Aurora B phosphorylation of KNL1 and Dsn1 was shown to sense and regulate the tension across kinetochore-microtubule attachments (Welburn et al., 2010, Kim and Yu, 2015).

The Mis12 complex is highly conserved from yeasts to higher vertebrate, binding KNL1 and the Ndc80 complex with a linear structure. Furthermore, it acts as a platform for the assembly of the outer as well as inner kinetochore layers. Dsn1-FLAG pulled down CENP-A, CENP-P, CENP-C and KMN network components in the affinity

purification in budding yeast (Akiyoshi et al., 2010). The localisation of kinetochore and kinetochore-associated components, HP1 (heterochromatin component), CENP-E (motor protein), CENP-H, CENP-A, Ndc80, Hsp90-Sgt1 chaperone and BubR1, is abolished in Mis12 depletion (Kline et al., 2006, Obuse et al., 2004, Davies and Kaplan, 2010). In addition, the Mis12 complex was shown to interact with the Ska complex (microtubule motor that binds and moves on depolymerizing microtubules) (Chan et al., 2012).

1.3.3.2 KNL1 complex

Knl1, another element of the KMN network, binds microtubules directly and acts as a platform for the recruitment of various proteins, including Zwint, BubR1, Bub1, Bub3 and CENP-F (Cheeseman and Desai, 2008, Kiyomitsu et al., 2007). Knl1/Blinkin/Sp105/Spc7 forms a heterodimer with Zwint, in humans, which is recruited to the outer kinetochore by the Mis12 complex (Varma et al., 2012b). Spc7, the fission yeast homologue of Knl1, was also shown to bind Sos7, which is a functional homologue of Zwint (Jakopec et al., 2012) - similarly in budding yeast Spc105 binds Kre28, the orthologue of Zwint (Pagliuca et al., 2009). The C-terminus of Knl1 contains key motifs for binding to the Mis12 complex and Zwint1, whereas regulatory Aurora B phosphorylation targets reside in the N-terminus (Lampson and Cheeseman, 2011).

Knl1 recruits PP1 in its N-terminal PP1-binding motif, which is followed by KI and MELT motifs ((M/I/LV)-(E/D)-(L/M/I/V)-(T/S)), as well as RWD domain in C-terminus. PP1 recruitment, in turn, triggers silencing of the spindle assembly checkpoint and hence mitotic exit (Meadows et al., 2011, Welburn et al., 2010, Liu et al., 2010). In addition, another phosphatase - PP2A-B56 - also localises to Knl1 MELT motifs, by binding phosphorylated Bub1/Bub3/BubR1 complex (SAC components; discussed in Chapter 1.4.1.2). Its localisation to Knl1 antagonises Aurora B activity by dephosphorylating the MELT motifs, where PP1 will be recruited (discussed more in detail in Chapter 1.4.5) (Espert et al., 2014, Nijenhuis et al., 2014). The PP1-binding activity of Knl1 is conserved across model organisms (Meadows et al., 2011, Welburn

et al., 2010, Liu et al., 2005, Rosenberg et al., 2011). In *C. elegans*, Knl1 may also recruit the Rod-Zwilch-Zw10 (RZZ) complex (Cheeseman and Desai, 2008, Essex et al., 2009, Varma et al., 2013).

The N-terminal domain of Knl1 ($Knl1^{1-250}$) precipitated Bub3, Bub1, BubR1 as well as Mad1, Mad2 and Cdc20 in humans in pull downs (Krenn et al., 2014). Bub1 and BubR1 contain Bub3 binding domain that interacts with the phosphorylated MELT motifs, located in the N terminal region of Knl1 (Yamagishi et al., 2012, Meadows et al., 2011, Heinrich et al., 2012, Krenn et al., 2014). Moreover, the KI motifs surrounding the MELT domains ($Knl1^{150-250}$) were shown to enhance the interaction between MELT domain and Bub1/BubR1 (Krenn et al., 2014). Mph1/MPS1 kinase also phosphorylates the MELT motifs, enabling the recruitment of Bub1, BubR1 and Bub3 to kinetochore; this regulatory mechanism is conserved in yeast and humans (Shepperd et al., 2012, Yamagishi et al., 2012, London et al., 2012). Mph1-dependent phosphorylation of the MELT motifs is antagonised by PP2A-B56 and PP1 activity, providing an opposing mechanism and thus providing robust and functional checkpoint signalling (London et al., 2012, Espert et al., 2014). The scheme of domains of Knl1 and its interacting proteins is shown in Figure 1.4.

Initially, Knl1 was identified during *C.elegans* RNAi screening, as a mutant with chromosome segregation defects and abolished kinetochore assembly (kinetochore null 1) (Desai et al., 2003). Despite complex formation with Ndc80 and Mis12, depletion of Knl1 in humans does not affect the recruitment of other subunits of the KMN network (Cheeseman et al., 2006, Kiyomitsu et al., 2007). In *C.elegans,* however, Knl1 affects the recruitment of the Ndc80 complex (Cheeseman and Desai, 2008, Gassmann et al., 2008, Essex et al., 2009). The first 500 amino acids of Knl1 have microtubule binding activity, as shown in the *in vitro* reconstitution of the KMN network (Cheeseman et al., 2006). Furthermore, a critical nine amino acids, responsible for Knl1 microtubule binding form a basic patch in the N-terminus of Knl1 (Espeut et al., 2012). siRNA of Knl1 results in chromosome missegregation as well as compromised formation of kinetochore-microtubule interactions (Cheeseman and Desai, 2008, Kiyomitsu et al., 2007, Schittenhelm et al., 2009).

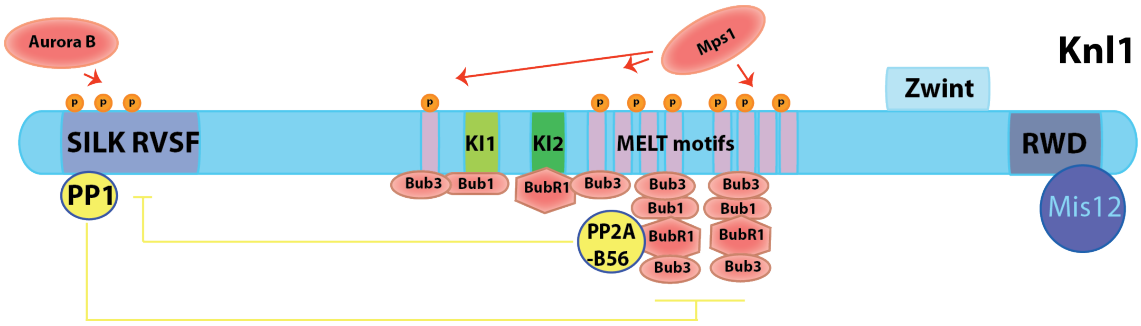

Figure 1.4. Scheme of Knl1 and its interacting proteins.

Knl1 is a widely conserved protein that acts as a scaffold for the recruitment of checkpoint and kinetochore components. Its N-terminus and the SILK RVSF motif (PP1-binding) bind microtubules, tightly regulated through phosphorylation by Aurora B and PP1. KI1 and KI2 motifs bind and enhance the binding of Bub1, Bub3 and BubR1 proteins. The main binding sites of Bub1/Bub3/BubR1 to Knl1 are the MELT motifs. The C-terminus of Knl1 binds Zwint and the RWD domain interacts with the Mis12 complex. Adapted from (Ghongane et al., 2014).

Zwint, on the other hand, targets the Rod-ZWILCH-ZW10 (RZZ) complex, which in turn brings Spindly then dynein-dynactin resulting in the recruitment of the Mad1-Mad2 complex to the kinetochore (Gassmann et al., 2008, Griffis et al., 2007). Coiled-coil Zwint forms a stable complex with Knl1 via its C-terminus (Petrovic et al., 2010). Zwint phosphorylation by Aurora B regulates the recruitment of dynein-dynactin and the RZZ complex, hence regulating SAC signalling and chromosome motility (Kasuboski et al., 2011, Famulski and Chan, 2007). This large 300 kDa Knl1 complex (Knl1 and Zwint) has multiple domains and functions that are required for proper kinetochore assembly, in terms of microtubule binding, checkpoint activation and silencing.

1.3.3.3 The Ndc80 complex

The Ndc80 complex is a heterotetramer consisting of Ndc80/Hec1, Nuf2, Spc25 and Spc24 proteins (Cheeseman and Desai, 2008). Ndc80 (nuclear division cycle 80) and Nuf2 were initially identified as components of the SPB in budding yeast (Rout and Kilmartin, 1990, Osborne et al., 1994, Wigge et al., 1998). However, only the research on highly expressed in cancer 1 (Hec1) in a retinoblastoma tumour suppressor screening

revealed the functional homology of Hec1 to Ndc80. Furthermore, antibody injections demonstrated that Ndc80/Hec1 localises to the kinetochore and has a role in chromosome movements (Chen et al., 1997). Later co-purification of Ndc80 resulted in the identification of three other tightly bound proteins – Nuf2, Spc24 and Spc25 (Figure 1.5a) (Wigge and Kilmartin, 2001, Osborne et al., 1994). During the 20 years since their discovery, significant progress has been made in characterising their structure and function. Ndc80/Hec1 was shown to be highly conserved from yeast to humans and to be essential for kinetochore function. The Ndc80 complex is required for kinetochore-microtubule attachments, chromosome movement and spindle assembly checkpoint signalling (Howe et al., 2001, Nabetani et al., 2001, McCleland et al., 2003, Williams et al., 2007). Disruption of the Ndc80 complex by antibodies, mutations or siRNA consistently shows the same phenotype – chromosome missegregation resulting from faulty kinetochore-microtubule attachments (Chen et al., 1997, Wigge and Kilmartin, 2001, Howe et al., 2001, Hori et al., 2003, McCleland et al., 2003, Desai et al., 2003, Cheeseman et al., 2004, Cheeseman and Desai, 2008, DeLuca et al., 2003, DeLuca et al., 2006, Deluca and Musacchio, 2011, Westermann et al., 2003, DeLuca and Musacchio, 2012).

The Ndc80 complex is a 57 nm long heterotetramer with two globular heads on both ends linked by coiled-coil regions (Wei et al., 2005, Ciferri et al., 2005). The crystal structure of an artificial human Ndc80 complex (called “bonsai”) was solved and two distinct regions were distinguished. Ndc80-Nuf2 globular domain, on one end, binds microtubules and Spc24-Spc25 head, on the opposite end, interacts (Ciferri et al., 2008) with other kinetochore proteins (Cheeseman and Desai, 2008, Guimaraes et al., 2008) – CENP-T (Suzuki et al., 2011, Gascoigne et al., 2011, Bock et al., 2012) and Dsn1 and Nsl1, components of the Mis12 complex (Hornung et al., 2011). Both Ndc80 and Nuf2 contain calponin homology (CH) domains, identified as microtubule binding sites. However, it is only the CH domain of Ndc80 together with its unstructured N-terminal tail that forms kinetochore-microtubule attachments, while the CH domain of Nuf2 supports the structure of the Ndc80 complex (Sundin et al., 2011, Alushin et al., 2010, Wilson-Kubalek et al., 2008, Tooley and Stukenberg, 2011). Ndc80 has five distinct

regions: N-terminal unstructured tail followed by the CH domain and a linker region and finally a coiled-coil domain disrupted by an internal loop (Figure 1.5b).

The loop region of Ndc80 is ~16 nm away from the MT-binding CH domain and creates a kink in the Ndc80 complex structure (Wang et al., 2008). The conserved sequence of the loop emphasises its importance. Studies in fission yeast generated mutants in the loop region - *ndc80-21* (L405P) and *ndc80-NH12* (L246P) - that have defective kinetochore-microtubule attachments and cause spindle collapse, as well as persistent spindle assembly checkpoint activation (Tang et al., 2013, Hsu and Toda, 2011). These studies showed that the loop region of Ndc80 recruits TACC and TOG proteins, namely Dis1/TOG (Hsu and Toda, 2011) and Alp7/TACC-Alp14/TOG (Tang et al., 2013) that create additional indirect microtubule binding sites from the Ndc80 loop region as well as functioning as a microtubule polymerases. In addition, deletion of the Ndc80 loop region in budding yeast showed that it is essential for recruitment of the Dam1 complex to the kinetochore (Maure et al., 2011). However there is a discrepancy with studies that suggest the CH domain of Ndc80 (Lampert et al., 2013, Gonen et al., 2012) is critical platform for the assembly of the ring structure composed of sixteen components of the Dam1 complex (Miranda et al., 2005, Westermann et al., 2005). A functional human homologue of the Dam1 complex exists as the Ska complex in humans and has similarly been shown to bind to the Ndc80 loop region (Zhang et al., 2012). In addition, Cdt1 (required for licensing of DNA replication origins) also localises to the analogous region of Ndc80 causing a conformational change in the Ndc80 complex *in vivo*. This activity is essential for the formation of stable kinetochore-microtubule attachments (Varma et al., 2012a, Varma et al., 2012b). These studies reveal an additional indirect microtubule-binding site within Ndc80 proteins – the loop region.

The linker region of Ndc80 is not very well characterised. Human Ndc80 has two α-helixes just after its CH domain (Ciferri et al., 2008). This region is referred to as a linker or a hairpin. Recently, the Trisha Davis group identified in budding yeast that the linker region influenced the microtubule binding of the Ndc80 complex. Moreover, mutations in the linker region abolished the Dam1 complex binding to microtubules (Tien et al., 2013). Another budding yeast study with *ndc80-Δ256-273* (the linker

region) truncation showed the reduced Ndc80-Dam1 interaction, and the mutant reduces the Ndc80 intramolecular flexibility in the Ndc80 complex (Lampert et al., 2013). The linker region might indirectly influence the Dam1 binding to Ndc80 *in vivo*, as the Dam1 complex was shown to localise to the loop region of Ndc80 (Maure et al., 2011). Further studies are needed in other model systems to assess the function of the conserved linker region of Ndc80. Its proximity to the CH domain makes it an attractive site to act as a protein recruitment platform or microtubule binding enhancer.

The main kinetochore-microtubule binding interface is the CH domain of Ndc80 protein, in particular the site called 'toe print' on the CH domain that steps on microtubules. The toe refers to the C-terminal end of the αG helix and short αB and αF helixes and is often described as a sensor of straight versus curled protofilaments, regulating the strength of the Ndc80 complex binding accordingly (strong and weak binding respectively). The toe binds at intra- and inter-dimer interfaces of tubulin heterodimers (Alushin et al., 2010). Mutations in this region and around it yield the kinetochore unable to form an attachment with microtubules (Tooley and Stukenberg, 2011). Moreover, the CH domain is highly phosphorylated by Aurora B (multiple sites)(Ciferri et al., 2008) and Nek2A (S165 in particular) (Wei et al., 2011) and has a role in the recruitment of spindle assembly checkpoint components such as Mad1, Mad2 and Mps1 (Guimaraes et al., 2008, Martin-Lluesma et al., 2002, Miller et al., 2008, Hewitt et al., 2010, Santaguida et al., 2011). S165 phosphorylation was shown to play a role in Mad1 and Mad2 recruitment as the mutations here lead to their mislocalisation as well as chromosome missegregation (Wei et al., 2011). Aurora B phosphorylation of the CH domain in addition to the N-tail acts as a tension sensor and it is essential for the recruitment of SAC components (Santaguida et al., 2011).

The N-tail is essential for microtubule binding, its truncation, depletion or mutations of Aurora B phosphorylation sites reduce the stability of kinetochore-microtubule attachments (Ciferri et al., 2008, Guimaraes et al., 2008, Sundin et al., 2011, DeLuca et al., 2006, Miller et al., 2008). Human studies have identified nine sites that are essential for microtubule binding as well as oligomerisation of the Ndc80 complexes on the microtubule (Alushin et al., 2010). The tail has positive patches that electrostatically

interact with negatively charged E-hooks of tubulin (Ciferri et al., 2008, Miller et al., 2008, Alushin et al., 2012). Furthermore, two Aurora B phosphorylation zones fine-tune the interactions of the Ndc80 complex with tubulin monomers (Zone 1) as well as between the neighbouring Ndc80 complexes to promote oligomerisation (Zone 2) (Alushin et al., 2012). However, recent work contradicts the cooperativity of the Ndc80 complexes, finding them to be very weak (if not at all) and not subject to phosphoregulation (Zaytsev et al., 2015). In addition, the phosphorylation of N-tail of Ndc80 is further emphasised as a rheostat controlling MT binding. Variable numbers of phosphorylation events induce different strengths of microtubule binding - less efficient interactions result from higher phosphorylation states (Zaytsev et al., 2015).

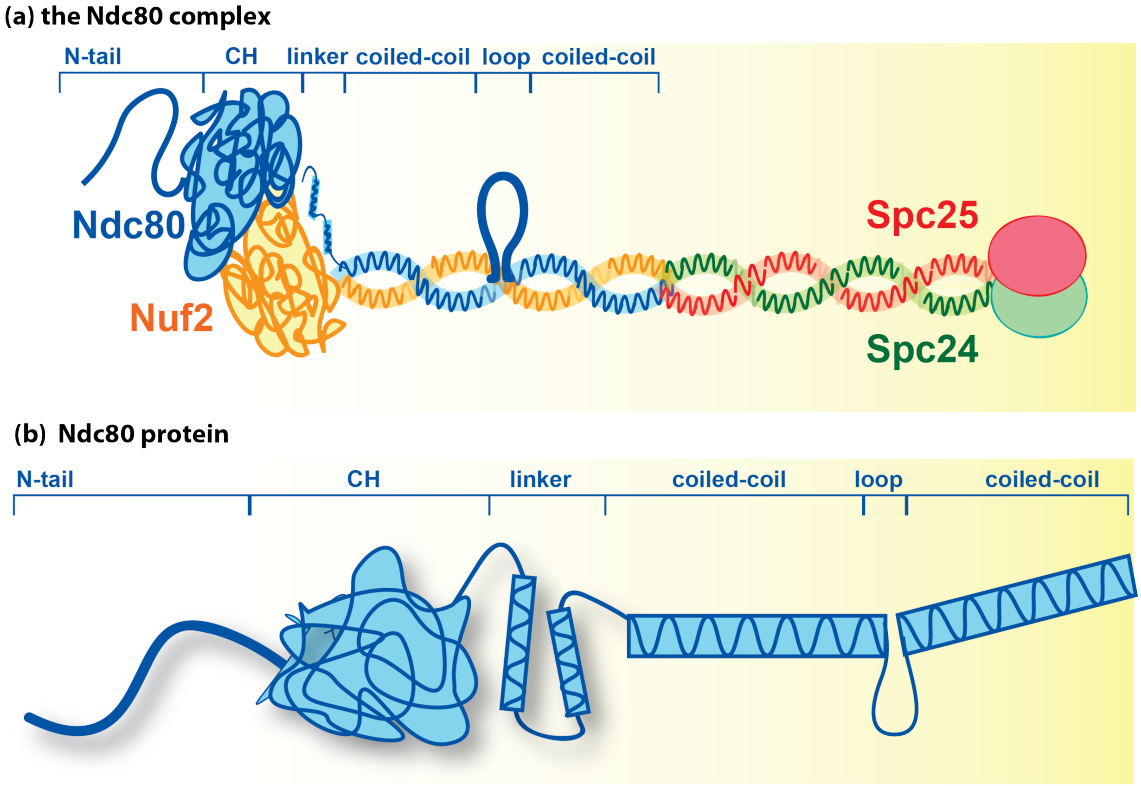

Figure 1.5. The Ndc80 complex.

(a) Scheme of the Ndc80 tetramer complex. Ndc80 and Nuf2 globular domains face the microtubule-binding site, whereas Spc24 and Spc25 anchor the protein to the kinetochore. The complex is held together through interaction of the coiled-coil regions of Spc25, Spc24, Nuf2 and Ndc80. (b) Ndc80 protein consists of an unstructured N-terminal tail (N-tail), followed by a calponin homology (CH) domain, an uncharacterised linker region and then coiled-coil domains disrupted by a loop structure.

1.3.4 Regulation of kinetochore-microtubule attachments

Kinetochore-microtubule attachment is critical to ensure faithful chromosome segregation and is therefore tightly regulated. To establish initial attachment, microtubules search for and eventually capture kinetochores through growth and shrinkage by pivoting movements. Subsequent bipolar attachment ensures correct segregation, as each kinetochore of sister chromatids is attached to opposite spindle pole (Figure 1.6a). This attachment is known as amphitelic attachment, but kinetochores can be in various states of mal-attachments if this is not achieved. Monotelic attachment exists if one kinetochore of the pair is attached to only a single pole (Figure 1.6b), whereas syntelic attachment occurs if both kinetochores of sister chromatids are attached to the same spindle pole (Figure 1.6c). Merotelic attachment is characterised by microtubules from the opposite poles attaching to the same kinetochore (Figure 1.6d). Additional errors in segregation can result from disruption of kinetochore, which can lead to unstable or weak attachment to microtubules. As mistakes can result in aneuploidy, the presence of surveillance mechanisms is critical for cell survival. Therefore, cells have evolved a mechanism for the detection of faulty attachments – the spindle assembly checkpoint (SAC) and a mechanism for correcting improper KT-MT attachments via the chromosomal passenger complex (CPC).

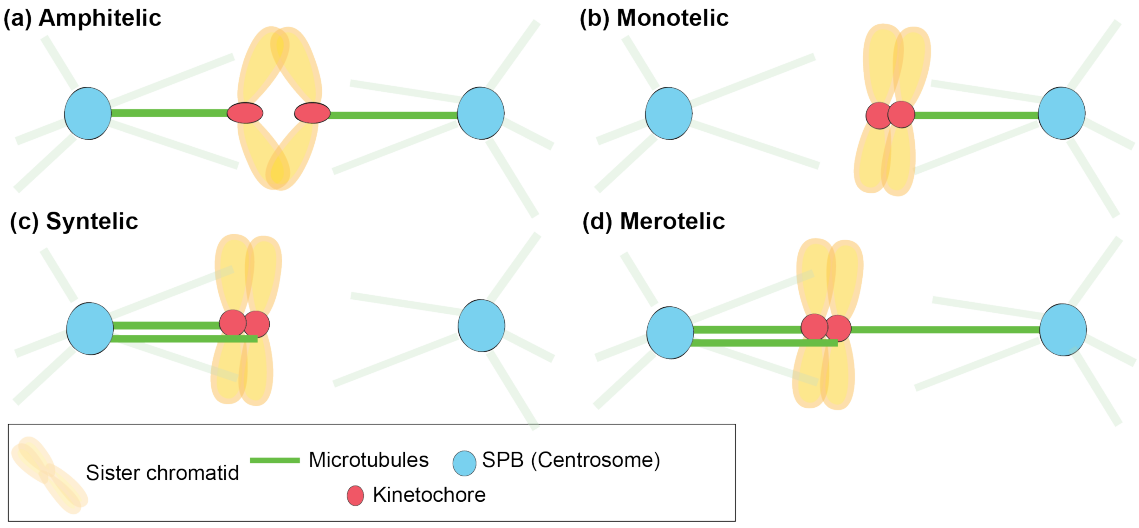

Figure 1.6. Kinetochore-microtubule attachments.

There are four types of kinetochore-microtubule attachments. (a) Amphitelic attachment, where the sister chromatids are attached to the opposite poles of SPBs, (b) monotelic where the attachment is only from one pole to one sister chromatid. Then,

(Figure 1.6. legend continued)
there is (c) syntelic attachment where both sister chromatids are attached to the same pole. In merotelic attachments (d) there are attachments from a single pole to both sister chromatids, as well as from the opposite pole.

Proper KT-MT attachments are regulated by kinases, including Aurora B, Nek2A, Mps1, Polo like kinase 1 (Plk1), CDK and Bub1, as well as phosphatases such as PP1 and PP2A-B56 that localise to the kinetochores to regulate the assembly of other substrates essential for cell division. For instance, Aurora B plays a key role in the detection of faulty attachments. *In vitro* studies using phosphomimetic and dephosphorylated Ndc80 proteins (Aurora B phosphorylation sites) bound to beads highlight the importance of Aurora B regulation. Phosphomimetic beads cannot track and stabilise microtubules, whereas dephosphorylated Ndc80 beads can (Umbreit et al., 2012). Furthermore, there is a graded response to microtubule binding, dependent on the phosphorylation of Ndc80 *in vitro* and *in silico* (Zaytsev et al., 2015). In general, phosphorylation by Aurora B has an inhibitory effect on the Ndc80 complex (Zaytsev et al., 2015, Alushin et al., 2012, Cheeseman et al., 2006, DeLuca et al., 2006), the Ska complex (Schmidt et al., 2012) and the Dam1 complex (Cheeseman et al., 2002). This correction mechanism needs to sense improper attachments only, and it was established that it is tension detected at the kinetochore (Kapoor et al., 2000, Li and Nicklas, 1995) rather than attachment to microtubules (Rieder et al., 1995) that is regulated by Aurora B phosphorylation (Zaytsev et al., 2015, Alushin et al., 2012). So how does it work? There is a spatial separation of Aurora B at the inner centromere from its substrates at outer kinetochore locations (Liu and Lampson, 2009). When kinetochores are under tension, the distance of Aurora B and its substrates increases two fold (up to ~100 nm), creating a decreasing phosphorylation gradient and thus reducing substrate phosphorylation (Wan et al., 2009, Wang et al., 2011). So that in amphitelic kinetochore attachment, Aurora B is physically away from the KMN network, whereas at syntelic attachments it would be closer enabling phosphorylation of KMN targets from improper attachment turnover. The scheme is shown on Figure 1.7.

The role of phosphatases in the regulation of KT-MT attachment is mostly in the timely removal of the mitosis-specific phosphorylation (Suijkerbuijk et al., 2012) for

progression to anaphase (Kruse et al., 2013, Espert et al., 2014, Liu et al., 2010). These mechanisms ensure the distinction between proper and improper kinetochore microtubule attachments, the latter switching on the spindle assembly checkpoint and chromosomal passenger complex (CPC) to ensure the efficient chromosome segregation.

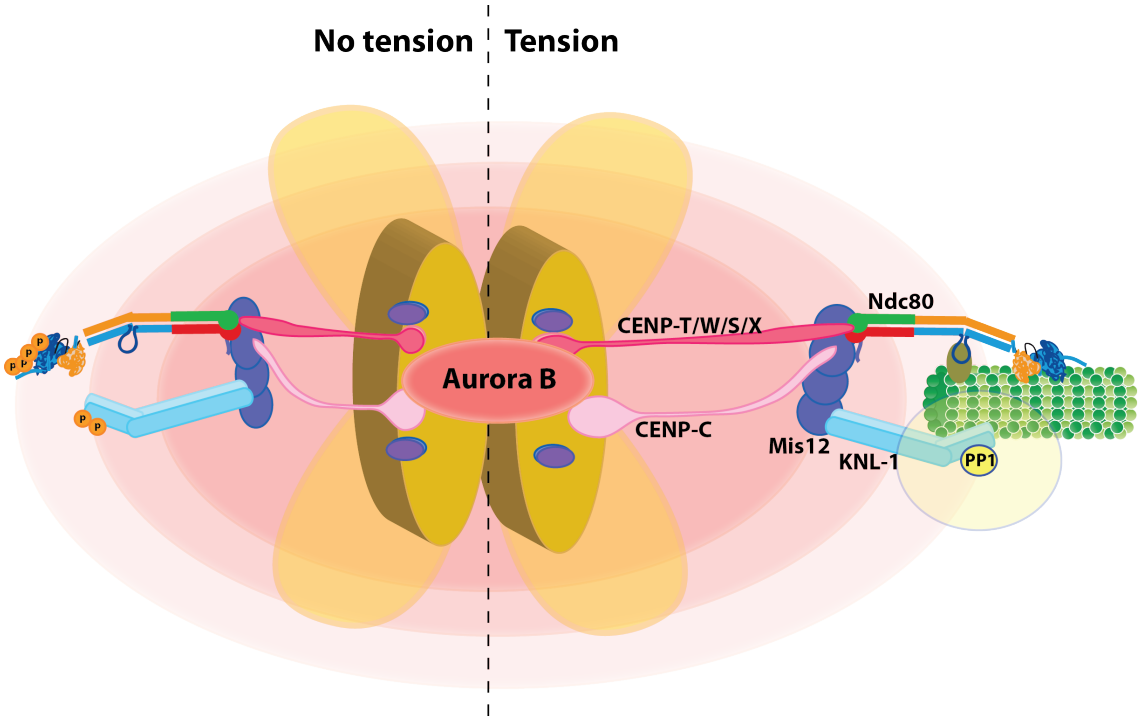

Figure 1.7. Regulation of kinetochore-microtubule attachment by phosphorylation zone.

The detection of the tension at kinetochore-microtubule attachment is primarily regulated by Aurora B. Aurora B creates a phosphorylation gradient and its substrates are phosphorylated based on the distance between them and Aurora B. When there is no tension at the kinetochore (left-hand side), the KMN network (primarily the Ndc80 complex) is phosphorylated and resulting in reduced microtubule binding. In the case of proper attachment that exerts tension at the kinetochore (right-hand side), the Ndc80 complex (and also CENP-T) stretches up to ~54 nm. This movement excludes it from the Aurora B phosphorylation zone, enabling the recruitment of its phosphatase antagonists including PP1.

1.4 Spindle assembly checkpoint

To ensure proper cell cycle progression, cells have developed 'checkpoint pathways', proposed originally by Hartwell and Weinert (Hartwell and Weinert, 1989), that monitor the transitions between cell cycle stages - G1/S, G2/M and the metaphase/anaphase boundary (Rhind and Russell, 2012). The checkpoints become active in response to defects at a particular stage and remain active until the errors have been corrected. The first identified checkpoint gene (in budding yeast), *rad9,* is involved in the DNA damage checkpoint. Mutation of *rad9* gene in the presence of X-irradiation led cells to undergo lethal cell division (Hartwell and Weinert, 1989). Together with ATR that senses breaks in single-stranded DNA and ATM kinase that senses double-stranded breaks in DNA, this checkpoint triggers the activation of downstream components ensuring that cells do not divide until the damage is repaired (Rhind and Russell, 2012). In addition, DNA replication and spindle assembly (mitotic) checkpoints are critical for successful cell survival.

Tensionless kinetochores activate the spindle assembly checkpoint (SAC) – the surveillance mechanism that halts mitotic progression until all attachments are properly established. The SAC is also called the mitotic, metaphase or kinetochore checkpoint and its first components were identified in 1991 in two landmark studies. In budding yeasts, mutant were isolated that were unable to arrest in mitosis in the absence of microtubules (Hoyt et al., 1991, Li and Murray, 1991). From these experiments mitotic arrest deficient – Mad1, Mad2 and Mad3 (Li and Murray, 1991), as well as budding uninhibited by benzimidazole – Bub1, Bub2 and Bub3 (Hoyt et al., 1991) were identified. The additional key kinases Aurora B/Ark1 and Mps1/Mph1 were also identified as SAC components. The SAC proteins are well conserved (Table 1.2). Laser ablation and cell biology experiments first identified that in the absence of tension, i.e. defective kinetochore-microtubule attachments, spindle checkpoint signalling is activated (Li and Nicklas, 1995). Restoration of tension or the removal of the unattached kinetochores by laser causes rapid mitotic exit (Rieder et al., 1995, Li and Nicklas, 1995). I will briefly introduce the key findings regarding the SAC components, their interactions and dependencies.

	S. pombe	*S. cerevisae*	*H. sapiens*
Key components	Mad2	Mad2	Mad2
	Mad1	Mad1	Mad1
	Mad3	Mad3	BubR1
	Bub1	Bub1	Bub1
	Bub3	Bub3	Bub3
	Mph1	Mps1	MPS1
	Ark1	Ipl1	Aurora B
	Slp1	Cdc20	Cdc20
RZZ complex	-	-	Zwilch
	-	-	Rod1
	-	Dsl1?	Zw10
Silencing	Dis2	Glc7	PP1
	-	-	Spindly
	-	-	$p31^{comet}$

Table 1.2. SAC components in different species.

1.4.1 Hierarchical assembly of SAC components at the kinetochore

The recruitment of SAC components to the kinetochore occurs in a hierarchical manner (Figure 1.8). Upon recognition of an unattached kinetochore, Aurora B will recruit Mps1 followed by the recruitment of Bub1, Bub3, BubR1/Mad3, Mad1 and Mad2. The ultimate goal of the SAC assembly cascade is the inhibition of Cdc20/Slp1 by the formation of the mitotic checkpoint complex (MCC). The MCC is an inhibitor of the anaphase-promoting complex/cyclosome (APC/C). Inhibition of the APC/C halts the degradation of securin/Cut2 and cyclin B/Cdc13, both of which are events required for anaphase onset (King et al., 1995, Cohen-Fix et al., 1996, Holloway et al., 1993).

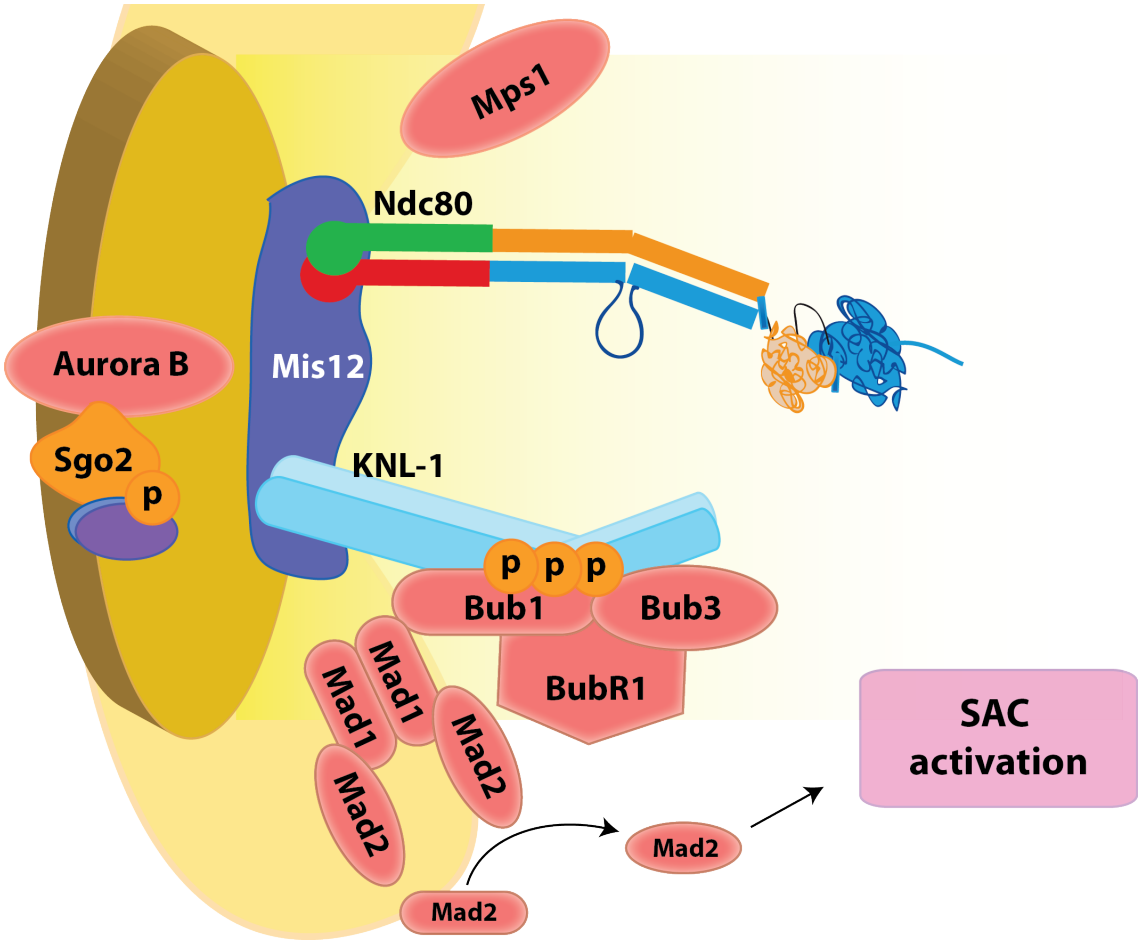

Figure 1.8. Spindle assembly checkpoint.

SAC components are recruited to the unattached kinetochore in a hierarchical manner. Aurora B and Mps1 are the first kinases to localise to kinetochore. Mps1 then phosphorylates Knl1, which in turn permits the localisation of Bub1/Bub3/BubR1 proteins. Recent studies in budding yeast indicate that Mad1, which forms a heterotetramer with Mad2, directly interacts with Bub1 at the kinetochore (London and Biggins, 2014a). A critical step is the conformational change of Mad2, from an "open" to "closed" conformation, that enable SAC activation.

1.4.1.1 Aurora B and Mps1

Aurora B and Mps1 are the most upstream components in the checkpoint signalling that are essential for the recruitment of Mad1, Mad2, BubR1/Mad3, Bub1 and Bub3 (Foley and Kapoor, 2013, Musacchio and Salmon, 2007). The sequence of the recruitment of Aurora B and Mps1 varies between model organisms. In budding yeast and *C. elegans* (no Mps1 homologue identified), Aurora B/Ipl1 plays a minor role in checkpoint

signalling (Essex et al., 2009, Foley and Kapoor, 2013, King et al., 2007). In fission yeast, *Xenopus* and mammalian cells there are some contradictions, yet clear interdependencies between Aurora B and Mps1/Mph1 exist. Reduction of Aurora B activity impairs Mps1 recruitment to the kinetochore (Hewitt et al., 2010, Santaguida et al., 2011, Saurin et al., 2011), yet on the other hand shRNA of Mps1 reduced Aurora B activity (Jelluma et al., 2008). In fission yeast deletion of Mps1/Mph1 reduced Aurora B/Ark1 levels, compared to wild type (Heinrich et al., 2012).

Aurora B (Ark1 in fission yeast, Ipl1 in budding yeast) is a mitotic kinase that senses tension at kinetochores and promotes the bi-orientation of chromosomes. The first isolated *ipl1* mutants showed faulty kinetochore bi-orientations, chromosome missegregation and later studies implicated Ipl1/Aurora B as a tension sensor at the kinetochore (discussed in Chapter 1.3.4) (Biggins et al., 1999, Foley and Kapoor, 2013, Liu and Lampson, 2009, Lampson and Cheeseman, 2011). Aurora B has multiple mitotic targets, including the Dam1 complex (budding yeast) (Cheeseman et al., 2002), the Ndc80 complex (DeLuca et al., 2006, Ciferri et al., 2008, Cheeseman et al., 2006, Akiyoshi et al., 2009), the Mis12 complex (Welburn et al., 2010) and the KNL1 complex (Welburn et al., 2010, Liu et al., 2010). Phosphorylation of these targets reduces their binding to microtubules (DeLuca et al., 2006, Welburn et al., 2010, Cheeseman et al., 2002, Kim and Yu, 2015). Using FRET to detect Aurora B kinase activity, the spatial phosphorylation zone of the substrates was established, and upon anaphase onset Aurora B substrates are dephosphorylated (Fuller et al., 2008, Lampson and Cheeseman, 2011).

Moreover, Aurora B localises to the inner centromeric region of chromosomes in early mitosis. Together with INCENP, Borealin and Survivin, Aurora B forms the chromosomal passenger complex (CPC), whose functions include the correction of attachment errors, regulation of chromosome segregation, spindle structures and mitotic progression. In metaphase, the CPC localises to the inner centromere, and is then transferred to the spindle midzone region and later to the cleave furrow at the end of mitosis (Ruchaud et al., 2007). Bub1 and Hrk1/Haspin pathways, as shown in fission yeast, mediate the localisation of the CPC to the centromere. Hrk1/Haspin

phosphorylates histone H3 at threonine 3, which interacts directly with Survivin/Bir1 and hence localises the entire CPC to the centromere (Yamagishi et al., 2010). Bub1 kinase activity is critical for localisation of shugoshin proteins ('guardian spirits' in Japanese; Sgo1 and Sgo2) that protect sister chromatid cohesion in mitosis and meiosis I. Bub1 was shown to phosphorylate histone H2A at serine 120 (threonine 121 in human), localising Sgo2 that is essential for localising Aurora B/Ark1 (Kawashima et al., 2010b). Additionally, Swi6/HP1 recruits cohesin to centromeres, which influences the localisation of Aurora B/Ark1 (Kawashima et al., 2007).

The DeLuca lab identified a subpopulation of Aurora B at the outer kinetochore, rather than the centromere, even after Ndc80 is dephosphorylated; however it remains to be further verified (DeLuca and Musacchio, 2012).

Mps1 (mono-polar spindle 1; called Mph1 in fission yeast) is a dual specificity kinase phosphorylating both tyrosine and serine/threonine (Zich and Hardwick, 2010). Mps1 is essential in budding yeast and vertebrates, but not in fission yeast (Foley and Kapoor, 2013). The first mutant isolated in budding yeast, *mps1-1,* was defective in establishing a bipolar spindle ascribable to deficiency in SPB duplication and caused cells to exit mitosis prematurely (Winey et al., 1991). Later, Mph1/Mps1 was shown to be the upstream component of SAC signalling, as its inhibition mislocalised Bub1, Bub3, BubR1/Mad3, Mad2, Mad1 and Zw10 (human only)(Maciejowski et al., 2010, Heinrich et al., 2012). Moreover, overexpression of Mps1 induces mitotic arrest (Hardwick et al., 1996), even if it does not localise to the kinetochore in an *ndc10-1* mutant that has no functional kinetochores as Ndc10 is critical in the deposition of CENP-A/Cse4 (Fraschini et al., 2001). Its function was assigned to be its regulatory (i.e. kinase activity), as Mph1/Mps1 has a high turnover rate at unattached kinetochores (Howell et al., 2004, Musacchio and Salmon, 2007).

Mps1 undergoes autophosphorylation, important for its function, as non-phosphorylatable mutants of Mps1 have a 40 fold decrease in kinase activity resulting in defective checkpoint signalling in budding yeasts (Mattison et al., 2007) and humans (Jelluma et al., 2008, Kang et al., 2007). Moreover, the autophosphorylation induces the

dimerization and activation of Mps1 *in vivo* and *in vitro* (Kang et al., 2007). In human cells, autophosphorylation at the TPR site was shown to regulate the function of Mps1 (Thebault et al., 2012). Residues 1-54 of Mps1 in humans are responsible for dimerization, as their deletion disables structural stability of Mps1 homodimers (Thebault et al., 2012).

Mph1/Mps1 localises to and functions at unattached kinetochores from prophase to anaphase (Castillo et al., 2002, Howell et al., 2004). Recently identified MELT motifs in KNL1 are phosphorylated by Mps1/Mph1, which in turn enables the recruitment of Bub1 and Bub3. Mutations in the MELT motifs result in defective checkpoint signalling, as there is no Bub1 or Bub3 recruitment to the kinetochore (Yamagishi et al., 2012, Heinrich et al., 2012, Shepperd et al., 2012). In metazoans, Mps1 additionally phosphorylates the RZZ complex that brings Mad1 and Mad2 to the kinetochores, however it also plays a role in checkpoint silencing (discussed in chapter 1.4.4) (Maciejowski et al., 2010, Essex et al., 2009, Karess, 2005, Santaguida et al., 2010). In addition, Mad1 and Mad2 are also substrates of Mph1/Mps1 (Hewitt et al., 2010, Brady and Hardwick, 2000), with Mph1-phosphorylation promoting the MCC assembly to the APC/C (Zich et al., 2012). Mps1 also exerts an effect on Aurora B activity by phosphorylating the CPC component - Borealin/Dasra (Jelluma et al., 2008).

In addition to its role in checkpoint signalling, Mph1/Mps1 has a function in chromosome alignment, as non-phosphorylatable *spc7-12A* mutants (Mps1/Mph1 phosphorylation targets) exhibit the chromosome mis-segregation phenotype and could not maintain minichromosomes (Yamagishi et al., 2012).

Recently crystallised Mps1/Mph1 was shown to contain an N-terminal extension (NTE), followed by a TPR domain and the C-terminal kinase domain (Lee et al., 2012, Zich and Hardwick, 2010). The TPR domain of Mps1 has a very similar fold to that of Bub1 and BubR1 (Thebault et al., 2012). Thebault et al. also an identified the LXXLL motif in the TPR domain that is critical for Mps1 to relocate from the cytosol to the nucleus at the G2/M phase (Thebault et al., 2012), as mutations here disable the shuffling. Furthermore, phosphorylation of the TPR domain of Mps1 by Aurora B helps localise it

to the kinetochore (Nijenhuis et al., 2013). The N-terminal domains of Mps1/Mph1 are critical for kinetochore localisation, as the truncations of 1-150 and 1-302 amino acids in fission yeast abolish checkpoint activation. This activity is then restored by tethering of Mph1/Mps1 to the kinetochore component (Mis12-Mph1, Mis12-Mph1-Δ1-302) (Heinrich et al., 2012). The main domains of human Mps1 are shown schematically on Figure 1.9.

Aurora B regulates the kinetochore localisation of Mps1 by controlling inhibitory effects of the TPR domain on the NTE of Mps1. In the presence of Aurora B, Mps1 can localise to the kinetochore (Nijenhuis et al., 2013). However, the exact localisation of Mps1/Mph1 to kinetochores remains mostly uncharacterised. Depletion of Ndc80 results in Mps1 mislocalisation, whereas combined Ndc80 and Aurora B depletion completely abolishes Mps1 localisation. The first 1-207 amino acids of Hec1 are critical for localising Mps1 to kinetochores in humans (Nijenhuis et al., 2013).

1.4.1.2 Bub1, Bub3 and BubR1/Mad3

The middle level of SAC hierarchical recruitment is composed of Bub1, Bub3 and BubR1/Mad3, all of which are highly conserved kinases. These proteins are recruited to conserved MELT and KI motifs in KNL1/Spc7/Spc105 – MELT and KI domains (Yamagishi et al., 2012, Shepperd et al., 2012, Heinrich et al., 2012, Bolanos-Garcia and Blundell, 2011, Krenn et al., 2014). The main domains of Bub1, Bub3 and BubR1 are shown schematically on Figure 1.9.

Bub1 is a true kinase, whereas BubR1 is a pseudokinase and its yeast homologue Mad3 lacks its kinase domain at its C-terminus. The N-termini of Bub1 and BubR1/Mad3 are well conserved; it contains the TPR (tetratricopeptide repeat-like fold) domain (Bolanos-Garcia and Blundell, 2011), followed by an unstructured region for Bub3 binding (also known as the GLEBS domain) (Windecker et al., 2009, Vanoosthuyse and Hardwick, 2009). Recent studies have also identified a middle region of Bub1 that binds Mad1 (Zhang et al., 2015, London and Biggins, 2014a, Brady and Hardwick, 2000,

Heinrich et al., 2014). Bub3, on the other hand, constitutes mostly of WD40 repeat domains that are the primary binding region to KNL1/Spc7/Spc105.

Bub1 and BubR1 bind Bub3 in a mutually exclusive manner, as they associate with the same site of Bub3 (Larsen et al., 2007). Bub1-Bub3 and BubR1-Bub3 are recruited to KI motifs 1 and 2 (conserved in vertebrates) respectively, via their TPR domains (Bolanos-Garcia and Blundell, 2011, Krenn et al., 2014).

Bub3 primarily binds with high affinity directly to Mps1-phosphorylated threonines of MELT ((M/I/LV)-(E/D)-(L/M/I/V)-(T/S)) motifs of KNL1; and this interaction is stabilised by Bub1 (Zhang et al., 2014, Primorac and Musacchio, 2013). Recruitment of the BUBs is related to the number of MELT motifs, as the sequential removal of MELTs motifs from KNL1 led to the reduced Bub1-Bub3 levels (Vleugel et al., 2013, Zhang et al., 2014). Further studies have shown different binding affinities of the Bub1-Bub3 complex to selected MELTs, for instance MELT2 did not restore SAC signalling, whereas MELT17 did (Vleugel et al., 2013).

The absence or reduction of Bub1 or Bub3 from the kinetochore leads to defective checkpoint signalling (Vanoosthuyse and Hardwick, 2009, Shepperd et al., 2012, Windecker et al., 2009). However in fission yeast checkpoint signalling is still retained in *bub3*Δ (Vanoosthuyse and Hardwick, 2009, Windecker et al., 2009, Tange and Niwa, 2008), indicating some additional function of this protein potentially as an inhibitory chaperone of Bub1 (Yamagishi et al., 2012).

Furthermore, the catalytic domains of Bub1 and BubR1 are required for chromosome bi-orientation, but not for checkpoint signalling (Bolanos-Garcia and Blundell, 2011). However work in *Xenopus* egg extracts with kinase-dead Bub1 showed a graded checkpoint response dependent on the concentration of nocodazole (weak response – no arrest; strong response – arrest), suggesting a potential role for Bub1 in response to weak checkpoint signals (Chen, 2004). The kinase domain of Bub1 is not required for its kinetochore recruitment, as kinase-dead and truncations of this domain still localise

to the kinetochore and arrest in mitosis (Klebig et al., 2009, Warren et al., 2002, Bolanos-Garcia and Blundell, 2011).

Initially, Bub1 kinase was shown to phosphorylate Bub3 and itself *in vitro* in budding yeast (Roberts et al., 1994), with later Mad1 characterised as a substrate *in vitro* (Seeley et al., 1999). Cdc20 was shown both *in vivo* and *in vitro* to be phosphorylated by Bub1; a debate exists surrounding the role of Bub1 in APC/C inhibition through the phosphorylation of Cdc20 by Bub1 most likely lies in amplification mechanism, as the non-phosphorylatable Cdc20 still retained some SAC activity (Bolanos-Garcia and Blundell, 2011). Additionally, Bub1 has a function in ensuring proper chromosome congression (Bolanos-Garcia and Blundell, 2011). In contrast to Bub1, BubR1 functions more specifically in stabilising the microtubule attachments (Meraldi et al., 2004, Bolanos-Garcia and Blundell, 2011) and in the formation of the MCC (discussed in Chapter 1.4.3) (Chen et al., 1999, Sczaniecka et al., 2008).

However, the key role of Bub1 kinase, characterised only recently, is the phosphorylation of histone H2A that is essential for the localisation of shugoshin proteins to centromeres (Kawashima et al., 2010a). In mitosis, Bub1 phosphorylates histone H2A at T120, to which Sgo1/Sgo2 localise and then further promote the recruitment of Aurora B/Ark1 to the inner centromeres (Caldas et al., 2013, Yamagishi et al., 2012).

1.4.1.3 Mad1 and Mad2

The last SAC components to be recruited to unattached kinetochores are Mad1 and Mad2 (Lara-Gonzalez et al., 2012, Foley and Kapoor, 2013). Mad1 depletion abolishes Mad2 localisation and cells are unable to arrest in mitosis (Heinrich et al., 2014, Martin-Lluesma et al., 2002, Luo et al., 2002, Essex et al., 2009). Furthermore, tethering of Mad1 to kinetochores results in constitutive Mad2 co-localisation and a metaphase-like arrest even with kinetochores properly attached to microtubules (Maldonado and Kapoor, 2011).

Mad1 recruits Mad2 to the kinetochore and forms a heterotetramer complex, with the N-terminus of Mad1 interacting with the C-terminus of Mad2 (Luo et al., 2002, Sironi et al., 2002). Mad1 dimerizes through its N-terminus domain, whereas the C-terminus contains a globular domain, resembling the structure of the Ndc80 complex (Kim et al., 2012). Moreover, truncation of the C-terminus of Mad1 was shown to affect its kinetochore localisation (Heinrich et al., 2014, Kruse et al., 2014), in particular the EDD sequence in fission yeast (Heinrich et al., 2014). A model was proposed where the Mad1 C-terminus folds back on its N-terminus, which may in turn trigger the conformational change of its binding partner Mad2 (discussed in Chapter 1.4.2) (Heinrich et al., 2014). The main domains of Mad1 and Mad2 are shown schematically on Figure 1.9.

The C-terminus of Mad1 contains also a RLK motif, which is hypothesised to bind Bub1 in yeasts (Brady and Hardwick, 2000, Heinrich et al., 2014). RLK mutants of Mad1 abolish the localisation to Bub1 and the reverse is true in the *bub1-cm1* mutant (a middle region of Bub1 that is important for localising Mad1 and Mad2 to the kinetochore) (Heinrich et al., 2014). In addition, budding yeast Mad1 and Bub1 were shown to interact directly *in vitro* and *in vivo*. The phosphorylation of the middle region of the Bub1 by Mps1 is essential for Bub1-Mad1 binding *in vitro* (London and Biggins, 2014a). The Bub1-Mad1 interaction *in vivo* requires Mad2 (Brady and Hardwick, 2000, Gillett et al., 2004) as well as Mps1 to be present (which is critical for phosphorylating Spc105/Knl1 to recruit the Bub1-Bub3 complex; alternatively there is some yet uncharacterised effect on Mps1 phosphorylating Mad1 (Hardwick et al., 1996)) (London and Biggins, 2014a). In yeast, Mad1 localises indirectly to Knl1/Spc7/Spc105 (through Bub1). In humans, however, Ndc80 was proposed to interact with the Mad1 N-terminus (Martin-Lluesma et al., 2002). Furthermore, multiple studies have shown that Ndc80 is required for Mad1 localisation to the kinetochores (Martin-Lluesma et al., 2002, DeLuca et al., 2003, McCleland et al., 2003), whereas other reports suggest that the RZZ complex brings Mad1-Mad2 to the KNL1 complex (through Zwint) (Varma et al., 2013). The most recent work in the Nilsson lab shows that Bub1 as a site required for the RZZ complex-mediated localisation of Mad1-Mad2 to the kinetochore (Zhang et

al., 2015). Reports in *C. elegans* also show that Bub1 is required for Mad1-Mad2 kinetochore localisation (Moyle et al., 2014).

Mad1 and Mad2 shuttle between the cytoplasm and the nucleus during the cell cycle. In interphase, they interact with the nuclear pore complex (NPC), in human and fission yeast (Rodriguez-Bravo et al., 2014, Schweizer et al., 2013, Heinrich et al., 2014) (S.Hauf, personal communication). Interphase Mad1 is needed to inhibit Cdc20 before M-phase, as the Mad1-Mad2-NPC localisation is required for the generation of the pre-mitotic 'wait' anaphase signal (Rodriguez-Bravo et al., 2014). This signal helps lowering the threshold for the MCC on-kinetochore signalling during mitosis (Rodriguez-Bravo et al., 2014) and it is partially regulated by Tpr (another component of the NPC) stabilising Mad1-C-Mad2 production, through SUMO pathway components from NPCs (Schweizer et al., 2013).

Mad2 deletions, in all model systems, cannot sustain checkpoint signalling and cells exit mitosis prematurely. Mad2 plays a critical role in a robust checkpoint response by undergoing a rapid conformational switch that is essential for the MCC formation (discussed in Chapter 1.4.3).

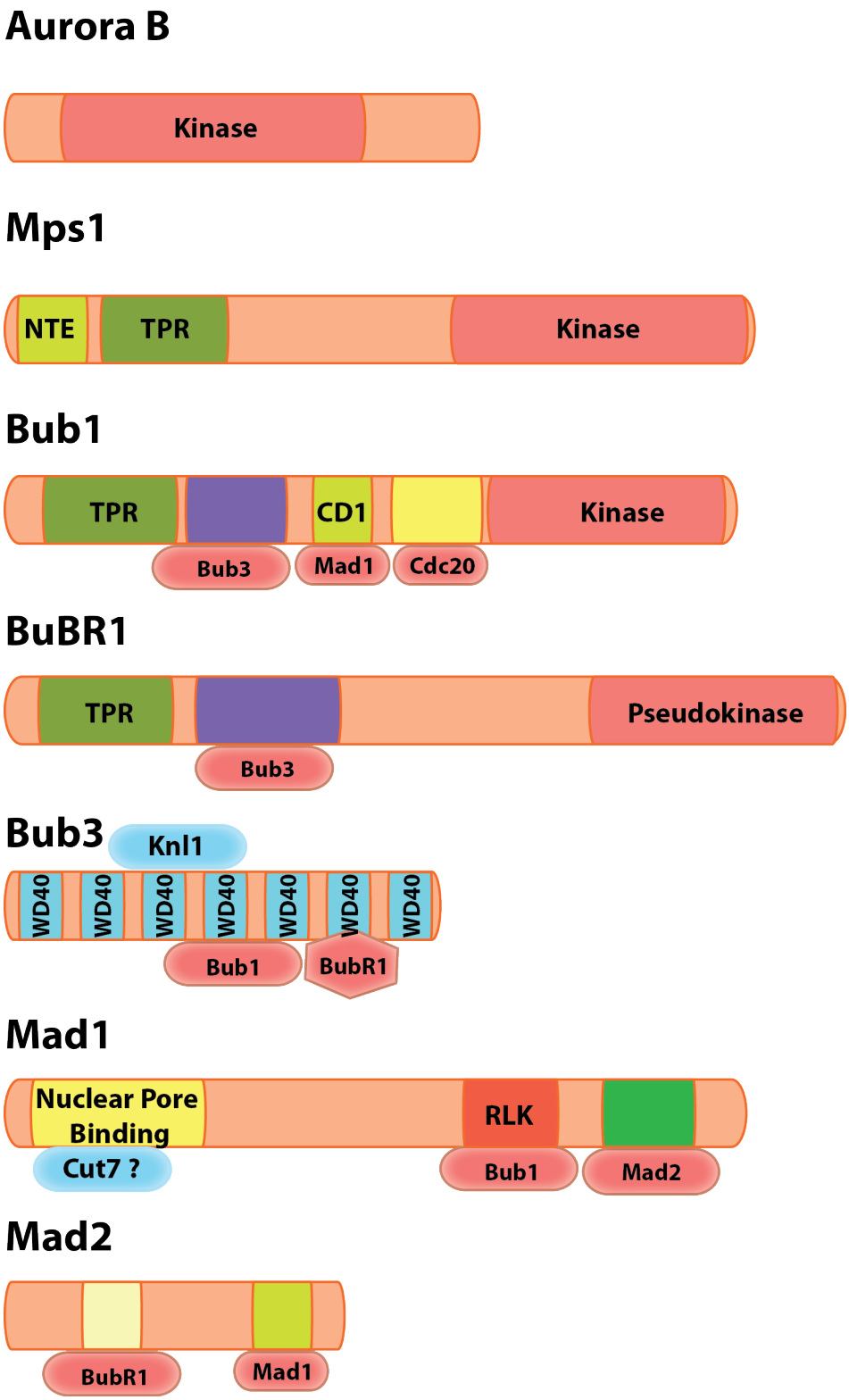

Figure 1.9. Domains and interacting partners of SAC proteins.

Summary of the main domains and interacting partners of SAC components in humans. Adapted from (London and Biggins, 2014b) and (Foley and Kapoor, 2013).

1.4.2 The 'Mad2-template' model

Cdc20, an activator of APC/C, needs to be inhibited in order to stop cell division until all improper kinetochore-microtubule attachments are correct. Mad2 was shown to bind Cdc20 as part of the mitotic checkpoint complex (MCC, discussed in Chapter 1.4.3). Mutants of the Mad2-binding region of Cdc20 fail to arrest in mitosis (Kim et al., 1998), similarly mutations in Mad2 have the same phenotype (De Antoni et al., 2005, Sironi et al., 2001). A single unattached kinetochore can cause a rapid SAC activation and halt cell division. The mechanistic explanation of this process is called the 'Mad2-template' model (De Antoni et al., 2005). Mad2 exists in two confirmations an inactive open-Mad2 (O-Mad2), and an active closed Mad2 (C-Mad2) that bind Mad1 and Cdc20 respectively (Sironi et al., 2001, Shah et al., 2004). Mad1 and Cdc20 have a similar Mad2-binding motif, which permits their interactions with Mad2 in a mutually exclusive manner (Sironi et al., 2002).

The conversion of Mad2 from open to closed was shown, in elegant FRAP studies, to occur at the kinetochore (Shah et al., 2004, Howell et al., 2004, Howell et al., 2000). Soluble pools of O-Mad2 (that exist in a huge amount) undergo catalytic conformational change at the C-terminus resulting in the formation of C-Mad2 (Luo et al., 2004, Luo et al., 2002, Sironi et al., 2002, Sironi et al., 2001). C-Mad2 can form strong interactions with Mad1 or Cdc20, as well as possessing an ability to dimerise with other O-Mad2 proteins (Mapelli and Musacchio, 2007, Screpanti et al., 2011). Mps1 was shown to play a role in the dimerization of Mad2, as its inhibition affected O-Mad2 but not Mad1-C-Mad2 (Hewitt et al., 2010).

The key step in the template model is the formation of a stable heterotetramer of Mad1-C-Mad2 (in a 2:2 ratio). These heterotetramers act as a template for binding another O-Mad2, triggering its confirmation change to C-Mad2, which is then released and binds Cdc20 instead (forming Cdc20-C-Mad2) (Mapelli and Musacchio, 2007, Sironi et al., 2001, Luo et al., 2004). Because of the Mad1-C-Mad2 template, soluble free O-Mad2 can be converted to C-Mad2 and form multiple Cdc20-C-Mad2 complexes in a rapid manner. This positive feedback loop ('Mad2-template') amplifies the checkpoint signal

from any single unattached KT leading to robust SAC activation (Rieder et al., 1995). The scheme of 'Mad2-template' is shown on Figure 1.10.

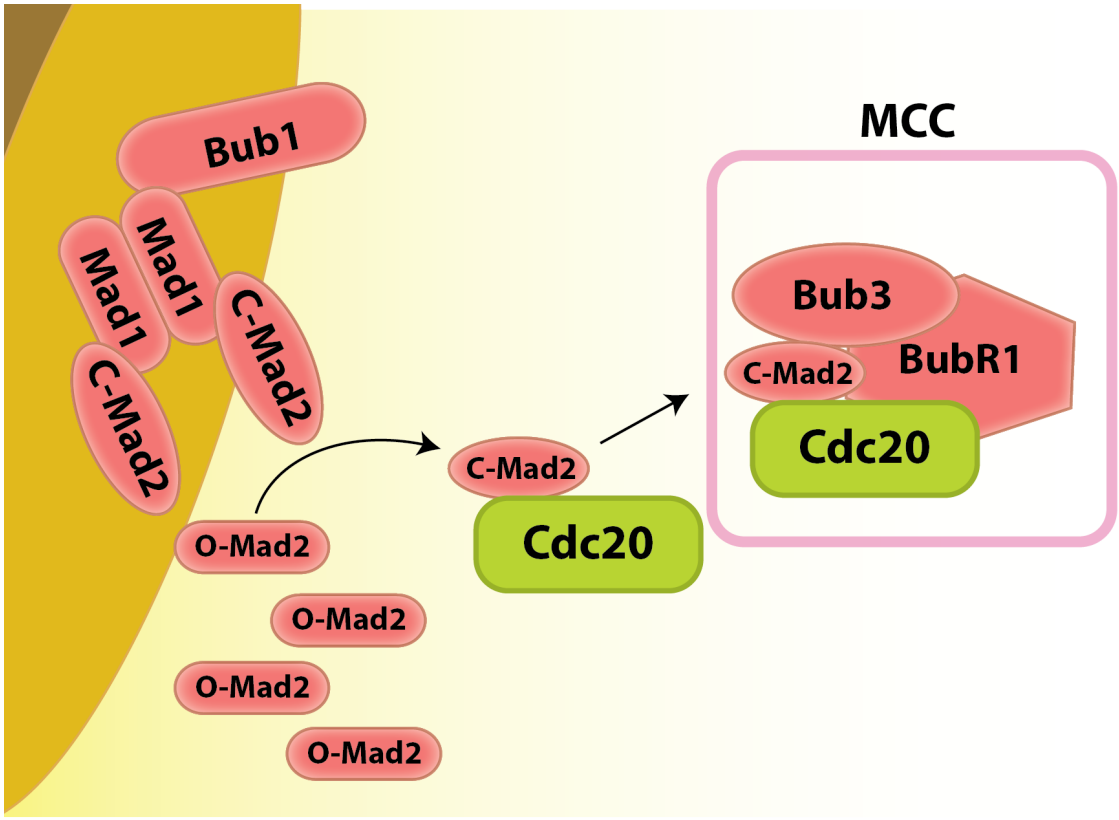

Figure 1.10. Mad2-template model.

Mad1-Mad2 complex is recruited to the kinetochore, most likely at the Bub1 site. O-Mad2 changes structural conformation to C-Mad2 and Mad1-C-Mad2 acts as a catalyst, triggering a prion-like reaction composed of the conversion of soluble O-Mad2 to C-Mad2. C-Mad2 can bind Cdc20, which then binds BubR1 and Bub3 to form the MCC.

1.4.3 Mitotic checkpoint complex (MCC)

The formation of Cdc20-C-Mad2 is a critical step towards blocking mitotic progression to anaphase. The purpose of this hierarchical recruitment of checkpoint components to unattached kinetochores is ultimately the formation of the mitotic checkpoint complex (MCC). Generally the MCC is a heterotretramer composed of Cdc20, C-Mad2, BubR1/Mad3 and Bub3 in a 1:1:1:1 ratio, however the stoichiometry is still under investigation (Figure 1.10) (Han et al., 2013, Nilsson et al., 2008). The MCC complex can form and function outside of the kinetochore (Kulukian et al., 2009).

Cdc20-C-Mad2 must bind BubR1/Mad3 and Bub3 (not present in the MCC in fission yeast) to form the MCC, as their deletions or truncations do not arrest cells in mitosis (Hardwick et al., 2000, Nilsson et al., 2008, Chen et al., 2002, Li et al., 2010). The final inhibitor of Cdc20 is BubR1/Mad3, as the two proteins Cdc20-BubR1 form a tight complex (Han et al., 2013). There are three key roles of BubR1/Mad3 (Han et al., 2013). Firstly, BubR1/Mad3 can directly interact with Mad2 and Cdc20 in the MCC (shielding C-Mad2 from potential dimerization with its O-Mad2 form) (Chao et al., 2012). Secondly, it provides spatial separation of Apc10 (the APC/C subunit) and Cdc20 and lastly it acts as a 'pseudo-substrate inhibitor' for Cdc20 (Burton and Solomon, 2007). The role of Bub3, on the other hand, still remains unknown. Furthermore, as mentioned earlier, Bub3 is not present in the MCC in fission yeast (Sczaniecka et al., 2008, Chao et al., 2012). During checkpoint silencing, Cdc20 needs to be ubiquitinated by APC/C, thus becoming its substrate rather than its activator (Lara-Gonzalez et al., 2012). As shown on Figure 1.11, the MCC blocks the proteolytic destruction of Cyclin B and securin, which are essential for the progression to anaphase.

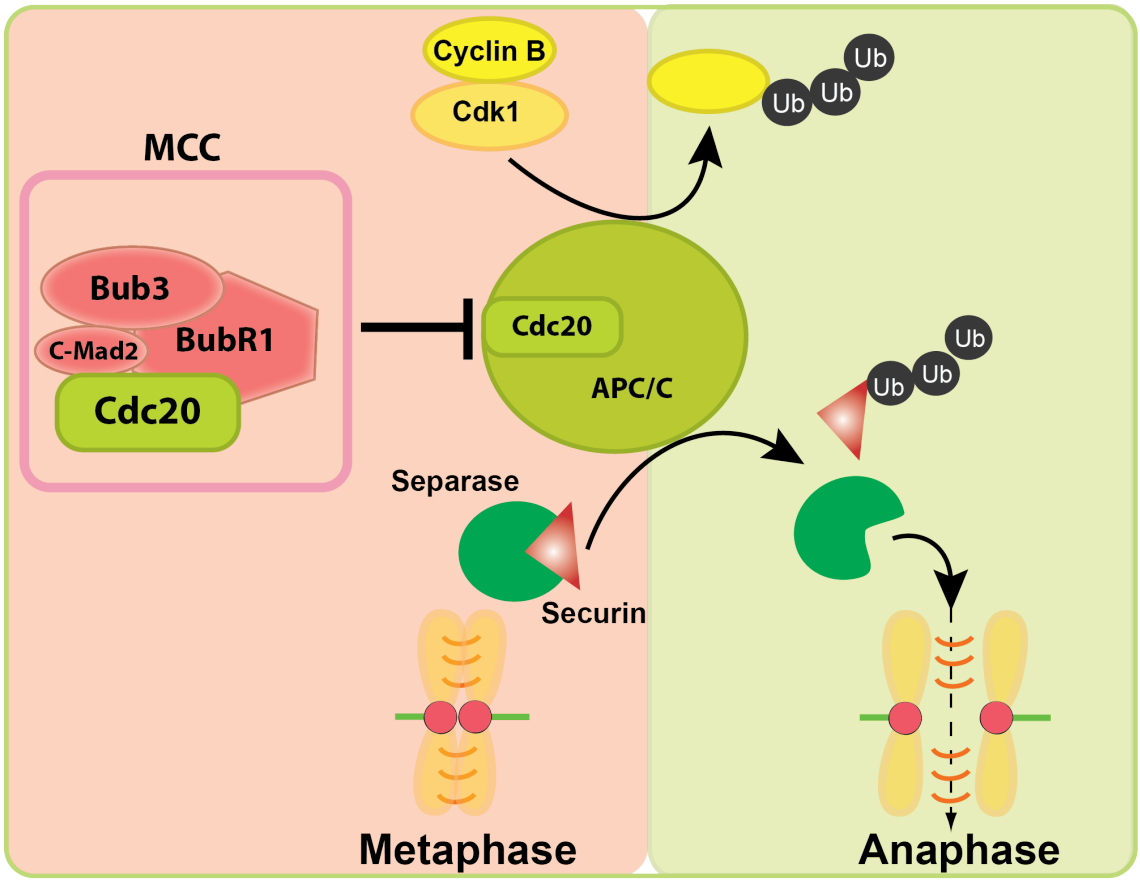

Figure 1.11. The role of the MCC.

Mitotic arrest is achieved by the formation of the mitotic checkpoint complex (MCC). It is formed from C-Mad2, BubR1, Bub3 (not present in the MCC in fission yeast) and Cdc20. The MCC inhibits the activity of the APC/C by preventing the destruction of its targets – cyclin B and securin. Cyclin B is a cofactor of Cdk1 while securin is protects separase from prematurely cleaving the cohesin and separating the sister chromatids.

1.4.4 Graded SAC response

A single unattached kinetochore was shown to arrest cells in mitosis and upon its laser ablation, cells immediately exited mitosis (Rieder et al., 1995). Moreover the response from a single or multiple unattached kinetochores was of a similar degree, and so this was called an 'all-or-none' checkpoint response, where a certain threshold needs to be satisfied (Foley and Kapoor, 2013).However, recently, the quantitative response of the checkpoint signal (also called 'graded') challenges this view (Kops et al., 2005).

Depending on the type of microtubule poison used, the checkpoint response varies. Nocodazole-arrested human cells with depolymerised microtubules have fully

unattached kinetochores and a strong SAC response. In contrary to cells with taxol-stabilised microtubules that lose kinetochore tension; concluded based on the amount of the MCC and the rate of SAC silencing (Collin et al., 2013, Westhorpe et al., 2011). Partial inhibition of Mps1 or Aurora B kinase activity also resulted in the reduced checkpoint response (Saurin et al., 2011). Another study, using laser-ablations of kinetochore fibres, showed a rapid accumulation of Mad2 on displaced chromosomes. The rate of securin degradation – an indicator of APC/C response - was dependent on the number of unaligned chromosomes (60 times faster for proper KT-MT attachments). Notably, the timing of the laser-sever was crucial, as there was 'a point of no return' where the cells would exit mitosis independent of the corrected attachments (Dick and Gerlich, 2013). Overexpression or reduction in the levels of SAC components also caused graded SAC responses. Mad2 overexpression causes mitotic arrest (Essex et al., 2009, He et al., 1997, Heinrich et al., 2013), whereas Mad1 overexpression causes a checkpoint defect instead (as it might bind more Mad2, inhibiting the formation of the MCC)(Heinrich et al., 2013). By modifying the promoters of Mad2, Mad1, Mad3 and Slp1/Cdc20 in fission yeast, it is possible to obtain active or defective checkpoint, and effects can be reversed by simultaneously modifying the levels of proteins – reduction of Mad2 and Cdc20/Slp1 (Heinrich et al., 2013).

These findings indicate that the checkpoint acts in a graded manner and its response depends on the relative levels of individual SAC proteins; in addition, there is a stage of irreversible progression to anaphase when the SAC is no longer activated.

1.4.5 Extinguishing the SAC at the kinetochore

Following the establishment of proper kinetochore-microtubule attachments, the activated checkpoint needs to be silenced in a robust manner. Checkpoint silencing is essential for mitotic progression, yet the mechanisms involved in the process are not fully understood. However, it is clear that the MCC disassembles, checkpoint proteins delocalise from the kinetochore and the mitosis-specific phosphorylation events are reversed. The main mechanisms include the dephosphorylation of mitotic targets,

stripping of SAC components from kinetochores and shielding Mad2 from forming the MCC (scheme on Figure 1.12).

The type 1 protein phosphatase (PP1) was identified as an important player for SAC silencing. PP1 localises to the SILK RVSF motif in the N-terminus of Knl1 and it is recruited to the kinetochore by kinesin-8 (Klp5-Klp6 in fission yeast) through interaction with the Alp7/Alp14 complex at the Ndc80 loop (Tang and Toda, 2015a, Rosenberg et al., 2011, Liu et al., 2010). Aurora B phosphorylates SILK RVSF site and upon its dephosphorylation PP1 is recruited, creating a feedback mechanism between activation and silencing (Liu et al., 2010, Espeut et al., 2012, Lesage et al., 2011). Another phosphatase, PP2A-B56 at least in metazoans, dephosphorylates this site (Espert et al., 2014, Nijenhuis et al., 2014), once it localises to Knl1, at the KI motif (KI2) through association with BubR1 (Krenn et al., 2014). Then, PP1 commences the dephosphorylation of mitosis-specific sites, i.e. dephosphorylation of the MELT motifs leads to the disassociation of Bub1, Bub3 and BubR1 from the kinetochore (Espeut et al., 2012). Deletion of the first 150 or 300 amino acids of Knl1 leads to the increased levels of BubR1 and Bub1 in comparison to wild type, indicating that PP1 negatively regulates their recruitment (London et al., 2012, Meadows et al., 2011, Zhang et al., 2014, Rosenberg et al., 2011). PP1 inhibition was shown to delay mitotic exit (Vanoosthuyse and Hardwick, 2009, Pinsky et al., 2009), and disruption of the PP1-Knl1 interaction leads to constitutive checkpoint activation (Rosenberg et al., 2011, Meadows et al., 2011, Liu et al., 2010). Depletion of PP2A-B56 was shown to abolish checkpoint silencing (Nijenhuis et al., 2014). Here emerge two feedback mechanisms of rapid checkpoint silencing: PP1 and PP2A-B56 counteracting Aurora B and Mps1 that prime and restrict the feedback until the appropriate time (Nijenhuis et al., 2014).

Another key player in checkpoint silencing, in humans, is $p31^{comet}$ that interacts with Mad2 (Habu et al., 2002). Successful $p31^{comet}$-O-Mad2 binding removes soluble population of Mad2 from the cell, thereby disabling further formation of the MCC complex. In addition, overexpression of $p31^{comet}$ results in formation of less Mad2-Cdc20 complex (Westhorpe et al., 2011). Cdc20 is ubiquitynated by the APC/C, regulated by Apc15/Mnd2 (APC/C component) (Foster and Morgan, 2012, Uzunova et

al., 2012). The absence of Apc15 was shown both in yeast and humans, to delay mitotic exit; in humans this is due to locking the confirmation of the MCC complex with Cdc20 (Foster and Morgan, 2012, Wang et al., 2014). $p31^{comet}$ therefore plays a key role in the disassembly of the MCC complex for checkpoint silencing.

Other checkpoint components also need to be removed from the kinetochore to silence the checkpoint. This process becomes evident from studies in which Mad1 or Mps1 is artificial tethered to attached chromosomes. Under this condition, prolonged mitotic arrest was observed, despite correct kinetochore-microtubule attachments (Jelluma et al., 2010, Maldonado and Kapoor, 2011). Dynein-mediated stripping of Mad1, Mad2 and BubR1 occurs in humans during checkpoint silencing. Dynein motors normally localise to kinetochores through RZZ-Spindly binding to the KNL1 complex (Howell et al., 2001, Barisic and Geley, 2011, Gassmann et al., 2010, Gassmann et al., 2008). There seems to be, however, some inhibition of dynein-dependent stripping of SAC components by CENP-I (Matson et al., 2012, Matson and Stukenberg, 2014). Interestingly, dynein-independent stripping mechanisms of Mad1 and Mad2 has also been observed in yeast and humans (Gassmann et al., 2010, Courtheoux et al., 2007).

Tight control of Mph1/Mps1 levels was also proposed to regulate the checkpoint silencing, as Mps1 levels decrease by anaphase onset (Howell et al., 2004, Palframan et al., 2006). Furthermore, Mph1/Mps1 regulates its own dissociation from the kinetochore (Jelluma et al., 2010, Hewitt et al., 2010).

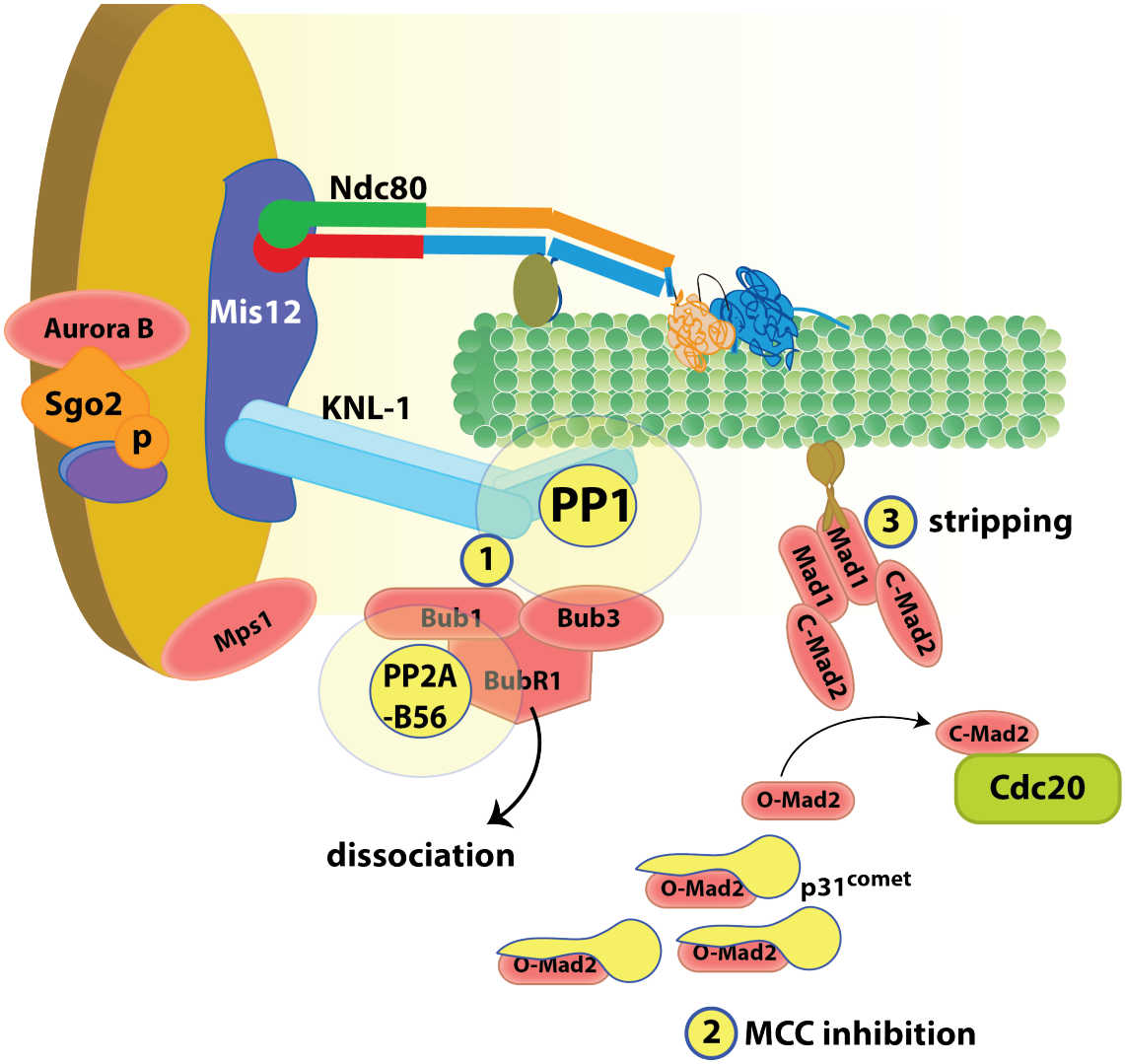

Figure 1.12. Silencing of the spindle assembly checkpoint.

The removal of SAC components from the kinetochore is critical for progression to anaphase. Dephosphorylation of Knl1 initially by PP2A-B56 and then PP1 leads to the dissociation of Bub1/Bub3/BubR1 from the kinetochore (1). PP1 dephosphorylation opposes Aurora B and creates a dephosphorylation zone affecting other proteins as well. (2) $p31^{comet}$ (present in humans) binds soluble O-Mad2 which can no longer undergo a conformational change to C-Mad2 and hence cannot form the MCC anymore. The insufficient levels of C-Mad2 reduce SAC activity. Furthermore, Mad1 and Mad2 proteins are stripped from the kinetochore by the RZZ complex with dynein and spindly. More studies are needed to further explore the mechanisms of checkpoint silencing.

1.5 Kinetochore proteins and cancer

Errors that arise during cell division by the formation of syntelic, monotelic or merotelic attachments can lead to improper chromosome segregation. This can result in the

formation of cells with abnormal numbers of chromosomes, a phenomenon known as aneuploidy. Aneuploidy is usually described as a hallmark of cancer; however it should also be noted that it is associated with premature ageing, infertility, spontaneous miscarriages and birth defects such as Down's syndrome (trisomy of chromosome 21) (Kops et al., 2005). During mitosis, there is a high probability of generating aneuploid offspring as the separated sister chromatid is irreversibly passed to them.

As the Ndc80 complex is a key kinetochore attachment factor, and therefore it is not surprising that it is misregulated in numerous cancers. Ndc80 or Hec1 (highly expressed in cancer 1) in humans is overexpressed in some cancers (Chen et al., 1997), in particular breast, prostate, colorectal and pancreatic types. Moreover, overexpression levels of Ndc80/Hec1 correlate with prognosis and tumour grade in breast, lung and pancreatic cancer patients (Bieche et al., 2011, Hayama et al., 2006, Meng et al., 2015). In addition, recent work in our lab suggests that overexpressed Ndc80 proteins absorb MAPs like Dis1, disrupting chromosome segregation and microtubule dynamics (Tang and Toda, 2015b). It has also been shown elsewhere that overexpression of Ndc80 leads to tumourigenesis as a result of hyper-activation of the SAC, especially stabilisation of Mad2 (Diaz-Rodriguez et al., 2008).

Mutations in and altered levels of Mad2, Mad1, Bub1, Bub3, BubR1 and Mps1 were observed in advanced stage tumours and various cancer cell lines (Shin et al., 2003, Olesen et al., 2001, Grabsch et al., 2003, Hernando et al., 2004). Overexpression of Mad2 in a mouse model promotes tumourigenesis by formation of multiple anaphase bridges and also chromosome gains and losses (Sotillo et al., 2007). However, other studies show that tumourigenesis as well as aneuploidy is linked with a decline in expression levels of SAC components, i.e. BubR1, Mad2 and Bub3 in mice (Kops et al., 2005). BubR1 mutations were identified in mosaic-variegated aneuploidy (MVA), characterised by microcephaly and childhood cancers (Hanks et al., 2004). Additionally mutations in the APC/C also contribute to increased chromosomal instability (CIN) (Fodde et al., 2001). A summary list of mitotic associated proteins and types of tumours linked with them is presented in Table 1.3.

Most solid tumours have aneuploidies, but they also have an accumulation of mutations in oncogenes and tumour-suppressors genes. Mouse models deficient for *Brca1* (breast cancer 1 protein; tumour suppressor gene) for instance had a decreased level of Mad2, Bub1, BubR1 and ZW10, which was reversed by the reconstitution of Mad2 (Wang et al., 2004). p53, another tumour suppressor commonly mutated in cancers, was also shown to alter the levels of Mad1 resulting in CIN (Kops et al., 2005).

Protein	Levels	Cancer
The Ndc80 complex	⇑	Lung, liver, breast, brain, colon, prostate
The Knl1 complex	⇑	Breast, colorectal, lung
The Mis12 complex	⇑	Colorectal, lymophoma
Mad2	⇓⇑	Breast, bladder
Mad1	⇑	Prostate, lymphoid, lung, breast
Bub1	⇓	Colon, lung, pancreatic
Bub3	⇓	Colorectal, cervical, head and neck
BubR1/Mad3	⇓	Colon, lymphoid, breast, MVA
Mps1/Mph1	ND	Renal, prostate
Aurora B/Ark1	⇑	Colorectal, stomach, cervical
TACC-TOG Alp7/Alp14	⇑	Breast, brain, sarcoma, colon
	⇓	Ovarian, thyroid
RZZ complex	⇑	Colon
Cdc20	⇑	Breast, lung, colorectal, ovarian, sarcoma

Table 1.3 Overview of the mitotic proteins mutated in cancers.

Table generated based on data from (Wang et al., 2004, Kops et al., 2005, Chen et al., 1997, Bieche et al., 2011, Hayama et al., 2006, Meng et al., 2015). Software's for confirming hits were the Human Protein Atlas (Uhlen et al., 2010) and Oncomine Platform from ThermoFisher Scientific. Legend: ⇑ - increased levels, ⇓ - decreased levels, ND – no data.

The increasing knowledge about kinetochore and checkpoint component is already contributing to their use as diagnostic markers as well as drug targets for cancer treatment. Further studies, especially at the molecular level, are critical to advance research in this field to help save lives further down the line.

1.6 Motivation for the study

Kinetochore-microtubule attachment is the key event ensuring proper chromosome segregation during cell division. It is critical to pass genetic information correctly to the daughter cells, as any mistakes result in aneuploidy, which is a hallmark of cancer. Studies have identified the KMN network as the major attachment site between the outer kinetochore and microtubules. Furthermore, this site, in particular Knl1 and Ndc80, is extensively regulated by phosphorylation and dephosphorylation, acting as a sensor of proper attachments and cell cycle progression. Aurora B and Mps1 are the major kinases detecting the tension at the kinetochore (Aurora B) and recruiting spindle assembly checkpoint proteins to unattached kinetochores (Mps1 and Aurora B) (Kapoor et al., 2000, Kim and Yu, 2015, London and Biggins, 2014b).

Ndc80/Hec1 is highly expressed in cancers, particularly in breast, prostate, lung and liver cancers (Meng et al., 2015, Chen et al., 1997, Hayama et al., 2006, Diaz-Rodriguez et al., 2008, Bieche et al., 2011) (discussed in Chapter 1.5). Its deletions or truncations were shown to lead to chromosome missegregation and affect the localisation of SAC proteins and others. Briefly, SAC activation halts cell division at metaphase until all chromosomes are properly attached. The levels and localisations of checkpoint proteins are critical for human health, as shown in cancers – e.g. lung (Mad1, Bub1), colon (Bub1, BubR1, Bub3), lymph (Mad1, Bub3) and breast (Mad2) cancers (Kops et al., 2005) (discussed in Chapter 1.5). Over the last 20 years, there has been a significant progress in determining the dependencies between checkpoint components, their localisations and activation mechanisms (mitotic checkpoint complex assembly), however it requires further investigation.

The first described platform for SAC component localisation is the Knl1 protein, where Bub1, Bub3 and BubR1 are recruited (Shepperd et al., 2012, Yamagishi et al., 2012, Heinrich et al., 2012). Recently, Mad1 and Mad2 were shown in yeast and humans to localise to Bub1 (London and Biggins, 2014b, London and Biggins, 2014a). However, the localisation of Aurora B and Mps1 to unattached kinetochore remains elusive. In the

literature, deletions or truncations of Ndc80 protein were shown to affect levels and localisation of Aurora B and Mps1, as well as Mad1, Mad2, Bub1, BubR1, Bub3 and RZZ complex. Therefore, I wanted to investigate whether Ndc80 acts as a platform for the recruitment of checkpoint components in fission yeast.

During my studies, I isolated thiabendazole (TBZ) sensitive mutants of *ndc80* in fission yeast. The purpose was to identify a potential link between checkpoint proteins and the Ndc80 complex as SAC proteins, which were initially identified by their microtubule poison sensitivity in budding yeast. I isolated an *ndc80* mutant whose checkpoint defect is characterised in Chapter 3. Detailed analysis of the checkpoint defective mutant is further described in Chapter 4 and Chapter 5. I summarise the discoveries of my studies and propose models of Ndc80 as the platform for SAC proteins recruitment in Chapter 6.

Chapter 2. Materials & Methods

2.1 Yeast methods and genetics

2.1.1 Strain growth and maintenance

Fission yeast cells were grown in standard conditions (Moreno et al., 1991). Cells were cultured on appropriate agar plates or in liquid cultures as stated in Table 2.1. Selective media were prepared by adding the appropriate drugs as shown in Table 2.2. The experiments with overexpression from *nmt* promoters were carried out using minimal media supplemented with thiamine, for cell growth, and upon washout of the reagent using a filtration system, the cells were grown in absence of thiamine for 24h (liquid culture) and 72h (plates). The yeast cells were stored in YFM media at -80˚C.

Name	Components	Use
EMM	14.7 mM potassium hydrogen phthalate, 15 mM Na_2HPO_4, 93.5 mM NH_4Cl, 2% w/v glucose, salt stock, vitamin stock, mineral stock (Moreno et al., 1991)	Minimal medium
EMM-L	Same as EMM but supplemented with 75 mg/l uracil (ura), adenine (ade), histidine (his), lysine (lys)	Minimal medium
EMM-L+T	Same as EMM-L but supplemented with 0.02mM thiamine	Minimal medium
YE	0.5% Difco yeast extract, 3% dextrose	Rich medium
YE5S	0.5% Difco yeast extract, 3% dextrose, 250 mg/ml uracil, adenine, histidine, lysine, leucine	Rich medium
YFM	YE5S with 15% glycerol	Freezing stock
LB (for *E.coli*)	170 mM NaCl, 0.5% w/v yeast extract, 1% w/v bactotryptone, pH7.0	Bacterial medium
MEA	3% Difco yeast extract, 75 mg/ml uracil, adenine, histidine, lysine, leucine	Mating medium

Table 2.1. Growth media composition

Name	Components
Aureobasidin A	YE5S + 0.5 **µ** g /ml aureobasidin (Takara Bio)
ClonNAT	YE5S + 100 **µ** g /ml nourseothricin (Werner Bio-agents)
Hygromycin B	YE5S + 300 **µ** g/ml hygromycin B (Roche)
Kanamycin	YE5S + 100 **µ** g /ml Geneticin (G418) (Sigma-Aldrich)
Phloxin B	YE5S + 7.5 **µ** g /ml Phloxin B (Sigma-Aldrich)

Table 2.2. List of drugs used for selection.

2.1.2 Yeast transformation

About 2 x10^8 mid-log phase cells were harvested by centrifugation at 3000 rpm for 3 minutes. The cells were then washed twice with LiAc/TE, and then resuspended in 100 µl of LiAc/TE. 7.5 µl of salmon sperm carrier DNA (10 mg/ml, Invitrogen, denaturated at 95˚C for 5 min) and 200 ng of DNA (PCR fragment or plasmid DNA) were added to the solution and gently mixed by rotation at room temperature for 10 minutes. 260 µl of LiAc/TE/40%PEG (polyethylene glycol; Sigma-Aldrich) was added and briefly vortexed. The sample incubated with shaking for 1-2 hours at 27˚C. 43 µl of DMSO was then gently added followed by heat shock for 5 minutes at 42˚C. The cells were then washed with YE5S and the pellet resupended in 500 µl of YE5S. Cells were incubated 1.5-2 hours at 27˚C. Cells were then plated on YE5S and incubated for 4-6 days at 27˚C.

For DNA integration with a selection marker, cells were replica plated from YE5S plates onto the appropriate selections after 24 hours. The cells were then grown for 4-5 days. For transformation of plasmid DNA with the budding yeast *LEU2* gene as a selection marker, cells were plated onto EMM-L+T and grown for 4-6 days at 27˚C.

2.1.3 Random spore analysis

Numerous strains in this study were constructed by mating followed by random spore analysis. For the mating, strains of opposite mating types h^+ and h^- were mixed together and grown on MEA plates for approximately 2 days at 27˚C. The formation of asci was confirmed by light microscopy. Then, cells were treated with 100 µl of 0.5% helicase (Biosepra) for 2-3 hours at 27˚C to digest the ascus walls. 43 µl of 100% ethanol was

then added to the cells and the tubes were vortexed for 30 minutes at the room temperature to kill non-sporulating cells. The spores were pelleted and resuspended in 100 µl of water. 1:100, 1:300 and 1:1000 dilutions were plated onto YE5S plates and cultured for 3 or 5 days at 30˚C and 27˚C respectively. Resultant colonies were replica plated on to the appropriate selection plates to genotype each colony.

2.1.4 Serial dilution assay (Spot test)

The desired strain was grown in liquid culture overnight to mid-log phase. The number of cells (cell number/ml) was measured using the KX-21N cell counter (Sysmex Corp) and dilution adjusted to collect $2x10^7$ cells/ml. Cells were resuspended in 200 µl of water and 10-fold dilutions of each sample were made in 96 wells plates. The cells were spotted on appropriate plates and incubated at various temperatures. Photographs of the plates were taken 2-4 days later.

The serial growth assay for mutant screening was carried out on YE5S, YE5S+PB and YE5S+thiabendazole plates at 19, 22, 25, 27, 30, 34 and 36˚C.

For the plasmid/integrated promoter experiments with *nmt* promoters, the EMM-Leu and EMM-Leu with 2mM Thiamine plates were used.

2.1.5 Gene tagging and manipulation

For endogenous gene tagging, the one-step PCR method was used (Bahler et al., 1998). Long oligonucleotides approximately 100 base pairs were used; 80 base pairs of homology to flanking sequences of the insertion site at the target gene endogenous locus and 20 base pairs of homology to the insertion cassette from the template plasmid. Various tags such as 3PK, 5FLAG, 3FLAG, 13myc with selection markers of nat^R and hph^R on the pFA6a template plasmid (Sato et al., 2005) were used for PCR amplification. The positive PCR product was ethanol precipitated and transformed into a wild type strain. After 1 day, cells were replica plated to appropriate selection plates. The presence of integrants on the appropriate endogenous locus was confirmed by colony PCR and sequencing.

2.1.6 Genomic DNA extraction from fission yeast cells

Freshly streaked growing cells were placed in 100 µl of Yeast Cell Lysis solution (EPICENTRE MasterPure Yeast DNA Purification Kit) and mixed thoroughly by vortexing. Cells underwent lysis at 65˚C for 15 minutes followed by immediate cooling on ice for 5 minutes. 50 µl of MPC Protein Precipitation Reagent was added to the sample and vortexed thoroughly for 10 seconds. Cells were then centrifuged for 10 minutes at 13,000 rpm. The pellet formed was discarded and supernatant was transferred to a new tube. 500 µl of isopropanol was added and sample mixed by inversion. The DNA was pelleted by centrifugation at 13,000 rpm for 10 minutes. DNA was subsequently washed with 500 µl of 70% ethanol and finally resuspended in 30 µl of water or TE.

2.2 Synchronisation of cells using hydroxyurea (HU)

Cells were synchronised in S phase using hydroxyruea (HU) to enrich for mitotic cells. Liquid cultures of 2-4 x10^6 cells/ml were treated with 12.5 mM of HU at 25˚C for 4 hours. Cells were then filtered, washed 3 times with water and placed in HU-free YE5S media.

2.3 Mitotic arrests

2.3.1 TBZ/CBZ conditions

Cells were synchronised in S phase using hydroxyurea (HU) for an accumulation of mitotic cells. Liquid cultures of 2-4 x10^6 cells/ml were treated with 12.5 mM of HU at 25˚C for 4 hours. Then the cells were filtered, washed 3 times with water and placed in HU-free YE5S media with 50 µg/ml TBZ and 60 µg/ml CBZ (Yamagishi et al., 2012). Samples were taken and fixed every 30 minutes for 3 hours and were later observed under the microscope. Alternatively, cells were used for live imaging after 30 minutes of growth in the presence of TBZ/CBZ.

2.3.2 *cut7-446* arrest

In order to accumulate mitotically-arrested cells, the strains were crossed to *cut7-446* strain. The *cut7-446* is defective in kinesin-5 mediated interdigitation of microtubules and elongation of mitotic spindles, hence the mutant displays defective spindles and chromosome overcondensation (Hagan and Yanagida, 1990). Cells were grown at 25˚C overnight until cultures reached mid-log phase. Cultures were then shifted to 36˚C for 90 minutes to arrest cells in a metaphase-like state. The cells were used for either fixation or live imaging.

2.3.3 *nda3-1828* arrest

To induce the spindle assembly checkpoint response, the attachments between kinetochore and microtubule need to be disrupted. Strains were crossed with the β-tubulin-defective, temperature-sensitive *nda3-1828* strain (Radcliffe et al., 1998). Cells were cultured at permissive temperature of 25˚C overnight until mid-log phase was reached. Cultures were then shifted up to 36˚C for 90 minutes to arrest cells in metaphase-like state. The cells were fixed every 30 minutes.

2.3.4 *nda3-KM311* arrest

Another β-tubulin mutant was used to arrest cells in mitosis. The *nda3-KM311* strain (Hiraoka et al., 1984) was crossed to the strains under investigation. Cells were grown overnight at the permissive temperature of 30˚C. Mid-log phase cultures were then shifted to the restrictive temperature of 19˚C for 6 hours. Samples were collected in 2-hour intervals, followed by fixation. The alternative temperatures were also tested: 30˚C and 20˚C (Hiraoka et al., 1984), 30˚C and 16˚C (Heinrich et al., 2012), 30˚C and 17˚C (Yamagishi et al., 2012), 30˚C and 18˚C (Meadows et al., 2011), permissive and restrictive temperatures respectively.

2.4 Yeast strain construction

2.4.1 Isolation of *ndc80* mutants

The previously constructed *ndc80*$^{+}$-*kan*^{r} strain containing a kanamycin-resistance marker gene (kan^{r}) in 3' flanking region of *ndc80*$^{+}$ (Hsu and Toda, 2011) was used. Genomic DNA from the *ndc80*$^{+}$-*kan*^{r} strain was extracted as described previously. The N-terminal fragment of *ndc80*$^{+}$-*kan*^{r} was randomly mutagenised using "error prone PCR". The unbalanced dNTP conditions (2.5mM 10x deoxyguanosine triphosphate (dGTP) in comparison to 0.25mM) and Vent DNA polymerase (New England Biolabs) were used to maximise the mutagenesis rate. The C-terminus of *ndc80*$^{+}$-*kan*^{r} was amplified by PCR using PrimeSTAR polymerase. The N and C terminal fragments of *ndc80*$^{+}$-*kan*^{r} were gel purified separately. Using an equimolar ratio of N and C, the fragments were fused together in a PCR reaction using PrimeSTAR polymerase. Then the amplified fusion fragments were concentrated by ethanol precipitation and transformed into the wild-type 513 strain and plated on YE5S. After 24 hours at 27˚C, the plates were replicated onto YE5S with kanamycin and incubated for 4 more days at 27˚C. Transformant colonies were then replicated onto YE5S, YE5S containing 10 μg/ml thiabendazole (TBZ, microtubule depolymerizing drug) and YE5S containing Phloxine B dye. Phloxine B dye is used to differentiate between live and dead cells - metabolically active live cells can remove the incorporated Phloxine B and so appear white/bright pink, whereas dead cells cannot export the dye and thus appear dark pink/red. YE5S with Phloxine B plates were incubated at 27˚C and 36˚C and YE5S with TBZ were incubated at 27˚C for 24 hours. Colonies that did not grow on either YE5S with Phloxine B at high temperature or on YE5S with TBZ or on both were selected.

This screening method was repeated until around 10,000 colonies had been screened. Temperature sensitive or TBZ sensitive colonies were picked up and their morphology was observed under the microscope. Isolates were then backcrossed to wild type 3D to ensure the proper integration of the randomly mutagenised *ndc80*$^{+}$-*kan*^{r} gene into the appropriate *ndc80*$^{+}$ locus. Mutants were described as temperature sensitive (2 colonies) or TBZ-sensitive (3 colonies).

2.4.2 Confirmation of mutation sites in *ndc80* mutants by sequencing

The gene of interest was amplified by PCR using PrimeSTAR polymerase (TaKaRa) and the amplified product was ethanol precipitated by QIAquick PCR extraction kit (Qiagen). Nucleotide sequencing was performed by Cancer Research UK, London Research Institute's in-house sequencing facilities. The sequences obtained were analysed using Serial Cloner 2-5, ApE and NCBI blast.

2.4.3 Confirmation of crosses by colony PCR

4-5 day old cells from YE5S plates were suspended in 40 mM NaOH with 0.01% sarcosyl. The samples were boiled at 95˚C for 15 minutes. After that they were cooled on ice, vortexed and centrifuged at 13,000 rpm for 30 seconds. The supernatant was used for a PCR reaction with Z-taq polymerase under the conditions depicted in Figure 2.1.

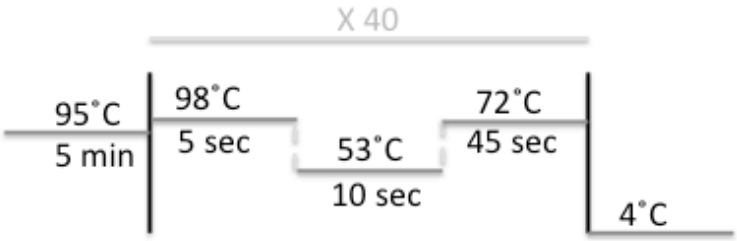

Figure 2.1. Colony PCR conditions.

2.5 Construction of plasmids

2.5.1 Construction of plasmids carrying *ndc80* gene

The open reading frame (ORF) of the truncated *ndc80*$^{+}$ gene was amplified by PCR and cloned into *Nde*I/*Bam*HI restriction sites of the pREP1 or pREP41-GFP vectors (Maundrell, 1993). pREP1 and pREP41-GFP carry the *nmt1* or *nmt41* promoter which is repressed in the presence of thiamine. The insertion of *ndc80* truncations into plasmids was confirmed by nucleotide sequencing.

2.5.2 Construction of plasmids carrying *mad2* gene

The open reading frame of *mad2*$^+$ gene was amplified by PCR. Then, the fragment was cloned into pREP41-GFP plasmid using *Sal*I/*Bam*HI restriction sites. The insertion was confirmed by nucleotide sequencing.

For the construction of pREP1-GFP-Mad2, the pREP41-GFP-Mad2 construct was used as a template for InFusion HD Cloning Kit (Clontech Laboratories. Briefly, GFP-Mad2 was PCR amplified using In-Fusion primers. PCR fragments were ethanol precipitated and plasmid was digested with *Nde*I/*Bam*HI, followed by gel extraction of the correct fragment using the QIAquick Gel Extraction (50) kit. 100 ng of purified PCR fragment (insert) was mixed with 25 ng of linearized plasmid in the presence of 5xIn-Fusion HD Enzyme Premix, to a total volume of 5 μl. The ligation was carried out at 50˚C for 15 minutes. Then, the product was transformed into Stellar Competent Cells.

2.5.3 Construction of plasmids carrying *mph1* gene

The open reading frame of *mph1*$^+$ gene was amplified by PCR. Then, the fragment was cloned into pREP41-GFP plasmid using *Sal*I/*Xma*I restriction sites. The insertion was confirmed by nucleotide sequencing.

For construction of pREP1-GFP-Mph1, the pREP41-GFP-Mph1 construct was used as a template for InFusion HD Cloning Kit (Clontech Laboratories). Briefly, GFP-Mph1 was PCR amplified using In-Fusion primers. PCR fragments were ethanol precipitated and plasmid was digested with *Nde*I/*Bam*HI, followed by gel extraction using the QIAquick Gel Extraction (50) kit. 100 ng of purified PCR fragment (insert) was mixed with 25 ng of linearized plasmid in the presence of 5xIn-Fusion HD Enzyme Premix, to a total volume of 5 μl. The ligation was carried at 50˚C for 15 minutes. Then, the product was transformed into Stellar Competent Cells.

2.6 Microscopy

Images were acquired by an Olympus IX70 PlanoApo 100x, NA 1.4, oil immersion objective on a Olympus IX70 wide-field inverted epifluorescence microscope. The DeltaVision-softWoRx system (softWoRx 3.3.0; Applied Precision Co.) with a Coolsnap HQ (Roper Scientific) camera was used for acquisition of all fluorescent microscopy data. Images were taken at 14 positions along the z-axis at 0.3 mm intervals. Then, images were deconvolved, compressed into the projection using the DeltaVision (DeltaVision-SoftWoRx; Applied Precision Ltd) maximum intensity algorithm. The later stages of image processing occurred in Adobe Photoshop CS5 and Adobe Illustrator CS5.1.

2.6.1 Signal quantification

For the fluorescent signal quantification, the live image observations of cells were performed. 200 µl of exponentially-growing cells were placed on a lectin-coated glass dish. Cells were photographed for 30-120 minutes depending on the experiment, with the time lapse images taken every 2 minutes. Deconvolved fluorescent images (DeltaVision-softWoRx (Applied Precission Ltd)) were used for quantification of the signals. The maximum signal intensity for an area of 4x4 pixels was recorded, as well as background noise in the proximity of the fluorescent spot (usually in the nucleus). The final read-out of signal intensity was obtained by subtracting the background intensity from the recorded one.

2.6.2 Paraformaldehyde sample fixation

For the quantification of mitotic cells, cells were fixed with 1.6% paraformaldehyde (PFA). 100 µl of 16% PFA was added to 900 µl of exponentially growing cell culture. After 10 minutes of incubation at room temperature, the sample was centrifuged and the pellet washed with 1 ml of PBS. The cells were then resuspended in 100 µl of PBS. 5 µl of the sample was placed on a glass slide with coverslip for observation under the microscope.

2.7 Biochemical analysis

2.7.1 Alkaline method

For rapid protein extraction to confirm protein tagging or checking protein expression levels, the alkaline fast extraction method was used (Matsuo et al., 2006). 1 ml of cells in exponential growth phase (around $6x10^6$ cells/ml) was collected by centrifugation 3,000 rpm for 3 minutes. The pellet was then washed with 1 ml of distilled water. Cells were centrifuged again at 3,000 rpm for 3 minutes, and the pellet resuspended in 300 µl of distilled water. 300 µl of 0.6 M NaOH was added and the sample incubated for 10 minutes at room temperature. Cells were then centrifuged at 7,000 rpm for 2 minutes and 70 µl of modified SDS-sample buffer (60mM Tris-HCl (pH6.8), 4% β-mercaptoethanol, 4% SDS, 0.01% BPB, and 5% glycerol) was added and mixed by pipetting. The sample was then boiled for 3 minutes at 95˚C and then cooled on ice. The samples were then loaded onto an SDS-PAGE gel for immunoblotting. The remaining sample was stored at -20˚C.

2.7.2 Protein extraction by glass beads

The mid-log phase cells, that were grown overnight, were collected and centrifuged at 3000 rpm for 3 minutes at 4˚C. The pellet was washed with 1 ml of STOP buffer and resuspended in 100 µl of IP2 buffer. Proteins were extracted using glass beads (Sigma Aldrich) in a Fast Prep FP120 apparatus (Savant Co., MN, USA) at setting 5.5k for 35 seconds, 6 times (each 2^{nd} time, the samples were put on ice for 1 minute). The protein extracts were then cleared from the cell debris and beads by 15 minutes of centrifugation at 13,000 rpm, 4˚C. The protein concentrations were then measured using Bedford assay (Bio-Rad).

2.7.3 Immunoblot analysis

20 µg of protein samples were boiled in Laemmli buffer for 5 minutes and loaded onto SDS-PAGE gels (4-12%, Bis-Tris gradient gel, Bio-Rad). After separation by electrophoresis, proteins were wet-transferred to immobilion PVDF membrane (Millipore) at 4˚C overnight at 30V or 1h at 120V. 5% skimmed milk in PBS was used to block the membrane for 30-90 minutes at room temperature. Primary antibody in 5%

skimmed milk/PBS was added to membrane for 1 h at room temperature or overnight at 4˚C. The blot was then washed 3 times with 0.1%PBST for 5 minutes. Then the secondary antibody in 5% skimmed milk/PBS was added for 30-60 minutes at room temperature, followed by three more sets of 5 minutes washes with 0.1% PBST. The antibody-bound membrane was developed on films for appropriate time using an ECL chemilluminescence kit (GE Healthcare Co.). The list of antibodies and their concentrations used in this study are summarised in Table 2.3.

Antibody	Clonality	Species	Concentration (for Immuno-blot)	Cat.No
Anti-PK	Monoclonal	Mouse IgG2	1:1000	ABD Serotec, MCA1360GA
Anti-GFP	Polyclonal	Rabbit	1:1000	Torrey Pines Biolab/AMSBio
Anti-Myc	Monoclonal	Mouse IgG1	1:1000	Babco, MMS-101P
Anti-FLAG (M2)	Monoclonal	Mouse IgG1	1:1000	Sigma-Aldrich, F-3165
Anti-Cdc2	Monoclonal	Mouse IgG1	1:2000 / 1:5000	ICRF (H.Yamano)

Table 2.3. List of primary antibodies used in the study.

2.7.4 Immunoprecipitation

2 mg of protein extracted by glass beads were used for coimmunoprecipitation. Extracts were added to protein A Dynabeads (Invitrogen Ltd., CA, USA) bound with 1:1000 anti-FLAG (M2, Sigma-Aldrich, UK) antibody and incubated at 4˚C for 1-1.5 hours on a rotor. Then, the beads were washed 5 times with wash buffer. 30 µl of Laemmli buffer was added and the samples were boiled for 5 minutes, followed by centrifugation at 5,000 rpm for 10 seconds. The samples were loaded onto SDS-PAGE gel (3-8%, Tris-Acetate, Bio-Rad), followed by immunoblot detection of the proteins.

2.8 Solutions and buffers

Solution	Components
TE	10 mM Tris-HCl pH 7.5, 1 mM EDTA
TAE	0.08 M Tris acetate, 2 mM Na_2EDTA
LiAc/TE	100 mM lithium acetate pH 7.4, 10 mM Tris-HCl pH 7.4, 1 mM EDTA pH 8.0
LiAc/TE/40% PEG3640	LiAc/TE, 40% polyethylene glycerol 3640 (Sigma-Aldrich)
6 x Loading dye	30% glycerol, 0.1% bromophenol blue
Transfer buffer	39 mM glycine, 48 mM Tris-base, 20% methanol
PBS	170 mM NaCl, 3 mM KCl, 10 mM Na_2HPO_4, 2 mM KH_2PO_4
PBST	PBS plus 0.1% Tween-20
STOP buffer	150 mM NaCl, 50 mM NaF, 10 mM EDTA, 0.007% v/v NaN_3
IP buffer	50 mM Tris-HCl pH 7.4, 1 mM EDTA pH 8.0, 500 mM Na Cl, 0.05% NP40, 0.1% Triton X-100, 10% glycerol
Wash buffer	IP buffer plus freshly added: 1 mM DTT, 15 mM PNPP, 1xprotease cocktail inhibitor (Sigma-Aldrich), 1 mM PMSF
2 x Sample buffer	125 mM Tris-HCl pH 6.8, 50% glycerol, 4% SDS, 0.02% bromophenol blue, 100 mM DTT
Alkaline sample buffer	60mM Tris-HCl (pH6.8), 4% β-mercaptethanol, 4% SDS, 0.01% bromophenol blue, 5% glycerol

Table 2.4 List of buffers and solutions.

2.9 Plasmids used in the study

Name	Gene	Origin
pREP1		Lab stock
pREP1-Ndc80	*ndc80*$^{+}$	Lab stock
pREP1-Ndc80-Δ211-270	*ndc80*	This study
pREP1-Ndc80-Δ211-248	*ndc80*	This study
pREP1-Ndc80-Δ249-270	*ndc80*	This study
pREP1-GFP-Mad2	*mad2*$^{+}$	This study
pREP1-GFP-Mph1	*mph1*$^{+}$	This study
pREP3-Mad2	*mad2*$^{+}$	Lab stock
pREP3-Mph1	*mph1*$^{+}$	Lab stock
pREP41		Lab stock
pREP41-GFP		Lab stock
pREP41-GFP-Ndc80	*ndc80*$^{+}$	Lab stock
pREP41-GFP-Ndc80-Δ211-270	*ndc80*	This study
pREP41-GFP-Ndc80-Δ211-248	*ndc80*	This study
pREP41-GFP-Ndc80-Δ249-270	*ndc80*	This study
pREP41-GFP-Mad2	*mad2*$^{+}$	This study
pREP41-GFP-Mph1	*mph1*$^{+}$	This study

2.10 Strains used in the study

Strain	Genotype
AEK004	*h*$^{-}$ *leu1 ura4 his2 ndc80-AK01-kan*
AEK00B	*WT 513 h*$^{-}$ *leu1 ura4*
AEK011	*h*$^{-}$ *leu1 ura4 ndc80-AK03-kan*
AEK014	*h*$^{+}$ *leu1 ura4 his2 ndc80-AK04-kan*
AEK020	*h*$^{-}$ *leu1 ura4 his2 ndc80-AK05-kan*
AEK047	*h*$^{-}$ *leu1 ura4 ndc80-AK02-kan*
AEK051	*h*$^{+}$ *leu1 his2 cut7-446*
AEK053	*h*$^{-}$ *leu1 ura4 mad2::LEU2*
AEK063	*h*$^{-}$ *ndc80-AK03-kan cut7-446*
AEK1007	*h*$^{+}$ *dis2::ura4*$^{+}$ *leu1 ura4 plo1-mCherry-hphR his2*

AEK1012	*h⁻ leu1 ndc80-AK01-kan dis2::ura4⁺ plo1-mCherry-hph ura4*
AEK1017	*h⁺ bub1⁺-GFP-kanR plo1-mCherry-hphR cut7-446 his2 leu1 ura4*
AEK1022	*h⁻ mad1⁺-GFP<<kanR cut7-446 plo1-mCherry-hphR*
AEK1031	*h⁺ leu1 ade6-M216 ura4 hph<<Pnm81<<mis12-(GGSG)2-mph1⁺-S(GGGGS)3-GFP<<kanR plo1⁺-mCherry<<natR ndc80-AK01-kan his2*
AEK1036	*h⁻ leu1 Hph>>Pnmt81>>mph1⁺-S(GGGGS)3-GFP<<kanR plo1⁺-mCherry<<natR ndc80-AK01-kan*
AEK1044	*h⁻ ndc80-AK01-kan aur1R-mCh-atb2 sid4-mRFP-natR nuf2-YFP-ura4 ura4 leu2*
AEK1058	*h⁻ mad1⁺-GFP<<kanR ndc80-Ak01-kanR plo1-mCherry-hphR cut7-446 leu2*
AEK1081	*h⁺ bub1⁺-GFP-kanR plo1-mCherry-hphR ndc80-AK01-kan cut7-446 leu1 ade6-M216 his2*
AEK1082	*h⁻ aur1R-mCh-atb2 sid4-mRFP-natR nuf2-YFP-ura4 ura4 leu2*
AEK1098	*h⁻ leu1 ura4 nuf2⁺-mCherry-ura4⁺ (pREP41-GFP-ndc80-Δ211-270)*
AEK1100	*h⁻ leu1 ura4 nuf2⁺-mCherry-ura4⁺ (pREP41-GFP-ndc80-Δ211-248)*
AEK1102	*h⁻ leu1 ura4 nuf2⁺-mCherry-ura4⁺ (pREP41-GFP-ndc80-Δ249-270)*
AEK1107	*h⁻ leu2 hph<<Pnmt81<<mis12-(GGSG)2-mph1⁺-GFP<<kanR mad2Δ::hygR plo1⁺-mCherry-natR ndc80-AK01-kanR*
AEK1110	*h⁻ leu1 ura4 pREP41-GFP-v*
AEK1114	*h⁻ leu1 ura4 bub3::ura4 pREP41-GFP-v*
AEK1116	*h⁻ leu1 ura4 mad3::ura4 pREP41-GFP-v*
AEK1118	*h⁻ leu1 ura4 mad2::natR pREP41-GFP-v*
AEK1188	*h⁺ leu1 ura4 his2 ndc80-3FLAG-kan*
AEK1189	*h⁻ leu1 ura4 pREP41-GFP-Mad2*
AEK1195	*h⁻ leu1 ura4 bub3::ura4 pREP41-GFP-Mad2*
AEK1197	*h⁻ leu1 ura4 mad3::ura4 pREP41-GFP-Mad2*
AEK1200	*h⁻ leu1 ura4 mad2::natR pREP41-GFP-Mad2*
AEK1201	*h⁻ leu1 ura4 pREP41-GFP-Mph1*
AEK1207	*h⁻ leu1 ura4 mad3::ura4 pREP41-GFP-Mph1*
AEK1209	*h⁻ leu1 ura4 mad2::natR pREP41-GFP-Mph1*
AEK1212	*h⁻ leu1 ura4 bub3::ura4⁺ pREP41-GFP-Mph1*
AEK1213	*h⁻ leu1 ura4 mph1-13myc-natR*
AEK1252	*h⁻ leu1 ura4 mph1-13myc-natR ndc80-3FLAG-kan*
AEK1274	*h⁻ leu1-32 ura4 mad1::ura4 pREP1-GFP-Mad2*
AEK1276	*h⁻ leu1 ura4 mad3::ura4 pREP1-GFP-Mad2*
AEK1278	*h⁻ leu1 ura4 mad3::ura4 pREP1-GFP-Mph1*
AEK1280	*h⁻ leu1 ura4 bub3::ura4 pREP1-GFP-Mad2*
AEK1282	*h⁻ leu1 ura4 mad2::natR pREP1-GFP-Mad2*
AEK1284	*h⁻ leu1 ura4 mad2::natR pREP1-GFP-Mph1*
AEK1288	*h⁻ ade6-216 his1 leu1 ura4 bub1::ura4 pREP1-GFP-Mad2*
AEK1290	*h⁻ ade6-216 his1 leu1 ura4 bub1::ura4 pREP1-GFP-Mph1*
AEK1292	*h⁻ leu1 ura4 his2 ndc80-AK01-kan pREP1-GFP-Mad2*
AEK1294	*h⁻ leu1 ura4 his2 ndc80-AK01-kan pREP1-GFP-Mph1*

AEK1302	*h⁻ leu1 ura4 pREP1-GFP-Mad2*
AEK1302	*h⁻ leu1 ura4 pREP1-GFP-Mad2*
AEK147	*h⁺ his2 ndc80-AK05-kan cut7-446 ura4 leu1*
AEK149	*h⁺ cut11-GFP-ura4⁺ leu1-32 ura4-D18*
AEK150	*h⁺ his2 cut7-446 mad2::LEU2*
AEK156	*h⁺ ndc80-AK01-kan cut7-446 leu1 his2*
AEK178	*h⁺ ndc80-AK01-kan cut11-GFP-ura4⁺ leu1-32 ura4-D18 his2*
AEK181	*h⁻ ndc80-AK03-kan cut11-GFP-ura4⁺ leu1-32 ura4-D18*
AEK188	*h⁻ cut11-GFP-ura4⁺ mad2::LEU2 leu1-32 ura4-D18*
AEK191	*h⁺ ndc80-AK05-kan cut11-GFP-ura4⁺ leu1-32*
AEK211	*h⁺ leu1 ura4 his2 nda3-KM311*
AEK220	*h⁺ his2 leu1 ura4 spc25-YFP-nat nuf2-mCherry-ura4 cut12-2CFP-hph*
AEK245	*h⁻ cut11-GFP-ura4⁺ mad2::LEU2 ura4-D18*
AEK309	*h⁻ Plo1-mCherry-hphR leu1 ura4 lys1*
AEK342	*h⁻ spc25-YFP-nat nuf2-mCherry-ura4 cut12-2CFP-hph ndc80-AK01-kan*
AEK344	*h⁻ spc25-YFP-nat nuf2-mCherry-ura4 cut12-2CFP-hph ndc80-AK03-kan*
AEK349	*h⁻ spc25-YFP-nat nuf2-mCherry-ura4 cut12-2CFP-hph ndc80-AK05-kan*
AEK373	*h⁻ ndc80-AK01-kan Plo1-mCherry-hphR leu1 ura4*
AEK383	*h⁺ leu1 ura4 his2 nda3-1828*
AEK400	*h⁻ ndc80-AK01-kan nda3-1828 leu1 ura4*
AEK401	*h⁺ ndc80-AK05-kan nda3-1828 leu1 ura4 his2*
AEK403	*h⁻ nda3-1828 mad2::LEU2 leu1 ura4*
AEK423	*h⁻ leu1-32 ura4 Mad1::ura4*
AEK423	*h⁻ leu1-32 ura4 Mad1::ura4*
AEK424	*h⁺ leu1 ura4 ade6-210 Mph1::ura4*
AEK425	*h⁻ ura4 ade6-216 Bub1::leu2*
AEK468	*h⁻ leu1 ura4 bub3::ura4⁺*
AEK501	*h⁻ Plo1-mCherry-hphR mad1⁺-GFP<<kanR lys1 ura4* (Heinrich et al., 2012)
AEK505	*h⁻ Plo1-mCherry-hphR mad2⁺-GFP-LEU2 leu1 lys1*
AEK507	*h⁻ ndc80-AK01-kanR mph1::ura4 leu1-32 ura4 leu2 ade6-210*
AEK510	*h⁻ ndc80-AK01-kanR bub1::leu2 ura4 leu1 ade6-M216*
AEK513	*h⁻ ndc80-AK01-kanR mad1::ura4 leu1-32 ura4*
AEK517	*h⁻ ndc80-AK01-kanR mad3::ura4 leu1 ura4*
AEK521	*h⁻ ndc80-AK01-kanR bub3::ura4 leu1 ura4*
AEK526	*h⁺ Plo1-mCherry-hphR mad3⁺-GFP<<kanR leu1 his2* (Heinrich et al., 2012)
AEK531	*h⁻ mph1⁺S(GGGGS)3-GFP<<kanR Plo1-mCherry-hphR leu1* (Heinrich et al., 2012)
AEK555	*h⁻ bub3⁺-S(GGGGS)3-GFP<<kanR plo1-mCherry-hphR leu1* (Heinrich et al., 2012)

AEK586	*h⁻ ndc80-AK01-kan mad2::leu2 leu1 ura4 lys1*
AEK590	*h⁺ ndc80-AK01-kanR bub1⁺-GFP-kanR plo1-mCherry-hph his2 ade6-210 ura4 lys1*
AEK595	*h⁻ ndc80-AK01-kanR mad2⁺-GFP-LEU2 Plo1-mCherry-hphR ura4*
AEK598	*h⁻ ndc80-AK01-kanR mad2⁺-GFP-LEU2 Plo1-mCherry-hphR cut7-446*
AEK600	*h⁺ bub1⁺-GFP-kanR plo1-mCherry-hphR his2 ade6-210 leu2 lys1 ura4* (Heinrich et al., 2012)
AEK618	*h⁻ ndc80-AK01-kanR plo1-mCherry-hphR mad1⁺-GFP<<kanR ura4 ade6-210 lys1*
AEK631	*h⁻ mad3⁺-GFP<<kanR ndc80-Ak01-kan plo1-mCherry-hphR*
AEK634	*h⁺ bub3⁺-S(GGGGS)3-GFP<<kanR ndc80-AK01-kanR plo1-mCherry-hphR leu2 his2*
AEK641	*h⁻ mad3⁺-GFP<<kanR ndc80-AK01-kanR plo1-mCherry-hphR leu2*
AEK645	*h⁺ mad3⁺-GFP<<kanR ndc80-AK01-kanR plo1-mCherry-hphR cut7-446 lys1 leu2 ura4? His2*
AEK669	*h⁻ mad3⁺-GFP<<kanR plo1-mCherry-hphR cut7-446 lys1 leu2 ade6?*
AEK697	*h⁻ mad2⁺-GFP-LEU2 plo1-mCherry-hphR cut7-446 ura4 leu1*
AEK700	*h⁻ leu1 ark1⁺-GFP<<kanR plo1-mCherry-hphR ndc80-AK01-kanR*
AEK704	*h⁻ Plo1-mCherry-hphR ark1⁺-GFP<<kanR leu2 lys1* (Heinrich et al., 2012)
AEK709	*h⁺ ndc80-AK01-kan mph1⁺-S(GGGGS)3-GFP<<kanR plo1-mCherry-hphR leu2 ura4 his2*
AEK752	*h⁺ mad1::ura4 mad2⁺-GFP-LEU2 ndc80-AK01-kanR plo1-mCherry-hphR his2 ura4 leu1*
AEK767	*h⁺ leu1-32 ura4 mad1::ura4 mad2⁺-GFP-LEU2 plo1-mcherry-hphR his2*
AEK779	*h⁺ leu1 ura4 ade6-210 Mph1::ura4 pREP1(v)*
AEK787	*h⁻ leu1 ura4 mad2::natR pREP1(v)*
AEK787	*h⁻ leu1 ura4 mad2::natR pREP1(v)*
AEK790	*h⁻ leu1 ura4 pREP1(v)*
AEK790	*h⁻ leu1 ura4 pREP1(v)*
AEK820	*diploid leu1 ura4 his7 ade6-216 ade6-210 ndc80::ura4⁺ ndc80⁺ (pREP1-vector)*
AEK821	*diploid leu1 ura4 his7 ade6-216 ade6-210 ndc80::ura4⁺ ndc80⁺ (pREP1-ndc80-FL)*
AEK826	*h⁻ leu1 ura4 his2 ndc80-AK01-kan pREP41(v)*
AEK835	*h⁻ leu1-32 ura4 Mad1::ura4 pREP1(v)*
AEK839	*h⁻ leu1 ura4 bub3::ura4⁺ pREP1(v)*
AEK842	*h⁻ ade6-216 his1 leu1 ura4 bub1::ura4⁺ pREP1(v)*
AEK843	*h⁻ ade6-216 his1 leu1 ura4 bub1::ura4⁺ pREP1(v)*
AEK845	*h⁻ leu1 ura4 Mad3::ura4 pREP1(v)*
AEK845	*h⁻ leu1 ura4 Mad3::ura4 pREP1(v)*
AEK862	*diploid leu1 ura4 his7 ade6-216 ade6-210 ndc80::ura4⁺ ndc80⁺ (pREP1-ndc80-Δ211-270)*
AEK871	*diploid leu1 ura4 his7 ade6-216 ade6-210 ndc80::ura4⁺ ndc80⁺*

	(pREP1-ndc80-Δ249-270)
AEK889	*h⁻ leu1 ura4 ndc80-NH12-kan* (Tang et al., 2013)
AEK893	*h⁻ leu1 ura4 nuf2-mCherry-ura4⁺ (pREP41-GFP(N))*
AEK894	*h⁻ leu1 ura4 nuf2-mCherry-ura4⁺ (pREP41-GFP-Ndc80-FL)*
AEK895	*h⁻ leu1 ura4 ndc80-NH12-kan (pREP1-vector)*
AEK896	*h⁻ leu1 ura4 ndc80-NH12-kan (pREP1-Ndc80-FL)*
AEK921	*h⁻ leu1 ura4 ndc80-NH12-kan (pREP1-ndc80-Δ211-270)*
AEK923	*h⁻ leu1 ura4 ndc80-NH12-kan (pREP1-ndc80-Δ211-248)*
AEK925	*h⁻ leu1 ura4 ndc80-NH12-kan (pREP1-ndc80-Δ249-270)*
AEK961	*h⁻ leu1 ura4 nuf2⁺-mCherry-ura4⁺ (pREP41-GFP-ndc80-Δ211-248)*
AEK986	*h⁻ leu1 ade6-M216? Hph>>Pnmt81>>mph1⁺-S(GGGGS)3-GFP<<kanR plo1⁺-mCherry<<natR*
AEK990	*h⁻ leu1 ade6-M216 hph<<Pnm81<<mis12-(GGSG)2-mph1⁺-S(GGGGS)3-GFP<<kanR plo1⁺-mCherry<<natR* (Heinrich et al., 2012)
AEK991	*h⁻ leu1 hph<<Pnmt81<<mis12-(GGSG)2-mph1⁺-S(GGGGS)3-GFP<<kanR mad2Δ::hygR plo1⁺-mCherry-natR* (Heinrich et al., 2012)
AEK996	*h⁻ ura4 bub1::leu2 plo1-mCherry-hphR ark1⁺-GFP-kanR leu2*

2.11 Oligonucleotides used in this study

For sequencing of *ndc80* mutants:

KSH17 F'-Ndc80 (-555)	AGGATATTTAGAATGCTACAC
KSH18 F'-Ndc80 (-175)	AATCCTGCCGTTGTCGATAT
KSH19 F'-Ndc80 (141)	GTACTTCAAGAACCAGTTTAG
KSH20 F'-Ndc80 (479)	TAATCGTTTCATGCCATCAAC
KSH21 F'-Ndc80 (807)	GTTCGCACATATCATTTGTAC
KSH22 F'-Ndc80 (1151)	AAGGGACTCTCTGAAGTATC
KSH23 F'-Ndc80 (1481)	CCATTTATTAATGAAGTTAGAC
KSH24 F'-Ndc80 (1811)	ACATGCTTGCATGGAGTACA
AEK04-F'-Ndc80(-476)	GCA GAT TAA AAT GAT ACC GAT TG
AEK05-R'-Ndc80(2265)	GTC GTG TAT ATG ATG TAT AAA AAC G

For colony PCR of *ndc80*:

Ndc80.DRS-R1	CTACTGACTTTGGATTGGTTCGTACCAGT ATCTC
Ndc80-F1	CACGTTCAAGACAGTTTGGAGGATTTGA AGATGG

For sequencing of *mad2* and *mph1* in plasmids:

AEK038-Mad2-F (158)	GAA GAC TTC AAA GTT GTT CGG AAA TAT

	GGA TTA AAT ATG C
AEK062-F (Mph1-925)	AAGCGTCAGCAGGAC
pREP-Forward	AGAGGAATCCTGGCATATCATC
pEP-Reverse	GCTTGAATGGGCTTCCATAG
GFP-505-F'	CACAACATTGAAGATGGAAGCGTTCAACTAG CAGACC

For colony PCR and sequencing of *mad1, mad2, mad3, bub1, bub3, mph1* and *ark1* tagged with GFP:

AEK035-Mad1-F (1951)	GTT GGT AAT CCA TCA GGC CCC GAA TTT GAG
AEK036-Mad1-R (3UTR 139)	TCG ACA TTG AAG GAT ATA TTG ATA TTA TTA GTT AAA CAA TCT ATT TCA TAA AAA AGT
AEK025-Mph1-R' (3'UTR 202)	GATATCAGGGGCCATATAATATGTGGTTCATTAAT C
AEK026-Mph1-F(5UTR -82)	ACG AAG TAA AAA TTT ATT GAT TAA CGC TTA ACA AAC AGT TGG AAA TTG GAA
AEK027-Bub1-F (5UTR -73)	GAA TAC TTG TCG TCG AAC CAA GTG CAG
AEK028-Bub1-R (3UTR 200)	GCA TGC ATA TTG CAG GTT TGT GAT CAT GAT
AEK023-Bub3-R'(3'UTR 125)	CTGAGGAAATATTGAACATTTACAACATTAAATA GGAGTGC
AEK029-Bub3-F (5UTR -237)	GTG AGG CAC AGA CTG TCA AAA TTT GTT GAA AAG AAG
AEK019-Mad3-R'(3'UTR 138)	ATAAATAAGATGCTTTATGTTAAGTTCGTATAACC CTTAAAATTCGCATGTTTC
AEK030-Mad3-F (5UTR-151)	CGT TCT TTC AAT AGA ATT GTA CTT GTC TAA ATA AAC TTT CCA ATA CTA
AEK031-Ark1-F (5UTR -30)	GTC AAA AGC CAA CAT CAG CGT TTT TTT ACG
AEK032-Ark1-R (3UTR 210)	GAA AAT CTG GAA AAC GAT TAG TTT ATG GTG GTG
AEK037-Mad2-F (5UTR -212)	GAG ATA GTG AAA TGA GTT TAA AAT GAC AGA TTA GTT ACT TTC AAG
AEK040-Mad2-R (3UTR 114)	TTC ACC GAA TTA TAG TTA AAC AAT ATG GCC GGA ATT TTG AGA TTT

For mutagenesis of *ndc80* for ts and TBZ screening:

1) N-terminal amplification

KSH01 F'-Ndc80-KanR	TCT TAT AAA TCT TTA TGA ATT TTG
NHT016 -aa280-R	CGT ACT TTT TAA AGC TTC TGT

2) C-terminal amplification

KSH21 F'-Ndc80 (807)	GTTCGCACATATCATTTGTAC

KSH02 R'-Ndc80-KanR	TAA ATT TTG AAC TAC TTT CAG C
3) fusion	
AEK04-F'-Ndc80(-476)	GCA GAT TAA AAT GAT ACC GAT TG
AEK05-R'-Ndc80(2265)	GTC GTG TAT ATG ATG TAT AAA AAC G

For site directed mutagenesis of *ndc80-AK01*:

1) For N-terminus	
AEK087-Ndc80-Ak01 ttg->ctg-F	CGCACATATCATTTGTACCCTGATGAATCACCCGAAGAAA
AEK05-R'-Ndc80(2265)	GTC GTG TAT ATG ATG TAT AAA AAC G
2) For C-terminus	
AEK04-F'-Ndc80(-476)	GCA GAT TAA AAT GAT ACC GAT TG
AEK088-Ndc80-AK01 ttg->ctg-R	TTTCTTCGGGTGATTCATCAGGGTACAAATGATATGTGCG
3) For fusion	
AEK091-Ndc80-F (5UTR-453)	ttatatatagcattatgttcaaaatgattgaat
AEK092-Ndc80-R (3UTR-227)	ttaaaatctgcaatcaataaaatatctgg

For tagging *mph1*:

AEK113-Mph1-tagging-F	GTAAGCACAAGCGATTAAATAAGGAACTTATTGATAGCATGGCTTATGATTGCGTTAGCAATTTACGAAAAATGCCAGAACGGATCCCCGGGTTAATTAA
AEK114-Mph1-tagging-R	CATTAAGAAACTCGTATGATGTTTGGGAAACTTTGTAAAAGATAAAACCTTTTTAAGAATAATCGGAAAATTTAGTGCCTGAATTCGAGCTCGTTTAAAC

For cloning *ndc80*, *mad2* and *mph1* to plasmids:

For *ndc80* :	
KSH03 F'-Ndc80 (NdeI)	CTG CAT ATG CAA GAT TCT TCC TCT
KSH04 R'-Ndc80 (BamHI)	TTT GGA TCC TTA CAG TTC CGA AC
For *mad2* :	
AEK037-Mad2-F (5UTR-212)	GAG ATA GTG AAA TGA GTT TAA AAT GAC AGA TTA GTT ACT TTC AAG
AEK040-Mad2-R (3UTR 114)	TTC ACC GAA TTA TAG TTA AAC AAT ATG GCC GGA ATT TTG AGA TTT
AEK103-Mad2-BamHI-R	AAA CAA GGA TCC CTA AG GAT TCA CTC GATATGC

	CACAAC GTCGAC A
AEK115-Mad2-SalI-F	ATGTCTAGCGTTCCCATAAGA
For *mph1* :	
AEK025-Mph1-R' (3'UTR 202)	GATATCAGGGGCCATATAATATGTGGTTCATTAA TC
AEK026-Mph1-F(5UTR -82)	ACG AAG TAA AAA TTT ATT GAT TAA CGC TTA ACA AAC AGT TGG AAA TTG GAA
AEK105-Mph1-XmaI-R	GCCTCCCGGGCTATTCTGGCATTTTTCGTAAATT GCTAA
AEK116-Mph1-SalI-F	ACGCGTCGACA ATG TCTAAGCGCA ATCCTCCTGT
For InFusion cloning:	
AEK121-pREP1 NdeI-GFP InF-GFP	CTTTGTTAAATCATATGAGTAAAGGAGAAGAACT T
AEK122-pREP1 Mad2-BamHI InF R	TTTTACCCGGGGATCCCTAAGGATTCACTCGATA TGCAAC
AEK123-pREP1 Mph1-BamHI InF R	TTTTACCCGGGGATCCCTATTCTGGCATTTTTCGT

For *ndc80* truncations of linker region:

AEK044-F (Ndc80-d211-269)	GTT TCA CTA ATT CAA TGC ACT GAA TAC AAT CAG ACA
AEK045-R (Ndc80-d211-269)	CGT ACT TTT TAA AGC TTC TGT CTG ATT GTA TTC AGT GCA TTG
AEK046-F (Ndc80-d211-248)	GTT GTT TCA CTA ATT CAA TGC ACT GAA TCA CCC GAA GAA AGT GAA
AEK047-R (Ndc80-d211-248)	CTC TGG TTC ACT TTC TTC GGG TGA TTC AGT GCA TTG
AEK048-F (Ndc80-d249-269)	TAT CAT TTG TAC CTT GAT GAA TAC AAT CAG ACA GAA
AEK049-R (Ndc80-d249-269)	CGT ACT TTT TAA AGC TTC TGT CTG ATT GTA TTC ATC AAG GTA CAA

Chapter 3. Isolation of *ndc80* mutants

In the current chapter I carried the mutagenesis screening of Ndc80 protein. I isolated and characterised in depth an *ndc80* mutant, which is sensitive to microtubule drugs.

3.1 Screening for *ndc80* temperature and thiabendazole sensitive mutants

The *ndc80*$^{+}$ gene is essential for cell viability (Hsu and Toda, 2011, Kim et al., 2010) and so it is not possible to construct a deletion strain of the *ndc80*$^{+}$ gene. Yeast genetics offer an alternative method - conditional mutants of the gene, which permit specific dissection of the functional differences between different Ndc80 domains. Ndc80 was shown to be involved in kinetochore capture as well as spindle assembly checkpoint signalling. Thus, single point mutations are beneficial for distinguishing the specific functions of Ndc80 regions in interaction with microtubules or checkpoint signalling (Cheeseman et al., 2006, Martin-Lluesma et al., 2002, McCleland et al., 2003, DeLuca et al., 2006). In my work, we wanted to address the role of the N-terminal domains of Ndc80. The unstructured N-tail, essential in fission yeast, but not in budding yeast (Kemmler et al., 2009, Akiyoshi et al., 2009, Hsu and Toda, 2011) is highly regulated by Aurora B/Ark1 phosphorylation, which in turn regulates electrostatic interactions with microtubules (Cheeseman et al., 2004, DeLuca et al., 2006, Ciferri et al., 2008). The calponin homology (CH) domain is another region of interest; it interacts with microtubules and is phosphorylated by Aurora B/Ark1 and other kinases in human cells (Alushin et al., 2012, Sundin et al., 2011, Chen et al., 2002). The linker region of Ndc80 has been uncharacterised up until now. These functional domains of Ndc80, being in the close proximity of microtubules and subjected to tight regulation, are interesting candidates for the control of mitotic progression and proper kinetochore-microtubule attachments.

The conditional mutants I isolated are sensitive to temperature and/or thiabendazole (TBZ). Temperature sensitive mutants grow normally at the permissive temperature of 27˚C, but show defective phenotypes at the restrictive temperature of 36˚C. TBZ is microtubule-depolymerising drug whose activity results in faulty kinetochore-microtubule attachments, which can be monitored by the spindle assembly checkpoint.

The TBZ-sensitive *ndc80* mutants may have either reduced microtubule-binding activities or defective checkpoint signalling. Therefore the TBZ-sensitive mutants were screened based on cell death on YE5S plates containing 10 μg/ml TBZ.

Briefly, we used an error-prone polymerase chain reaction (PCR) with a 10 times excess of deoxyguanosine triphosphate (dGTP) and Vent DNA polymerase to randomly mutagenise the N-terminal region of *ndc80*$^{+}$ gene. The PCR products were then fused to wild-type C-terminus of *ndc80*$^{+}$ gene with kanamycin resistance marker and then transformed into wild type (513) strain. Due to the presence of homologous 5' (460bp upstream) and 3' (315bp downstream) regions of the *ndc80* locus, the mutagenised gene can replace the endogenous allele and be selected for based on kanamycin resistance. The cells were initially plated on YE5S plates at 27˚C, to enable efficient more homologous recombination and after 3 days replica plated to kanamycin selection plates. Following that, replica plating was made to YE5S with Phloxine B plates at permissive (27˚C) and restrictive (36˚C) temperatures, and YE5S with TBZ (10μg/ml) plates at 27˚C. The selection was based on the colonies growth between selection and normal growth conditions. The experimental scheme of the mutant isolation procedure is shown in Figure 3.1.

Five independent sets of screenings yielded a total of 8,000-10,000 colonies for analysis. Overall, 5 candidate mutants were isolated for further study. The number of isolated mutants was expected to be higher, but probably due to short size of the N-terminal fragment that was mutagenised (1.7kb), the frequency of mutations was lower. Alternatively, it is also possible that conditional mutations in the N-tail are infrequent. The *ndc80* mutant screening, performed by previous lab members, involving error-prone PCRs of the entire *ndc80*$^{+}$ gene (1,875bp), resulted in 12 (Kuo-Shun Hsu) and 18 mutants (Ngang Heok Tang). Of these, 30% of isolated mutants showed mutations in the N-terminus of the *ndc80* gene (unpublished data). All the *ndc80* mutants isolated in this study were backcrossed to wild type to eliminate the chances of extragenic mutations as the cause of phenotypes.

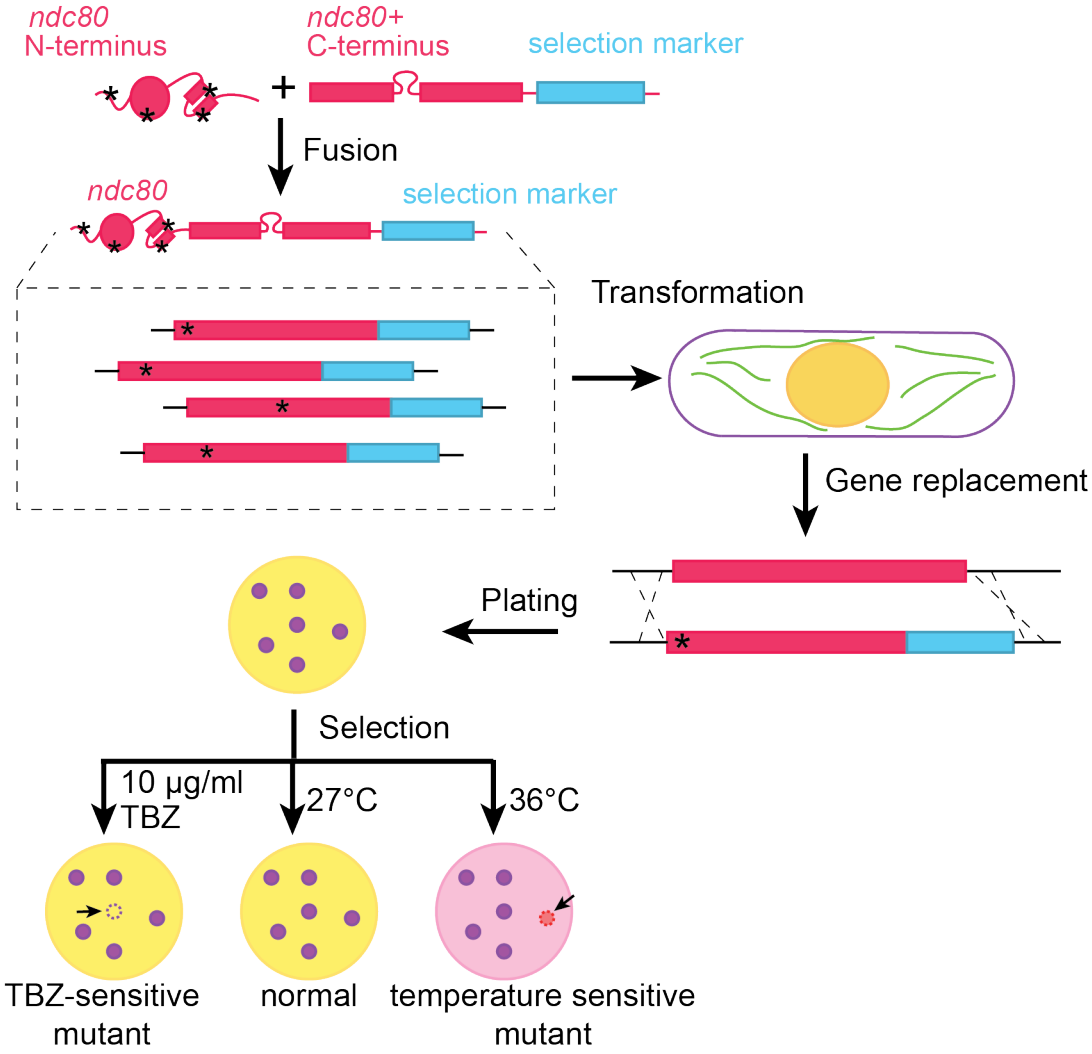

Figure 3.1. Temperature/TBZ sensitive mutant isolation

The randomly mutagenised N-terminal fragment of the *ndc80* gene was fused with a C-terminal construct containing a kanamycin selection marker. Asterisks represent introduced mutations, which were then transformed into wild type fission yeast cells. The endogenous *ndc80*$^{+}$ gene should be replaced by the mutated *ndc80-kan*^{R} through homologous recombination. Transformants were plated on YE5S plates at 27˚C, and after 24 hours they were replica plated onto kanamycin plates. After 4 days, cells were again replica plated to selection plates – YE5S containing Phloxine B placed at permissive (27˚C) and restrictive (36˚C) temperatures or YE5S with 10 µg/ml TBZ at 27˚C. Temperature sensitive mutants cannot grow at the restrictive temperature, while TBZ sensitive mutants cannot grow on TBZ plates.

3.2 Characterisation and analysis of isolated *ndc80* mutants

The difference between temperature and TBZ sensitivity of *ndc80* mutants was determined by serial dilution spot tests. 5 x 10^4 cells were spotted on the first lane

followed by 10-fold dilutions in consecutive lanes. The candidate strains were spotted on YE5S containing Phloxine B, which stains dead cells dark red (see Materials and Methods). The plates were incubated at temperatures ranging from 27˚C to 36˚C and observed after 3 days. The TBZ sensitivity of *ndc80* mutants was checked on YE5S plates containing 5, 7.5, 10, 12.5, 15 and 20 μg/ml of TBZ grown at 27˚C for 3 days (Figure 3.2).

Using the above-mentioned approach, I have isolated five *ndc80* mutants. In brief, *ndc80-AK02*, *ndc80-AK03* and *ndc80-AK04* are both temperature and TBZ sensitive with varying degrees. *ndc80-AK02* is a strong ts-mutant, *ndc80-AK03* shows mild sensitivity and *ndc80-AK04* has an intermediate temperature sensitivity. They also show TBZ sensitivity. *ndc80-AK02* is a strong TBZ-sensitive mutant whereas *ndc80-AK03* and *ndc80-AK04* are intermediate. On the other hand, *ndc80-AK01* and *ndc80-AK05* show TBZ but not temperature sensitivity. *ndc80-AK01* and *ndc80-AK05* show strong TBZ-sensitivity comparable to the *mad1* deletion (Figure 3.2).

TBZ is a microtubule-depolymerising agent that destroys mitotic spindles, leading to unattached kinetochores, hence spindle assembly checkpoint activation. If the checkpoint signalling is defective, untimely mitotic progression leads to premature cytokinesis with improperly segregated chromosomes. In the presence of a destabilising drug, these defects are exhibited as impaired growth, when compared to the wild type. Notably, the initial identification of checkpoint components in budding yeast also relied on a microtubule-depolymerising drug benomyl (Li and Murray, 1991, Roberts et al., 1994, Hardwick and Murray, 1995).

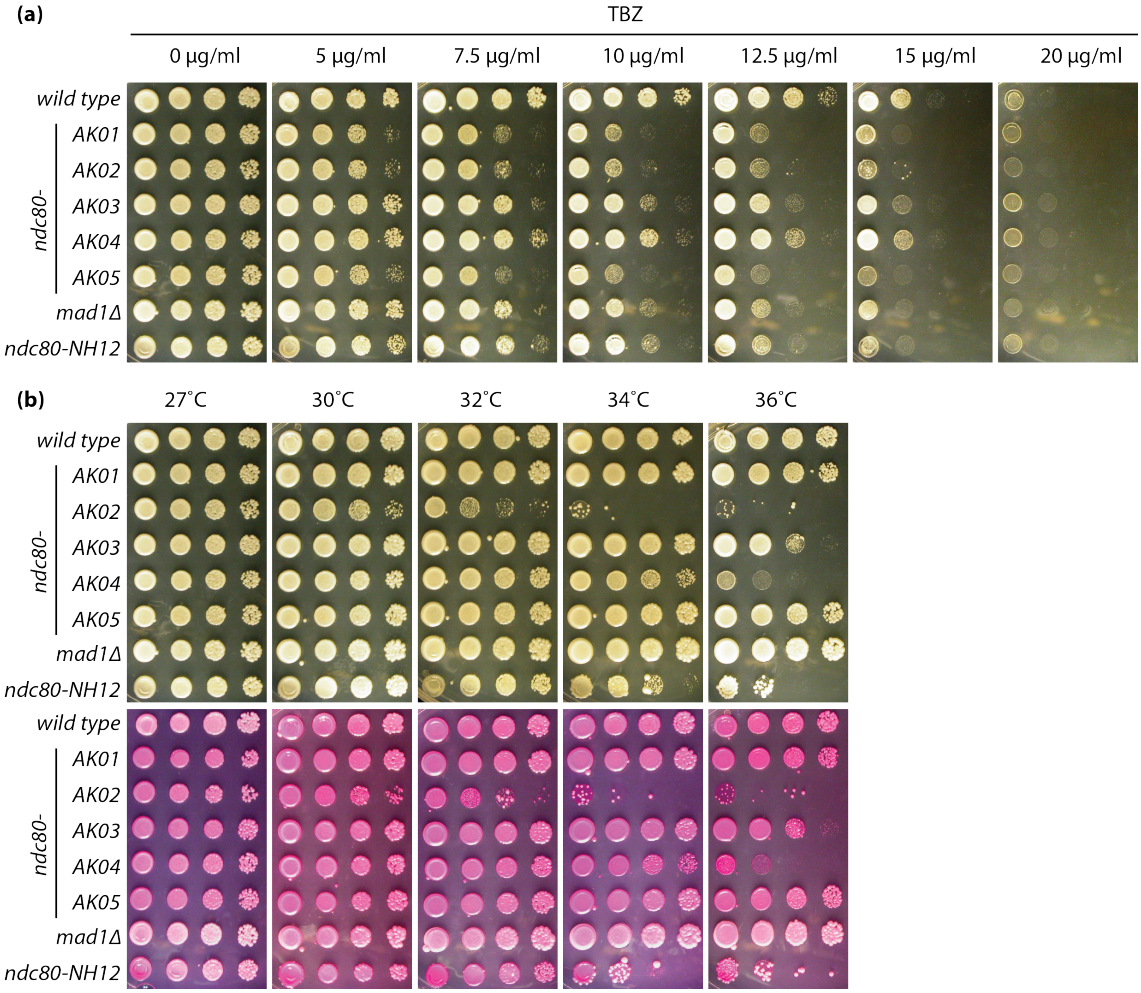

Figure 3.2. Serial dilution spot assay for temperature and TBZ sensitivity of isolated *ndc80* mutants.

The five candidates isolated in the screening of 8,000-10,000 clones were tested for temperature (b) and TBZ sensitivity (a) by serial dilution assays. Spot tests (5 x 10^4 cells in the first spot were followed by 10-fold dilutions subsequently) were performed (a) Cells were plated on YE5S containing indicated concentrations of TBZ for 3 days at 27˚C. (b) Cells were plated on YE5S in the presence (red) and absence of Phloxine B. Plates were incubated at the indicated temperatures for 3 days.

3.3 Sequencing of *ndc80* mutants and homology alignments

The phylogenetic tree of Ndc80 reveals that the protein is highly conserved in virtually all the organisms (Figure 3.3). When looking at the sequence homology the N-terminus of Ndc80 is also well conserved, especially the CH domain. Furthermore, the crystal structure of human Hec1/Ndc80 has been solved (Ciferri et al., 2008). The same function of the CH domain in the microtubule binding was confirmed in budding and fission yeast as well as humans (Sundin et al., 2011, Alushin et al., 2010, Wilson-Kubalek et al., 2008, Tooley and Stukenberg, 2011, Yamagishi et al., 2014, Cheeseman, 2014).

The *ndc80* genes of candidate mutants were sequenced to determine which domain of the protein might be responsible for the sensitivity to temperature and/or TBZ (Figure 3.2).

We isolated two mutations *ndc80-AK02* (N281D) and *ndc80-AK04* (L547P) in the coiled-coil domain of Ndc80. They both show temperature and TBZ sensitivity. The mutation in *ndc80-AK04* is not aimed for our screening, as the random mutagenesis of the N-terminal region was only carried only until residue 302. But it is possible that PCR fragments containing the 302th amino acid, which was not intended to be error-prone, contained this mutation.

ndc80-AK03 has a mutation in the highly conserved CH region - R183G. This mutation in the αF helix changes the polar arginine residue to a non-polar glycine, possibly reducing a binding affinity of the Ndc80 complex to the microtubules. The calponin homology domain sequence is highly conserved among species (Figure 3.4). *ndc80-AK03* mutant exhibits TBZ sensitivity and weak temperature sensitivity.

ndc80-AK01 contains a mutation at the position L246P. This mutation introduces a change from a hydrophobic residue to the helix-breaking residue (proline). This site is located in the αH helix of the uncharacterised Ndc80 linker region, which is in large conserved among species – hydrophobic in *H sapiens* (methionine), *X. laevis*

(methionine), *S. pombe* (leucine) and *S. cerevisiae* (leucine) (Figure 3.4). According to the PISA method (which determines residues in close proximity, based on salt bridges, hydrogen bridges formation, a distance of less than 4 Å away) (Ciferri et al., 2008, Krissinel and Henrick, 2007), the residue in this position in human Hec1/Ndc80 is in contact with the Nuf2 protein.

The last mutant *ndc80-AK05* (N272D) also has a mutation at the end of the linker region, at the beginning of the αJ domain. Both budding and fission yeasts have a polar uncharged asparagine at this site, whereas *X. laevis* and *D. melanogaster* have non-polar residues (Figure 3.4). Both *ndc80-AK01* and *ndc80-AK05* have shown only TBZ sensitivity, indicating the potential novel function of the linker region that needs to be investigated further.

To better visualise the mutations sites of *ndc80-AK01, ndc80-AK03* and *ndc80-AK05,* they were marked on the human "bonsai" Ndc80 complex crystal structure (Figure 3.5). All information regarding the mutations is summarised on Figure 3.6.

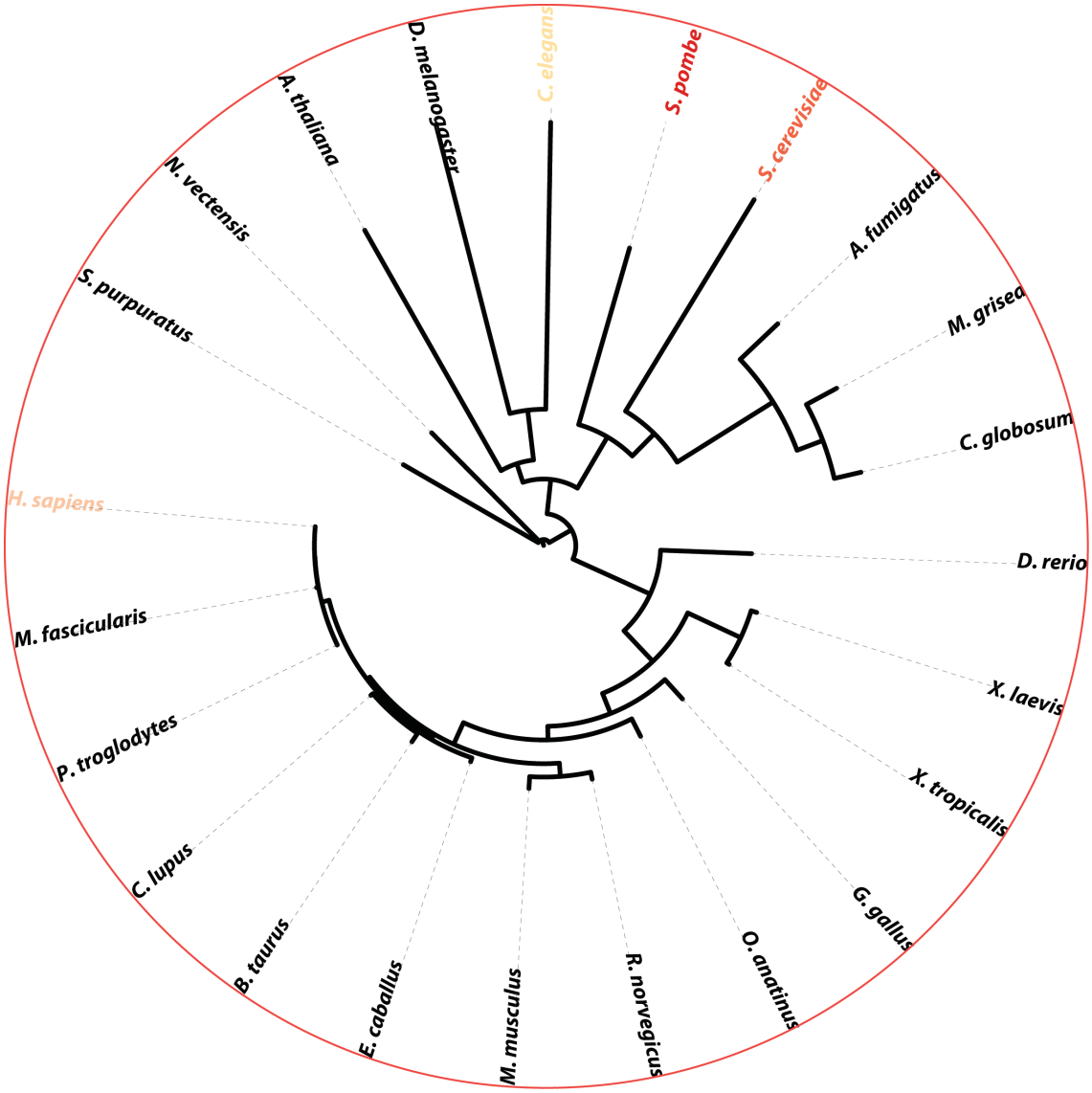

Figure 3.3. Evolutionary relation between Ndc80 and its homologues

Phylogram representing the evolutionary relationships among eukaryotic Ndc80 proteins. A maximal likelihood unrooted tree was made using ClustalW multiple alignments (Larkin et al., 2007) in PHYLIP (Felsenstein, 1989). The radial rendering was carried out with iTOL (Letunic and Bork, 2011). The excavate *S.purpuratus* was an outgroup (top left corner), from which one in a clockwise direction taxa fan out. The scale bar represents one unit of evolutionary distance along the branches according to computed Jones-Taylor-Thornton method (Jones et al., 1992).

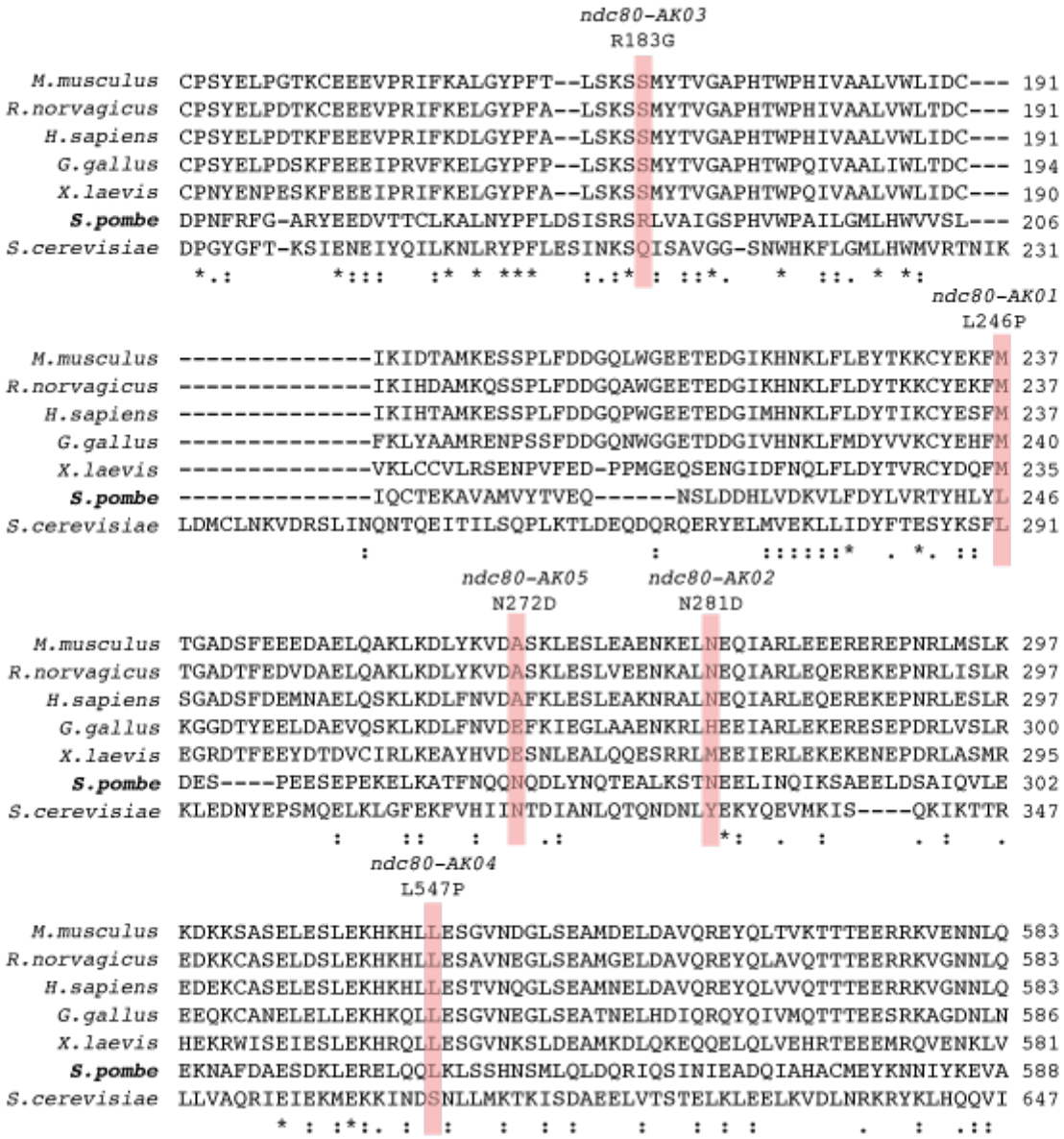

Figure 3.4. The amino acid alignment of Ndc80 proteins from different organisms

Sequences were obtained from UniProt database (http://www.uniprot.org/uniprot/?query=ndc80&sort=score) and were aligned using ClustalX online (http://www.ebi.ac.uk/Tools/msa/clustalw2/) . Sequences of Ndc80 from 7 different species were aligned: *M. musculus, R. norvagicus, H. sapiens, G. gallus, X. laevis, S. pombe* and *S. cerevisiae*. Only the regions surrounding *ndc80* mutant alleles are presented.

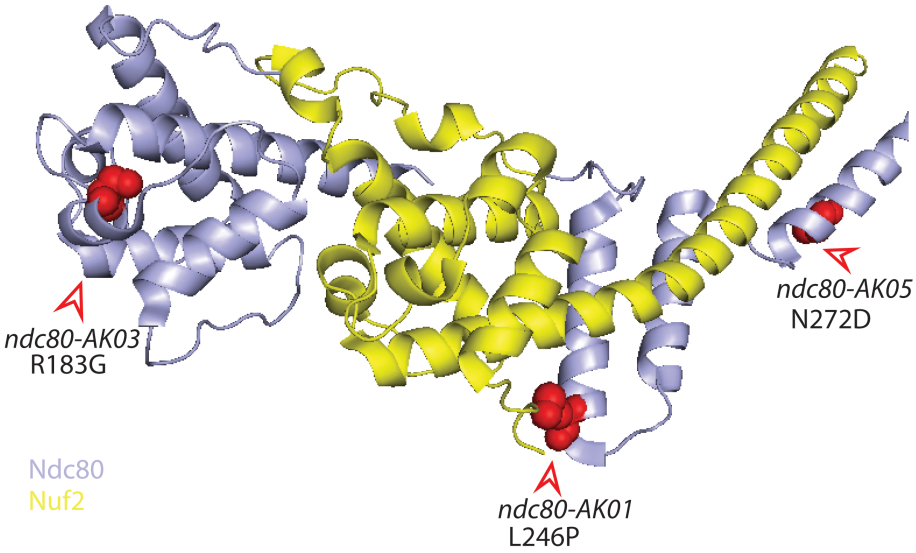

Figure 3.5. The location of the *ndc80* mutation sites in human "bonsai" Ndc80 complex.

The crystalised structure of the human Ndc80 "bonsai" complex is shown together with positions of mutated amino acids. This complex consists of a heterodimer comprising two chimeric proteins, Ndc80-Spc25 and Nuf2-Spc24, which contain calponin homology domains and shortened coiled-coil regions (Ciferri et al., 2008). Only Ndc80 (blue) and Nuf2 (yellow) proteins are shown on the scheme. The mutation sites (red ball and stick structures, indicated with red arrowheads) were marked based on the homology alignments to human Ndc80/Hec1. R183G in *ndc80-AK03* is located in calponin homology domain and is buried inside the structure. L246P in *ndc80-AK01* is located in the linker region at αH, in the proximity of unstructured regions of Nuf2. N272D in *ndc80-AK05* on the other hand is located at the beginning of the coiled-coil region of Ndc80. RCSB accession number: 2VE7.

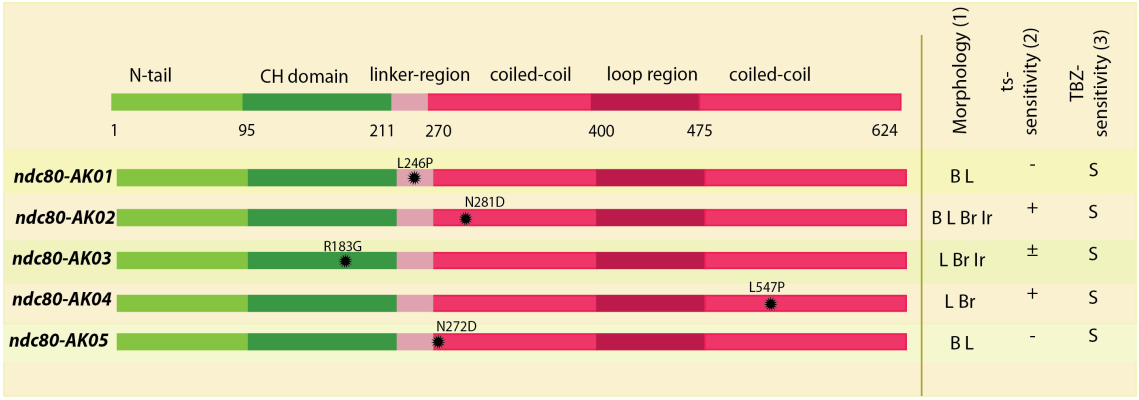

Figure 3.6. Summary of *ndc80* mutants initial assessment.

Schemes of Ndc80 protein domains are shown. The mutation site in each *ndc80* mutant was marked. Cell morphology, temperature sensitivity and TBZ sensitivity were recorded and marked according to the legend:
(1) Morphology was recorded: B- big, L- long, Br – branched, Ir – irregular;
(2) ts-sensitivity: + -strong, ± - moderate, - - none;
(3) TBZ sensitivity: S – sensitive.

3.4 Initial characterisation and classification of isolated *ndc80* mutants

To help an initial classification of isolated mutants in terms of defective phenotypes, I have checked the cellular morphology, the growth curves and the viability of cells of each mutant.

3.4.1 Analysis of growth in liquid cultures

To confirm the defects observed on the serial dilution assay, liquid culture analysis was conducted to determine the appearance of the growth defects in media over several hours. Cells were cultured overnight in YE5S media and split in two, each with the cell counts of 2 x 10^6 cells/ml. The cells were then placed in the permissive or restrictive conditions. For the temperature shift, there is a clear growth defect in *ndc80-AK02*, *ndc80-AK03* and *ndc80-AK04* (Figure 3.7). As *ndc80-AK02* and *ndc80-AK04* mutants occur in the coiled-coil region, these mutants will not be studied any further. Only their initial characterisation was carried out (growth curves, morphology observations and spotting assays) (Figure 3.2, Figure 3.4, Figure 3.7 and Figure 3.9).

The mutants of interest for further analysis have mutations in the calponin homology domain (*ndc80-AK03*) and the uncharacterised linker region (*ndc80-AK01* and *ndc80-AK05*). The linker region mutants grow as well as wild type at 36˚C, whereas *ndc80-AK03* does not (Figure 3.7). Next, we tested the growth of mutants in YE5S liquid culture in the presence of 50 μg/ml TBZ, starting at 4 x 10^6 cells/ml. The mutants grew slower than wild type in the presence of TBZ (Figure 3.8). The snapshots of their phenotypes are shown in Figure 3.9. To further characterise *ndc80* mutants, I tested cell viability in liquid culture in presence of TBZ by a plating assay (Figure 3.10).

3.4.2 Cell morphology

The morphology of mutant cells under the restrictive conditions was observed. Mutant cells were collected in their exponential growth phase and observed after 3 hours in liquid culture at 36˚C. *ndc80-AK01*, *ndc80-AK03* and *ndc80-AK05* mutants, liquid

cultures were also observed in the presence of 50 μg/ml TBZ. Cells were bigger and longer after 150 min under restrictive conditions and were occasionally branched (Figure 3.9). Their morphologies are summarised in Figure 3.6.

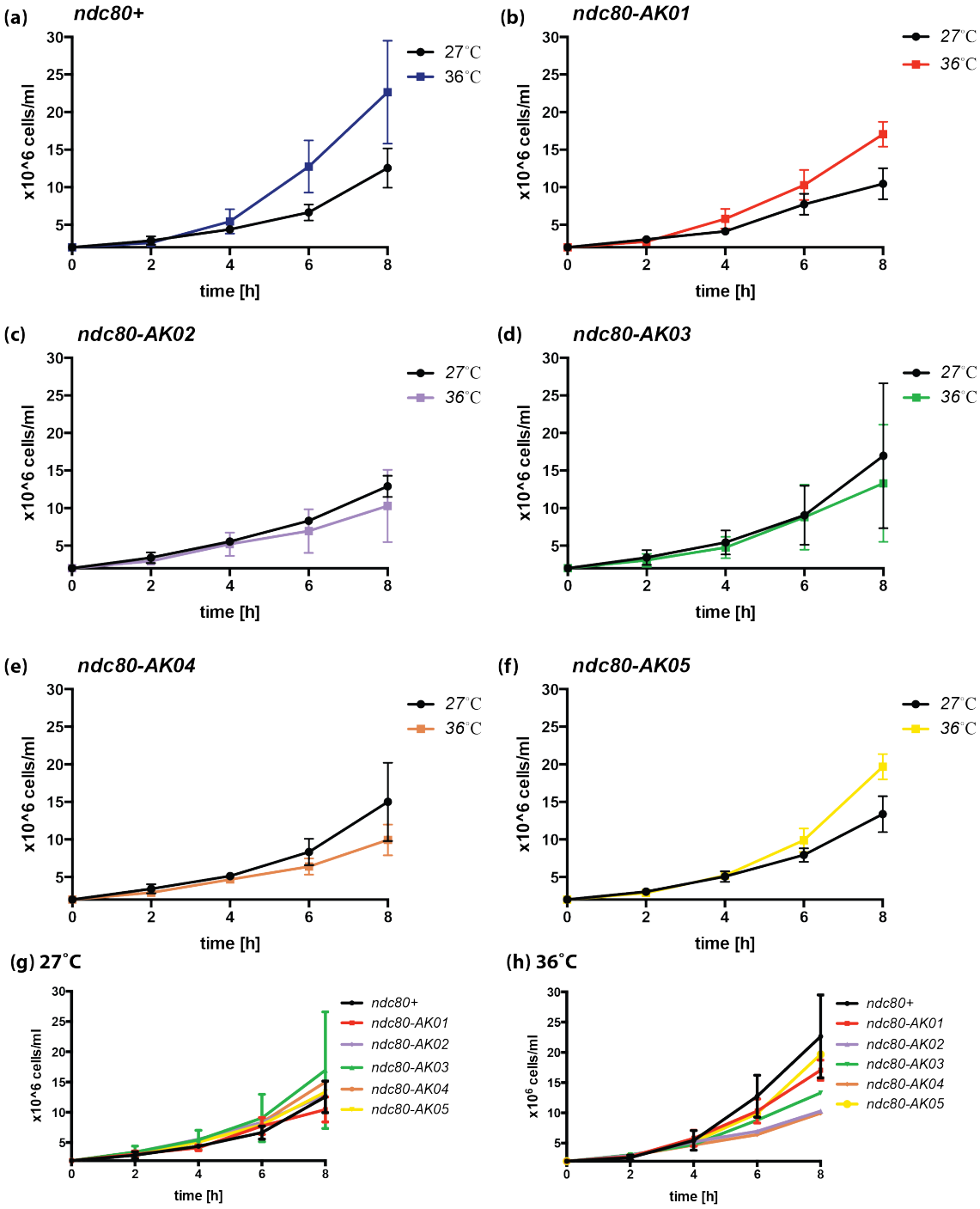

Figure 3.7. Growth curves of *ndc80* mutants.

Cells grown overnight in YE5S medium were diluted into two identical cultures at the concentration of 2 x 10^6 cells/ml. One culture was placed at 27˚C and the other was

(Legend to Figure 3.7 continued)
shifted up to 36˚C. Cell numbers were counted every 2 hours. (a)-(f) Individual mutant compared to *ndc80*$^{+}$. Combined mutant growth curves at 27˚C (g) and 36˚C (h).

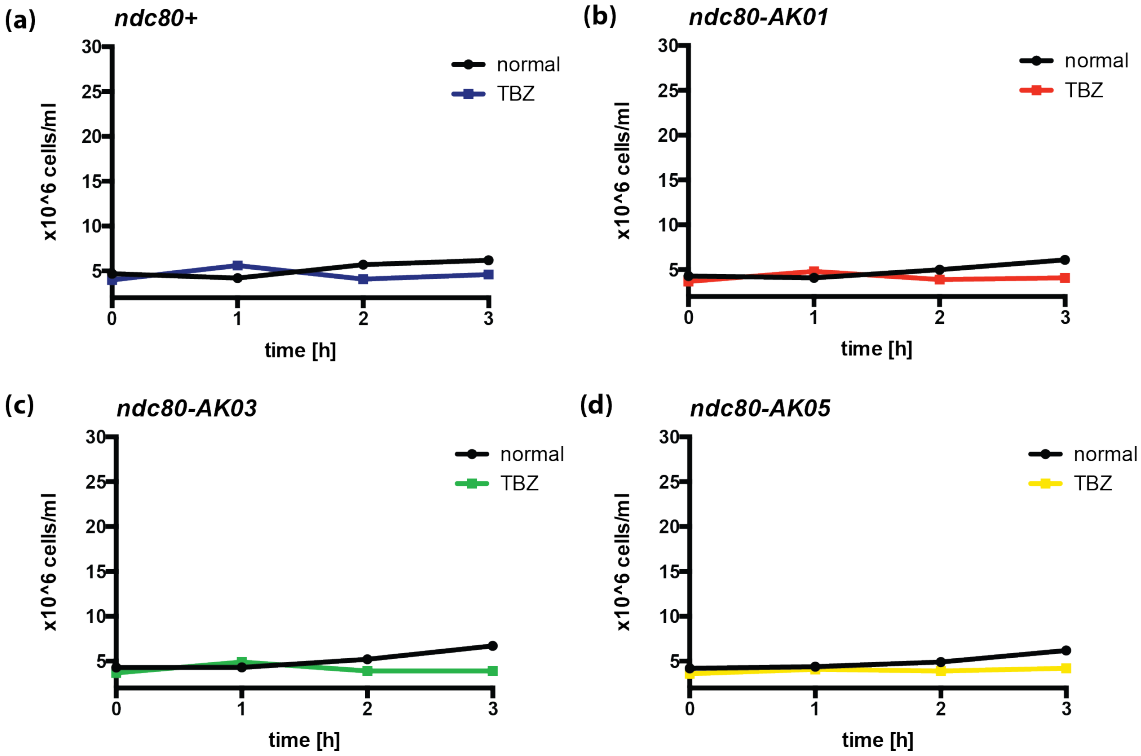

Figure 3.8. Growth curves of *ndc80* mutants in TBZ conditions.

Cells grown overnight in rich medium were split into two identical cultures at a concentration of 4 x 10^6 cells/ml. To one culture 50 µg/ml TBZ was added and the other culture was left drug-free. Both cultures were then placed at 27˚C. Cells were counted every hour.

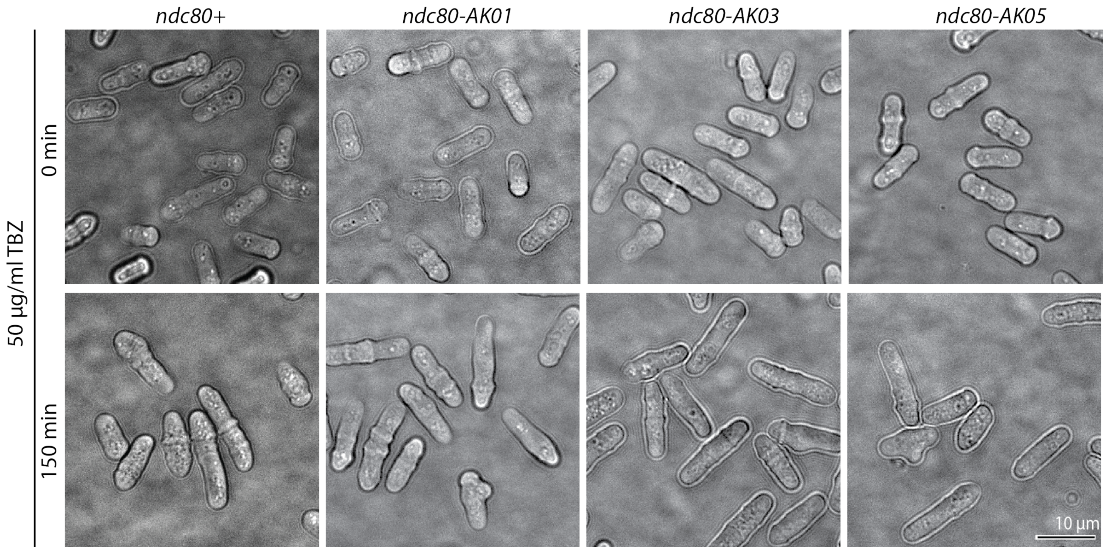

Figure 3.9. Morphology of *ndc80* mutants in permissive and restrictive conditions.

Observations of *ndc80* mutants under permissive and restrictive conditions. *ndc80-AK01, ndc80-AK03* and *ndc80-AK05* were grown overnight at 27˚C and then the exponential growing cells were split into two. One was placed at 27˚C and the other in restrictive conditions in the presence of 50 µg/ml TBZ. The samples were fixed with 1.6% PFA after 150 min in the presence of drugs. Scale bar, 10 µm.

3.4.3 Analysis of cell viability of *ndc80* mutants

To confirm *ndc80-AK01, ndc80-AK03* and *ndc80-AK05* mutants' hypersensitivity to TBZ when grown on plates, a cell viability test was carried out. Cells grown overnight in rich medium were diluted to 2 x 10^6 cells/ml and cultured in YE5S medium containing 50 µg/ml TBZ. Samples were taken hourly during 4 hours and plated onto YE5S plates at 200-500 cells per plate. Viability was calculated for each time point as a percentage from the number of colonies growing in TBZ against those grown at 0 hours. Figure 3.10 shows that in the presence of TBZ, the viability of wild type cells fluctuates around the same levels (95-100%). The viability of control *mad1*Δ declines over long exposure to the drug - after 3 and 4 hours in TBZ, the number of surviving colonies falls by 60% and 70% respectively *ndc80-AK01* and *ndc80-AK05* also have a clear decline in viability from 1 hour onwards. After 4 hours, less than 50% of colonies remain in *ndc80-AK01, ndc80-AK03* and *ndc80-AK05*. All mutants, similar to *mad1*Δ are unable to arrest in mitosis, induced by microtubule poisons, suggesting the defect in spindle assembly checkpoint activation. The initial identification of spindle assembly

checkpoint components in budding yeast was also utilised a growth viability test and serial dilution assays in the presence of benomyl (Li and Murray, 1991, Roberts et al., 1994, Hardwick and Murray, 1995).

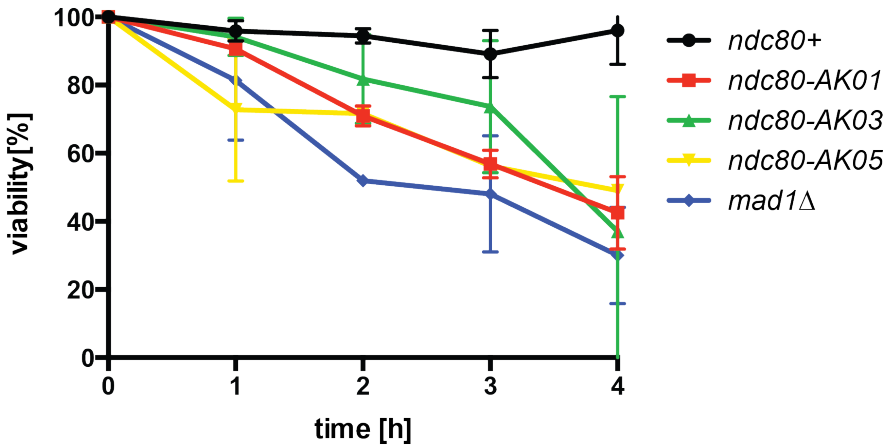

Figure 3.10. Viability test of *ndc80* mutants in the presence of a microtubule drug.
Overnight cell cultures grown in YE5S at 27˚C were diluted to 2 x 10^6 cells/ml. The cells were placed into YE5S containing 50 µg/ml TBZ. Cells were counted every hour and 200-500 cells were plated on YE5S plates and incubated at 27˚. After 3 days the number of viable colonies was counted and viability calculated against the cell number.

3.5 The Ndc80 complex is intact in mutant backgrounds

Before proceeding into further phenotypic characterisation of the potential checkpoint-defective mutants, it is critical to check if the structure of the Ndc80 complex is not impaired by *ndc80* mutant alleles. Examination of other Ndc80 tetramer complex components Nuf2-mCherry and Spc25-YFP by imaging will allude to any problems in complex formation or stability.

3.5.1 Integrity of the Ndc80 complex in mutant background is not impaired

To address the question of complex integrity in mutant strains, Nuf2-mCherry and Spc25-YFP were introduced. Mutant cells expressing the fluorescent Ndc80 complex were grown overnight then diluted to 2 x 10^6 cells/ml for synchronisation at S-phase by 12.5mM hydroxyurea (HU). After 4 hours at 25˚C, HU was washed out and the cells were released into rich media with 50 µg/ml TBZ and 60 µg/ml of carbendazim (CBZ),

another microtubule destabilising drug (Yamagishi et al., 2012), for 3 hours, followed by fixation in 1.6% PFA. As shown in Figure 3.11, Spc25 and Nuf2 colocalise in both WT and mutant cells. Also, there is no statistically significant difference of Nuf2 and Spc25 signal intensity between WT and mutant cells. The strains also expressed Cut12-2CFP, marking the SPB, to further verify that protein expression levels are the same in mutants (data not shown). These data indicate that the Ndc80 complexes are intact in mutant backgrounds.

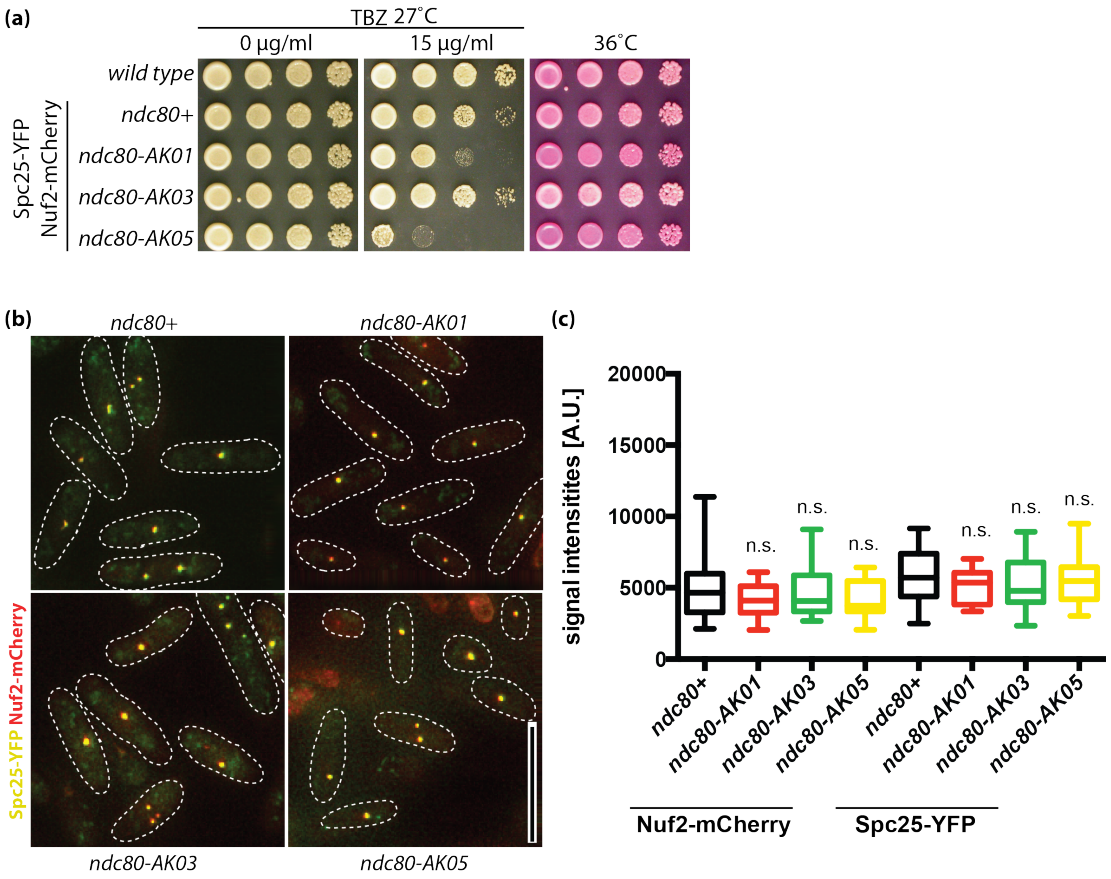

Figure 3.11. Stability of the Ndc80 complex is intact in mutant backgrounds

Exponentially growing cells (4x10^6 cells/ml) were synchronized in early S phase with 12.5mM hydroxyurea (HU) at 25˚C for 4 hours and then released into HU-free media containing 50 µg/ml TBZ and 60 µg/ml carbendazim (CBZ) at 27˚C. Samples were fixed with 1.6% PFA and visualised after 180 minutes using Spc25-YFP and Nuf2-mCherry. (a) A serial dilution assay of strains used in the current study. The number of initial spot cells (far-left) was 5 x 10^4 cells. Cells were plated on YE5S, YE5S containing 15 µg/ml TBZ at 27˚C and YE5S containing Phloxine B at 36˚C. (b) Representative images showing the integrity of the Ndc80 complex The Spc25-YFP and Nuf2-mCherry were visualised. n>200 cells for examination, in the current study. Scale bar, 10 µm. (c) Quantification of signal intensities in >20 cells. An unpaired t-test shows no significant differences (n.s.) between the wild type and mutant *ndc80* strains.

3.6 Characterisation of the *ndc80* mutants under mitotic arrest conditions

To further characterise the potential defect in spindle assembly checkpoint signalling in *ndc80-AK01, ndc80-AK03* and *ndc80-AK05,* I performed liquid culture experiments using three different mitotic arrest conditions. Firstly, using the microtubule drugs – TBZ/CBZ, I arrested the cells in mitosis. Secondly, the *cut7-446* kinesin-5 conditional mutant that is characterised by monopolar spindle formation and also arrests the cells in mitosis. Thirdly, *nda3* conditional mutants, where β-tubulin is impaired and cells can not form microtubules in restrictive conditions – at high (36˚C) or low temperature (19˚C), *nda3-1828* (Radcliffe et al., 1998) and *nda3-KM311* (Hiraoka et al., 1984) respectively and so I investigated *ndc80* mutant phenotypes under these conditions.

3.6.1 TBZ/CBZ

Firstly, I synchronised the cells in early S phase using HU, then washed out the drug and placed the cells in rich media containing 50 μg/ml TBZ and 60 μg/ml of CBZ, drugs that depolymerise microtubules (Yamagishi et al., 2012). Cells were collected every 30 min after 1 hour of incubation (Figure 3.12).

Cells exiting mitosis in the absence of microtubules can be identified by septum formation and accumulation of dead cells with improperly divided chromosomes, which can be visualised using Calcofluor staining. In the presence of microtubule depolymerizing drugs, wild type cells arrest at a mitotic stage as the spindle assembly checkpoint is activated. For the first 90 minutes, cells stay unseptated, but I start to observe the accumulation of cells exiting mitosis (with septum) (120-180 min) due to checkpoint silencing or slippage through the checkpoint. In contrast, the control *mad2*Δ strain has an inactive SAC and hence does not arrest in mitosis. Cells can exit mitosis prematurely with improper chromosome segregation, often resulting in cell death. *mad2*Δ cells exit mitosis prematurely, at 150 min 32% of cells have exited mitosis, in comparison to wild type where 10% have exited at this time point (Figure 3.12).

In *ndc80-AK01* and *ndc80-AK05* cells, a *mad2* deletion-like phenotype was observed (Figure 3.12a) - quantification shows that at 150 min, the percentage of septated/dead cells reached 32% and 28% respectively (Figure 3.12b). In contrast, *ndc80-AK03* showed 24% septated/dead cells at 0 min and this figure remained within this range throughout the experiment (Figure 3.12). Our results suggest that similar to a *mad2*-deletion, *ndc80-AK01* and *ndc80-AK05* cells are defective in spindle checkpoint activation or maintenance, while the *ndc80-AK03* phenotype may not be linked to the spindle checkpoint.

Since the septation phenotype is associated with mitotic exit, we decided to further characterise the *ndc80* mutant alleles using mitotic markers under the same growth conditions as above. First, Cut11-GFP was introduced into the mutant cells (Figure 3.13c). *cut11*$^{+}$ encodes an SPB-anchoring protein, which is homologous to budding yeast and human Ndc1. It localises to the nuclear envelope in interphase cells, and during mitosis it shows SPB localisation from early prophase to mid anaphase (West et al., 1998).

In a wild type strain, 2-4% of cells show a Cut11-GFP signal at the SPB from 0 to 90 min and their number increasing to 18% at 120 min and 30% at 180 min (Figure 3.13). These data suggest that at the entry into mitosis (around 120 min), the spindle checkpoint is active and cells with Cut11-GFP at the SPB accumulate at mitosis. In the case of *mad2*Δ, the cell numbers remained in the range of 0-15% throughout the duration of the experiment. These results are in accordance with our predictions, since there is no active spindle checkpoint and cells can exit mitosis. The mitotic cells' peak observed at 150 min corresponds to the increase in synchronised cells entering mitosis. *ndc80-AK01* and *ndc80-AK05* cells have very similar profiles to *mad2*Δ. In both cases, the number of mitotic cells was ranged from 2-8% during the entire experiment, showing high similarity to data from the *mad2*Δ control, albeit not identical. Similar to the previous septation experiment, the *ndc80-AK03* mutant had a relatively high percentage of mitotic cells (11%) already at 0 min and levels remained at a similar level throughout the experiment. The data from the Cut11-GFP experiment (Figure 3.13) is in accordance with the septation experiment (Figure 3.12).

In summary, the linker region mutants *ndc80-AK01* and *ndc80-AK05* so far behave similarly to the *mad2*Δ strain, indicative of a defect in SAC function, whereas *ndc80-AK03* behaves differently and appears to have another type of defects.

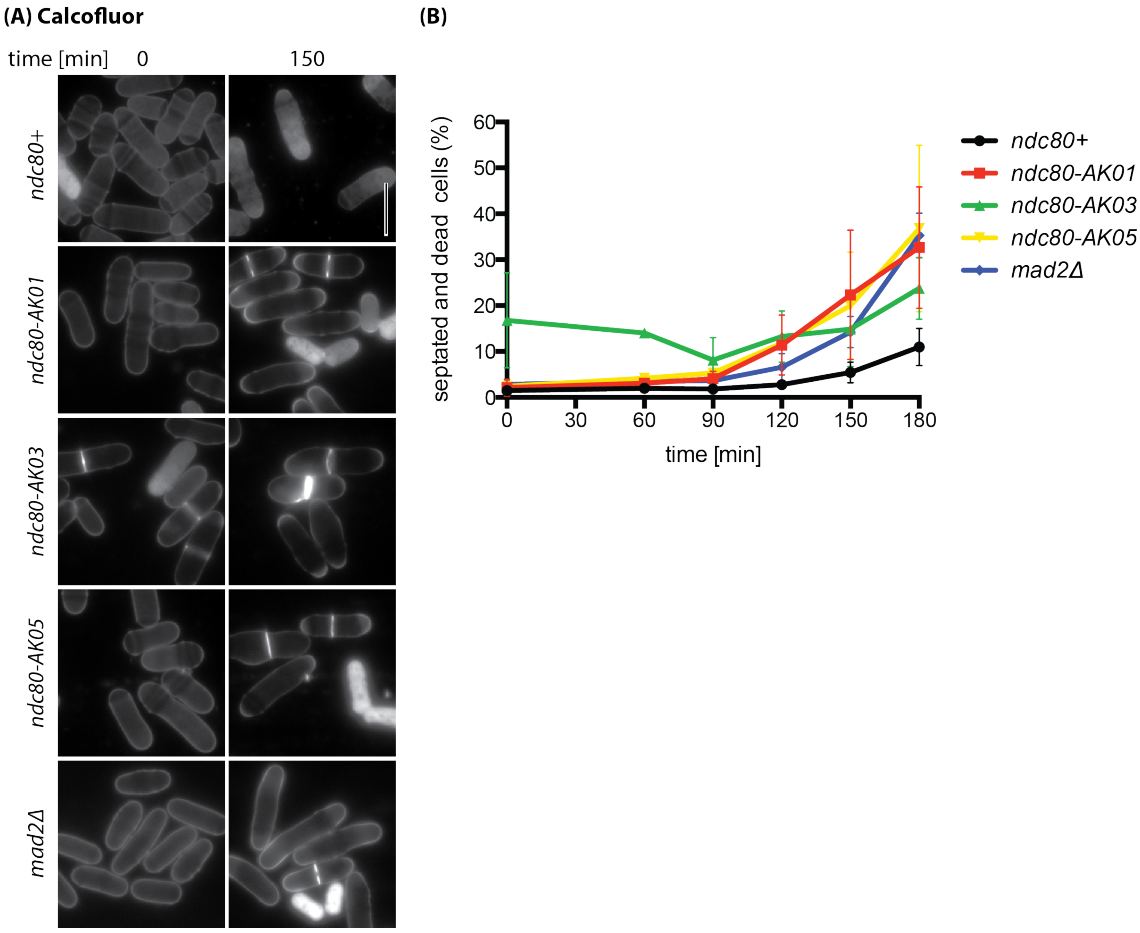

Figure 3.12. *ndc80* mutants are defective in spindle checkpoint activation.

Exponentially growing cells (4 x 10^6 cells/ml) were synchronised with 12.5mM HU at 25˚C for 4 hours. HU was then washed out and cells were placed in YE5S with 50 µg/ml TBZ and 60 µg/ml of CBZ at 27˚C. Samples were fixed with 1.6% PFA and stained with Calcofluor every 30 minutes during 3 hours of incubation. (A) The phenotypes of wild type, *ndc80-AK01, ndc80-AK03, ndc80-AK05* and *mad2*Δ are shown at 0 and 150 minutes. Septated and dead cells were observed in mutants. Scale bar, 10 µm. (B) Quantification of septated and dead cells during the experiment. 150 cells were counted for each time point. Values are averages from three repeats. Error bars represent standard deviations.

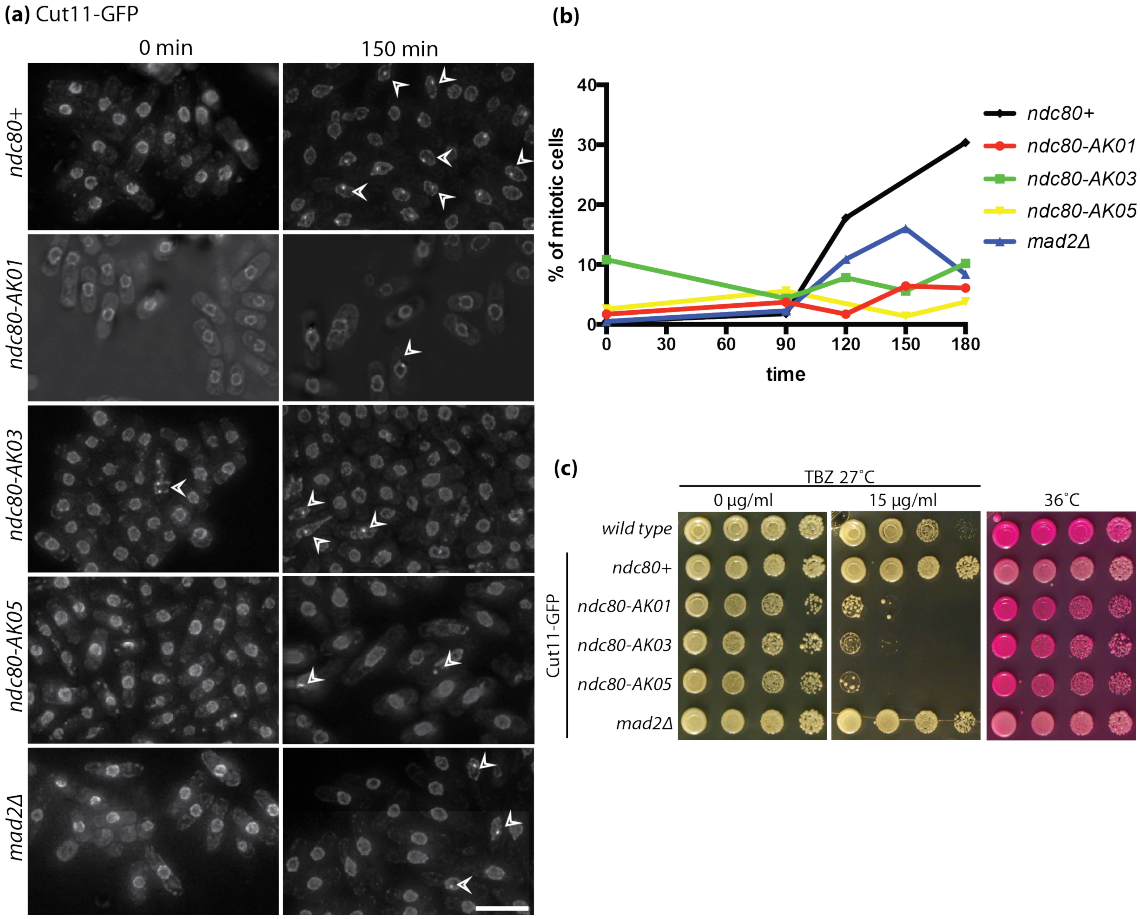

Figure 3.13. Cut11-GFP localisation in the *ndc80* mutants.

Exponentially growing cells (4 x 10^6 cells/ml) were synchronised using 12.5mM HU at 25˚C for 4 hours and then released into YE5S with 50 µg/ml TBZ and 60 µg/ml of CBZ at 27˚C. Samples were fixed with 1.6% PFA and Cut11-GFP localisation was observed every 30 minutes for 3 hours. The phenotypes (a) and their quantifications (b) for *ndc80* mutants, wild type and *mad2*Δ containing Cut11-GFP are shown. For each time point more than 150 cells were counted. The percentage of cells that displayed a cumulative Cut11-GFP signal accumulated at the SPB (indicated with white arrowheads) was calculated. The values are averages from two experiments. Scale bar, 10 µm. (c) The serial dilution assay of the strains used in the current study compared to wild type (513).

3.6.2 cut7-446

To further characterise the defective spindle checkpoint phenotypes, we decided to use a different method for inducing mitotic arrest. The *cut7*$^+$ gene encodes the kinesin-5 responsible for interdigitating and elongating mitotic spindles (Hagan and Yanagida, 1990). Temperature sensitive mutants (e.g. *cut7-446*) arrest with overcondensed chromosomes and display defective spindle formation at 36˚C (Hagan and Yanagida,

1990, Hagan and Yanagida, 1992). Therefore, c*ut7-446* mutants are recognised by the SAC, which delays mitotic progression (Kim et al., 1998).

The *ndc80* mutant alleles were crossed with *cut7-446* cells (Figure 3.14a) for imaging. Initial trials with Calcofluor staining, at the permissive temperature of 27˚C, and a long time-course experiment (6h) were unsuccessful. The optimised experimental conditions were subsequently established, including DAPI staining, the usage of lower permissive temperature (25˚C) and a shorter time-course (3.5h) with sample fixation every 40 min. 4',6-diamidino-2-phenylidole (DAPI) is a fluorescent dye that binds in the minor groove of DNA. In the *cut7-446* strain, after shift to restrictive conditions (36˚C), the cells are arrested in mitosis, which is observed with DAPI as an accumulation of overcondensed chromosomes (Figure 3.14b-d). In *mad2Δ cut7-446* on the other hand, there is an accumulation of cut-phenotype cells that are exiting mitosis with improperly segregated genetic material, indicating that the checkpoint is defective. The *ndc80-AK01 cut7-446* mutant behaves similarly to *mad2Δ cut7-446.* Improperly divided cells exit mitosis and there is no mitotic arrest. 40% of *ndc80-AK01 cut7-446* cells have the cut-phenotype after 160 min, similar to 50% for *mad2*Δ *cut7-446*. Neither *ndc80-AK03 cut7-446* nor *ndc80-AK05 cut7-446* show this checkpoint defect; in both mutants, cells arrest in mitosis with overcondensed chromosomes (Figure 3.14b-d). *ndc80-AK05 cut7-446* cells strongly resemble those of the wild type background in terms of both overcondensation and cut-phenotypes (Figure 3.14b-d), whereas *ndc80-AK03 cut7-446* does not seem to have a spindle checkpoint defect at all.

Data from several of our assays suggest that *ndc80-AK03* does not appear to have a spindle checkpoint defect. Therefore, the *ndc80-AK03* mutant was excluded from subsequent analysis. For the *ndc80-AK05* mutant we decided to further analyse its spindle checkpoint defect, as the data of *ndc80-AK05 cut7-446* was inconsistent with previous observations (see Figure 3.12 and Figure 3.14).

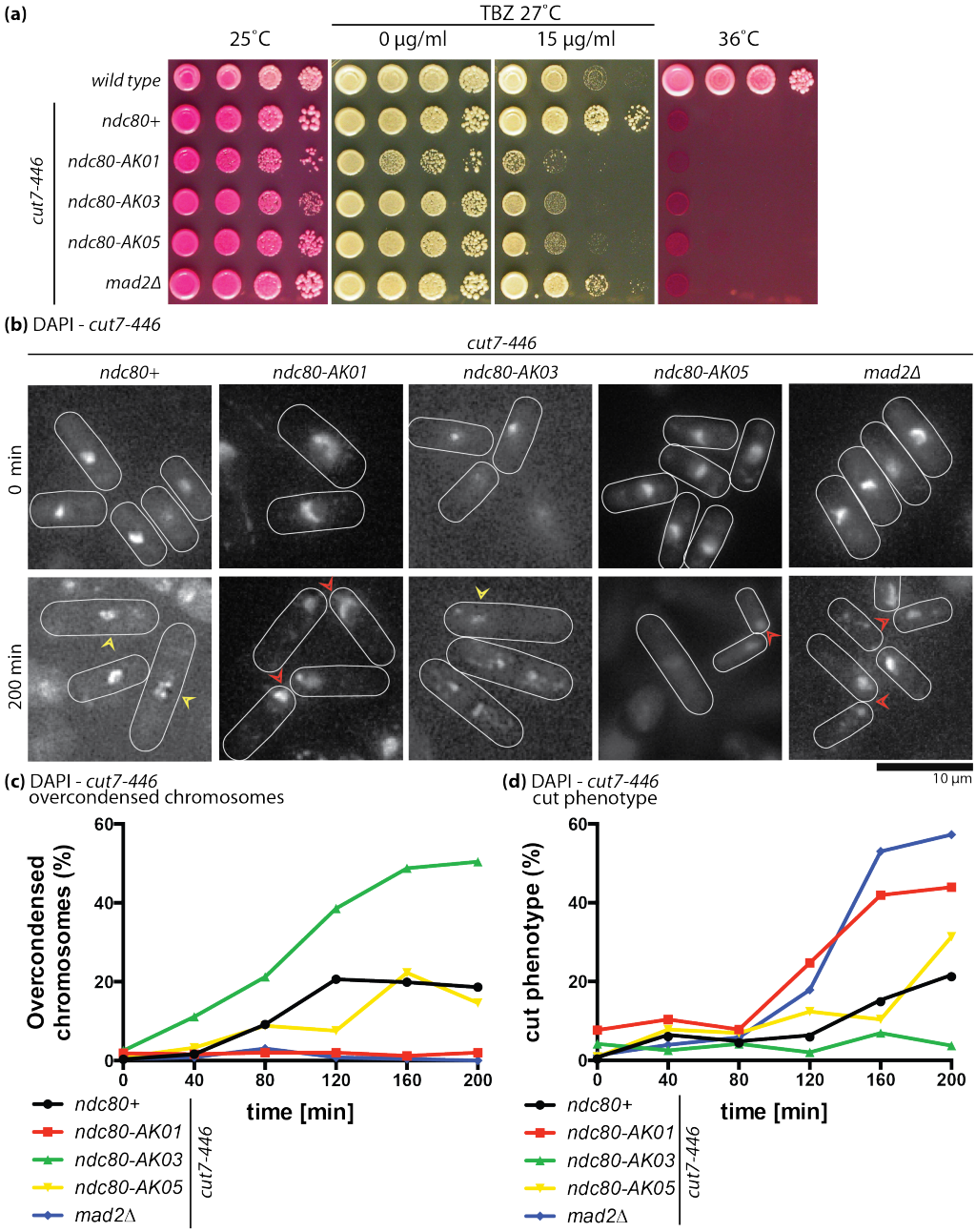

Figure 3.14. *ndc80-AK01* has a checkpoint defect in the *cut7* mutant background.

(a) Serial dilution spot assay of *ndc80* mutants in the temperature sensitive *cut7-446* mutant background. 5 x 10^4 cells were plated in the first lane (far-left), followed by tenfold dilution. Cells were grown for 3 days under the indicated conditions. (b,c,d) Cells were grown in YE5S at 25˚C, diluted to 4 x 10^6 cells/ml and shifted up to 36˚C. The samples were fixed with 1.6% PFA every 40 minutes for 200 minutes. The cells were then stained with DAPI and images were taken (b,c). The percentage of cells displaying overcondensed chromosomes (c) and the "cut" phenotype (d) is shown. For each time point, more than 150 cells were counted. Yellow arrowheads indicate overcondensed chromosomes and the red arrowheads indicate cells with the cut-phenotype. The periphery of cells is outlined with dotted lines. Values are averages from two experiments. Scale bar 10 µm.

3.6.3 Additional cold sensitive phenotype of *ndc80* mutants

To further examine the checkpoint-defective phenotypes of *ndc80-AK01* and *ndc80-AK05*, we intended to use the cold sensitive β-tubulin *nda3-KM311* allele as an alternative way of activating the SAC (Hiraoka et al., 1984). At the restrictive temperature (19˚C), *nda3-KM311* cells are unable to form microtubules and the cells show a delay in mitosis. However, isolates of *ndc80-AK01 nda3-KM311* and *ndc80-AK05 nda3-KM311* double mutants were very difficult to obtain. Therefore, we hypothesised that the *ndc80* mutations caused additional cold sensitive phenotypes. A serial dilution assay (Figure 3.15a) confirmed our assumptions of cold-sensitivity from *ndc80-AK01* and *ndc80-AK05* cells. However, shifting mutants to the restrictive temperature (19˚C) did not cause any mitosis-associated phenotypes (Figure 3.15b-d). Therefore, defects must be of different nature and were not analysed further in the current study. Eventually, we managed to obtain progeny of *ndc80-AK01 nda3-KM311* and *ndc80-AK05 nda3-KM311*, but could not observe any mitotic delay or exit under restrictive conditions, similar to the *ndc80* mutants alone (Figure 3.16). This phenotype can result from an incorrect assignment of the *nda3-KM311* gene in the cross or the *ndc80* mutants masking the effects of *nda3-KM311* at the restrictive temperature. Therefore, I decided to use another *nda3* conditional allele *(nda3-1828)* to verify the phenotype of the *ndc80* mutants.

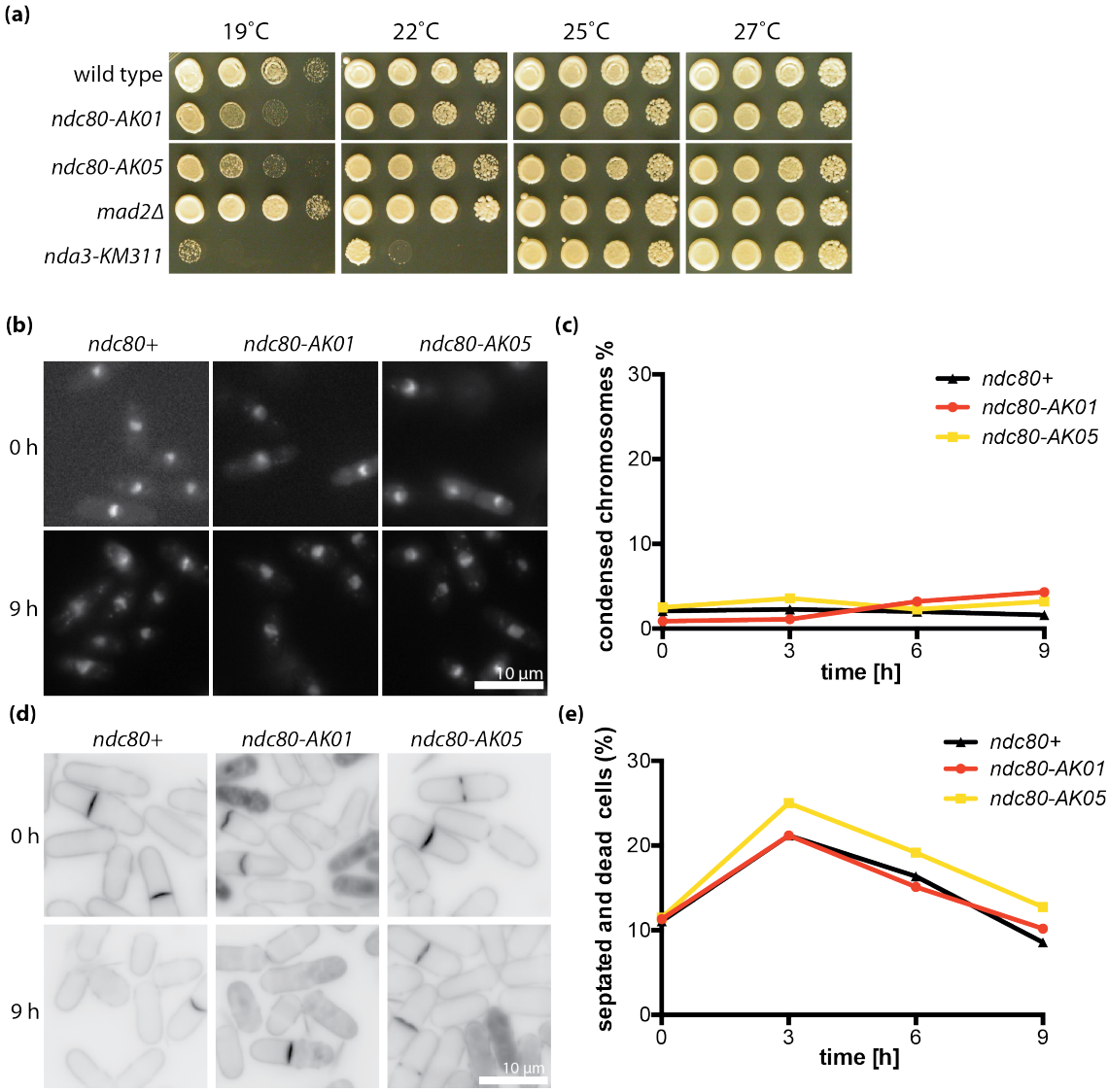

Figure 3.15. Novel cold sensitive phenotype of *ndc80-AK01* and *ndc80-AK05*.

(a) Serial dilution assay (5 x 10^4 cells in the first spot, 10-fold dilutions subsequently) were performed on YE5S media and the plates were incubated at the indicated temperatures (upper panel) for 3 days. (b-e) 4 x 10^6 cells were shifted down to 19^0C and were observed every 3 hours for 9 hours. Samples were fixed with 1.6% PFA and stained with DAPI (b, c), and Calcofluor (d, e). Quantifications for overcondensed chromosomes (c), and septated cells (e) are shown on DAPI (b) and Calcofluor (d) stained cells appropriately. For each time point, more than 150 cells were counted. Scale bars, 10 µm.

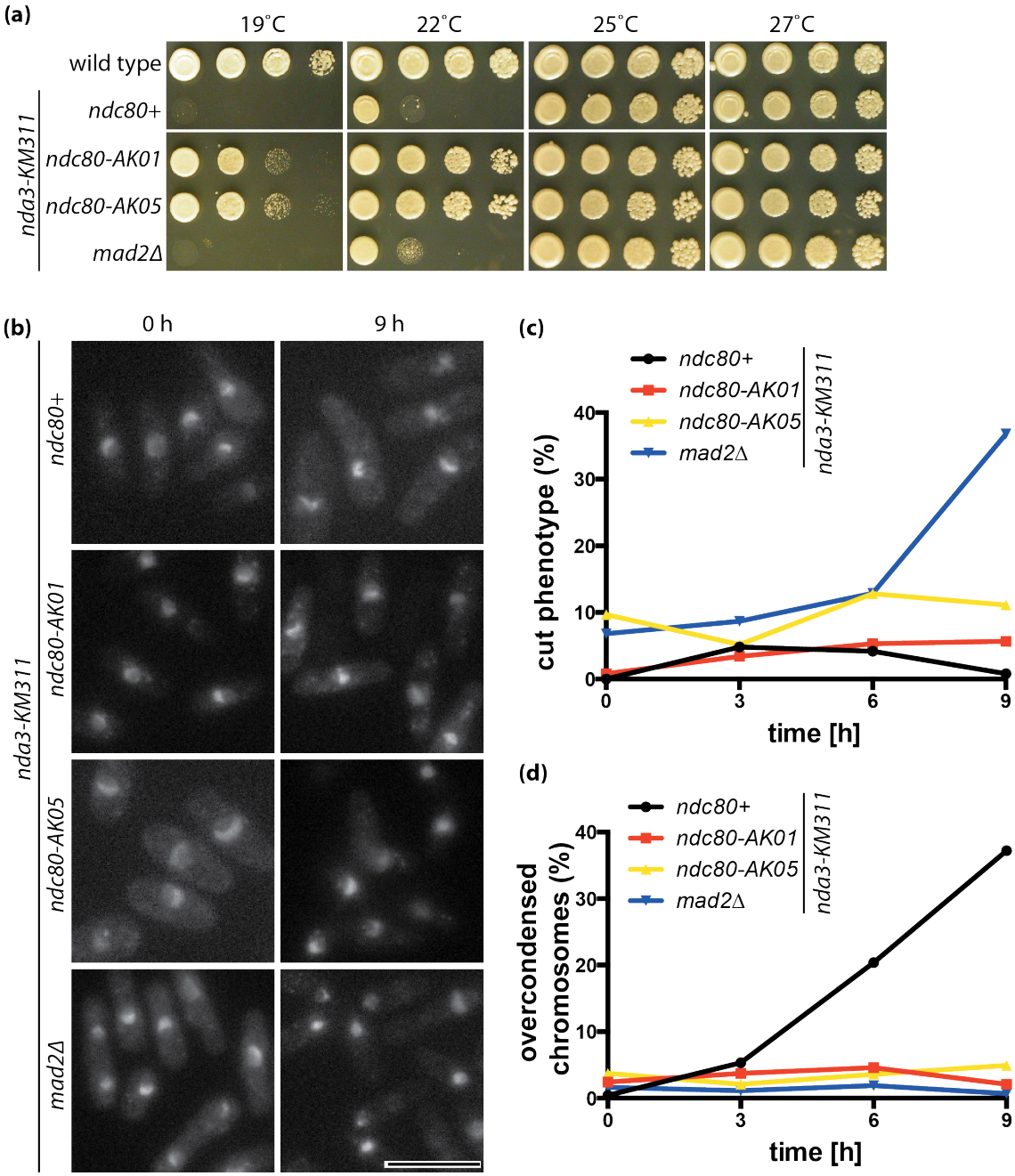

Figure 3.16. There is a mitotic arrest in *ndc80-AK01 nda3-KM311* and *ndc80-AK05 nda3-KM311* cells.

(a) Serial dilution assay (5 x 10^4 cells in the first spot, 10-fold dilutions subsequently) were performed on YE5S media and the plates were incubated at the indicated temperatures (upper panel) for 3 days. (b-d) 4 x 10^6 cells were shifted down to 19˚C and were observed every 3 hours for 9 hours. Samples were fixed with 1.6% PFA and stained with DAPI (b). Quantifications for septated cells (c) and overcondensed chromosomes (d) are shown. For each time point, more than 150 cells were counted. Scale bars, 10 µm.

3.6.4 *nda3-1828*

Since we could not activate the SAC at cold-induced conditions (*nda3-KM311*), we used the second β-tubulin *nda3-1828* allele, which is temperature-sensitive at 36˚C (Radcliffe et al., 1998). The *ndc80* mutant alleles were backcrossed to *nda3-1828.* Exponentially growing cells were shifted up to 36˚C and samples were collected every 40 minutes (Figure 3.17). Samples were fixed and stained with DAPI to observe chromosome condensation and cut-phenotypes similarly to the *cut7-446* experiment.
When the SAC is inactivated by the deletion of *mad2* in the *nda3-1828* background, the mitotic delay cannot be sustained and cells exit mitosis with improperly divided chromosomes. In *ndc80-AK01 nda3-1828*, similarly, no mitotic delay is observed (Figure 3.17). However, in *ndc80-AK05 nda3-1828* there is accumulation of overcondensed chromosomes rather than the cut-phenotype.

For future analysis we decided to omit *ndc80-AK05,* because it does not appear to have defects in the SAC - Figure 3.14 and Figure 3.17. A potential explanation can be difference in tensions exerted on by weaker induction of the checkpoint signalling in the presence of TBZ/CBZ drugs that cannot be repeated when using conditional mutants.
Accordingly, the following studies focus only on *ndc80-AK01* as this mutant displays phenotypes consistently with a checkpoint defect. I would like to determine the nature of the SAC defect in *ndc80-AK01* mutant.

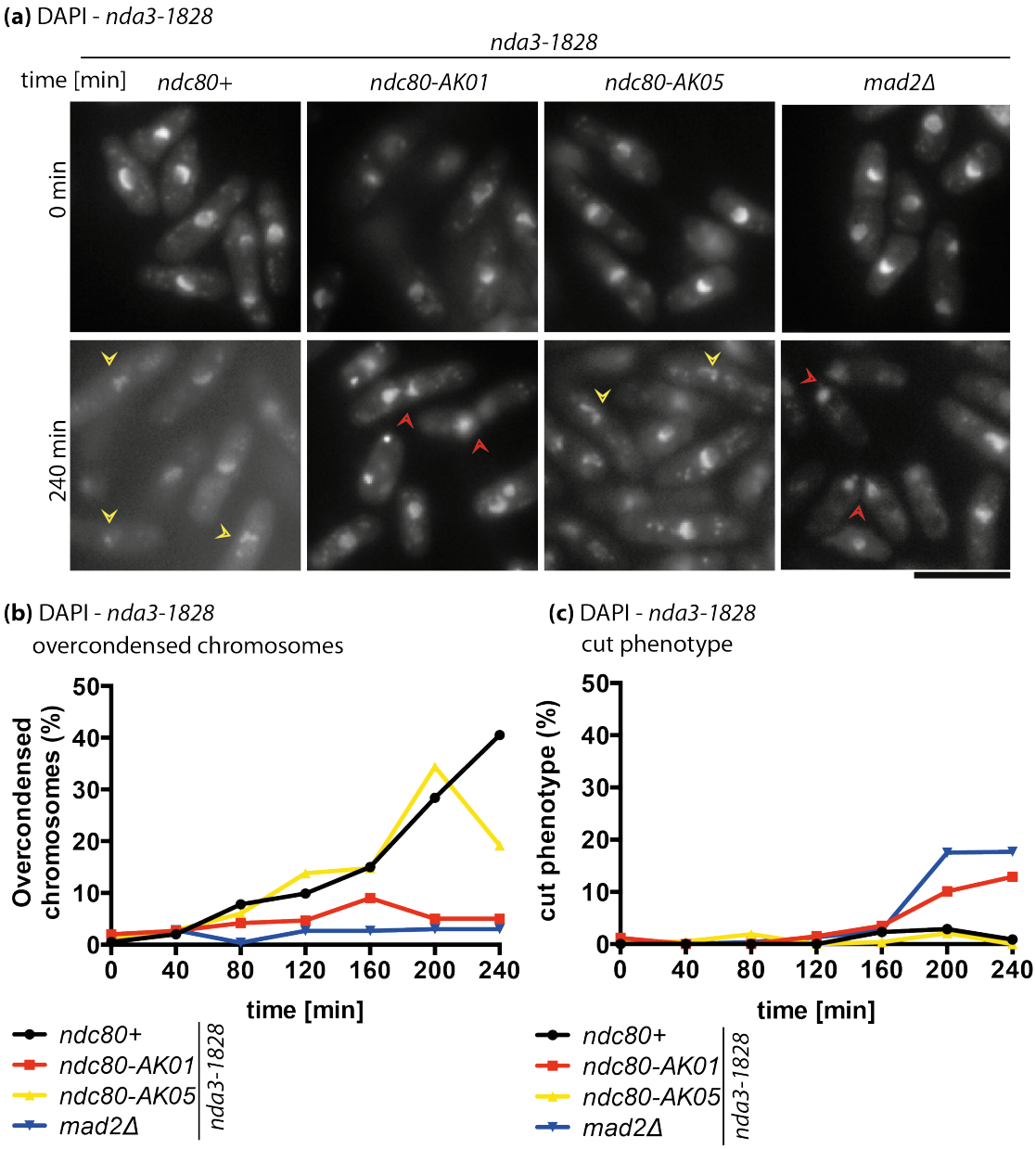

Figure 3.17. *ndc80-AK01 nda3-1828* displays a checkpoint defect.

Exponentially growing cells (4 x 10^6 cells/ml) at 27°C were shifted to 36°C and samples were taken every 40 minutes for 240 minutes, then fixed with 1.6% PFA. Cells were then stained with DAPI (a) and phenotypes were quantified according to two criteria: chromosome overcondensation (b) and cut-phenotypes (c). Red arrowheads indicate cells with cut-phenotypes, whereas yellow arrowheads indicate overcondensed chromosomes. For each time point, more than 150 cells were counted. The values are averages from two experiments. Scale bar, 10 µm.

3.7 The linker region of Ndc80 is essential for its function at the kinetochore

As *ndc80-AK01* has a mutation in the previously uncharacterised linker region of Ndc80, we decided to look into the function of this domain in more detail. To this end, various truncations of the Ndc80 linker region were constructed. Ndc80-Δ211-248, Ndc80-Δ249-270 and Ndc80-Δ211-270 were made in pREP1 and pREP41-GFP plasmids. Ndc80-Δ211-249 has a deletion of the αH helix that directly follows the calponin-homology domain; the region affected in *ndc80-AK01* (L246P). Ndc80-Δ249-270 has a deletion of the αI helix and Ndc80-Δ211-270 does not contain any of the linker region (Figure 3.18). The study of this uncharacterised domain of Ndc80 will provide more insight into its role and function.

3.7.1 Viability test

Firstly, I asked whether the linker region on its own is essential for cell viability. Using the truncation constructs in pREP1 (with the *LEU2* budding yeast gene that complements the fission yeast *leu1* mutation), the plasmids were episomally introduced into a diploid strain containing the heterozygous deletion, with one endogenous *ndc80*$^+$ replaced by the *ura4*$^+$ cassette (Figure 3.19). Once the plasmids were transformed into diploid strains, they were allowed to sporulate and the spores were plated on the selection plates, EMM-Leu and EMM-Leu-Ura. This allowed the isolation of haploids containing plasmid with Ndc80 truncations in the *ndc80*$^+$ wild type background or *ndc80*$^+$ deletion by *ura4*$^+$. If plasmids could complement the *ndc80* deletion, the number of segregants on EMM-Leu plates is expected to be double compared to EMM-Leu-Ura according to Mendel's inheritance principles, which is the case for wild type Ndc80 (Ndc80-wt). However, no colonies were observed for a vector, Ndc80-Δ211-248, Ndc80-Δ249-270 or Ndc80-Δ211-270, indicating that the haploid *ndc80* deletion strains (by *ura4*$^+$) were not rescued by any of Ndc80 truncation constructs. This indicates that both αH and αI helices are essential for cell viability and required for Ndc80 function. More than 10 colonies were observed on EMM-Leu-Ura plates, but were in fact diploid as confirmed by microscopy observations.

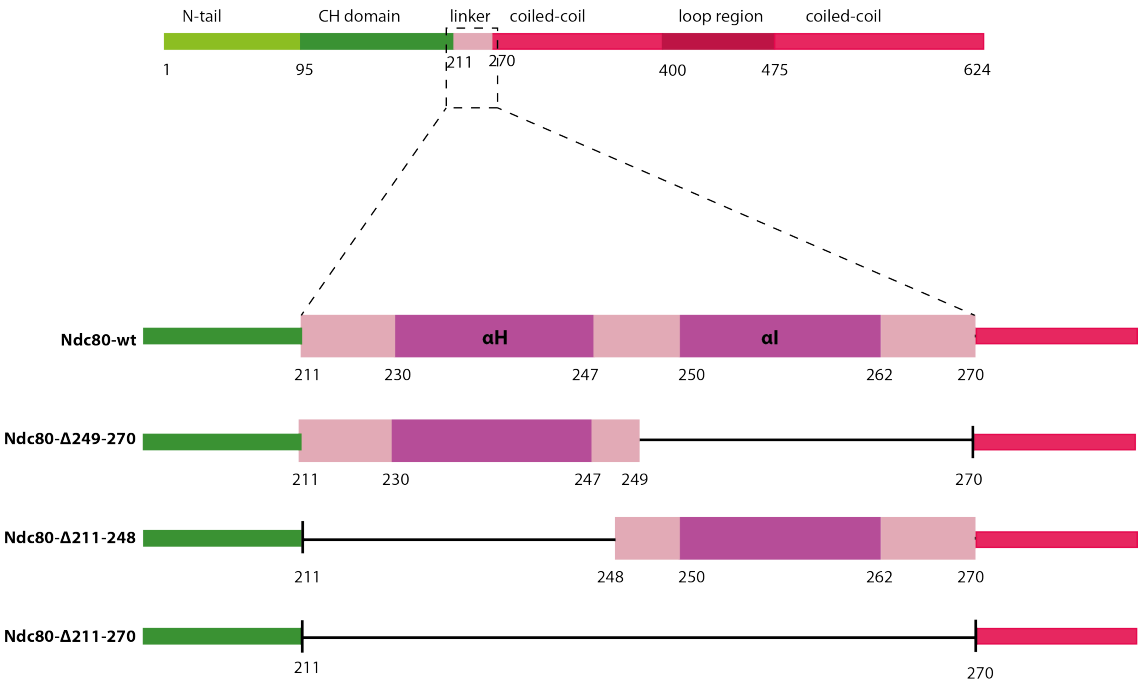

Figure 3.18. Scheme of Ndc80 linker region truncations.

The truncations of Ndc80 linker region were designed as shown on the scheme. The αH and αI helices' positions were based on alignments with Hec1 boundaries determined by the crystal structure (Ciferri et al., 2008).

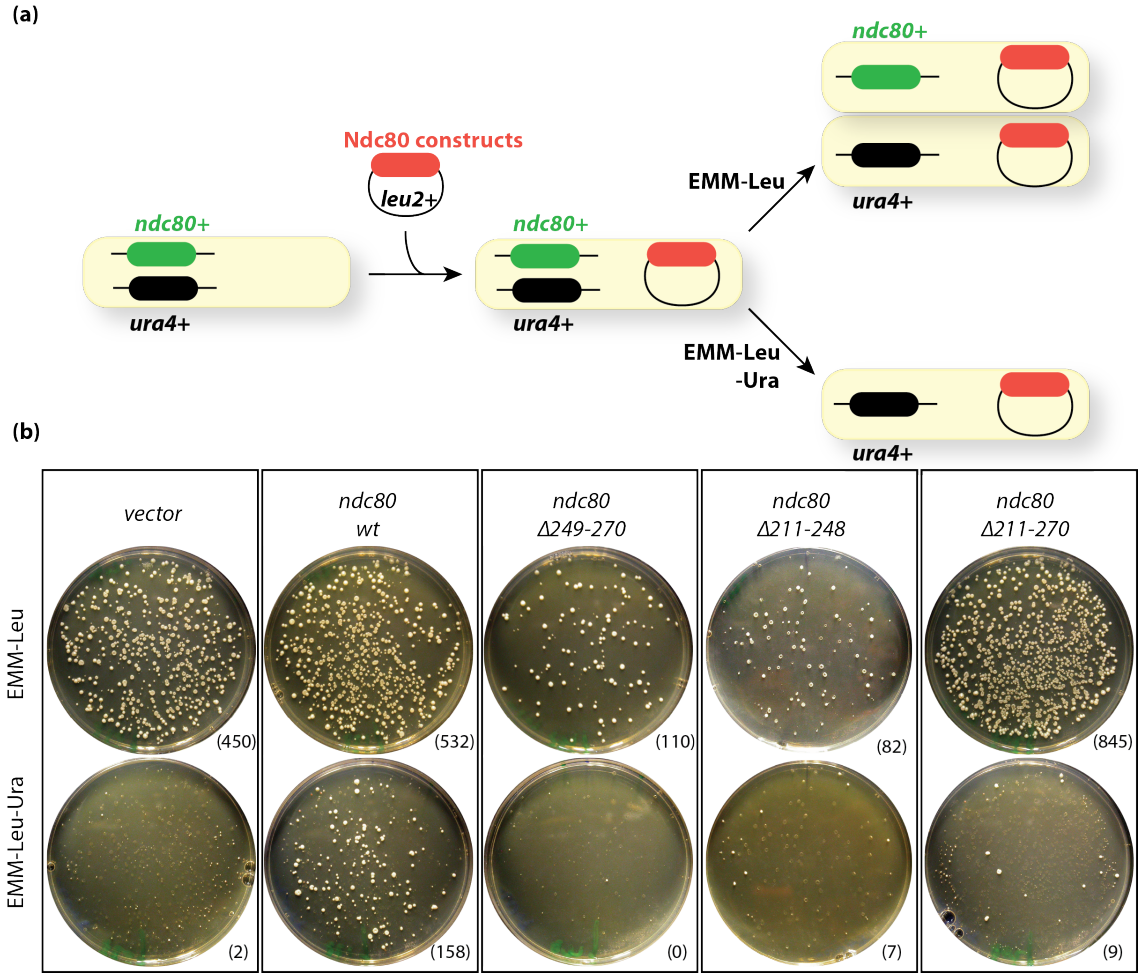

Figure 3.19. The Ndc80 linker region is essential for cell viability.

(a) Scheme of the experimental strategy for checking the viability of Ndc80 linker region truncations. Ndc80 truncations were cloned into pREP1 vector, with the *LEU2* marker. Constructs were introduced into heterozygous diploid cells, in which a *ura4*$^{+}$ marker replaces one copy of *ndc80*$^{+}$. Transformed cells were allowed to sporulate and the same numbers of cells were plated on (1) EMM-Leu and (2) EMM-Leu-Ura plates for appropriate marker selection. Note that thiamine was added at all times to repress the expression from the *nmt1* promoter (i.e. to avoid overexpression). (b) Pictures of colonies grown on each plate (EMM-Leu, top; EMM-Leu-Ura, bottom) that was incubated at 27˚C for 5 days are shown. The number of colonies grown was counted.

3.7.2 The linker region is essential for function of the Ndc80 complex

As the linker region is essential for cell viability, the next question to address is its function at the kinetochore. Ndc80 truncations under the *nmt1* promoter were transformed into the *ndc80-NH12* internal loop mutant (Tang et al., 2013) that was previously isolated in our lab. A mutation in the Ndc80 loop region causes chromosome alignment defects, missegregation and impaired localisation of Alp7/Alp14 to kinetochores during late mitosis at the restrictive conditions (36˚C) (Tang et al., 2013). A serial dilution assay was performed in the presence and absence of thiamine at permissive and restrictive temperatures. Ndc80-wt manages to rescue the temperature sensitivity of *ndc80-NH12,* whereas the linker truncations do not, though very modest suppression of growth at the high temperature might be noticeable by Ndc80-Δ211-248 or Ndc80-Δ211-270 (Figure 3.20). Furthermore, it is clear that there is no dominant negative effect when overexpressing Ndc80 truncations, as there is normal growth in absence of thiamine at 27˚C (Figure 3.20).

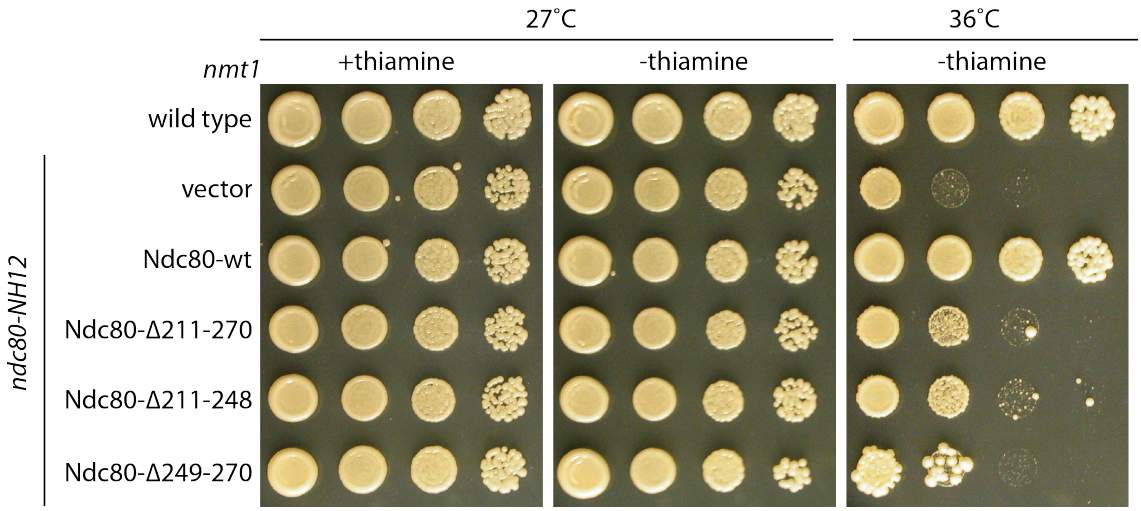

Figure 3.20. The linker region of Ndc80 is essential for functionality of the Ndc80 complex at the kinetochore.

A serial dilution spot assay was performed on *ndc80-NH12* strains containing Ndc80-wt, Ndc80-Δ211-248, Ndc80-Δ249-270 and Ndc80-Δ211-270 expressed from the *nmt1* promoter. 5 x 10^4 cells were placed onto the first spot and then tenfold dilutions were carried on rich media (YE5S) in the presence and absence of thiamine at 27˚C and 36˚C and incubated for 3 days.

3.7.3 The linker region of Ndc80 is important for proper kinetochore localisation

Next, to characterise the linker region truncations of Ndc80, we have observed the localisation of these Ndc80 constructs. The linker-less Ndc80 proteins may be able to localise to the kinetochore or accumulate in the cells elsewhere, causing the misplacement of their endogenous binding partner(s) from their canonical loci. The observed phenotypes might result from mislocalisation of potential binding partners rather than directly from Ndc80 linker truncations. New pREP41 plasmids with N-terminally tagged GFP containing Ndc80-Δ211-248, Ndc80-Δ249-270 and Ndc80-Δ211-270 were transformed into wild type Nuf2-mCherry strains. Constructs were expressed in EMM-Leu with and without thiamine for 12, 14, 16 and 18 hours. Overexpression for 16 and 18 hours in liquid culture resulted in high aggregation of the GFP-Ndc80 proteins; therefore only the 12 and 14 hours experiments are presented in Figure 3.21. In Ndc80-wt, GFP-Ndc80 localises to Nuf2-mCherry as expected, in the presence or absence of thiamine (this indicated that repression of *nmt41* promoter by 2mM thiamine is not fully efficient and some protein can be produced). In the truncations of the Ndc80 linker region, there is no localisation to the kinetochores, despite overexpression of the protein (Figure 3.21). Furthermore, to check cell growth and overexpression levels in all strains, we performed a spotting assay in the presence and absence of thiamine. The cell pellet after 14 hours overexpression from the *nmt41* promoter was collected and protein levels examined by immunoblotting (Figure 3.22). As shown in Figure 3.22, for GFP-Ndc80-Δ249-270 the amount of protein loaded and expression levels were lower compared to other constructs. Ndc80-Δ211-248 and Ndc80-Δ211-270 showed growth and overexpression levels similar to Ndc80-wt. Data from Figure 3.21 and Figure 3.22 indicate that in the absence of the linker region the Ndc80 protein can not localise to kinetochore, hence the non-functional Ndc80 truncations observed in Figure 3.20.

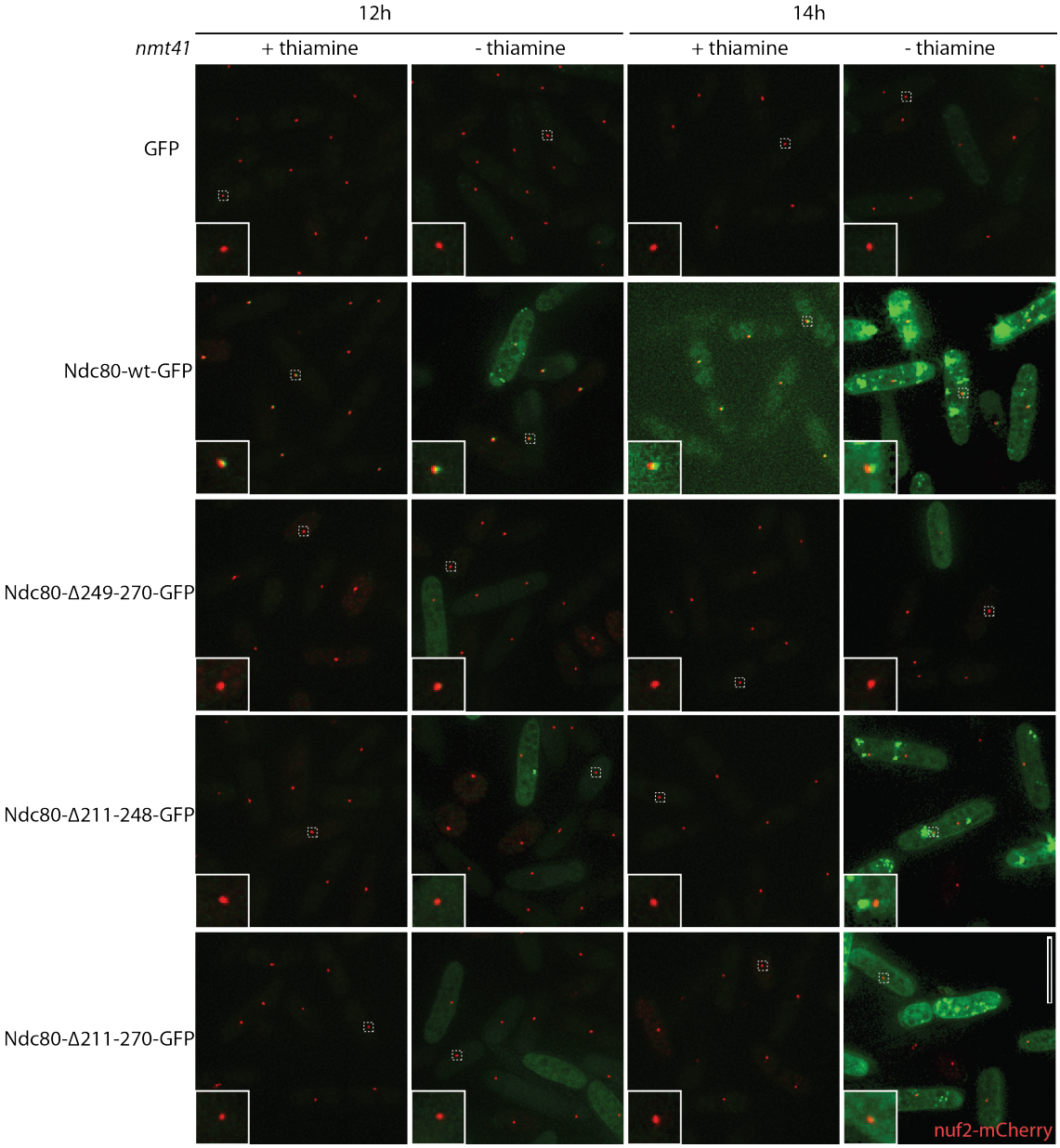

Figure 3.21. Localisation of Ndc80 linker region truncations at the kinetochore.

Cells containing Nuf2-mCherry were transformed with pREP41-GFP plasmids carrying the indicated Ndc80 constructs. Cells were precultured in EMM-Leu+Thiamine and then they were split into two – one culture into EMM-Leu+Thiamine and the other into EMM-Leu. After 12 and 14 hours at 27˚C, the samples were imaged. Insets show enlarged images corresponding to kinetochore regions. Only Ndc80-wt-GFP localises to kinetochores. Scale bar, 10 μm.

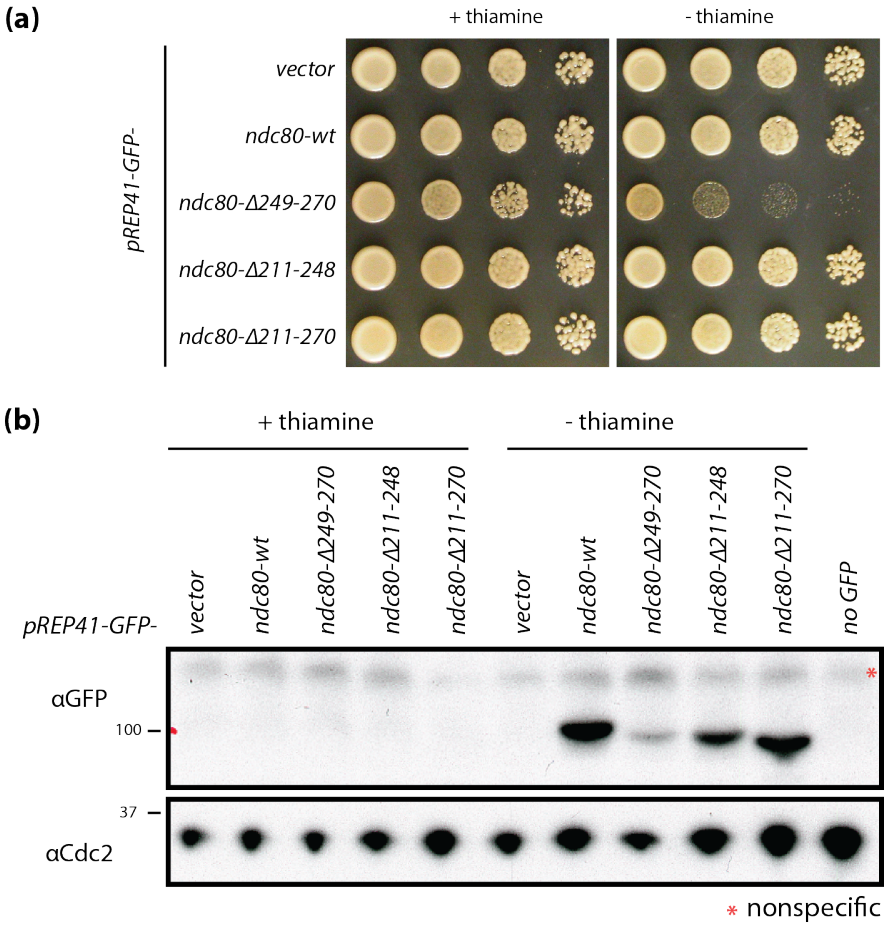

Figure 3.22. Levels of overexpression of Ndc80 linker region truncations.

(a) Serial dilution assay of cells with pREP41-GFP containing Ndc80-Δ211-248, Ndc80-Δ249-270 and Ndc80-Δ211-270. 5 x 10^4 cells in the first spot were followed by 10-fold dilutions and plated on EMM-Leu+Thiamine and Emm-Leu. Plates were incubated at 27˚C for 3 days. (b) Cells were cultured in liquid EMM-Leu with or without thiamine at 27˚C for 14 hours. 20 µg of protein extract was loaded and run on a gel for immunoblotting. Anti-GFP antibody was used for the detection of GFP-Ndc80 truncation mutant proteins. The protein loading control Cdc2 was detected by anti-Cdc2 antibody.

3.8 Summary

In this chapter, I have firstly screened for *ndc80* mutants based on temperature and thiabendazole-sensitivity. From five independent screenings, I isolated 2 temperature sensitive and 3 TBZ mutants of the *ndc80* alleles. Initial assessment of these mutants included looking at cell morphology, growth curves, the degree of temperature and thiabendazole sensitivity as shown on spotting assays, as well as sequencing analysis.

Each of the isolated mutants has a point mutation either in the calponin-homology domain, linker region or coiled-coil region.
Two temperature sensitive mutants, *ndc80-AK02* and *ndc80-AK04,* were omitted from future analysis as they had mutations in the coiled-coil region, which was not our primary focus.

Notably, the stability of the Ndc80 complex was confirmed in three mutants (*ndc80-AK01, ndc80-AK03* and *ndc80-AK05*) that were characterised for potential defects in spindle assembly checkpoint signalling. Under a mitotic arrest condition, induced by TBZ/CBZ or *cut7* and *nda3* mutants, the mutant phenotypes were observed by live imaging. Based on these data, I decided to focus further work on the *ndc80-AK01* allele, which is consistently defective in checkpoint signalling. This linker region mutant behaves similarly to previously characterised checkpoint defective deletions of *mad1* or *mad2*. Moreover, truncations of the linker region reveal that the region is essential for cell viability, functionality of the Ndc80 complex and its localisation to kinetochore.

3.9 Discussion

As shown throughout metazoan studies, Ndc80/Hec1 is a key element in kinetochore-microtubule attachments. The extensive work on its structure, binding partners, regulation and kinetochore-microtubule attachment has been underway in human cell lines and it has become clear that misregulation of Ndc80/Hec1 is intimately linked to human cancer, especially in breast and prostate cancers. Moreover, there is evidence that Ndc80 overproduction levels are linked with tumour grade and patient prognosis (Bieche et al., 2011). Tumourigenic features of Ndc80/Hec1 were also studied in mice, where the overexpression of Ndc80 increases the frequency of cancer occurrence (Diaz-Rodriguez et al., 2008).

However, relatively little is known about $ndc80^{+}$ in fission yeast. The overexpression of wild type Ndc80 is not toxic to cells, however the $ndc80^{+}$ is essential in fission yeast. Furthermore, in experiments in our lab, with overexpression of wild type and Ndc80-loop-less proteins, microtubule associated proteins including Dis1 (a homologue of ch-

TOG/XMAP215) localise most likely to the additional Ndc80 sites outside kinetochore (Tang and Toda, 2015b).

To identify other regions in Ndc80 with distinct functions, we have carried out the random mutagenesis screening of the N terminal regions of the protein, that bind microtubules and are essential for cell integrity (Ciferri et al., 2008, Cheeseman et al., 2006, Hsu and Toda, 2011). The screening for both temperature and thiabendazole sensitive mutations led us to the isolation of mutants in these Ndc80 domains. I expected a higher number of mutants, but it is possible that the homologous recombination rate is much lower in the N-terminus of *ndc80*$^{+}$ or that there were no mutations introduced due to the insufficiently long fragment for errors in polymerase chain reaction to occur. As previously mentioned, it may be that the N-terminus plays an important role in cell viability; and so may have a very low tolerance for conditional mutations.

The two temperature sensitive mutants isolated (*ndc80-AK02* and *ndc80-AK04*) have the mutations in the coiled-coil region, which firstly was outside our scope of interest and secondly they might loosen the stiffness of the whole Ndc80 complex structure by affecting the dimerisation of Ndc80 and Nuf2 through coiled-coil regions.

The *ndc80-AK03* mutant showed TBZ sensitivity and weak temperature sensitivity. It is the only mutation that was isolated in the calponin homology domain (R183G), which is buried inside the structure. It is possible that this mutation affects the interaction between Ndc80 and microtubules. As there was no clear phenotype except the overcondensation of chromosomes we decided to omit *ndc80-AK03* from future studies.

The *ndc80-AK05* (N272D) mutant, on the other hand, showed initially clear checkpoint defect phenotype (in presence of TBZ/CBZ) but the data was not recapitulated in the *cut7* and *nda3* mutant backgrounds. It is highly unlikely that the mutation is unstable, as isolated *ndc80* mutant alleles were backcrossed, their TBZ sensitivity in each mutant background was verified and they were sequenced. The difference might arise rather from the difference in their microtubule depolymerising activity on the tension along

the microtubule in *nda3* conditional mutants and TBZ (Kawashima et al., 2007, Sawin and Nurse, 1998, Hiraoka et al., 1984, Umesono et al., 1983b, Umesono et al., 1983a, Millband and Hardwick, 2002, Radcliffe et al., 1998). As the mutation is not directly in the linker region of Ndc80, due to time constraints and the inconsistency of the observations, we decided to exclude it from further studies.

The only mutant we decided to analyse further was *ndc80-AK01*, which has a clear checkpoint defect as observed under all mitotic arrest conditions used (TBZ/CBZ, *cut7* and *nda3* conditional mutants). It was a clear TBZ sensitive mutant with reduced viability (Figure 3.10), an increase in the number of cells exiting mitosis (observed as cut cells (Figure 3.12)) and no accumulation of mitotic cells (Cut11-GFP (Figure 3.13)). We hypothesise that the *ndc80-AK01* mutation may affect the localisation of spindle assembly checkpoint components to the kinetochore. Recent papers published during my studies suggest a role for the N-terminal domains in the recruitment of Mph1/MPS1 to kinetochores (Zhu et al., 2013, Nijenhuis et al., 2013). In budding yeast, on the other hand, Dam1 (microtubule associated protein) interacts directly or indirectly with the linker region of Ndc80 (Lampert et al., 2013), rather than loop (Maure et al., 2011) or N-tail as previously shown (Tien et al., 2010). However, in the *ndc80-AK01* mutant we do not observe microtubule defects (seen as defects in chromosome segregation), but this notion requires further analysis.

The current observations of the mutation in the Ndc80 linker region prompted us to look into this region in greater detail. The region consisting of unstructured sequences and two alpha helices between the calponin homology domain and the coiled-coil is a good candidate for interactions with other proteins. Firstly, this region is essential for Ndc80 complex formation, as truncations of the linker region do not localise (Figure 3.21) nor function at the kinetochore (Figure 3.20). The linker region was also shown to be essential for cell viability (Figure 3.19) and so might be required for proper dimerisation of Ndc80 and Nuf2, as it is located just after the calponin homology domain. Therefore the study of the *ndc80-AK01* mutant allele will provide us with more information about this domain.

Chapter 4. Detailed characterisation of the *ndc80-AK01* mutant reveals a crucial role of the Ndc80 linker region in spindle assembly checkpoint

4.1 Live image analysis of *ndc80-AK01*

To further describe the *ndc80-AK01* defect, the analysis of spindle assembly checkpoint (SAC) components was conducted. Time-lapse live image analysis was carried out for exponentially growing cells at 27˚C that were transferred to lectin-coated culture dish and imaged in Deltavision live microscope equipped with temperature-controlling system. As the *ndc80-AK01* mutant has a checkpoint defect, it is vital to determine if this is because of mislocalisation or degradation of SAC components from the kinetochore and/or failure in inactivation of the APC/C.

4.1.1 Spindle microtubules are intact in *ndc80-AK01*

Initially, time-lapse imaging was carried out to observe microtubules. Mitotic progression was observed using mCherry-Atb2 and Sid4-RFP to visualise microtubules and spindle poles respectively and Nuf2-YFP, a component of the Ndc80 complex, was used to observe mitotic division as shown in Figure 4.1. Chromosome segregations seem normal in *ndc80-AK01*, however a centromere-specific probe, such as *cen2*-GFP (centromere 2 marked with GFP) should be used to fully assess sister centromere movements. The microtubule structures are intact in the mutant and the distance between SPBs (pole-to-pole) is similar in $ndc80^{+}$ and *ndc80-AK01* cells (Figure 4.1b). Furthermore, the microtubule dynamics of $ndc80^{+}$ and *ndc80-AK01* are similar (Figure 4.1b).

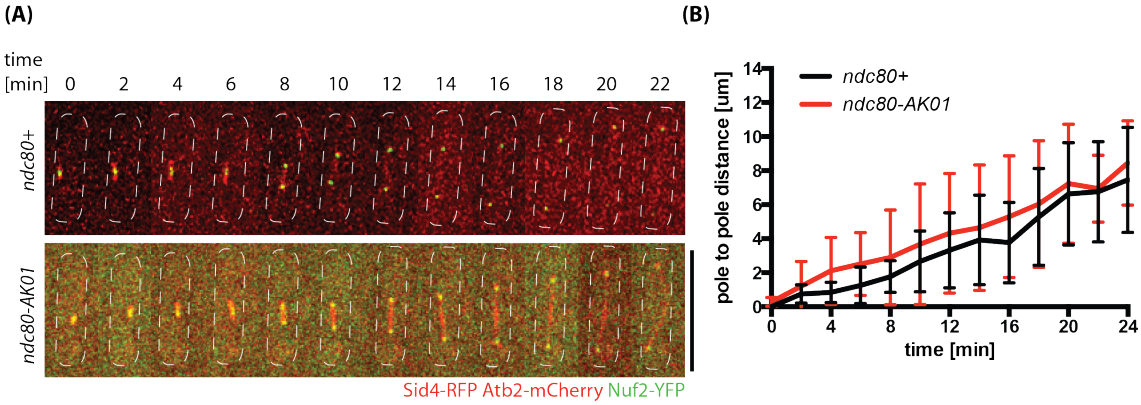

Figure 4.1. The chromosome segregation and microtubules are normal in *ndc80-AK01*.

Exponentially growing cells (4 x 10^6 cells/ml) were placed in YE5S at 27˚C. Samples were live imaged for 60 minutes. The localisation of Sid4-mRFP, mCherry-Atb2 and Nuf2-YFP was observed. (a) Representative images of *ndc80*$^+$ and *ndc80-AK01* are shown. Scale bar, 10 µm. (b) Quantification of spindle lengths in µm. n > 10 cells were counted. Error bars represent standard deviations.

4.1.2 ndc80-AK01 does not influence checkpoint silencing

The next thing I looked at was the relationship between *ndc80-AK01* and checkpoint silencing. Previous characterisation of the mutant indicates that *ndc80-AK01* is defective in checkpoint activation as there is no mitotic arrest, observed as an accumulation of mitotic cells as visualised with Cut11-GFP (Figure 3.13), or premature exit from mitosis visualised with DAPI and Calcofluor (Figure 3.12, Figure 3.14, Figure 3.17). To determine if Ndc80 exerts any effect on checkpoint silencing in addition to spindle assembly checkpoint activation, the double mutants of Δ*PP1*^{dis2} and *ndc80-AK01* with Plo1-mCherry acting as a mitotic marker were constructed. PP1^{Dis2} is a key phosphatase of spindle assembly checkpoint silencing that is recruited once proper kinetochore-microtubule attachments are established to allow anaphase onset and chromosome segregation (Vanoosthuyse and Hardwick, 2009). To determine any potential role of *ndc80-AK01* in checkpoint silencing, a spotting assay was carried out (Figure 4.2a). There was no additional sensitivity to TBZ observed in Δ*PP1*^{dis2} *ndc80-AK01* double mutants (Figure 4.2a). Furthermore, live imaging was carried out for *ndc80*$^+$, *ndc80-AK01* and double mutants with Δ*PP1*^{dis2} with Plo1-mCherry, in microtubule depolymerising conditions (TBZ/CBZ). Cell cultures in exponential

growing phase were placed at 27˚C in rich media containing 50 µg/ml TBZ and 60 µg/ml of CBZ. No difference in mitotic duration was observed between the *ndc80*$^{+}$ and *ndc80*$^{+}$ Δ*PP1*^{dis2}, which is slightly unexpected. A prolonged mitotic arrest in *pp1*Δ$^{dis2\Delta}$ mutants is usually caused by an inability to silence the checkpoint without PP1 (Figure 4.2b). *ndc80-AK01* and *ndc80-AK01* Δ*PP1*^{dis2} spend less than 20 minutes in mitosis, which is half as long as wild type (Figure 4.2b). As there are no additional phenotypes in double mutant of *ndc80-AK01* Δ*PP1*^{dis2} compared to controls (Figure 4.2), *ndc80-AK01* does not seem to play a role in checkpoint silencing. From the analyses of *ndc80-AK01* mutants in Figure 3.12, Figure 3.13, Figure 3.14 and Figure 3.17, the defect is linked with SAC activation and any potential silencing defect might rather be linked with impaired SAC activation.

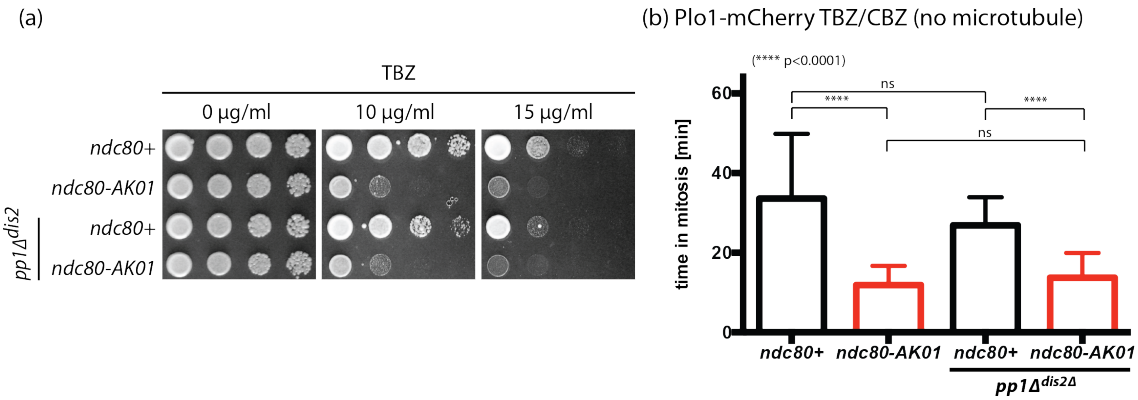

Figure 4.2. *ndc80-AK01* has no additive effect on checkpoint silencing.

(a) Spot tests of *ndc80*$^{+}$, *ndc80-AK01, ndc80*$^{+}$ Δ*PP1*^{dis2} and *ndc80-AK01* Δ*PP1*^{dis2} (5 x 10^4 cells in the first spot were followed by 10-fold dilutions subsequently) were performed. Cells were plated on YE5S containing indicated concentrations of TBZ for 3 days at 27˚C. (b) Exponentially growing cells (4 x 10^6 cells/ml) were placed in YE5S with 50 µg/ml TBZ and 60 µg/ml of CBZ at 27˚C. Samples were imaged for 60 minutes. Plo1-mCherry localisation at SPBs was observed as an indication of mitotic arrest. n=20 cells for each time point. Error bars represent standard deviations. Unpaired t-tests were carried out.

4.1.3 ndc80-AK01 does not display any additional phenotypes with SAC components deletions

To determine which of the checkpoint components is affected by *ndc80-AK01*, I have crossed the *ndc80-AK01* with individual deletions of SAC components - *mad1, mad2, mad3, bub1, bub3* and *mph1* - to observe if there is any additive effect on TBZ sensitivity in these strains.

Serial spotting dilution assay were employed to examine TBZ sensitivity in the double mutants. Any changes in TBZ sensitivity in double mutants should provide information on the function of *ndc80-AK01* in the checkpoint-signalling cascade and the most likely affected components. Furthermore, the effects of the Ndc80 mutant could result from compromised pathways other than SAC that show additive defects; therefore the spotting assay can provide preliminary information in this regard. As shown in Figure 4.3, there is no additional sensitivity to TBZ; the double mutant copies the sensitivity of *ndc80-AK01* or one of the SAC deletions. These results indicate that *ndc80-AK01* affects the checkpoint-signalling cascade directly, as there were no additive sensitivities observed.

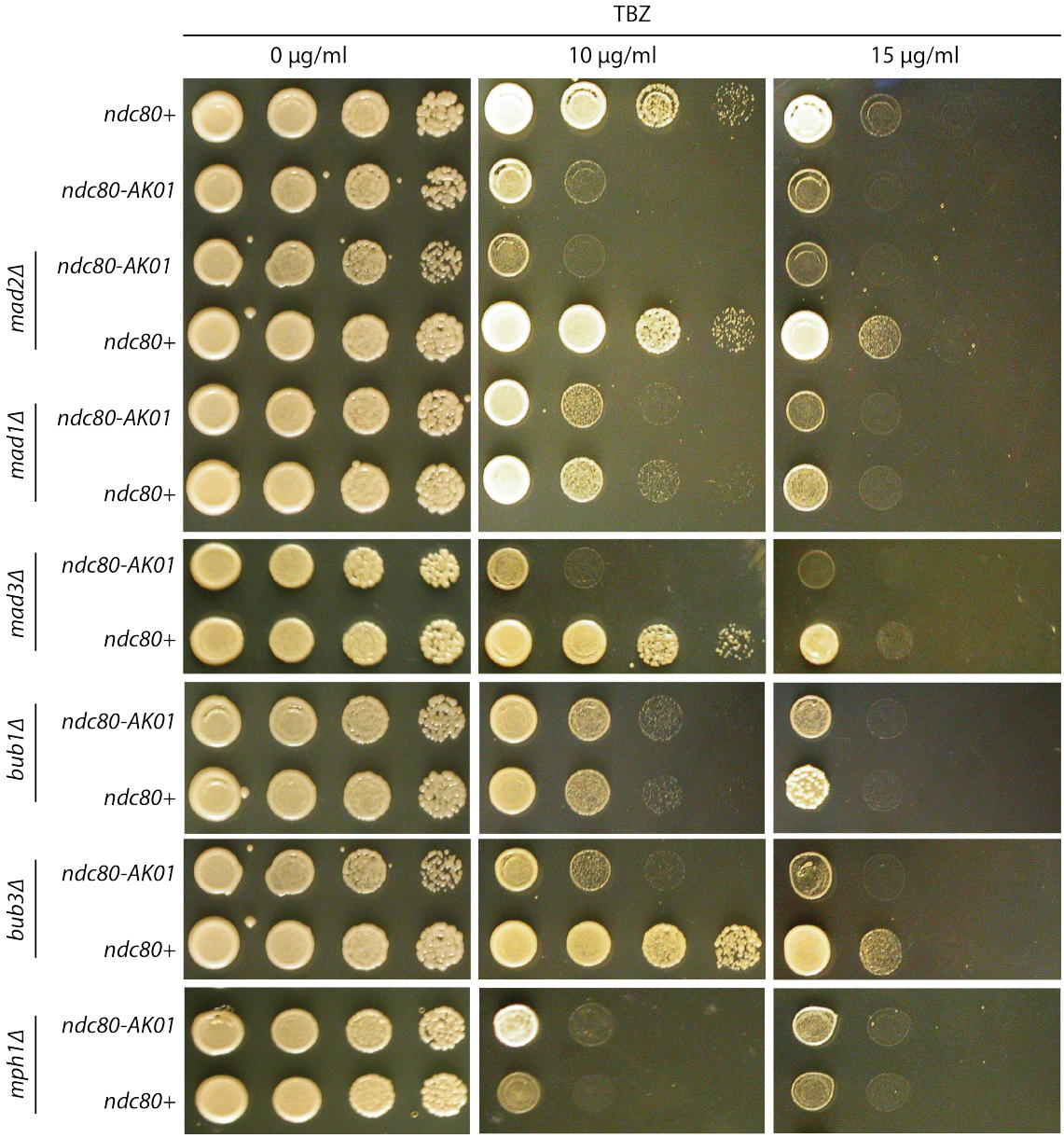

Figure 4.3 *ndc80-AK01* has no additional TBZ sensitivity when combined with deletion of SAC components.

Spot tests of *ndc80*$^{+}$ and *ndc80-AK01* in SAC deletion backgrounds (5 x 10^4 cells in the first spot were followed by 10-fold dilutions subsequently) were performed. Cells were plated on YE5S containing indicated concentrations of TBZ for 3 days at 27˚C.

4.1.4 Protein levels of GFP-tagged SAC components remains unchanged in *ndc80-AK01*

I wished to characterise *ndc80-AK01* by observing the localisation of GFP tagged SAC components. Silke Hauf kindly provided strains containing Mad1, Mad3, Bub1, Bub3, Ark1 and Mph1. As there were additional phenotypes observed in *ndc80-AK01* upon marker switch from *kan*^{r} to *hph*^{r} or *nat*^{r} for unknown reasons (as all the SAC-GFP strains were kan-resistant, if we had Ndc80-hph or Ndc80-nat, it would make constructions of double mutants easier). But either Ndc80-hph^r or Ndc80-nat^r displayed additional SAC-independent phenotypes (data not shown), the strains (doubly tagged with kan markers) were checked in detail. Firstly, the levels of GFP-tagged SAC components in *ndc80*$^+$ and *ndc80-AK01* were measured by immunoblotting. Cells were grown overnight, diluted to 4 x 10^6 cells/ml and then they were incubated for 3 hours at 27˚C in the presence or absence of 50 μg/ml TBZ and 60 μg/ml of CBZ for 3 hours. Using anti-GFP antibodies, the levels of SAC components were assessed in the *ndc80-AK01* background (Figure 4.4a-b). The levels of Mad1, Mad3, Bub1, Bub3, Mph1 and Ark1 in *ndc80*$^+$ and *ndc80-AK01* are very similar (Figure 4.4a-b). Mad2-GFP levels are slightly elevated in *ndc80-AK01*, which is discussed further in Chapter 4.4. Furthermore, the TBZ sensitivity of *ndc80-AK01* SAC-GFP component strains is the same as original *ndc80-AK01* mutant, making the strains available and suitable for the experiments (Figure 4.4c).

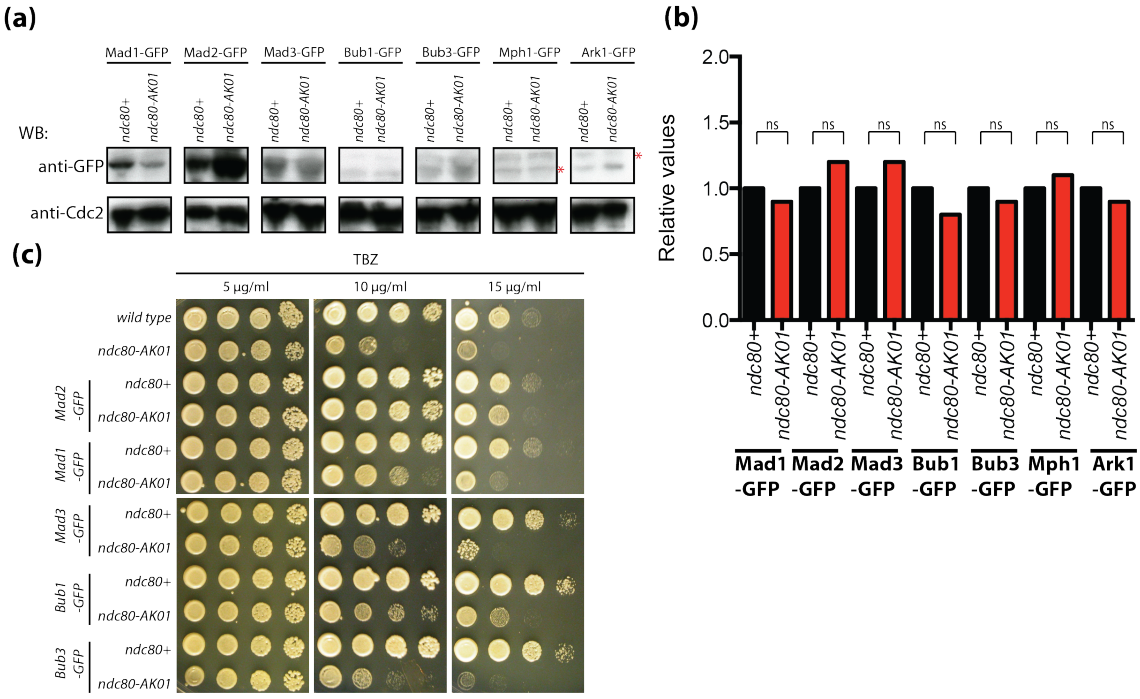

Figure 4.4. GFP-tagged SAC components are expressed at normal levels in *ndc80-AK01*.

(a) Protein extracts were prepared from indicated strains grown in YE5S medium overnight at 27˚C. Immunoblotting was performed with affinity-purified anti-GFP (top) and anti-Cdc2 antibody (bottom). 20 μg of protein extracts was loaded in each lane. Red asterisks indicate nonspecific bands. (b) Relative intensities of GFP-tagged SAC components in *ndc80*$^{+}$ and *ndc80-AK01* were calculated against Cdc2 (GFP/Cdc2). Error bars represent standard deviations from 3 independent immunoblots. An unpaired t test was carried out. (c) A serial dilution assay of strains tagged with GFP used in the current study. The number of initial spot cells (far-left) was 5 x 10^4 cells followed by ten fold dilutions. Cells were plated on YE5S, YE5S containing indicated amounts of TBZ and grew for 3 days at 27˚C.

4.2 Downstream spindle assembly checkpoint components are not recruited to the kinetochore in *ndc80-AK01* under mitotic arrest conditions

The next part of the analysis of *ndc80-AK01* mutant phenotypes was live imaging to observe the localisation of GFP-tagged SAC components localisation during cell division, with Plo1-mCherry used as a mitotic marker. *ndc80*$^{+}$ and *ndc80-AK01* were observed under mitotic arrest conditions, induced by TBZ/CBZ microtubule depolymerising drugs or the *cut7-446* conditional mutant. Live imaging was carried out

at 27˚C in the presence of 50 μg/ml TBZ and 60 μg/ml of CBZ, or alternatively in a *cut7-446* background upon shift up to 36˚C.

4.2.1 Mad2 and Mad1 are absent from kinetochores in *ndc80-AK01*

Some of the first identified 'mitotic arrest deficient' mutants have critical roles in checkpoint signalling (Li and Murray, 1991). More importantly, these components are widely conserved in model organisms (Li and Murray, 1991). Mad1 and Mad2 form dimers individually and collectively assemble into a tetramer. During interphase Mad1-Mad2 localise to nuclear pore complexes and then to the kinetochore in mitosis (Schweizer et al., 2013, Rodriguez-Bravo et al., 2014, Kruse et al., 2014).

First of all, I carried out live imaging to examine the localisation patterns of Mad1 and Mad2 in the *ndc80-AK01* mutant. In the presence of TBZ/CBZ, Mad2-GFP localises to kinetochores throughout mitosis in wild type cells (Figure 4.5a-b). However, in *ndc80-AK01*, Mad2-GFP accumulates in the nucleus but does not localise to kinetochores (Figure 4.5a-b), suggesting that *ndc80-AK01* is defective in recruiting Mad2. The levels of Plo1-mCherry remain the same in $ndc80^{+}$ and *ndc80-AK01* (Figure 4.5c). Furthermore, $ndc80^{+}$ cells spend more than 40 minutes in mitosis on average, whereas *ndc80-AK01* spends around 16 minutes (Figure 4.5d). When the mitotic arrest was induced by monopolar spindle formation in the *cut7-446* background, 30 minutes after shift up to 36˚C, similar phenotypes were observed (Figure 4.6). Mad2-GFP retained its nuclear localisation, but could not localise to kinetochores in *ndc80-AK01* (Figure 4.6a-c). Additionally, when looking at Plo1-mCherry levels, there is no difference between $ndc80^{+}$ and *ndc80-AK01*. Also the mitotic arrest observed is shorter for *ndc80-AK01* compared to wild type (Figure 4.6c).

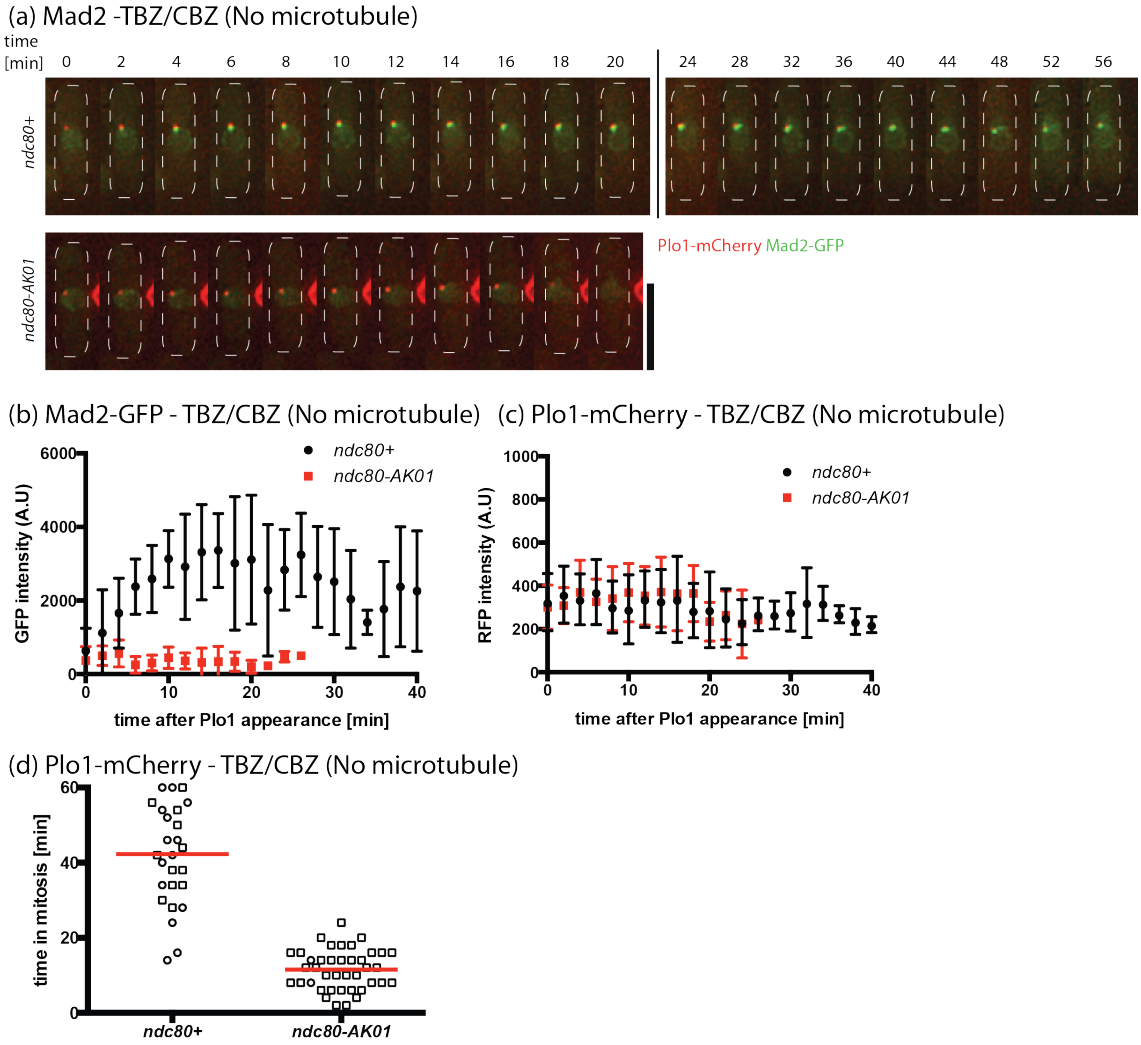

Figure 4.5. Mad2-GFP does not localise to the kinetochore in *ndc80-AK01* under mitotic arrest conditions.

Exponentially growing cells (4 x 10^6 cells/ml) were placed in YE5S with 50 µg/ml TBZ and 60 µg/ml of CBZ at 27˚C. After 30 minutes, live samples were placed on lectin-coated dishes and imaged for 60 minutes. (a) Representative images of *ndc80*$^+$ and *ndc80-AK01* with Mad2-GFP and Plo1-mCherry. Scale bar, 10 µm. Quantification of Mad2-GFP (b) and Plo1-mCherry (c) signal intensities. n > 10 cells for *ndc80*$^+$ and *ndc80-AK01*. (d) Time in mitosis measured as the duration of Plo1-mCherry accumulation at SPB. n > 30 cells.

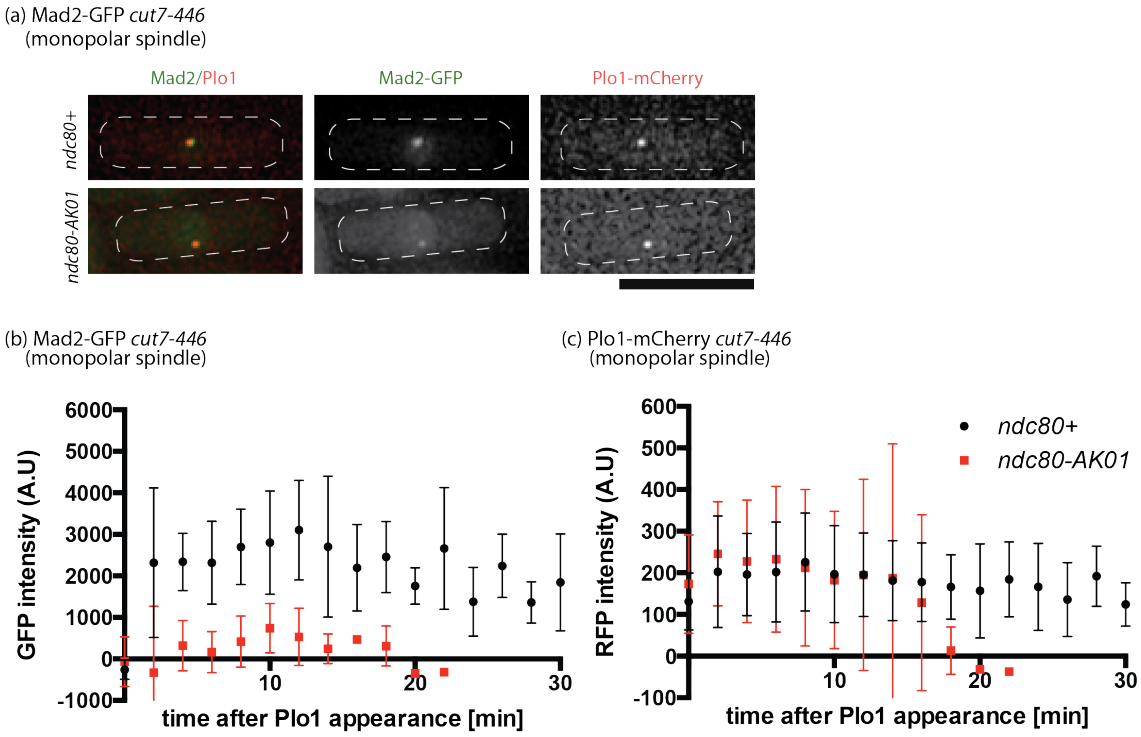

Figure 4.6. Mad2-GFP is reduced from kinetochore in *ndc80-AK01* in *cut7-446* background.

Exponentially growing cells (4 x 10^6 cells/ml) at 27˚C were shifted to 36˚C in YE5S. After 30 minutes the live samples were placed on lectin-coated dishes and imaged for 60 minutes. (a) Representative images of *ndc80*$^+$ and *ndc80-AK01* with Mad2-GFP and Plo1-mCherry. Scale bar, 10 µm. Quantification of Mad2-GFP (b) and Plo1-mCherry (c) signal intensities. n > 10 cells were counted for *ndc80*$^+$ and *ndc80-AK01*.

As Mad2-GFP localisation was reduced in *ndc80-AK01* in mitotic arrest condition, Mad1-GFP, which forms a tetramer with Mad2 (Luo et al., 2002, Sironi et al., 2002), was studied next. In the presence of TBZ/CBZ, Mad1-GFP localises to the nucleus in interphase with the misplacement of Mad1-GFP from the kinetochore during mitosis in *ndc80-AK01* (Figure 4.7a-c). In wild type cells, mitotic arrest lasts twice as long as in *ndc80-AK01* (Figure 4.7d). Furthermore, the observations of Mad1-GFP localisation in the *cut7-446* background gave the same conclusions (Figure 4.8). There is no Mad1-GFP localising to kinetochores in *ndc80-AK01 cut7-446* and the time in mitosis for mutant is 20 minutes shorter than *ndc80*$^+$ *cut7-446* (Figure 4.8a-c). Mad2 and Mad1 are the most downstream components in the SAC signalling cascade and their kinetochore localisation is abolished from the kinetochore upon deletion of any of the other components – *bub1*Δ, *mad3*Δ, *mph1*Δ or *ark1*Δ (Heinrich et al., 2012).

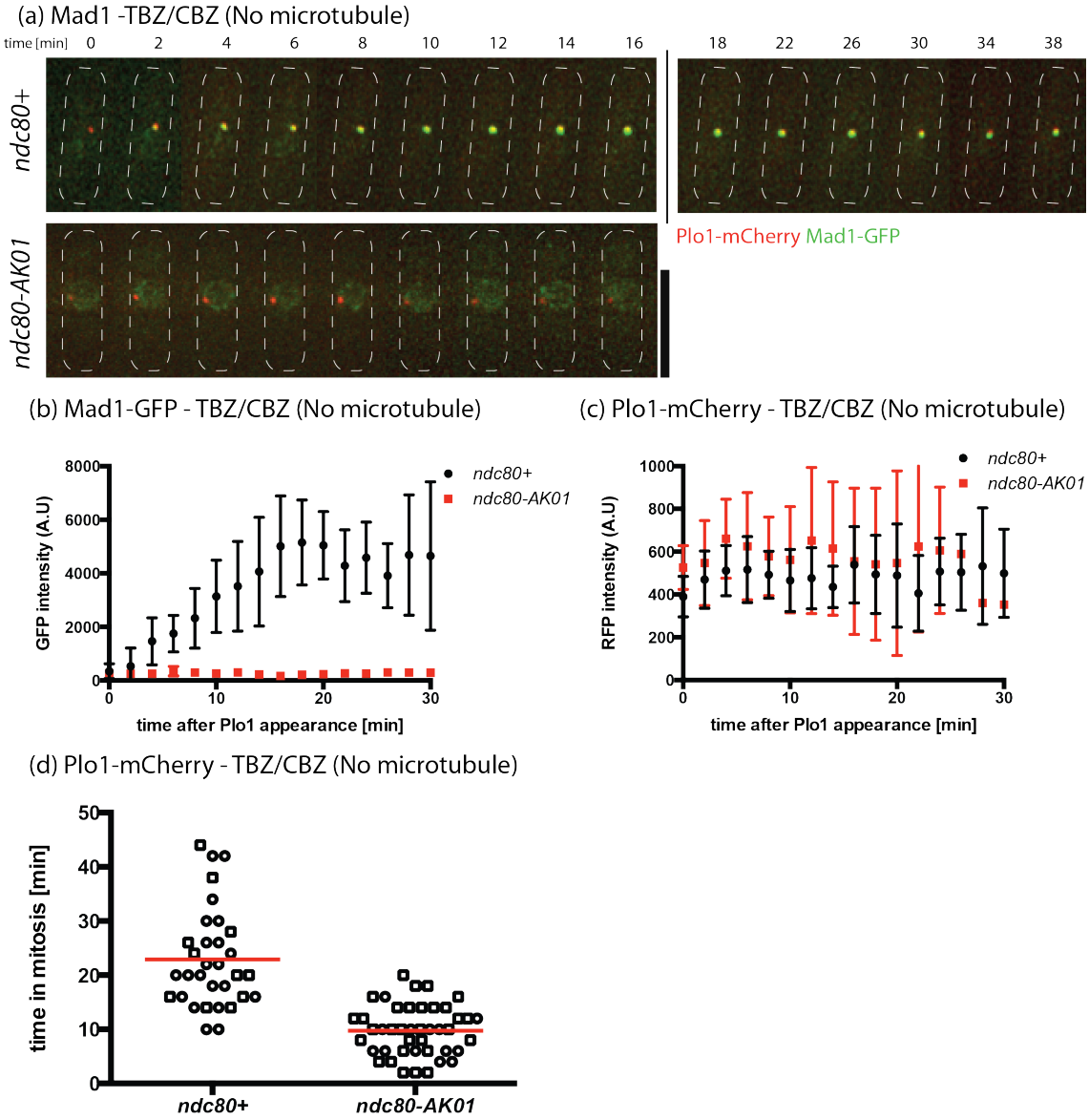

Figure 4.7. Mad1-GFP is absent from kinetochore in *ndc80-AK01* in absence of microtubules.

Exponentially growing cells (4 x 10^6 cells/ml) were cultured in YE5S with 50 µg/ml TBZ and 60 µg/ml of CBZ at 27˚C. After 30 minutes the live samples were placed on lectin-coated dishes and imaged for 60 minutes. (a) Representative images of *ndc80*$^+$ and *ndc80-AK01* with Mad1-GFP and Plo1-mCherry. Scale bar, 10 µm. Quantification of Mad1-GFP (b) and Plo1-mCherry (c) signal intensities. n > 10 cells for *ndc80*$^+$ and *ndc80-AK01*. (d) Time in mitosis measured as the duration of Plo1-mCherry accumulation at SPB. n > 30 cells.

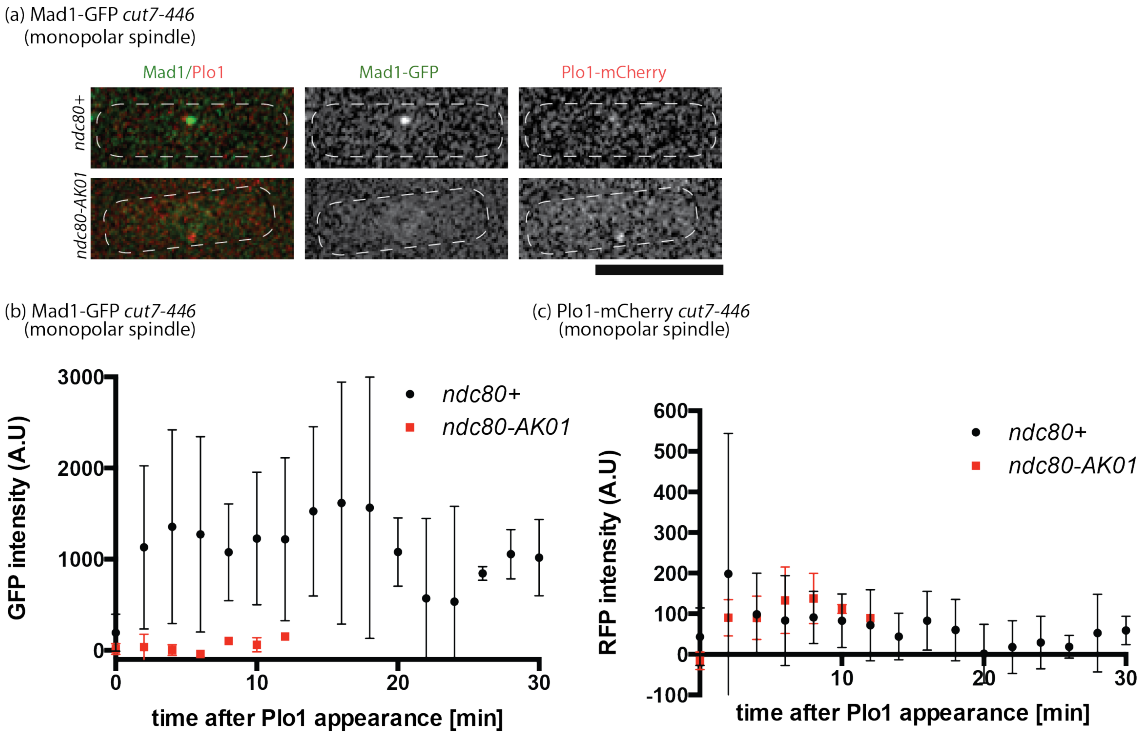

Figure 4.8. Mad1-GFP is mislocalised from kinetochore in *ndc80-AK01 cut7-446*.

Exponentially growing cells (4 x 10^6 cells/ml) at 27˚C were shifted to 36˚C in YE5S. After 30 minutes the live samples were placed on lectin- coated dishes and imaged for 60 minutes. (a) Representative images of *ndc80*$^+$ and *ndc80-AK01* with Mad1-GFP and Plo1-mCherry. Scale bar, 10 µm. Quantification of Mad1-GFP (b) and Plo1-mCherry (c) signal intensities. n >10 cells for *ndc80*$^+$ and *ndc80-AK01*.

4.2.2 Mad3, Bub1 and Bub3 are also absent from the kinetochore in *ndc80-AK01*

Subsequently, the localisation patterns of Mad3 (BubR1 in human), Bub1 and Bub3 tagged with GFP were analysed in *ndc80-AK01* under mitotic arrest conditions. These proteins were recently shown to localise to KNL-1/Spc7 upon phosphorylation of the MELT motifs by Mph1/MPS1 (Yamagishi et al., 2012, Shepperd et al., 2012). It was shown that Bub1-Bub3 form a complex and their recruitment is essential for Mad1 and Mad2 localisation to the kinetochore (Yamagishi et al., 2012, Shepperd et al., 2012, Heinrich et al., 2012). Recently, in budding yeast, it was further shown that Bub1, upon phosphorylation by Mps1, is a receptor for Mad1 kinetochore localisation (London and Biggins, 2014a). Therefore, localisation patterns of Mad3, Bub1 and Bub3 in mitotic arrest conditions were examined.

As shown in Figure 4.9, in TBZ/CBZ conditions, Mad3-GFP localises to the kinetochore in *ndc80*$^{+}$ and this localisation is abolished in *ndc80-AK01*. There is no accumulation of Mad3-GFP at the kinetochore (Figure 4.9b) despite the similar levels of Plo1-mCherry signals in *ndc80*$^{+}$ and *ndc80-AK01* (Figure 4.9c). Additionally, the duration of mitosis is on average 20 minutes shorter in *ndc80-AK01* compared to wild type in TBZ/CBZ conditions (Figure 4.9d). Moreover, Mad3-GFP does not localise to the kinetochore in *ndc80-AK01* under *cut7-446* conditions (Figure 4.10). In restrictive conditions (36˚C), the time in mitosis is 26 minutes and 10 minutes for *ndc80*$^{+}$ and *ndc80-AK01* respectively (Figure 4.10c). This duration is shorter than in TBZ/CBZ conditions but the difference most likely results from a different experimental setup; higher temperatures that accelerate cellular processes such as mitosis.

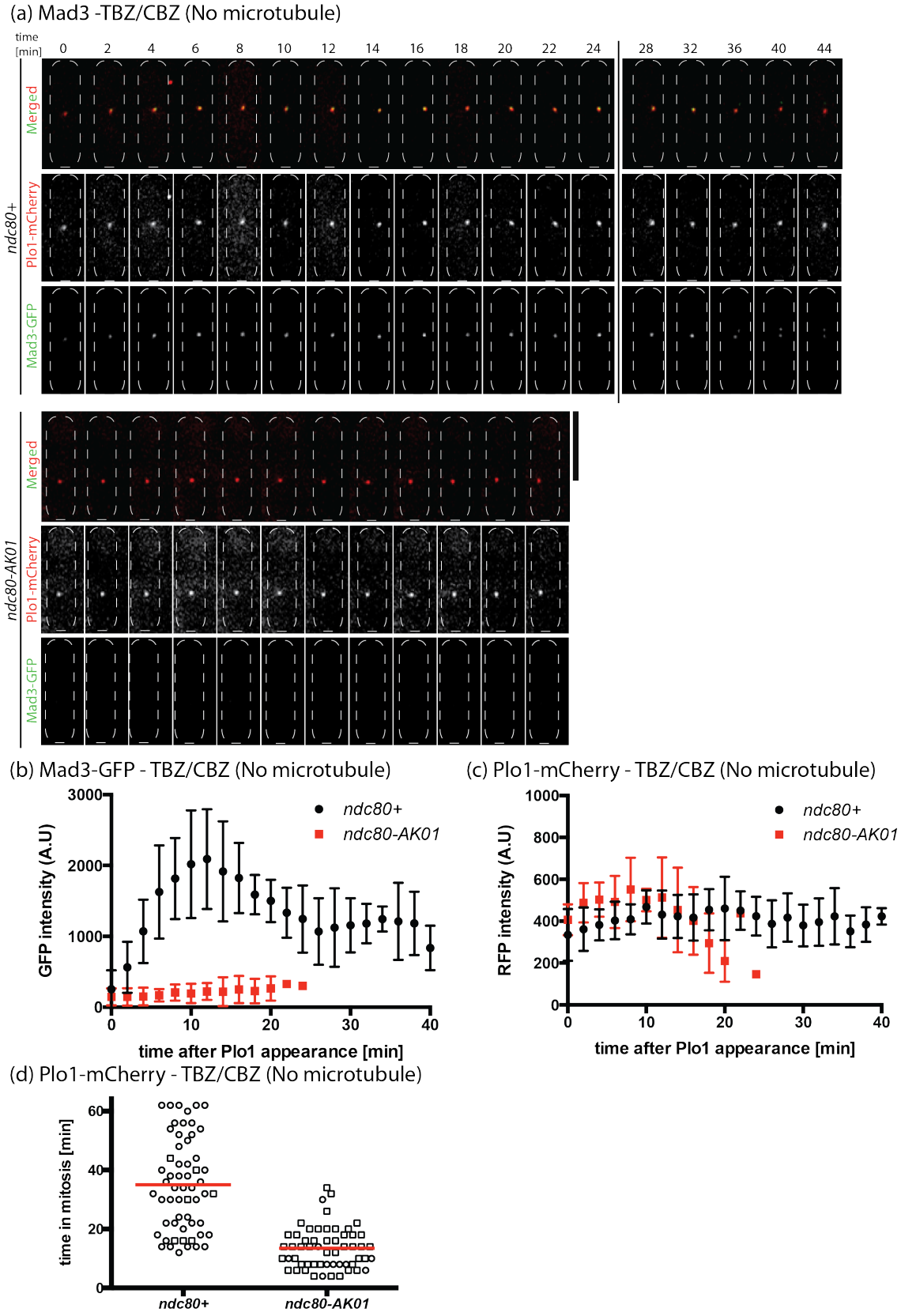

Figure 4.9. Mad3-GFP is absent from kinetochore in *ndc80-AK01*.

(Legend from Figure 4.9 continued)
Exponentially growing cells (4 x 10^6 cells/ml) were placed in YE5S with 50 µg/ml TBZ and 60 µg/ml of CBZ at 27˚C. After 30 minutes the samples were placed on lectin coated dishes and live imaged for 60 minutes. (a) Representative images of *ndc80*$^+$ and *ndc80-AK01* with Mad3-GFP and Plo1-mCherry. Scale bar, 10 µm. The quantification of Mad3-GFP (b) and Plo1-mCherry (c) signal intensities. More than 10 cells were counted for *ndc80*$^+$ and *ndc80-AK01*. (d) The time in mitosis counted as the duration of Plo1-mCherry accumulation at SPB. More than 30 cells were counted.

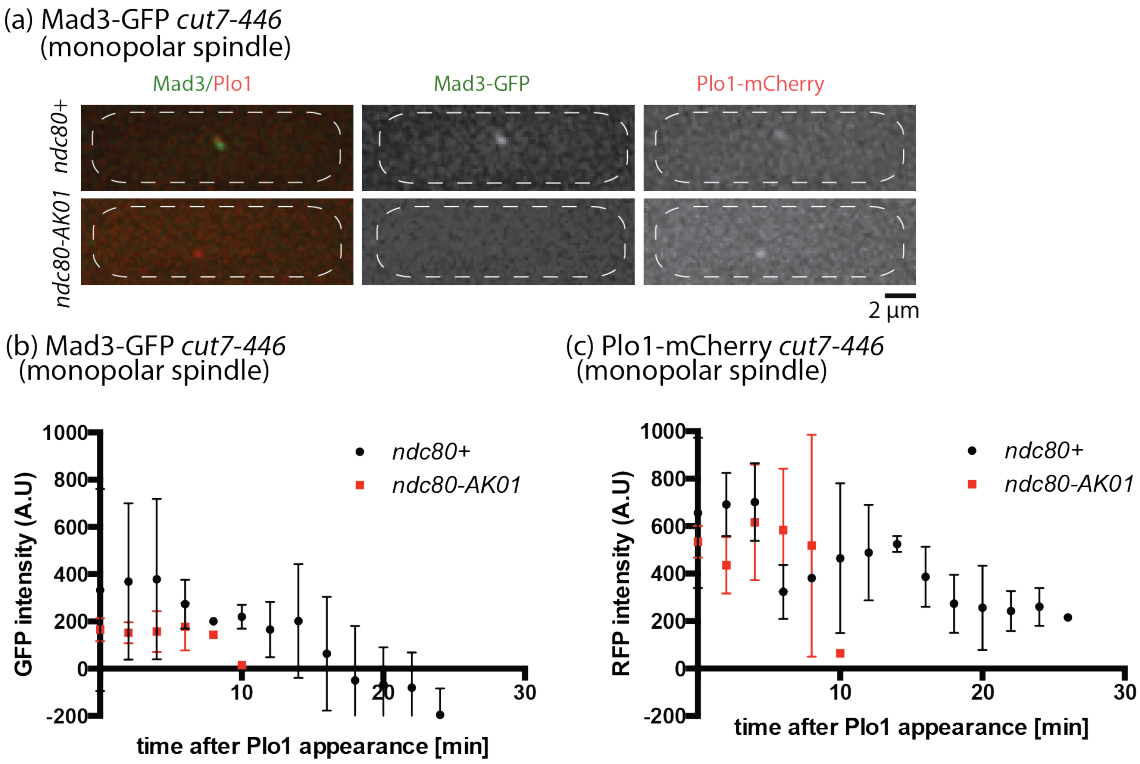

Figure 4.10. Mad3-GFP does not localise to kinetochores in *ndc80-AK01 cut7-446*.

Exponentially growing cells (4 x 10^6 cells/ml) at 27˚C were shifted to 36˚C in YE5S. After 30 minutes the live samples were placed on lectin-coated dishes and imaged for 60 minutes. (a) Representative images of *ndc80*$^+$ and *ndc80-AK01* with Mad3-GFP and Plo1-mCherry. Scale bar, 10 µm. Quantification of Mad3-GFP (b) and Plo1-mCherry (c) signal intensities. n > 10 cells for *ndc80*$^+$ and *ndc80-AK01*.

Next, the localisation of Bub1 tagged with GFP was observed. In the presence of 50 µg/ml TBZ and 60 µg/ml of CBZ, Bub1 does not localise to the kinetochore in *ndc80-AK01* (Figure 4.11a-c). GFP-tagged Bub1 levels are reduced to background values in *ndc80-AK01*, despite Plo1-mCherry levels remaining similar in wild type and *ndc80-AK01* (Figure 4.11b-c). Furthermore, there is no mitotic arrest observed in the mutant

background, cells spent an average of 18 minutes in mitosis compared to 40 minutes for wild type (Figure 4.12d). Furthermore, the analysis of Bub1-GFP in *ndc80-AK01 cut7-446* background is in accordance with previous experiments, where Bub1-GFP is absent from the kinetochore in TBZ/CBZ, as shown in Figure 4.12. As the data in *cut7-446* experiments was in accordance with the observations in TBZ/CBZ conditions, mitotic arrests experiments induced only by TBZ/CBZ were carried out in the following experiments.

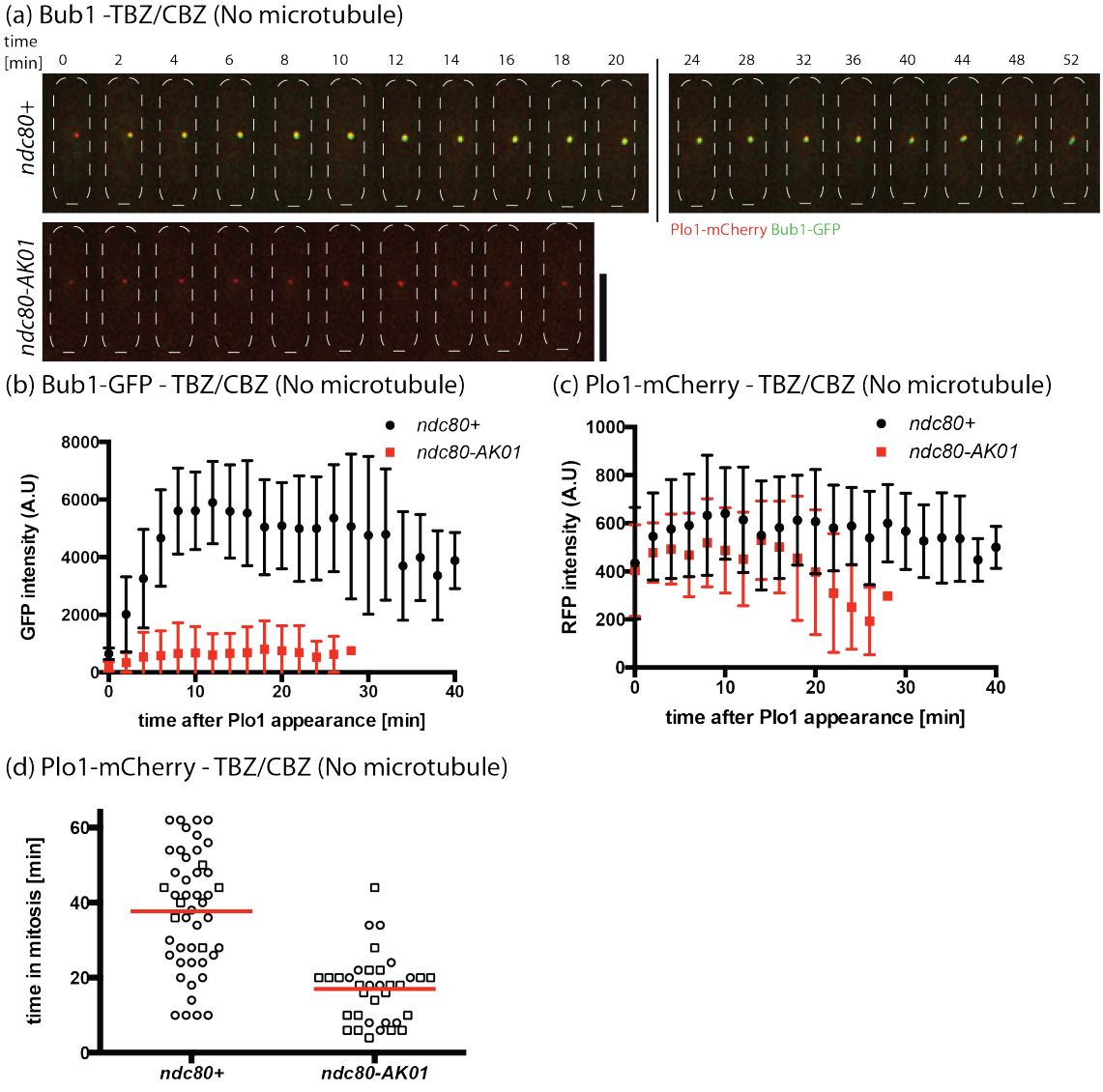

Figure 4.11. Bub1-GFP is absent from kinetochore in *ndc80-AK01*.

Exponentially growing cells (4 x 10^6 cells/ml) were placed in YE5S with 50 µg/ml TBZ and 60 µg/ml of CBZ at 27˚C. After 30 minutes the live samples were placed on lectin coated dishes and imaged for 60 minutes. (a) Representative images of *ndc80*$^+$ and *ndc80-AK01* with Bub1-GFP and Plo1-mCherry. Scale bar, 10 µm. Quantification of

(Legend from Figure 4.11 continued)
Bub1-GFP (b) and Plo1-mCherry (c) signal intensities. n > 10 cells for *ndc80*$^{+}$ and *ndc80-AK01*. (d) The time in mitosis counted as the duration of Plo1-mCherry accumulation at SPB. n > 30 cells.

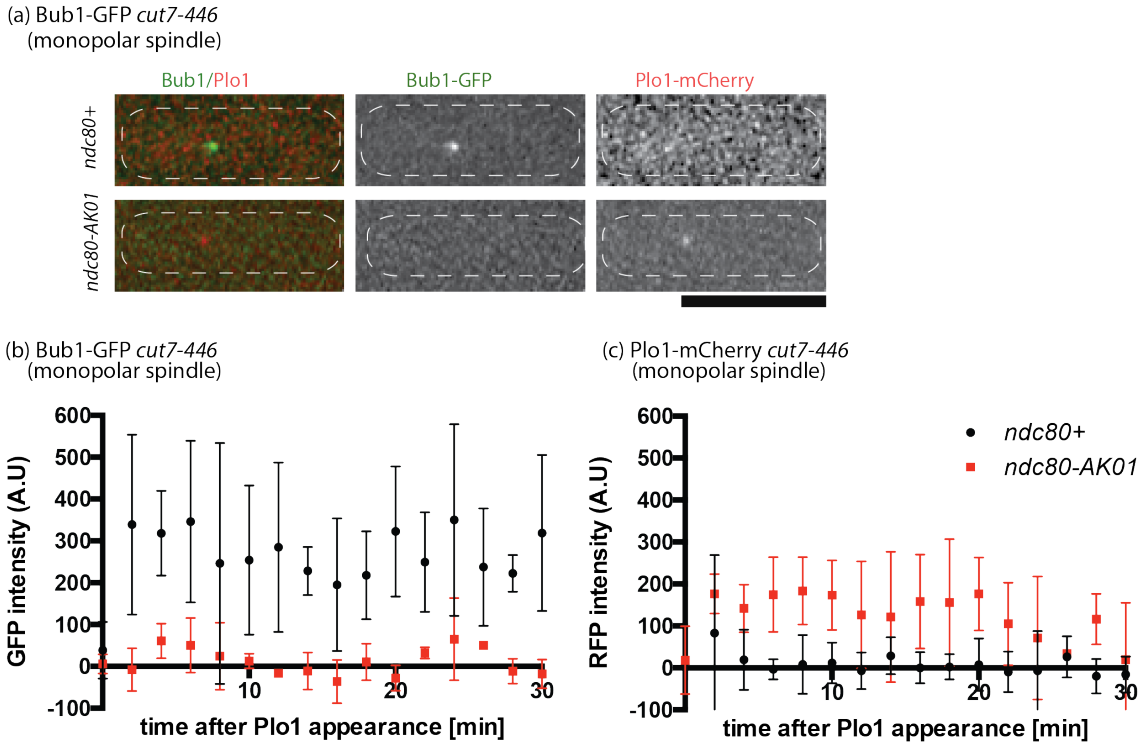

Figure 4.12. Bub1-GFP does not localise to kinetochore in *ndc80-AK01* in *cut7-446*.
Exponentially growing cells (4 x 10^{6} cells/ml) at 27˚C were shifted to 36˚C in YE5S. After 30 minutes the live samples were placed on lectin-coated dishes and imaged for 60 minutes. (a) Representative images of *ndc80*$^{+}$ and *ndc80-AK01* with Bub1-GFP and Plo1-mCherry. Scale bar, 10 µm. Quantification of Bub1-GFP (b) and Plo1-mCherry (c) signal intensities. n > 10 cells for *ndc80*$^{+}$ and *ndc80-AK01*.

As Bub1 and Bub3 form complex on KNL-1/Spc7, the localisation of Bub3-GFP to the kinetochore was also verified. As shown in Figure 4.13, in TBZ/CBZ conditions, Bub3-GFP does not localise to kinetochores in *ndc80-AK01*. Furthermore, there is a clear difference in duration of mitotic arrest between mutant and wild type - 22 minutes shorter for *ndc80-AK01* (Figure 4.13d).

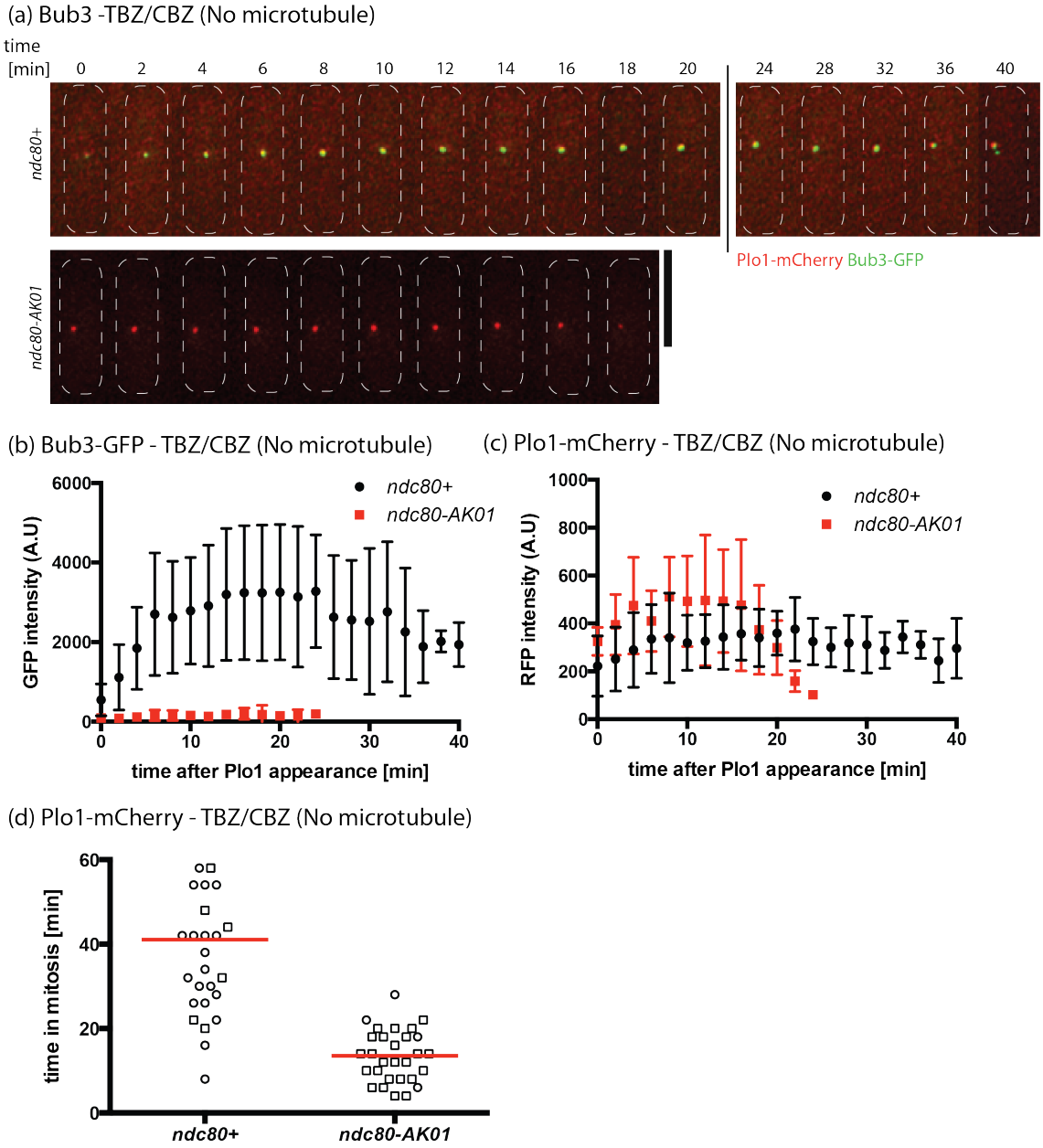

Figure 4.13. Bub3-GFP is absent from kinetochore in *ndc80-AK01*.

Exponentially growing cells (4 x 10^6 cells/ml) were placed in YE5S with 50 µg/ml TBZ and 60 µg/ml of CBZ at 27˚C. After 30 minutes the live samples were placed on lectin-coated dishes and imaged for 60 minutes. (a) Representative images of *ndc80*$^+$ and *ndc80-AK01* with Bub3-GFP and Plo1-mCherry. Scale bar, 10 µm. Quantification of Bub3-GFP (b) and Plo1-mCherry (c) signal intensities. n > 10 cells for *ndc80*$^+$ and *ndc80-AK01*. (d) The time in mitosis counted as the duration of Plo1-mCherry accumulation at SPB. n > 30 cells.

4.2.3 Mph1 and Ark1 are absent from the kinetochore in *ndc80-AK01* under mitotic arrest conditions

Localisation of Bub1, Bub3 and Mad3 is linked with the phosphorylation of KNL-1/Spc7 by Mph1/MPS1 (Yamagishi et al., 2012, Shepperd et al., 2012), therefore Mph1-GFP localisation required investigation. Additionally, Ark1/Aurora B is another upstream component in checkpoint signalling. There is a debate about the localisation of Ark1/Aurora B/Ipl1 in regards to Mph1/MPS1 and their dependencies between model organisms (Heinrich et al., 2012, Yamagishi et al., 2014). Therefore localisation of both components needs to be observed in *ndc80-AK01*.

GFP-tagged Mph1 and Ark1 were analysed in *ndc80*$^{+}$ and *ndc80-AK01* in mitotic arrest conditions, at 27˚C in presence of 50 μg/ml TBZ and 60 μg/ml of CBZ. For Mph1-GFP in TBZ/CBZ conditions, there is no localisation of Mph1 to kinetochores in *ndc80-AK01,* despite Plo1-mCherry remaining at the same level (Figure 4.14a-c). Similar to previous data, the time in mitosis is halved in *ndc80-AK01* (Figure 4.14d).

Next, the localisation of Ark1-GFP at the kinetochore in mitotic arrest conditions by TBZ/CBZ was observed. There is no Ark1-GFP signal observed in mitotic cells in *ndc80-AK01* (Figure 4.15a-c). Furthermore, the time cells spent in the arrested state is 18 minutes shorter in the mutant compared to wild type *ndc80*$^{+}$ (Figure 4.15d). These results may suggest that Ark1, as the most upstream component in fission yeast SAC signalling, is mislocalised from kinetochores and is primarily responsible for the observed mislocalisation of downstream components (Mph1, Bub1, Bub3, Mad3, Mad2 and Mad1).

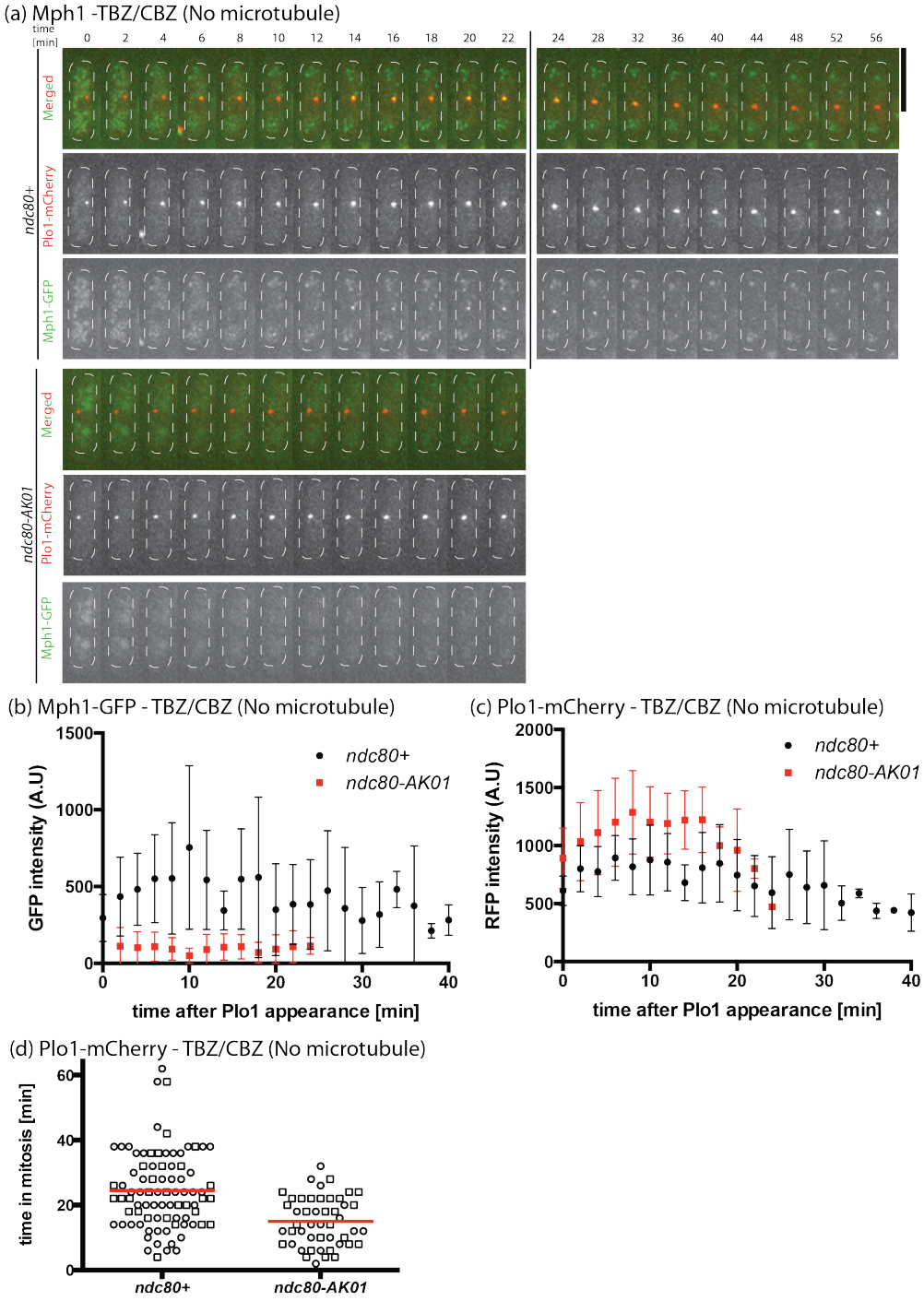

Figure 4.14. Mph1-GFP is absent from kinetochore in *ndc80-AK01*.

Exponentially growing cells (4 x 10^6 cells/ml) were placed in YE5S with 50 µg/ml TBZ and 60 µg/ml of CBZ at 27˚C. After 30 minutes the live samples were placed on lectin-coated dishes and imaged for 60 minutes. (a) Representative images of *ndc80*$^+$ and *ndc80-AK01* with Mph1-GFP and Plo1-mCherry. Scale bar, 10 µm. Quantification of Mph1-GFP (b) and Plo1-mCherry (c) signal intensities. n > 10 cells for *ndc80*$^+$ and *ndc80-AK01*. (d) The time in mitosis counted as the duration of Plo1-mCherry accumulation at SPB. n > 30 cells were counted.

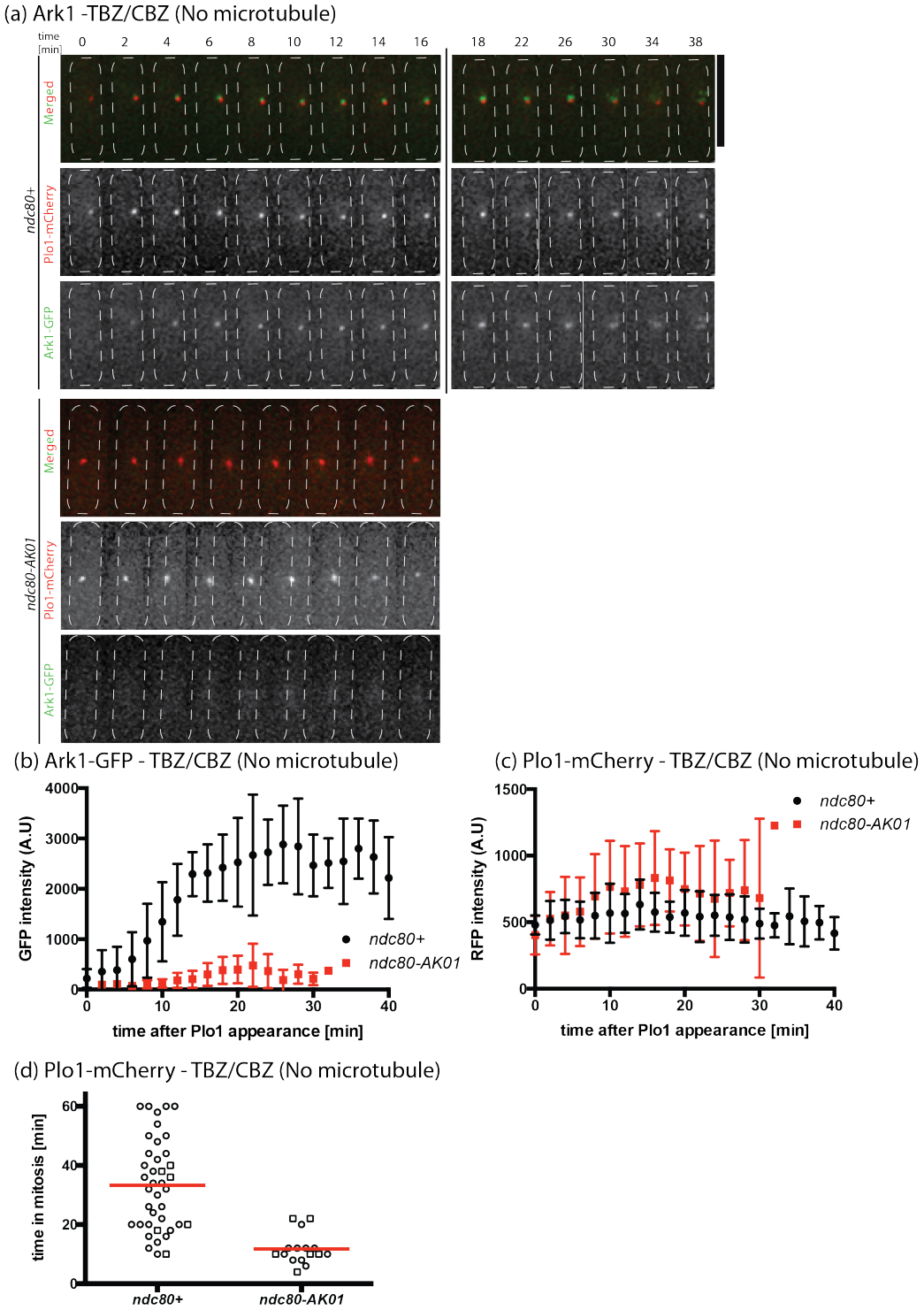

Figure 4.15. Ark1-GFP is absent from kinetochore in *ndc80-AK01*.

Exponentially growing cells (4 x 10^6 cells/ml) were placed in YE5S with 50 µg/ml TBZ and 60 µg/ml of CBZ at 27˚C. After 30 minutes the live samples were placed on lectin-coated dishes and imaged for 60 minutes. (a) Representative images of *ndc80*$^+$ and *ndc80-AK01* with Ark1-GFP and Plo1-mCherry. Scale bar, 10 µm. Quantification of Ark1-GFP (b) and Plo1-mCherry (c) signal intensities. n > 10 cells for *ndc80*$^+$ and

(Legend from Figure 4.15 continued)
ndc80-AK01. (d) The time in mitosis counted as the duration of Plo1-mCherry accumulation at SPB. n > 30 cells.

4.2.4 The reduction of Ark1 levels at the kinetochore may be attributed to the absence of Bub1 from the kinetochore

Despite the notion that Ark1 is the most upstream component of the SAC signalling pathway, recent observations of Ark1-GFP localisation and levels in *nda3-KM311*-mitotic arrest conditions show a clear reduction of GFP signals at the kinetochore in *bub1*Δ and *mph1*Δ of 90% and 70% respectively (Heinrich et al., 2012). Also in asynchronously growing cells at 30˚C, there is more than 50% reduction in signal intensities in *bub1*Δ. A feedback loop may exist from Bub1 kinase, which is essential in phosphorylating H2A-S121, leading to centromeric recruitment of Sgo2 where in turn more Ark1/Aurora would localise (Kawashima et al., 2010b, Lin et al., 2014). Therefore, the localisation of Ark1-GFP was investigated in *bub1*Δ under mitotic arrest conditions used in my experimental design.

There is a reduction in Ark1-GFP levels at the kinetochore in *bub1*Δ*,* similar to *ndc80-AK01* (Figure 4.16a-c). This reduction is similar to that observed in *bub1*Δ *nda3-KM311* (Heinrich et al., 2012), despite slightly altered experimental conditions (the presence of TBZ/CBZ at 27˚C, rather than *nda3-KM311*). Additionally, there is more than 50% reduction in the amount of time the cells spent in mitosis in *bub1*Δ and *ndc80-AK01*, when compared to wild type (Figure 4.16d). Therefore, the reduction of Ark1-GFP from the kinetochore in *ndc80-AK01* might result from the feedback from Bub1, which is absent from kinetochores in *ndc80-AK01*.

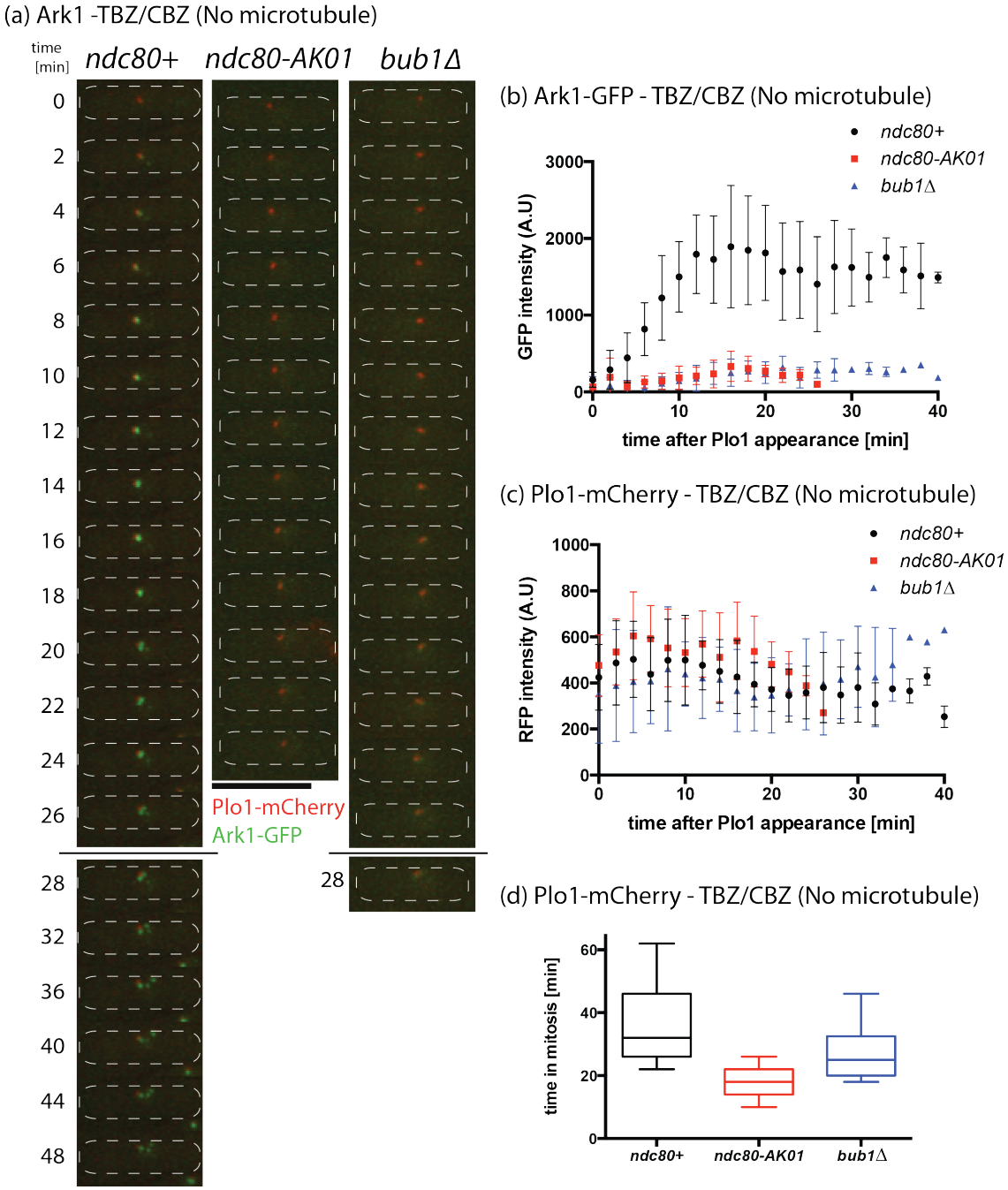

Figure 4.16. Reduction of Ark1-GFP from kinetochore is linked with Bub1 absence.

Exponentially growing cells (4 x 10^6 cells/ml) were placed in YE5S with 50 µg/ml TBZ and 60 µg/ml of CBZ at 27˚C. After 30 minutes the live samples were placed on lectin-coated dishes and imaged for 60 minutes. (a) Representative images of *ndc80*$^+$ and *ndc80-AK01* with Ark1-GFP and Plo1-mCherry. Scale bar, 10 µm. Quantification of Ark1-GFP (b) and Plo1-mCherry (c) signal intensities. n > 10 cells for *ndc80*$^+$, *ndc80-AK01* and *bub1*Δ. (d) The time in mitosis counted as the duration of Plo1-mCherry accumulation at SPB. n > 30.

4.3 Recruitment of spindle assembly checkpoint components to the kinetochore is impaired in *ndc80-AK01* under unperturbed conditions

After the analysis of SAC components during mitotic arrest, the localisation of GFP-tagged SAC components was observed by live imaging at 27˚C during unperturbed cell division cycle. Exponentially growing cells at 4 x 10^6 cells/ml were placed on lectin-coated plates and imaged using Deltavision system.

4.3.1 Mad1, Mad3, Bub3, Bub1 and Mph1 are absent from kinetochore in *ndc80-AK01*

The localisation of Mad1-GFP in unperturbed conditions (Figure 4.17) is very similar to the one observed under mitotic arrest (Figure 4.7 and Figure 4.8). Firstly, Mad1-GFP nuclear localisation during interphase is clearly observed in *ndc80*$^+$ and *ndc80-AK01*. Secondly, there is a reduction of GFP signals from the kinetochore in *ndc80-AK01* (Figure 4.17), analogously to that during mitotic arrest conditions, there is no Mad1-GFP detected at the kinetochore in *ndc80-AK01* (Figure 4.7a-b, Figure 4.8a-b).

Next, Mad3-GFP localisation was observed in unperturbed conditions. There is a clear reduction of the protein from kinetochore in *ndc80-AK01* (Figure 4.18). This data is in accordance with reductions of Mad3-GFP kinetochore levels in mitotic arrest conditions (Figure 4.9 and Figure 4.10).

Subsequently, the localisation of Bub1 and Bub3 tagged with GFP was examined in unperturbed conditions. Similar to Mad3-GFP, both Bub1 and Bub3 proteins do not localise to the kinetochore in *ndc80-AK01* (Figure 4.19 and Figure 4.20). This data is consistent with observations of Bub1-GFP and Bub3-GFP in *ndc80-AK01* under both types of mitotic arrest conditions (Figure 4.11 and Figure 4.13) and (Figure 4.12).

Bub1, Bub3 and Mad3, normally localising to phosphorylated KNL-1/Spc7, were reduced at the kinetochore, what prompted me to investigate Mph1/Mps1 kinase

localisation. As shown on Figure 4.21, there is a reduction or absence of Mph1 from the kinetochore in *ndc80-AK01* under unperturbed conditions. This data supports the observations of Mph1-GFP localisation in *ndc80-AK01* in the absence of microtubules (Figure 4.14).

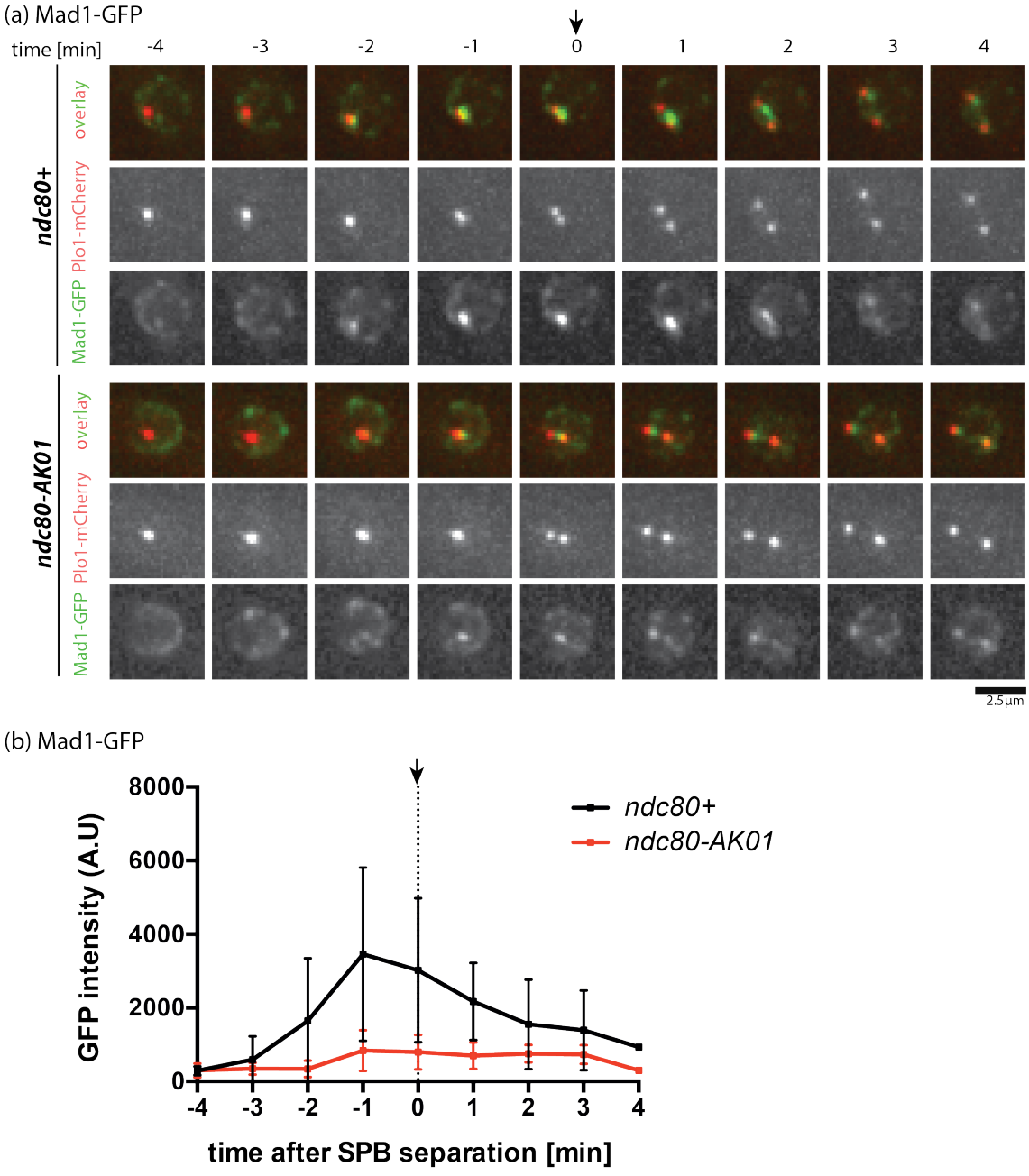

Figure 4.17. Mad1-GFP is reduced from kinetochore in *ndc80-AK01*.

Exponentially growing cells (4 x 10^6 cells/ml) were placed in YE5S at 27˚C. The live samples were placed on lectin-coated dishes, left for 10 minutes and imaged for 30 minutes. (a) Representative images of *ndc80*$^+$ and *ndc80-AK01* with Mad1-GFP and

(Figure 4.17, legend continued)
Plo1-mCherry. Scale bar, 2.5 µm. (b) Quantification of Mad1-GFP signal intensities. n > 10 cells.

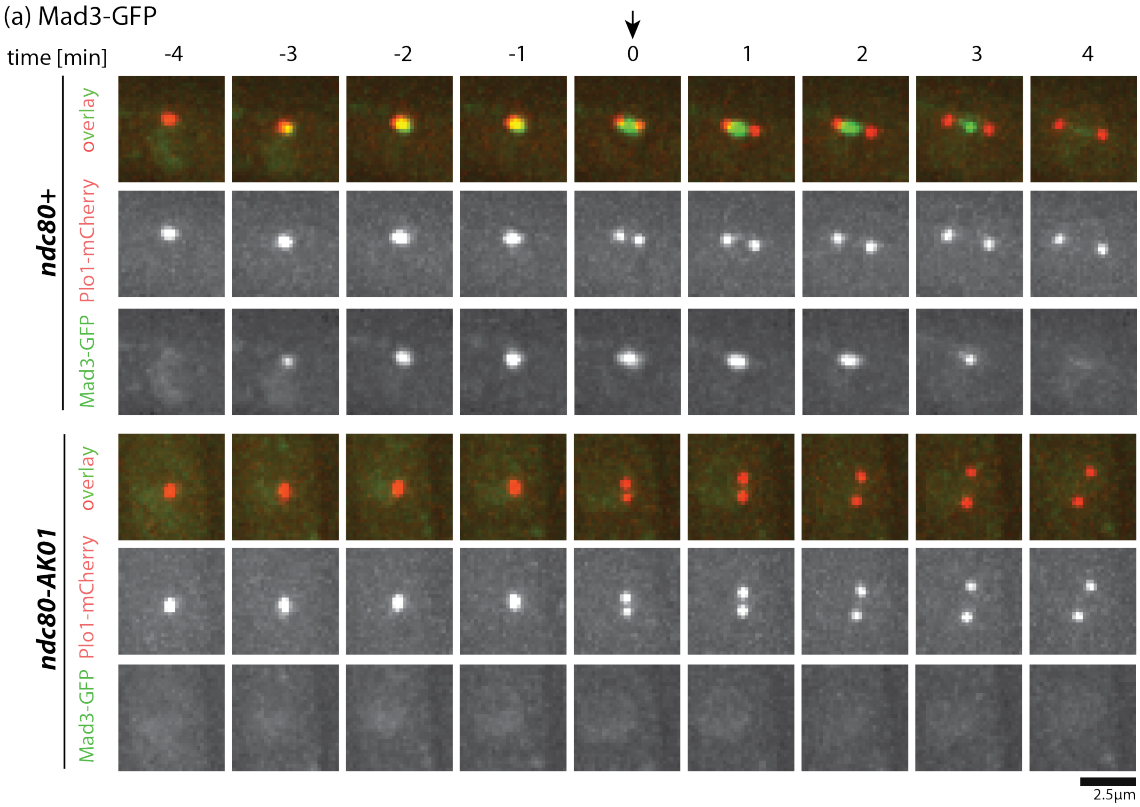

Figure 4.18. Mad3-GFP does not localise at kinetochore in *ndc80-AK01*.

Exponentially growing cells (4 x 10^6 cells/ml) were placed in YE5S at 27˚C. The live samples were placed on lectin-coated dishes, left for 10 minutes and imaged for 30 minutes. (a) Representative images of *ndc80*$^+$ and *ndc80-AK01* with Mad3-GFP and Plo1-mCherry. Scale bar, 2.5 µm. (b) Quantification of Mad3-GFP signal intensities. n >10 cells.

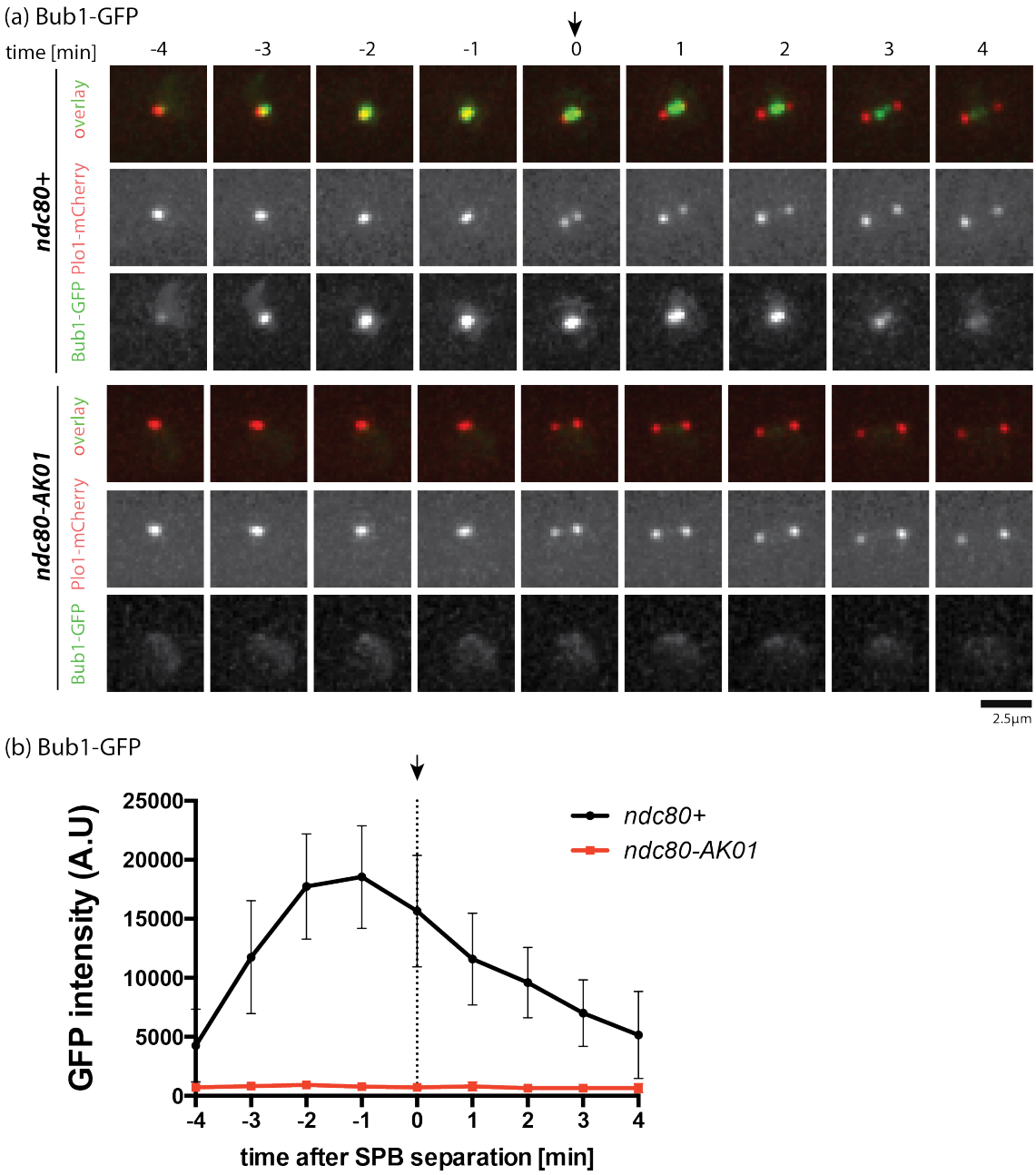

Figure 4.19. Bub1-GFP does not localise to kinetochore in *ndc80-AK01*.

Exponentially growing cells (4 x 10^6 cells/ml) were placed in YE5S at 27˚C. The live samples were placed on lectin-coated dishes, left for 10 minutes and imaged for 30 minutes. (a) Representative images of *ndc80*$^+$ and *ndc80-AK01* with Bub1-GFP and Plo1-mCherry. Scale bar, 2.5 µm. (b) Quantification of Bub1-GFP signal intensities. n > 10 cells.

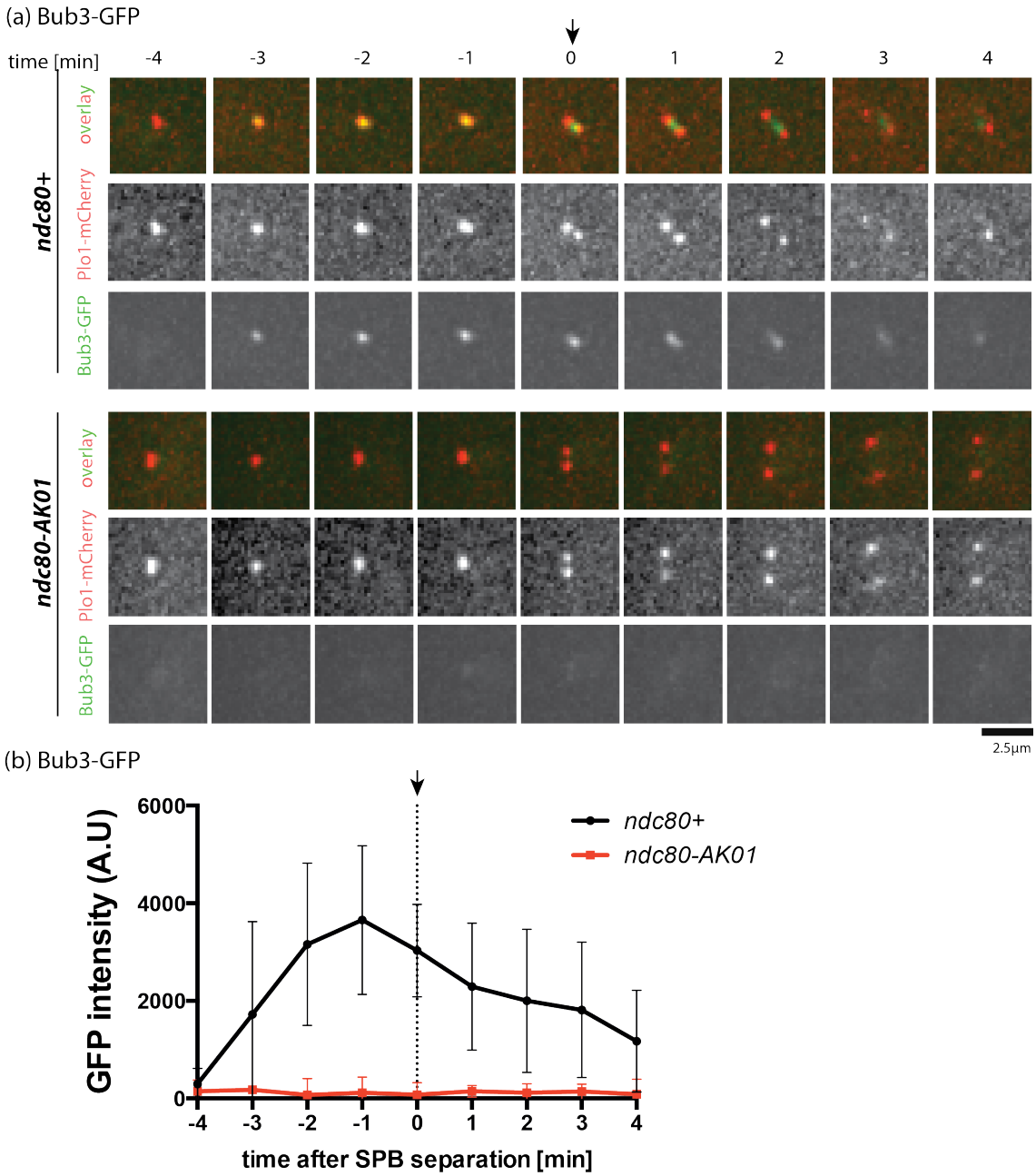

Figure 4.20. Bub3-GFP does not localise to kinetochore in *ndc80-AK01*.

Exponentially growing cells (4 x 10^6 cells/ml) were placed in YE5S at 27˚C. The live samples were placed on lectin-coated dishes, left for 10 minutes and imaged for 30 minutes. (a) Representative images of *ndc80*$^+$ and *ndc80-AK01* with Bub3-GFP and Plo1-mCherry. Scale bar, 2.5 µm. (b) Quantification of Bub3-GFP signal intensities. n > 10 cells.

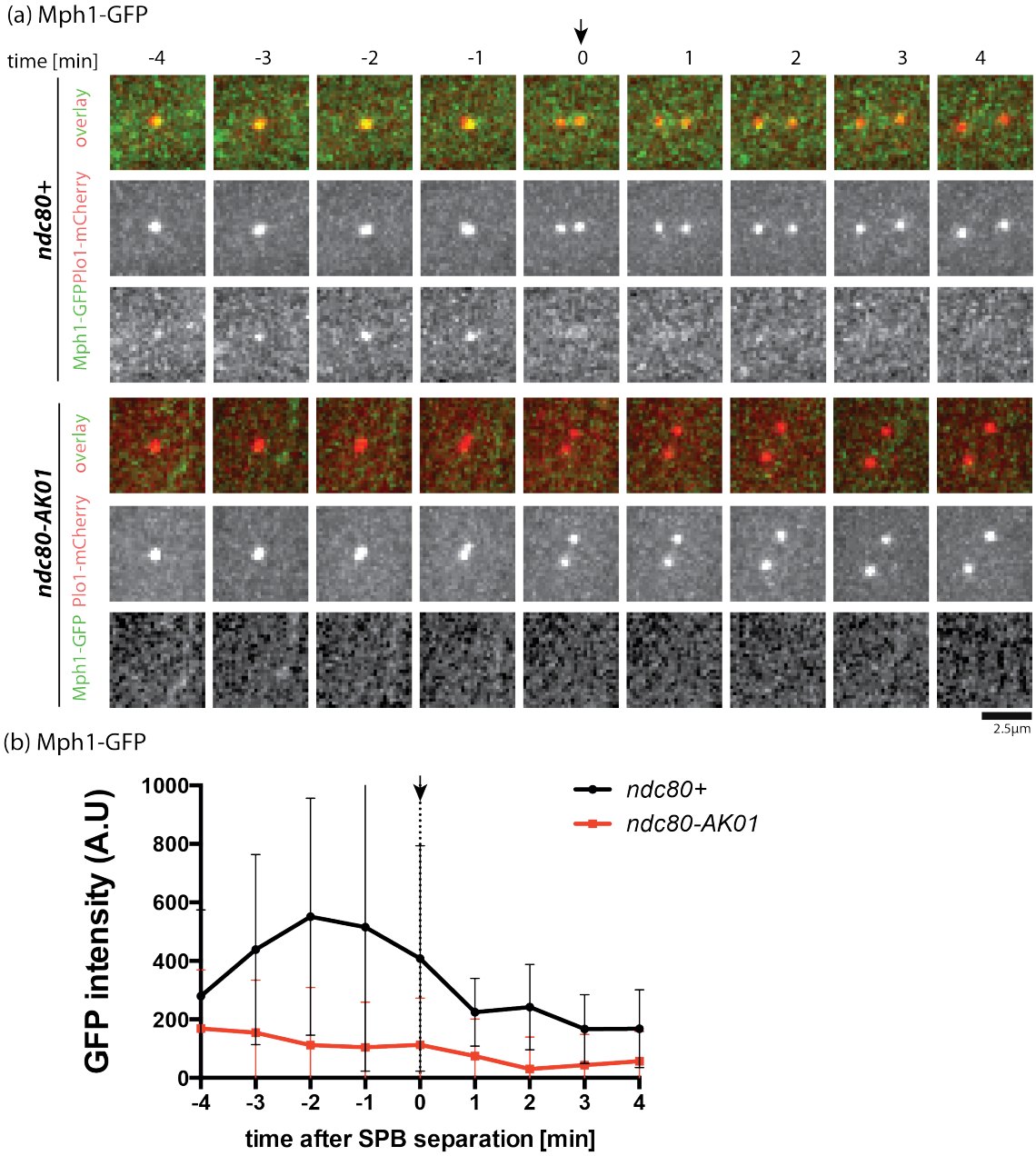

Figure 4.21. Mph1-GFP does not localise to kinetochore in *ndc80-AK01*.

Exponentially growing cells (4 x 10^6 cells/ml) were placed in YE5S at 27˚C. The live samples were placed on lectin-coated dishes, left for 10 minutes and imaged for 30 minutes. (a) Representative images of *ndc80*$^+$ and *ndc80-AK01* with Mph1-GFP and Plo1-mCherry. Scale bar, 2.5 µm. (b) Quantification of Mph1-GFP signal intensities. n > 10 cells.

4.3.2 Mad2 and Ark1 are reduced from kinetochore in the *ndc80-AK01* mutant under unperturbed conditions

The localisation of the last two remaining spindle assembly checkpoint components (Mad2 and Ark1) was also analysed in the *ndc80-AK01* background under unperturbed conditions.

For Mad2-GFP, as shown earlier, in the absence of microtubules (Figure 4.5) or presence of monopolar spindles (Figure 4.6), there is a clear mislocalisation of the protein from kinetochores in *ndc80-AK01*. However, there is a strong interphase nuclear localisation, which seems to persist at the nuclear envelope even in the mutant background (Figure 4.5). In unperturbed conditions, however, Mad2-GFP localises normally to kinetochore in *ndc80-AK01,* even with similar expression levels to $ndc80^{+}$ (Figure 4.22). The contradiction regarding Mad2-GFP kinetochore localisation in the unperturbed and mitotic arrest conditions might be due to different depletion levels of Mad1 at the kinetochore. As the localisation of Mad2 is linked with the presence of Mad1-GFP at the kinetochore (Heinrich et al., 2012) and there is still some Mad1-GFP observed (Figure 4.17) in *ndc80-AK01*, that may already lead to Mad2-GFP accumulation at the kinetochore (even at low levels of Mad1 observed) in *ndc80-AK01* (see Chapter 4.3.3, Figure 4.24).

When looking at Ark1-GFP levels, there was also no reduction of GFP levels at the kinetochore in *ndc80-AK01* at 27˚C (Figure 4.23). This is in contrary to the observations of Ark1-GFP in *ndc80-AK01* in the absence of microtubules, where there is no Ark1-GFP left at the kinetochore (Figure 4.15). As shown, the reduction was linked with the feedback loop from Bub1, which is absent in *ndc80-AK01* (Figure 4.16). The localisation of Ark1-GFP in *bub1*Δ remains to be determined. However, it is possible that regulation of Bub1 "feedback" toward Ark1 is weaker in unperturbed conditions than mitotic arrest (also the amount of Bub1 accumulated in mitotic arrest (Figure 4.11 and Figure 4.12) appears bigger than in experiments at 27˚C (Figure 4.19)).

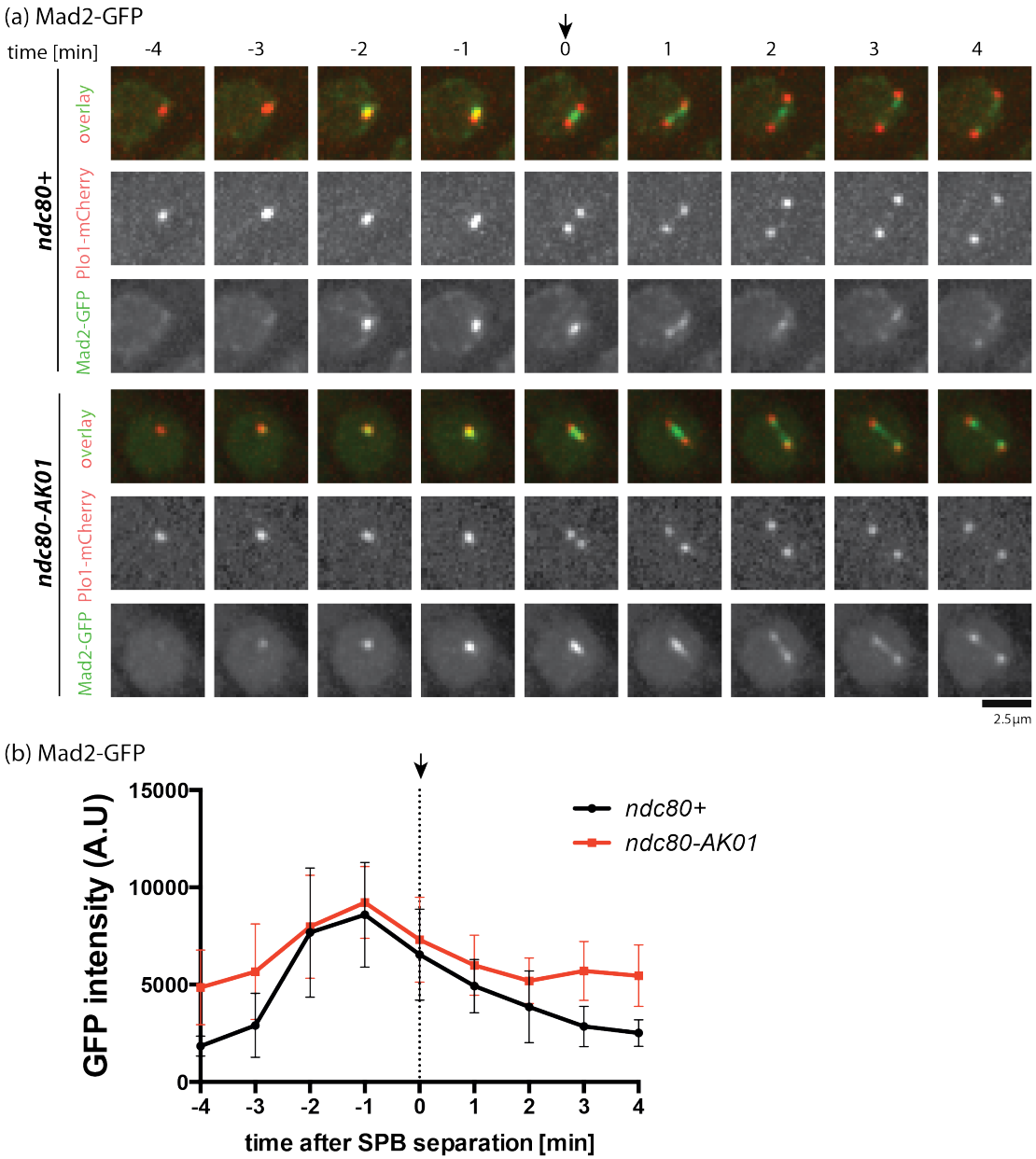

Figure 4.22. Mad2-GFP levels remain the same in *ndc80-AK01* in unperturbed conditions.

Exponentially growing cells (4 x 10^6 cells/ml) were placed in YE5S at 27˚C. The live samples were placed on lectin-coated dishes, left for 10 minutes and imaged for 30 minutes. (a) Representative images of *ndc80*$^+$ and *ndc80-AK01* with Mad2-GFP and Plo1-mCherry. Scale bar, 2.5 µm. (b) Quantification of Mad2-GFP signal intensities. n > 10 cells.

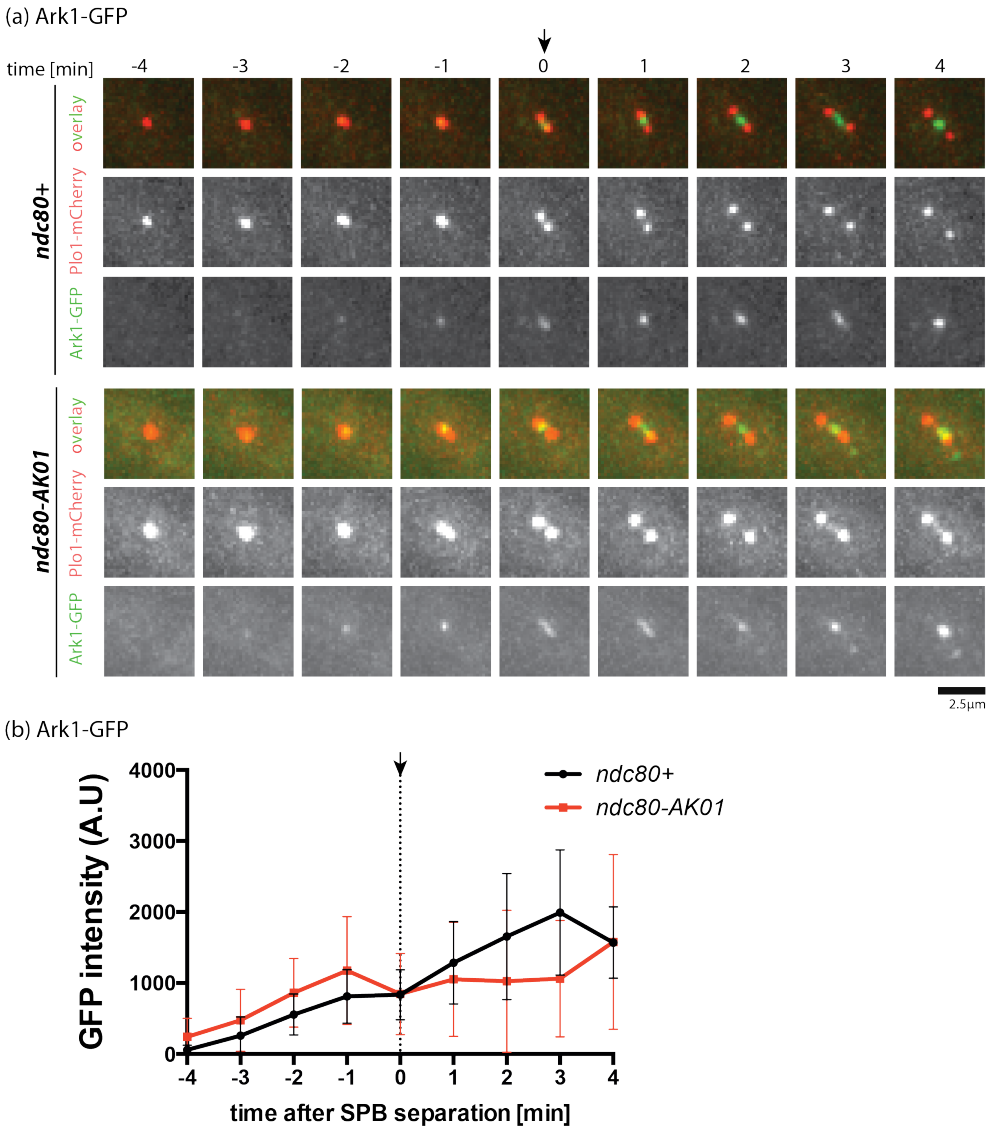

Figure 4.23. Ark1-GFP levels are reduced in *ndc80-AK01*.

Exponentially growing cells (4 x 10^6 cells/ml) were placed in YE5S at 27˚C. The live samples were placed on lectin-coated dishes, left for 10 minutes and imaged for 30 minutes. (a) Representative images of *ndc80*$^+$ and *ndc80-AK01* with Ark1-GFP and Plo1-mCherry. Scale bar, 2.5 µm. (b) Quantification of Ark1-GFP signal intensities. n > 10 cells.

4.3.3 Mad2 persistence at kinetochores is linked to Mad1 levels

To verify if Mad2-GFP persistence is linked to the levels of Mad1 at the kinetochore, Mad2-GFP localisation in a *mad1*Δ background was studied. In unperturbed conditions, Mad2-GFP is absent from the kinetochore in *mad1*Δ and *mad1*Δ *ndc80-AK01* (Figure 4.24). Recently, it was reported that in human cells, the Mad1-Mad2 complex is already

formed during interphase and it directly interacts with the nuclear pore complex (NPC) (Rodriguez-Bravo et al., 2014). In addition, in budding yeast the similar localisation of the Mad1-Mad2 complex (Chen et al., 1999) and its interaction with Nup53p is known (Iouk et al., 2002). Furthermore, recent immunoprecipitation and mass spectrometry in fission yeast have also identified Nup211 (a component of the nuclear pore complex) as a potential interaction partner with Mad1 (Heinrich et al., 2014). Therefore, the human and fission yeast data might indicate that the unaltered levels of Mad2-GFP in *ndc80-AK01* at the kinetochore (Figure 4.22) are linked to the reduced residual amount of Mad1-GFP that might be below the detection threshold at the kinetochore.

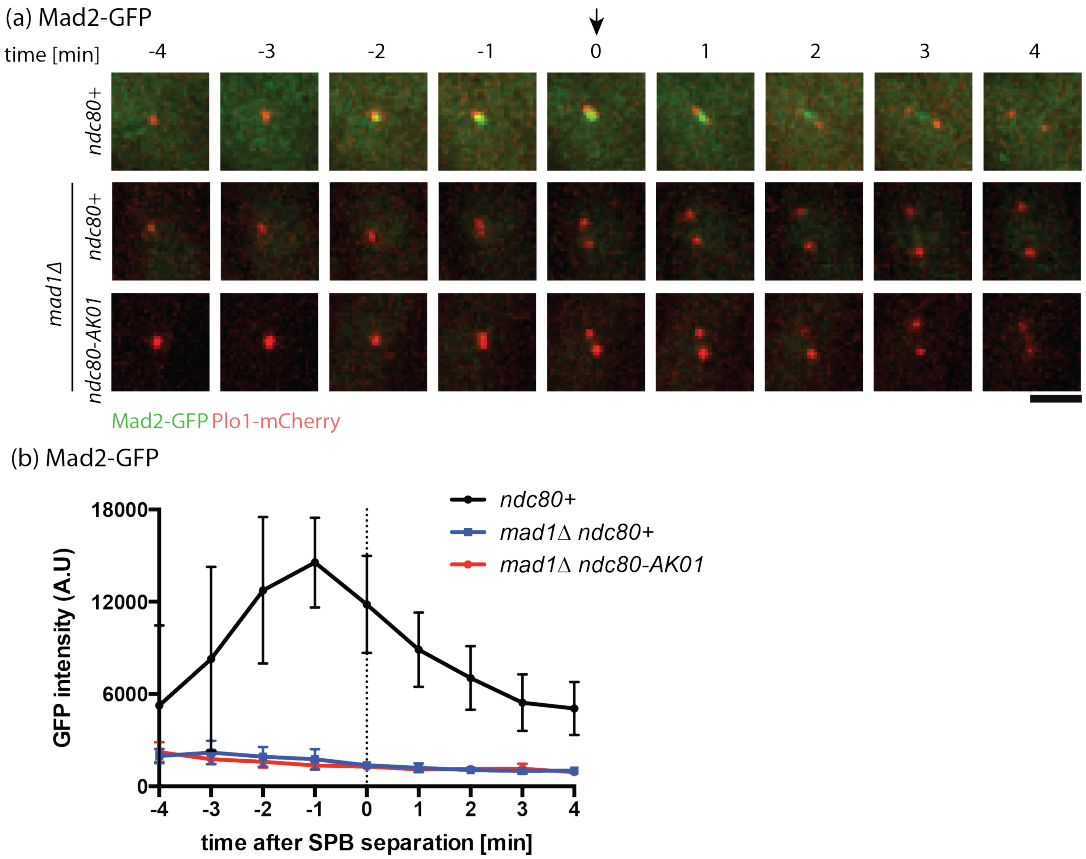

Figure 4.24. Reduction of Mad2-GFP from the kinetochore is linked to Mad1.

Exponentially growing cells (4 x 10^6 cells/ml) were placed in YE5S at 27˚C. The live samples were placed on lectin coated dishes, left for 10 minutes and imaged for 30 minutes. (a) Representative images of *ndc80*$^+$, *mad1*Δ *ndc80-AK01* and *mad1*Δ *ndc80*$^+$ with Mad2-GFP and Plo1-mCherry. Scale bar, 2.5 µm. (b) Quantification of Mad2-GFP signal intensities. n > 10 cells.

4.4 Summary and Discussion

In this chapter, I have characterised the *ndc80-AK01* mutant phenotype. First of all, I confirmed an intact microtubule structure in *ndc80-AK01* (Figure 4.1). Subsequent analyses focused on determining which of the GFP-tagged SAC is affected by *ndc80-AK01*. Levels of SAC-GFP proteins in *ndc80*$^{+}$ and *ndc80-AK01* were confirmed to be identical (no significant difference between data sets) and TBZ sensitivity in the mutant backgrounds was the same as in the originally isolated *ndc80-AK01* mutant (Figure 4.4). The localisation of GFP-tagged SAC components was analysed in unperturbed cell cycle (Chapter 4.3) and under mitotic arrest conditions induced either by TBZ/CBZ or *cut7-446* (Chapter 4.2).

Recent work in fission yeast has uncovered a three-layer interdependent hierarchy of SAC components (Heinrich et al., 2012). Ark1 and Mph1 are the most upstream components that are required for the recruitment of the other SAC proteins. Bub1, Bub3 and Mad3 constitute the middle level of the hierarchy. The Bub1-Bub3 complex localises to KNL-1/Spc7 upon phosphorylation of MELT motifs by Mph1/MPS1 (Yamagishi et al., 2012, Shepperd et al., 2012, London et al., 2012). Mad1, Mad2 and Mad3, on the other hand, are classified as the most downstream components in SAC signalling. Mad1 and Mad2 (also Mad3) are the last factors to be recruited, dependent on the kinetochore localisation of the above listed SAC components (Heinrich et al., 2012).

In mitotic arrest conditions by TBZ/CBZ, GFP-tagged Mad2, Mad1, Mad3, Bub1, Bub3, Mph1 and Ark1 are absent from kinetochores in *ndc80-AK01* (Figure 4.5, Figure 4.6, Figure 4.7, Figure 4.8, Figure 4.9, Figure 4.10, Figure 4.11, Figure 4.12, Figure 4.13, Figure 4.14 and Figure 4.15). These data suggest that Ark1 or Mph1 is the primary components recruited to the Ndc80 linker region and that their mislocalisation abolishes the recruitment of downstream components to unattached kinetochores.

To distinguish between Mph1 and Ark1/Aurora B as the component localising to Ndc80, the feedback loop from Bub1 to Ark1 was investigated. Bub1 is a kinase that

phosphorylates H2A-S121, which is a site of Shugoshin 1 (Sgo1) and Shugoshin 2 (Sgo2) recruitment, which in turn stimulates Ark1 localisation to the centromere (Kawashima et al., 2010b, Lin et al., 2014). As shown in Figure 4.16, Ark1-GFP reduction at the kinetochore in *ndc80-AK01* is linked with the misplacement of Bub1 from the kinetochore; the decrease in Ark1-GFP intensities is almost the same, if not identical, between *bub1*Δ and *ndc80-AK01* (Figure 4.16). This is in accordance with the literature, where *bub1*Δ causes 50% decline in Ark1-GFP accumulation at the kinetochore (Heinrich et al., 2012). We can hypothesise therefore that Mph1 is the primary kinase recruited to the Ndc80 complex and Ark1 reduction in *ndc80-AK01* is due to the absence of Bub1. However, we cannot fully exclude at this stage the possibility that Ark1 localises not only to the Sgo1/Sgo2 sites at the centromere but also to the Ndc80 linker region.

In addition, under unperturbed conditions, where the checkpoint components are non-essential, I have found that in *ndc80-AK01* cells all of GFP tagged SAC components delocalise from the kinetochore with similar degrees. Bub1, Bub3, Mad3 and Mph1 are absent from the kinetochore, whereas Mad1 is reduced in *ndc80-AK01* (Figure 4.17, Figure 4.18, Figure 4.19, Figure 4.20 and Figure 4.21). Ark1-GFP is retained at the kinetochore, however Aurora B/Ark1 has multiple roles in the cells, in addition to checkpoint signalling. It is involved in chromosome bi-orientation, monitoring tension at kinetochores and correcting faulty kinetochore-microtubule attachments by formation of the chromosomal passenger complex (CPC). Ark1 was shown to localise to the inner centromere (corresponding to *dg/imr* heterochromatin regions in fission yeast (Yamagishi et al., 2014)), however additional localisation to the outer kinetochore cannot be fully excluded experimentally at this time (Kawashima et al., 2010b, Lin et al., 2014). The further discussion of potential models is found in Chapter 6.

In *ndc80-AK01*, unlike mitotic arrest conditions, during normal cell cycle, Mad2-GFP appeared to localise to the kinetochore during M phase (Figure 4.22). As shown earlier (Figure 4.24), this may be due to Mad1 still localising to kinetochores as in *mad1*Δ, there is no Mad2-GFP at the kinetochore. This suggests that there is still residual Mad1-GFP at the kinetochore in *ndc80-AK01*, which cannot be detected with our microscope.

The data presented here indicate that Ndc80 acts most likely as a platform for Mph1/MPS1 recruitment to the kinetochore. The *ndc80-AK01* mutant disrupts the kinetochore localisation of SAC components by having a direct or indirect effect derived from the failure of Mph1 to be recruited to the kinetochore.

Chapter 5. Ndc80 is required for the recruitment of Mph1 to the kinetochore

Analyses of the recruitment of GFP-tagged SAC components led us to hypothesise that Mph1 is the factor recruited by Ndc80 and this localisation is impaired in *ndc80-AK01*. Lack of Mph1 recruitment to the kinetochore would have direct effects on the remaining SAC components and even indirectly on Ark1/Aurora B. This hypothesis requires further experiments for validation. For this, Mph1 was tethered to the outer kinetochore component Mis12 to see if this would rescue the phenotype of *ndc80-AK01* cells. Furthermore, the potential direct interaction between Mph1 and Ndc80 was studied by co-immunoprecipitation. In addition the overexpression of Mph1 was observed in *ndc80-AK01* background to check for phenotype rescue with Mad2 overexpression as a control.

5.1 Tethering of Mph1 to the kinetochore restores spindle assembly checkpoint in *ndc80-AK01*

Mph1 was tethered to the outer kinetochore component through a fusion protein with Mis12 (denoted Mis12-Mph1) (Heinrich et al., 2012). This fusion construct was expressed under the endogenous *nmt81* promoter from the *mph1*$^{+}$ locus. The promoter is repressed in the presence of thiamine whereas upon thiamine washout, the protein is expressed. The strain was kindly provided by Silke Hauf. It was shown that constructs are maintained at the kinetochore, with activated SAC signalling resulting in a pronounced delay in mitosis and also growth defects (Heinrich et al., 2012). Previous reports have already indicated that persistent Mps1 tethering to kinetochore causes the activation of the checkpoint in human cells (Jelluma et al., 2010, Yamagishi et al., 2012).

As reported earlier (Heinrich et al., 2012), Mis12-Mph1 overexpression in otherwise wild type cells leads to cell death due to constitutive checkpoint activation; cells arrest in mitosis and eventually die. In *mad2*Δ, however, the tethering of Mph1 to the

kinetochore has no effect on cell viability (Figure 5.1). This is due to the fact that downstream Mad2 is absent, which is essential for MCC formation. Despite the proper recruitment of Bub1, Bub3, Mad3 and Mad1 to kinetochores due to Mph1, the MCC cannot be activated without Mad2 (Heinrich et al., 2012). As shown earlier, Mph1-GFP in *ndc80-AK01*, on the other hand, does not normally localise to kinetochores (Figure 5.1), thus the checkpoint is defective. Once Mph1-GFP is tethered to Mis12 in the mutant background, mitotic arrest and growth defects are observed. This observation suggests that presence of Mis12-Mph1 restores the checkpoint activity to *ndc80-AK01* cells that normally cannot arrest (Figure 5.1). In the double mutant of *ndc80-AK01 mad2*Δ containing Mis12-Mph1, reduction in the mitotic cells population and normal growth on the plates were observed, suggesting defective checkpoint activation (Figure 5.1).

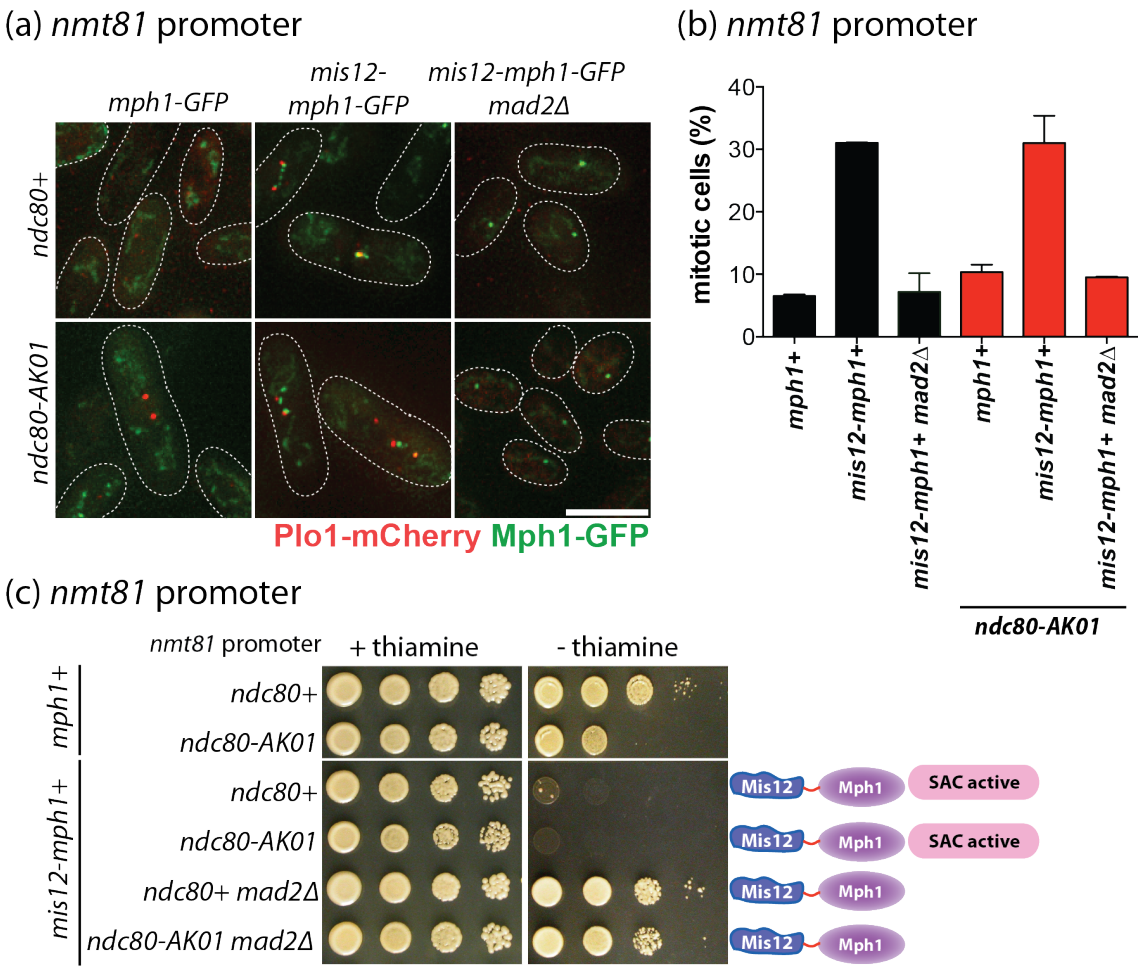

Figure 5.1. Mph1-Mis12 does not rescue *ndc80-AK01* phenotype.

Cells containing the *nmt81* promoter at the endogenous *mph1* locus were grown overnight at 27˚C in EMM-Leu+Thiamine. (a) Thiamine was then washed-out and cells were placed in EMM-Leu for 14 hours at 27˚C. Samples were then fixed in 1.6% PFA and imaged. Mitotic cells were identified by the presence of Plo1-mCherry at SPBs. Scare bar, 10 µm. (b) The percentage of mitotic cells was counted. n>200 cells. (c) A serial dilution spot assay was performed for the indicated Mph1 constructs expressed from the *nmt81* promoter. 5 x 10^4 cells were placed onto the first spot and then tenfold dilutions were confirmed on EMM-Leu media in the presence and absence of thiamine at 27˚C and incubated for 3 days.

5.2 Ndc80 and Mph1 interactions

As the linker region of Ndc80 plays a role in the recruitment of Mph1/MPS1 to the kinetochore, the next question to address is whether there is a physical interaction between Ndc80 and Mph1/MPS1. Ndc80 tagged with 3FLAG or 3PK was crossed with Mph1-13myc or Mph1-5FLAG. Cells were cultured overnight at 27˚C and exponentially growing cells (4 x 10^6 cells/ml) were collected and prepared for the immunoprecipitation.

5.2.1 Co-immunoprecipitation of Mph1 and Ndc80

Initially, asynchronous cultures grown at 27˚C in YE5S were used for the experiment. Despite the detection of both Ndc80 and Mph1 in cell extracts, there is no co-immunoprecipitation detected between Ndc80 and Mph1 when using dynabeads coated with anti-FLAG (Figure 5.2a). Observation of Mph1 and Ndc80 interaction is difficult as the accumulation of Mph1-GFP signals at the kinetochore in unperturbed conditions at 27˚C lasts only 4 minutes during the entire cell cycle (Figure 4.21).

Therefore, cultures were synchronised using HU and then cells were arrested in mitosis using TBZ/CBZ. In *ndc80*$^+$ cells under these mitotic arrest conditions, Mph1-GFP accumulates at the kinetochore for 20 minutes, on average (Figure 4.14). Despite the synchronisation, there was no improvement in detecting an interaction between Mph1 and Ndc80. Both tagged Mph1 and tagged Ndc80 are present in the indicated strains however there is no interaction observed (Figure 5.2b).

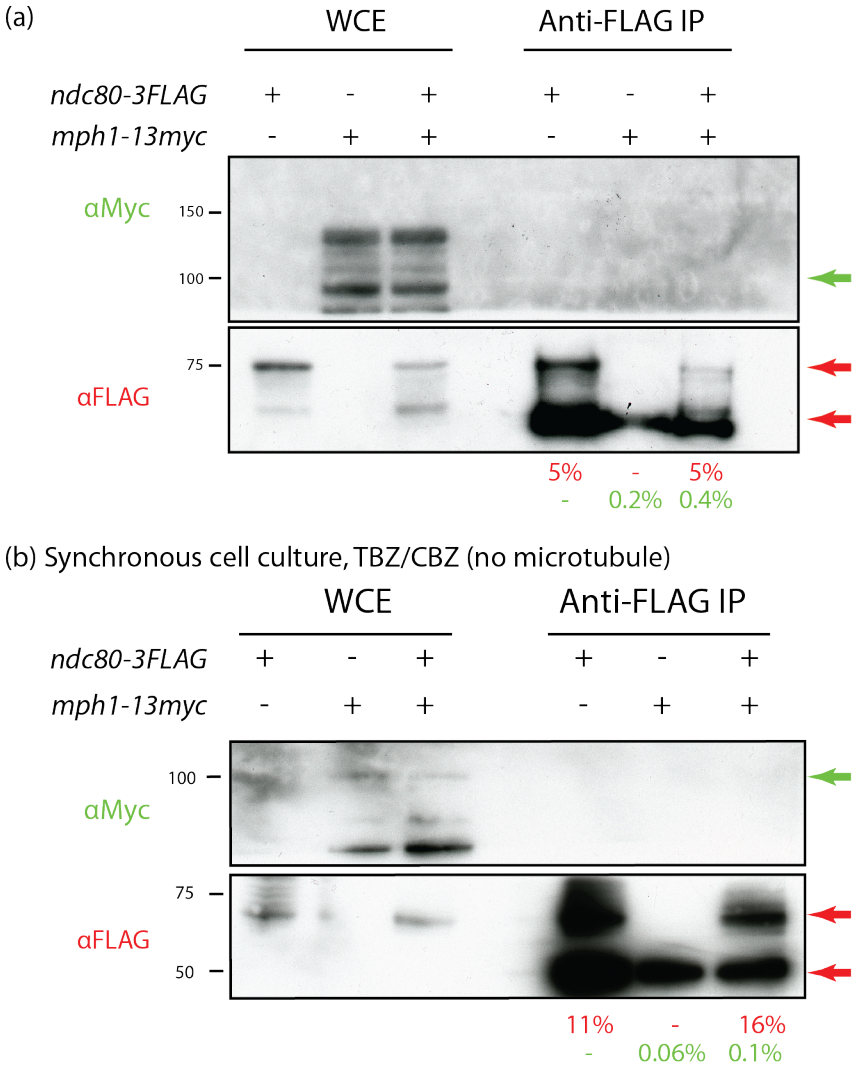

Figure 5.2. Co-immunoprecipitation experiments between Ndc80 and Mph1.

2mg of protein extract was prepared from the indicated cells grown in unperturbed (a) and (b) perturbed conditions. Exponentially growing cells (4 x 10^6 cells/ml) were synchronised with 12.5mM HU at 25˚C for 4 hours. HU was then washed out and cells were placed in YE5S with 50 µg/ml TBZ and 60 µg/ml of CBZ at 27˚C. Protein extracts were collected and immunoprecipitation was performed. WCE, 50 µg. Percentage of IP values relative to WCE was calculated for Myc (green) and FLAG (red) tagged proteins. WCE is 1% of IP input. The arrowheads indicate Mph1-13Myc and Ndc80-3FLAG bands.

Next, the Ndc80-3PK and Mph1-5FLAG were tested under the same conditions (data not shown). Unfortunately, interactions were not observed between Ndc80 and Mph1 in asynchronous and synchronous cell cultures. As there was no interaction observed between Mph1 and wild type Ndc80, the interaction in *ndc80-AK01* mutant was not studied.

5.3 Ectopic overproduction of Mad2 and Mph1 are toxic to *ndc80-AK01*

Alternative approach to study Mph1 was therefore employed – overexpression of Mph1 was carried out, with Mad2 overexpression as a control. Overexpression of Mad2 in a wild type background results in cells arresting in a metaphase-like state, with cells exhibiting hypercondensed chromosomes and short mitotic spindles (He et al., 1997). *mad2*$^{+}$ overexpression mimics normal checkpoint activation without causing a defective spindle (induced by *nda3*^{cs} mutants (Kanbe et al., 1990) or microtubule destabilising drugs (Walker, 1982)). Eventually, the cells will bypass anaphase and exit mitosis without sister chromatids separation or spindle elongation (He et al., 1997). In the current study, using pREP3, pREP1 and pREP41, we tried overexpressing Mad2 and Mph1 to observe their effect on *ndc80-AK01* to determine the relationships.

It was shown previously that Mph1, when fused to Ndc80 (expressed under *nmt41*), is toxic to wild type, *mph1*Δ and *bub3*Δ cells, whereas normal cell growth was observed under *nmt41* induced expression of Mph1 in *mad1*Δ, *mad2*Δ, *mad3*Δ and *bub1*Δ backgrounds (Ito et al., 2012). These results suggest that growth arrest and toxicity to cells result from the checkpoint activation and Mph1 acts most upstream of SAC signalling (note that Bub3 has been shown that is not an SAC components, instead it is important for SAC silencing (Yamagishi et al., 2012, Tange and Niwa, 2008, Windecker et al., 2009, Vanoosthuyse and Hardwick, 2009). However, there was no toxicity observed in my experiments (Appendix - 7.1.1; Figure 7.1), so the alternative approaches were tested.

Mad2 overexpression from pREP3x-Mad2 resulted in metaphase arrest, similar phenotypes were observed in *mad1*Δ, *bub1*Δ and *bub3*Δ (data not shown), which indicated their localisation upstream of Mad2 (Millband and Hardwick, 2002). *mad3*Δ on the other hand, grew well in the overexpression of Mad2, indicating that Mad3 acts downstream of or together with Mad2 in the checkpoint signalling cascade (Millband and Hardwick, 2002).

pREP1 plasmids containing GFP-tagged Mad2 and Mph1 were constructed and transformed into SAC deletion (*mad1*Δ*, mad2*Δ*, mad3*Δ*, bub1*Δ*, bub3*Δ and *mph1*Δ) and *ndc80-AK01* strains. Effects of the overexpression were studied by serial dilution spotting assay (Figure 5.3b-c) and protein expression levels were measured 18 hours after overexpression in EMM-Leu (Figure 5.3a). Expression levels of GFP-Mad2 were similar in all SAC deletion backgrounds, although there were higher levels of Mad2 in *ndc80-AK01*. For Mph1, the expression levels were the same in *mad2*Δ*, mad3*Δ and *bub1*Δ backgrounds. Overexpression of Mad2 from the pRPEP1 plasmid in wild type, *mad1*Δ*, mad2*Δ*, bub1*Δ*, bub3*Δ and *mph1*Δ and *ndc80-AK01* resulted in high toxicity and no cell growth when compared with controls (empty vector) (Figure 5.3b). Cells overexpressing Mad2 from the *nmt1* promoter in *mad3*Δ show normal growth, on the other hand. The observation of Mad2 effects in SAC deletion backgrounds, used as controls in the current study, are in accordance with literature, where pREP3-Mad2 was used (Millband and Hardwick, 2002). However, overexpression of Mph1 from *nmt1* resulted in high toxicity and no cell growth in *mad2*Δ*, mad3*Δ and *bub1*Δ (Figure 5.3).

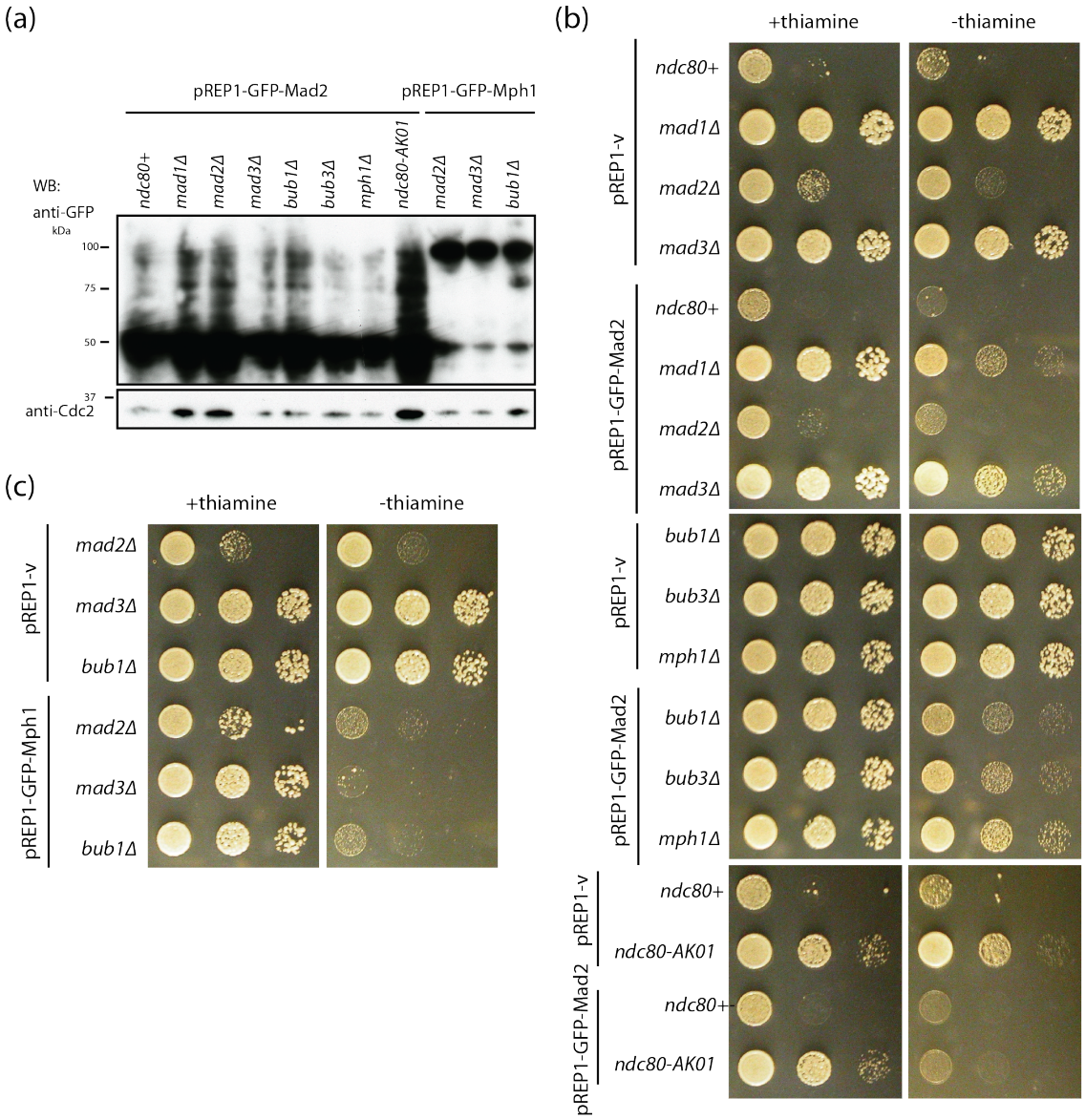

Figure 5.3. Overexpression of Mad2 and Mph1 from pREP1 results in high toxicity and cell death.

(a) Cells containing pREP1-GFP-Mad2 or pREP1-GFP-Mph1 were precultured in EMM-Leu+Thiamine and then placed for 18 hours in liquid EMM-Leu at 27˚C. 4 x 10^6 cells/ml were collected and protein extracts were prepared using the alkaline method. Equal protein extracts were loaded and prepared for immunoblotting. Anti-GFP antibody was used to detect GFP-Mad2 and GFP-Mph1 proteins. The protein loading control Cdc2 was detected by anti-Cdc2 antibody. (b) Serial dilution assay of cells with pREP41-GFP-Mad2 and pREP41-GFP-Mph1. 5 x 10^4 cells in the first spot were followed by 10-fold dilutions and plated on EMM-Leu+Thiamine and Emm-Leu. Plates were incubated at 27˚C for 3 days.

5.4 Summary and Discussion

To summarise, tethering of Mph1 to the outer kinetochore component Mis12 in wild type cells resulted in checkpoint activation, observed as permanent mitotic arrest with high mitotic indexes and cell death (Figure 5.1). In *ndc80-AK01*, the checkpoint activation is restored upon tethering of Mph1 to Mis12, indicated by no growth and high mitotic indexes. In *mad2*Δ and double mutants *mad2*Δ *ndc80-AK01*, the checkpoint is not functional and even as Mis12-Mph1 brings Bub1, Bub3, Mad3 and Mad1 to kinetochore, the checkpoint is still defective as expected. These data further confirm the role of Ndc80 as a platform for Mph1 kinetochore localisation.

There were also alternative Mph1 tethered constructs available in the literature. In Tomohiro Matsumoto's lab, expression of Mph1 fused to Ndc80 in pREP81 plasmid resulted in persistent activation of the spindle checkpoint; this also occurs when expressing Mph1-Ndc80-GFP from an endogenous *nmt81* locus (Ito et al., 2012). On the other hand, in Yoshinori Watanabe's lab, Mph1 was tethered to Cnp3C/CENP-C, leading to robust SAC activation that results in impaired cell growth (Yamagishi et al., 2012). Reports in budding yeast, further suggest that Mps1 localises to Ndc80 (Kemmler et al., 2009, Aravamudhan et al., 2015). There is a broad range of work in human cells showing Hec1/Ndc80 as a platform for Mps1/Mph1 kinetochore localisation, the details of which will be discussed extensively in Chapter 6 (Nijenhuis et al., 2013, Hiruma et al., 2015, Ji et al., 2015, Zhu et al., 2013) together with proposed models.

The interaction between Ndc80 and Mph1 was not shown by immunoprecipitation (Figure 5.2). This is most likely due to the very low abundance of Mph1 and the short time during which it localises to kinetochore. Studies have shown difficulty in confirming the binding partners of SAC components – using mass spectrometry or immunoprecipitation (Heinrich et al., 2014)(also personal communication with S.Hauf and Y.Watanabe). In humans, no interaction between Mps1/Mph1 and Hec1/Ndc80 was detected *in vivo*, despite interactions detected using *in vitro* reconstitution of the complex (Zhu et al., 2013, Nijenhuis et al., 2013, Hiruma et al., 2015, Ji et al., 2015).

However, it is possible that there is an intermediate binding partner present that mediates Mph1 localisation to Ndc80 in fission yeast.

To summarise, the ectopic overexpression of Mad2 and Mph1 showed high toxicity in SAC deletion backgrounds (Figure 5.3). The exception was pREP1-GFP-Mad2 overexpression in *mad3*Δ (Figure 5.3). Expression from pREP41 did not provide sufficient overexpression to lead to any toxicity that could help in classifying a role in checkpoint signalling (Figure 7.1). Overexpression of Mad2 in *ndc80-AK01* was toxic, placing Ndc80 upstream in SAC signalling hierarchy. Overexpression of Mph1 from the *nmt1* on the other hand, was toxic in all investigated conditions (Figure 5.3). To address the poor growth of the construct on EMM-Leu+Thiamine plates, the genetic background of the strains needs to be discussed. All of them contain *ura4* mutation that impacts the growth in EMM media. Furthermore, from the observations and discussions with lab members it seems that WT513 has difficulty growing when transformed with plasmids; even an empty vector reduces its viability. Moreover, the expression of Mad2 from *nmt41* promoter showed no toxicity or rescue indicating a weak expression that cannot affect checkpoint signalling (Figure 7.1). Since Mph1 overexpression from pREP41-GFP in *mad2*Δ is toxic, this suggests that there is a checkpoint-independent toxic effect in contrary to the expectations from the literature. There is normal cell growth when using pREP41-Mph1, but that was using a much higher cell concentration than spotting assays usually do. Experiments with pREP81-Mph1-GFP in *mad2*Δ show no toxic effect, but this is the weakest promoter (Ito et al., 2012). Unfortunately, the overexpression experiments did not produce any results that can verify the localisation and function of Mph1 in regard to Ndc80.

Overall, the additional strategies need to be employed to finalise the hypothesis on Mph1/Mps1 localising to Ndc80, at the kinetochore, during cell division. The tethering experiments provided a valid proof supporting the hypothesis. Also, the metazoan and budding yeast research supports the current working model. The additional experiments will need to be conducted to verify the hypothesis and they will be discussed in Chapter 6.

Chapter 6. Discussion

6.1 Overall summary

Understanding of kinetochore assembly at the centromere region has moved forward during the last 20 years. CENP-A localisation marks the site for kinetochore formation triggering the assembly of other CCAN components. The kinetochore is a dynamic ensemble of more than 100 components that are essential for proper chromosome segregation (Foley and Kapoor, 2013, Cheeseman, 2014). In the outer kinetochore, the KMN network (Knl1 complex/Mis12 complex/Ndc80 complex) directly binds to microtubules. CENP-C and the CENP-T/W/S/X complex serve as a bridge from the inner kinetochore to the KMN network, thereby stabilising kinetochore structure (Nishino et al., 2012, Suzuki et al., 2011, Gascoigne et al., 2011). Furthermore, the Mis12 complex stabilises the Ndc80 complex and Knl1 (Hornung et al., 2011)(Welburn et al., 2010). The Knl1 complex can bind microtubules, but its primary role is the recruitment of spindle assembly checkpoint components and silencing factors (PP1 and PP2A-B56) that regulate microtubule attachment (DeLuca and Musacchio, 2012, Foley and Kapoor, 2013, Cheeseman, 2014, Ghongane et al., 2014). The Ndc80 complex, consisting of Ndc80, Nuf2, Spc24 and Spc25, is a major microtubule binder (Ciferri et al., 2008). The Ndc80 complex forms a dumbbell structure with calponin-homology (CH) domains of Ndc80 and Nuf2 facing the microtubules and Spc24-Spc25 stabilising the interactions by binding the Mis12 complex and CENP-T (Cheeseman and Desai, 2008, Guimaraes et al., 2008, Suzuki et al., 2011, Gascoigne et al., 2011, Bock et al., 2012, Hornung et al., 2011, Cheeseman, 2014, Yamagishi et al., 2014, Ciferri et al., 2008). Ndc80 binds microtubules in a tripartite manner (Tooley et al., 2011). Firstly, the unstructured N-tail interacts via electrostatic interactions upon its dephosphorylation (Alushin et al., 2010). Its binding is tightly regulated by Aurora B phosphorylation, making it a sensor of kinetochore-microtubule attachment (Zaytsev et al., 2015). Then the CH domain of Ndc80 is the major microtubule-binding site (Alushin et al., 2010, Ciferri et al., 2008). The loop region of Ndc80 is an indirect MT-binding site; microtubule-associated proteins (Alp7/Alp14, Dis1, the Dam1 complex, Cdt1 and the Ska complex) localise here in mitosis, creating additional microtubule binding

interfaces (Varma et al., 2012b, Zhang et al., 2012, Varma et al., 2012a, Hsu and Toda, 2011, Maure et al., 2011, Tooley et al., 2011, Tang et al., 2013).

Proper chromosome segregation is a result of correct kinetochore-microtubule attachments in mitosis, which are ensured by the spindle assembly checkpoint (SAC). Improper kinetochore-microtubules attachment, and/or rather a lack of tension at kinetochores is detected by Aurora B kinase, which enables the recruitment of SAC components. The SAC components - Aurora B/Ark1, Mps1/Mph1, Bub1, Bub3, BubR1/Mad3, Mad1 and Mad2 – need to localise to unattached kinetochores and halt mitotic progression until the proper attachments are established (Essex et al., 2009, Foley and Kapoor, 2013). This mechanism is hierarchical and very robust, responding even to a single unattached kinetochore (Foley and Kapoor, 2013). The first stage involves the localisation of Aurora B/Ark1 and Mps1/Mph1 kinases to the kinetochore, and phosphorylation of targets including the Ndc80 complex and Knl1 (Cheeseman et al., 2002, DeLuca et al., 2006, Ciferri et al., 2008, Cheeseman et al., 2006, Akiyoshi et al., 2009, Welburn et al., 2010, Liu et al., 2010). Phosphorylated Knl1/Spc7 is a recruitment site for Bub1, Bub3 and BubR1/Mad3 (Meadows et al., 2011, Welburn et al., 2010, Liu et al., 2010). Bub1 was shown only recently to localise the Mad1-Mad2 complex in yeasts and humans (Heinrich et al., 2014, Zhang et al., 2015, London and Biggins, 2014a, Brady and Hardwick, 2000). Once at the kinetochore Mad2 undergoes conformational changes (from open (O-Mad2) to closed (C-Mad2)) that enable its binding to Cdc20/Slp1, together with BubR1/Mad3 and Bub3 (not in fission yeast) (Mapelli and Musacchio, 2007, Sironi et al., 2001, Luo et al., 2004, Screpanti et al., 2011). Subsequent inhibition of Cdc20, an activator of the APC/C, halts the progression to anaphase as securin and cyclin B cannot be degraded (Lara-Gonzalez et al., 2012, Han et al., 2013, Chao et al., 2012).

Only during last 20 years, there was substantial progress in unravelling SAC signalling; the proteins involved, their localisations, interactions between them and their functions. However, there are still open questions remaining. The current scheme of SAC signalling in humans is shown in Figure 6.1.

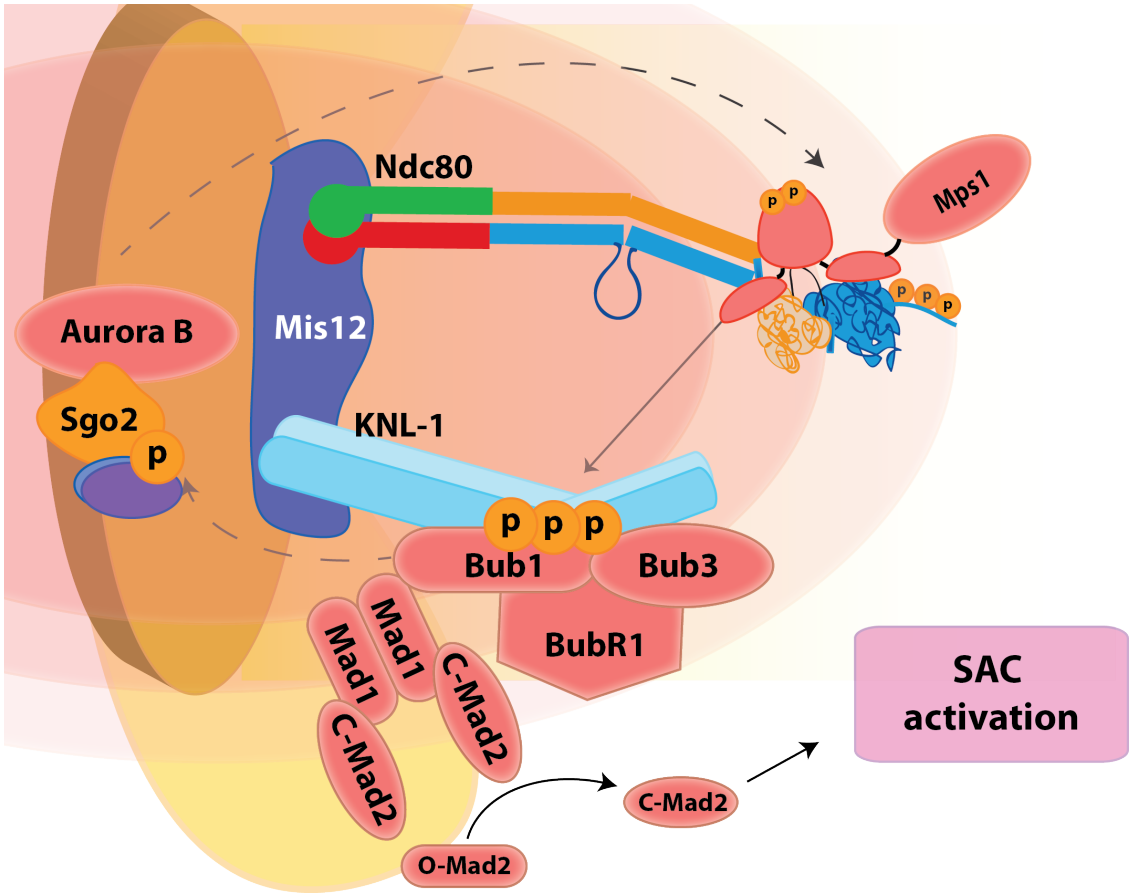

Figure 6.1. SAC signalling.

Scheme of checkpoint signalling cascade in humans. The first step is localisation of Aurora B to the inner centromere (phosphorylated histone H2A, where Sgo2 is recruited). Aurora B creates a phosphorylation gradient and the tensionless kinetochore (unattached) recruits SAC components. Mps1 localises to two motifs in the Ndc80 complex - the NTE domain of Mps1 localises to the CH domain of Ndc80, upon TPR phosphorylation by Aurora B, and the MR/IRK region localises to the CH domain of Nuf2. Then, Mps1 becomes activated and phosphorylates Knl1, where in turn Bub1, Bub3 and BubR1 are recruited. Bub1 recruits also the Mad1-Mad2 heterotetramer, which becomes activated and the soluble Mad2 undergoes conformational changes to form the MCC complex.

As the Ndc80 complex is an outer kinetochore component that is tightly regulated by Aurora B and deletions or truncations of Ndc80 result in mislocalisation of SAC components, I wanted to explore the link between Ndc80 and checkpoint signalling. Therefore, I carried out random mutagenesis of the N-terminal domains (N-tail, CH domain, linker region) of Ndc80 that are essential for the localisation of Mps1/Mph1, Bub1, BubR1/Mad3, Bub3, Mad2 and Mad1.

I have isolated a mutant, *ndc80-AK01,* that has a single substitution of Leucine to Proline at position 246. L246 is situated within a relatively conserved linker (or hairpin) region of Ndc80. *ndc80-AK01* is sensitive to TBZ and is defective in checkpoint signalling. *ndc80-AK01* cells exit mitosis in the absence of microtubules (TBZ/CBZ; Figure 3.12, Figure 3.14 and Figure 3.17) and do not accumulate mitotic cells (Figure 3.13).

In Chapter 4, I have characterised the nature of the checkpoint defect in *ndc80-AK01*. By doing systematic localisation analyses of GFP-tagged SAC components under mitotic arrest conditions, I have determined that *ndc80-AK01* causes the mislocalisation of Ark1/Aurora B, Mph1/Mps1, Bub1, Bub3, Mad3/BubR1, Mad1 and Mad2 from unattached kinetochores (Figure 4.5, Figure 4.6, Figure 4.7, Figure 4.8, Figure 4.9, Figure 4.10, Figure 4.11, Figure 4.12, Figure 4.13, Figure 4.14 and Figure 4.15). The working hypothesis was that the localisation of the most upstream component in SAC signalling is affected in *ndc80-AK01*, and its absence impairs the recruitment of other downstream components. Mph1/Mps1 and Ark1/Aurora B, the most upstream components (some model systems place Ark1/Aurora B on top, whereas other put Mph1/Mps1 as the first one to be recruited) (London and Biggins, 2014b, Yamagishi et al., 2014, Heinrich et al., 2012) are the main candidates whose localisation could be perturbed by the mutation in the linker region of Ndc80.

To distinguish between Ark1/Aurora B and Mph1/Mps1, the localisation of Ark1 was investigated in the deletion of Bub1. Bub1 is known to enhance Ark1 localisation to the kinetochore. Bub1 phosphorylates histone H2A on S120 where Sgo2 is recruited. Sgo2 then localises then Ark1/Aurora B to the pericentromeric regions (Kawashima et al., 2010b). In *bub1*Δ cells, GFP-tagged Ark1/Aurora B appears absent from the kinetochore (Figure 4.16), indicating that its mislocalisation in *ndc80-AK01* is because of impaired localisation of Bub1. Therefore the hypothesis of Ark1/Aurora B being directly influenced by *ndc80-AK01* is less probable. However, it cannot be fully excluded, as there might be some population of Ark1/Aurora B that localises to the outer kinetochore region. In DeLuca's lab, in human cell lines, Aurora B was proposed

to localise to Ndc80 (DeLuca and Musacchio, 2012), however these discoveries were not verified any further.

The possibility of Ark1/Aurora B localising to the linker region of Ndc80 is not likely, given the currently proposed mechanisms of Aurora B phosphorylation gradient that detects tension at the centromere/kinetochore region (Wan et al., 2009, Wang et al., 2011). According to this model, Aurora B localising to the inner centromere creates a phosphorylation gradient that is dependent on distance. The main attachment is through the Ndc80 complex, which has three microtubule binding regions – direct binding through the N-tail, the CH domain and indirectly by localising MAPs to the loop region. Proper kinetochore-microtubule attachment results in the Ndc80 complex to undergo a conformational stretch (length increased by ~50 nm), which is linked with decreased phosphorylation by Aurora B (Zaytsev et al., 2015, Alushin et al., 2012, Cheeseman et al., 2006, DeLuca et al., 2006). Therefore, the highly phosphorylated N-tail of Ndc80 attaches to microtubules more strongly upon dephosphorylation. A lack of attachment results in phosphorylated Ndc80 complex, which has a lower binding affinity to the microtubules (Zaytsev et al., 2015, Alushin et al., 2012). Therefore, tension detection by Aurora B and the phosphorylation gradient comprises a critical regulator of the KT-MT attachments (Zaytsev et al., 2015, Kapoor et al., 2000, Li and Nicklas, 1995) and it seems unlikely that Aurora B/Ark1 would also localise to the Ndc80 complex, as it would interrupt the phospho-regulation of the Ndc80 complex.

Mps1/Mph1 is more likely to be the kinase whose localisation is impaired in *ndc80-AK01*. Multiple studies for the last two years indicate that Ndc80 is essential for the recruitment of Mps1 to the kinetochore (Dou et al., 2015, Ji et al., 2015, Hiruma et al., 2015, Nijenhuis et al., 2013, Thebault et al., 2012, Zhu et al., 2013). The NTE and TPR domains of Mps1 are the primary kinetochore localisation signals, binding to the CH domain of Ndc80 *in vitro* (Zhu et al., 2013, Ji et al., 2015). The TPR domain has an inhibitory effect on NTE, and upon phosphorylation by Aurora B, inhibition is eliminated and Mps1 can localise to the kinetochore via NTE and TPR domains (Figure 6.2) (Nijenhuis et al., 2013). In addition, a new region – called the MR (middle region) or IRK (internal region of kinetochore localisation) of residues 261-300 in humans, is

also responsible for proper kinetochore localisation of Mps1 (Ji et al., 2015, Dou et al., 2015). However, NTE, TPR and MR domains bind different regions of the Ndc80 complex. NTE requires the CH domain of Ndc80 for localisation to the kinetochore, whereas the MR region binds to that of Nuf2 in humans (Ji et al., 2015, Dou et al., 2015).

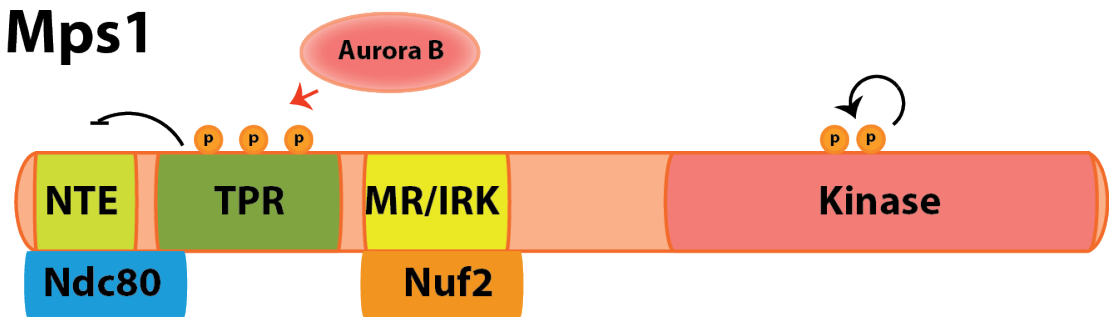

Figure 6.2. Domains of Mps1.

The N-terminal extension (NTE) interacts with the CH domain of Ndc80. The TPR domain, regulated by Aurora B phosphorylation, has an inhibitory effect on the NTE. Upon TPR phosphorylation, the NTE is no longer inhibited and Mps1 can localise to the Ndc80 complex. Another region, which was recently identified, is the MR/IRK, which is critical for the localisation of Mps1 to Nuf2. The kinase domain of Mps1 has autophosphorylation activity, thereby triggering the activation of Mps1.

Moreover, it was suggested that there is a sequential localisation of Mps1 motifs to its kinetochore platforms. In early prophase, inactive Mps1 localises to Nuf2 through its MR/IRK motif, dependent (Ji et al., 2015) or independent (Dou et al., 2015) of Aurora B phosphorylation; further studies are needed to address the dependency. Once at the kinetochore, Mps1 undergoes autophosphorylation (Dou et al., 2015, Thebault et al., 2012) and changes in conformation, where the NTE domain is freed to bind Ndc80, in an Aurora B-dependent manner (Dou et al., 2015). Moreover, phosphorylation by Aurora B and localisation of Mps1 to the kinetochore are linked with incorrect kinetochore-microtubule attachment (Dou et al., 2015, Hewitt et al., 2010, Santaguida et al., 2011, Saurin et al., 2011). Competitive binding of the Ndc80 complex to microtubules or Mps1 was shown. In the presence of microtubules, the CH domain of Ndc80 does not bind Mps1 and the reverse is also true (Dou et al., 2015, Ji et al., 2015, Hiruma et al., 2015). Studies in budding yeast show that tethering Mps1 at various

positions has different effects on SAC signalling (Aravamudhan et al., 2015). The proximity to Mps1's phosphorylation targets (aka MELT motifs) is critical for checkpoint activation, however even artificial tethering of Mps1 did not prevent checkpoint silencing once proper kinetochore-microtubule attachments were established (Aravamudhan et al., 2015). This might be due to intra-kinetochore stretch between Ndc80 and Knl1 that creates spatial separation of Mps1 from its substrates (Aravamudhan et al., 2015, Maresca and Salmon, 2010).

As truncations and mutations of the Ndc80 protein were shown to impair the recruitment of Mps1, it was hypothesised that the *ndc80-AK01* mutants affects Mph1/Mps1 localisation. Moreover, artificial tethering of Mph1 to the outer kinetochore (Mis12) restored the checkpoint signalling in *ndc80-AK01* (Figure 5.1), which would not occur if the localisation of Ark1/Aurora B was impaired in *ndc80-AK01*. Under this condition, I observed no growth and high mitotic indexes in *ndc80-AK01* (Figure 5.1). This situation is similar to wild type cells in which Mph1 is tethered to the kinetochore (Ito et al., 2012, Yamagishi et al., 2012, Heinrich et al., 2012). Therefore, the localisation of Mph1 is impaired in *ndc80-AK01*. I envision the following three scenarios are possible.

Firstly, there might be a direct interaction between Mph1/Mps1 and the linker region of Ndc80 (Figure 6.3a). *In vitro* work in humans shows direct binding between Ndc80 and Mph1/Mps1 (Zhu et al., 2013). The CH domain of Ndc80 is essential for localisation of Mps1 to kinetochores. The interaction with Ndc80 is mediated by the NTE of Mps1 (Hiruma et al., 2015, Zhu et al., 2013), however in fission yeast it is the middle region (150-302 amino acids) that is essential for Mph1/Mps1 localisation to the kinetochore (Heinrich et al., 2012). Moreover, there is no conserved TPR domain or NTE in fission yeast. As Mph1 is mislocalised in *ndc80-AK01*, a linker region mutant, it is possible that this is the main region directly binding to Mph1. The linker region is located directly after the CH domain of Ndc80; therefore Mph1/Mps1 would be in very close proximity to the CH domain, similar to humans. And since no critical regions of Mph1/Mps1 and their binding platforms were currently described, it is possible that the middle 150-302 residues of Mph1/Mps1 localises it to the linker region of Ndc80, and

this interaction is disrupted in *ndc80-AK01* cells. As it is currently technically difficult to show any interaction *in vivo* (Figure 5.2), future studies should look *in vitro* at the binding of Ndc80 and Mph1/Mps1. Potentially, mass spectrometry analysis and yeast two hybrids assays could be used to show Ndc80-Mph1 interactions and their abolishment in *ndc80-AK01* cells.

The second hypothesis involves indirect binding between Mps1 to Ndc80, which is also disrupted in *ndc80-AK01* cells (Figure 6.3b). Potentially, one of the MAPs that localises to the Ndc80 complex can bring Mph1/Mps1 to kinetochores. The Dam1 complex in budding yeast is a likely candidate that was shown initially to bind the loop region of Ndc80, and later the linker region (Lampert et al., 2013). It is possible that this complex brings Mph1/Mps1 in the proximity of the CH domain of Ndc80, where Mps1 would localise and become active. Furthermore, the Dam1 complex was suggested to block the activity of Mps1 (kinases) and phosphatases, acting as a regulator of mitosis in space (Aravamudhan et al., 2015). Therefore, it is possible that other MAPs are localising to the linker region, thereby in turn recruiting Mph1/Mps1 to kinetochores and their localisation is impaired in the *ndc80-AK01* background. Potentially MAPs would localise to Ndc80 – however we can probably exclude Dis1, Alp7/Alp14 and Klp5/Klp6, which localise to the loop region of Ndc80, and their tethering to the kinetochore restores checkpoint signalling (Tang et al., 2013, Tang and Toda, 2015a, Hsu and Toda, 2011). Mass spectrometry analysis, potentially with cross-linking or SILAC, could provide more information on proteins localising directly or indirectly to the linker region of Ndc80.

A third possible model to explain the mislocalisation of Mph1/Mps1 from the kinetochore in *ndc80-AK01* cells is disrupted binding to Nuf2 (Figure 6.3c). Ndc80-AK01 has a mutation of leucine to the helix breaker proline, causing a kink in the structure between αH and αI helices. This structural change may disrupt some interactions with Nuf2. This additional kink in the structure, which does not disrupt the Ndc80-Nuf2 interaction as the stability of the Ndc80 complex is intact in *ndc80-AK01* (Figure 3.11), can affect access to the nearby CH domain of Nuf2 (Figure 3.5). Notably, Nuf2 has been shown to bind Mps1 (Hiruma et al., 2015). A ΔCH domain truncations of

Nuf2 has reduced interaction with the MR (middle region; 261-300) of Mps1. In particular, an N126A mutation in Nuf2 impairs the binding to Mps1 (Hiruma et al., 2015) and fails to restore mitotic arrest in the presence of Aurora B inhibitors (Ji et al., 2015). Therefore, the mutation in the linker region could affect the localisation of Mph1/Mps1 to Nuf2.

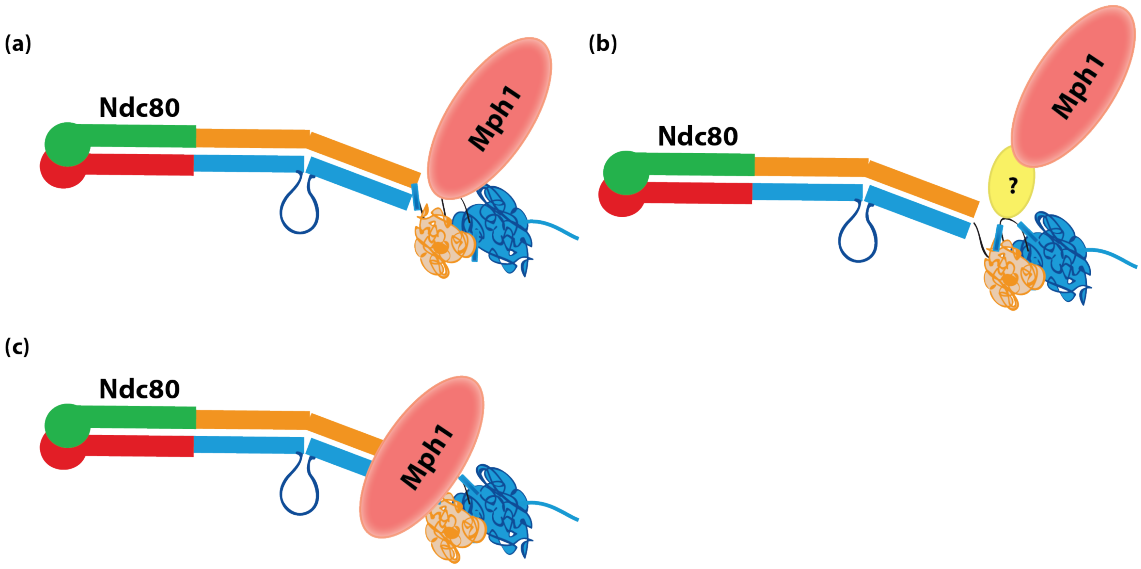

Figure 6.3. Models of the Mph1 localisation to the Ndc80 complex.

Models showing the potential localisations of Mph1 to the Ndc80 complex in fission yeast. (a) Mph1 localising directly to the linker region of Ndc80. (b) Mph1 recruitment to the kinetochore involving indirect binding to the linker region via some unknown partner. (c) Mph1 localising to the CH domain of Nuf2 and the mutation in the linker region of Ndc80 impairs this proper localisation.

To summarise, the *ndc80-AK01* mutation affects the localisation of Mph1/Mps1. Recent studies in humans shed some light on the potential mechanisms of interaction in fission yeast. The Ndc80 complex-Mps1 interaction was shown to be directly through NTE to the CH domain of Ndc80 and MR/IRK to the Nuf2 protein (Ji et al., 2015, Hiruma et al., 2015, Zhu et al., 2013). Mph1/Mps1 in fission yeast requires its middle region (150-302; different from human) for kinetochore localisation instead (Heinrich et al., 2012), suggesting a similar function for middle region of Mph1/Mps1 in fission yeast as in humans. Further studies are needed to distinguish the interactions and binding domains required for the Ndc80 complex-Mph1/Mps1 interaction. However, it remains clear that the mutation in the linker region disrupts the localisation of Mph1/Mps1 either by

abolishing direct/indirect interactions to the site or shielding the access to Nuf2. In addition to the recruitment platform function, the linker region of Ndc80 is essential for the conformation structure of the Ndc80 complex. Truncations are not viable or functional and do not localise to kinetochores (Figure 3.19, Figure 3.20 and Figure 3.21).

The most up-to-date model of SAC signalling in fission yeast, similar to humans, is the hierarchical recruitment of SAC components to the kinetochore (a scheme shown in Figure 6.4). Ark1 localisation to the inner centromere creates a phosphorylation gradient essential for establishing kinetochore-microtubule attachments and sensing tension (Yamagishi et al., 2014). Mph1 localises to the Ndc80 complex, as shown in my current work. Once Mph1 is localised properly, it phosphorylates Spc7, where in turn Bub1, Bub3 and Mad3 proteins are recruited (Heinrich et al., 2012, Meadows et al., 2011, Yamagishi et al., 2012). Next, Mad1 localises to Bub1 (however there are no direct interactions shown in fission yeast) (Heinrich et al., 2014). Mad1 forms a complex with Mad2 that is essential for the robust checkpoint response. C-Mad2 binds Slp1, together with Mad3 forming the MCC (Yamagishi et al., 2014). Progression to anaphase is halted until all the attachments are corrected. Once proper tension is detected at kinetochores by Ark1, $PP1^{Dis2}$ is brought to the kinetochore by Klp5/Klp6 that indirectly interact with the Ndc80 loop (Tang and Toda, 2015a).

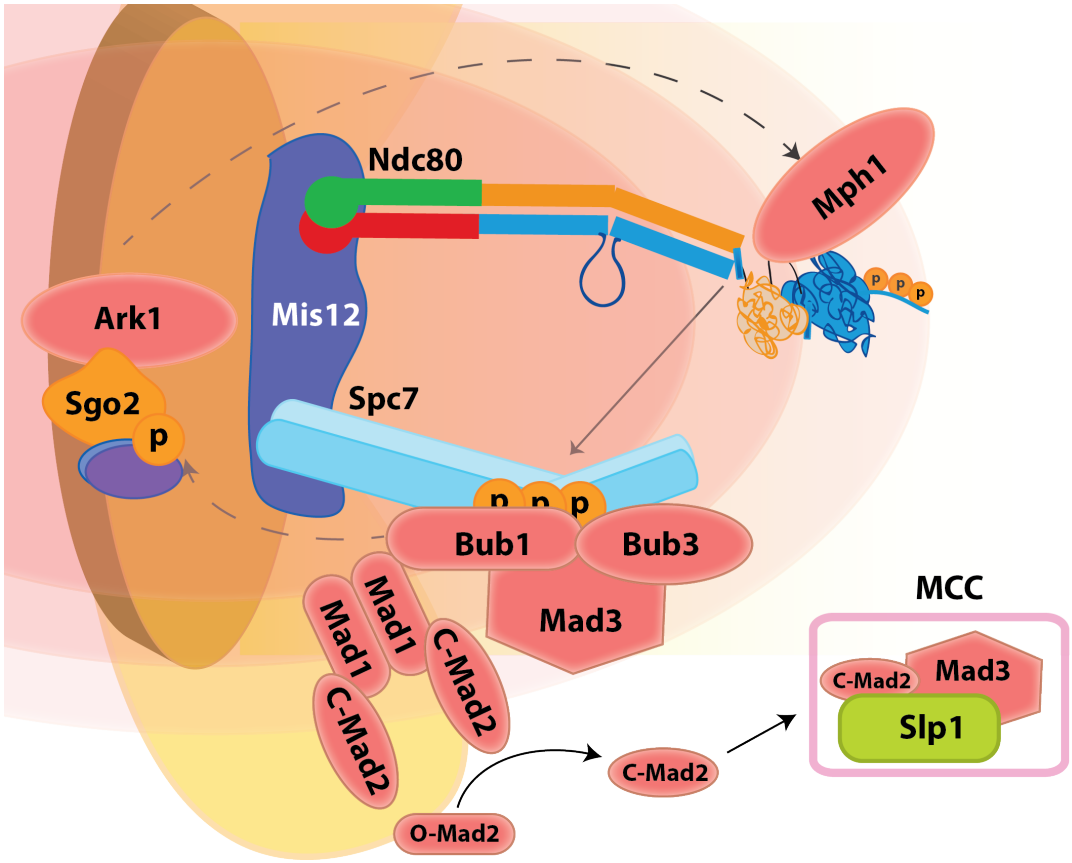

Figure 6.4. SAC signalling in fission yeast.

Ark1 is recruited first to the centromere/kinetochores and then Mph1 localises to the Ndc80 complex (current work). Once Mph1 localises and becomes active, Spc7 is phosphorylated and Bub1, Bub3 and Mad3 are recruited together with the Mad1-Mad2 heterotetramer complex. The sequential conformation changes of Mad2 result in the formation of the MCC (C-Mad2-Mad3-Slp1).

The current studies contribute to the understanding of checkpoint signalling, which has implications in the prevention of aneuploidy. Both Ndc80 and Mph1/Mps1 proteins are often mutated and overexpressed in cancers (Chapter 1.5) therefore detailed characterisation is critical for future therapies.

6.2 Future directions

Recent studies on human Mps1 have shown that there is a novel MR or IRK region that is critical for primary localisation of Mps1 to the Ndc80 complex (Dou et al., 2015, Ji et al., 2015). Fission yeast contain a similar domain, as studies by Silke Hauf showed that truncations of 1-302 and 1-150 amino acids of Mph1/Mps1 had different phenotypes.

The GFP-tagged truncation of Δ1-302 of Mph1 did not accumulate at the kinetochore and did not arrest in mitosis, similarly to *mph1*Δ. Mph1Δ1-150 on the other hand, still had normal localisation and showed checkpoint arrest. This data indicate that 151-301 region of Mph1 is crucial for Mph1 localisation. Artificial tethering of Mph1 Δ1-302 to Mis12 did restore checkpoint signalling (Heinrich et al., 2012). Therefore, future studies should elucidate the key residues important for localising Mph1 to the kinetochore, most likely revealing the same phenotype as *ndc80-AK01*. Human studies already indicate the critical role of the MR/IRK domain; it remains to be seen if this region, and its function, is conserved in fission yeast.

An additional question to answer would regard the competitive binding of Mph1 and microtubules to the Ndc80 complex. As shown in recent studies, the Ndc80 complex can bind either Mps1 or microtubules (Dou et al., 2015, Ji et al., 2015, Hiruma et al., 2015), although a transient stage in which both Mps1 and microtubule bind to the Ndc80 complex was also proposed (Dou et al., 2015). It would be interesting to check if there is similar competition in fission yeast, despite the fact that the linker region of the Ndc80 complex plays a role in localising Mph1/Mps1 rather than the CH domain, which directly binds microtubules and Mps1 (Dou et al., 2015, Ji et al., 2015, Hiruma et al., 2015). In addition, it would be very interesting to check how the phosphorylation of the Ndc80 N-tail by Ark1 regulates Mph1 recruitment to the Ndc80 complex in fission yeast. This phosphorylation was shown recently to regulate Mps1 kinetochore localisation (Zhu et al., 2013).

Chapter 7. Appendix

7.1.1 Overexpression of Mad2 and Mph1 from the *nmt41* promoter

The expression of GFP-tagged Mad2 or Mph1 from pREP41 was carried out in SAC deletion backgrounds (*mad1*Δ, *mad2*Δ, *mad3*Δ and *bub3*Δ) and then later in *ndc80-AK01*. Overexpression of Mad2 under *nmt41* resulted in normal cell growth in *mad3*Δ and *bub3*Δ (Figure 7.1). Overexpression of Mph1 from pREP41 also grew normally in *mad3*Δ and *bub3*Δ (Figure 7.1). Toxic effects of Mph1 overexpression on *bub3*Δ cells can be explained by the lack of activation or effect of Bub3 by Mph1, in contrary to the other SAC components. Mph1 overexpression under *nmt41* (Figure 7.1) is partially in accordance with the literature, as there is a normal cell growth in *mad3*Δ, however there are no toxic effects observed in *bub3*Δ as anticipated; furthermore there is an unexpected toxicity in *mad2*Δ. Overexpression from pREP41-GFP-Mph1 will therefore not be used further.

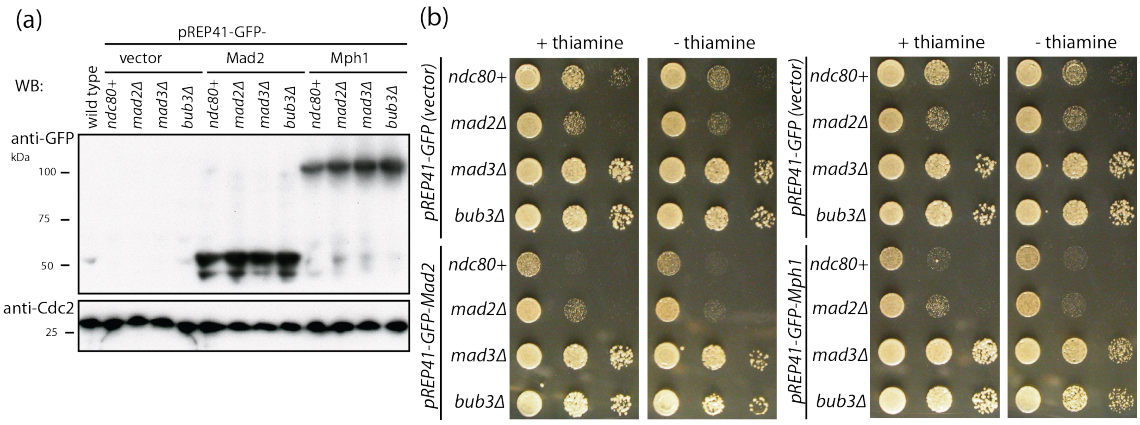

Figure 7.1. Overexpression of Mad2 and Mph1 from pREP41 has very weak effect on cells.

(a) Cells containing pREP41-GFP-Mad2 or pREP41-GFP-Mph1 were precultured in EMM-Leu+Thiamine and then placed for 18 hours in liquid EMM-Leu at 27˚C. 4 x 10^6 cells/ml were collected and protein extracts were prepared using alkaline method. Equal amounts of protein extracts were loaded and prepared for immunoblotting. Anti-GFP antibody was used to detect GFP-Mad2 and GFP-Mph1 proteins. The protein loading control Cdc2 was detected by anti-Cdc2 antibody. (b) Serial dilution assay of cells with pREP41-GFP-Mad2 and pREP41-GFP-Mph1. 5 x 10^4 cells in the first spot were followed by 10-fold dilutions and plated on EMM-Leu+Thiamine and Emm-Leu. Plates were incubated at 27˚C for 3 days.

Reference List

AKIYOSHI, B., NELSON, C. R., RANISH, J. A. & BIGGINS, S. 2009. Analysis of Ipl1-mediated phosphorylation of the Ndc80 kinetochore protein in Saccharomyces cerevisiae. *Genetics,* 183**,** 1591-5.

AKIYOSHI, B., SARANGAPANI, K. K., POWERS, A. F., NELSON, C. R., REICHOW, S. L., ARELLANO-SANTOYO, H., GONEN, T., RANISH, J. A., ASBURY, C. L. & BIGGINS, S. 2010. Tension directly stabilizes reconstituted kinetochore-microtubule attachments. *Nature,* 468**,** 576-9.

ALUSHIN, G. M., MUSINIPALLY, V., MATSON, D., TOOLEY, J., STUKENBERG, P. T. & NOGALES, E. 2012. Multimodal microtubule binding by the Ndc80 kinetochore complex. *Nat Struct Mol Biol,* 19**,** 1161-7.

ALUSHIN, G. M., RAMEY, V. H., PASQUALATO, S., BALL, D. A., GRIGORIEFF, N., MUSACCHIO, A. & NOGALES, E. 2010. The Ndc80 kinetochore complex forms oligomeric arrays along microtubules. *Nature,* 467**,** 805-10.

AMARO, A. C., SAMORA, C. P., HOLTACKERS, R., WANG, E., KINGSTON, I. J., ALONSO, M., LAMPSON, M., MCAINSH, A. D. & MERALDI, P. 2010. Molecular control of kinetochore-microtubule dynamics and chromosome oscillations. *Nat Cell Biol,* 12**,** 319-29.

ARAVAMUDHAN, P., GOLDFARB, A. A. & JOGLEKAR, A. P. 2015. The kinetochore encodes a mechanical switch to disrupt spindle assembly checkpoint signalling. *Nat Cell Biol,* 17**,** 868-879.

BARISIC, M. & GELEY, S. 2011. Spindly switch controls anaphase: spindly and RZZ functions in chromosome attachment and mitotic checkpoint control. *Cell Cycle,* 10**,** 449-56.

BASILICO, F., MAFFINI, S., WEIR, J. R., PRUMBAUM, D., ROJAS, A. M., ZIMNIAK, T., DE ANTONI, A., JEGANATHAN, S., VOSS, B., VAN GERWEN, S., KRENN, V., MASSIMILIANO, L., VALENCIA, A., VETTER, I. R., HERZOG, F., RAUNSER, S., PASQUALATO, S. & MUSACCHIO, A. 2014. The pseudo GTPase CENP-M drives human kinetochore assembly. *Elife,* 3**,** e02978.

BIECHE, I., VACHER, S., LALLEMAND, F., TOZLU-KARA, S., BENNANI, H., BEUZELIN, M., DRIOUCH, K., ROULEAU, E., LEREBOURS, F., RIPOCHE, H., CIZERON-CLAIRAC, G., SPYRATOS, F. & LIDEREAU, R. 2011. Expression analysis of mitotic spindle checkpoint genes in breast carcinoma: role of NDC80/HEC1 in early breast tumorigenicity, and a two-gene signature for aneuploidy. *Mol Cancer,* 10**,** 23.

BIGGINS, S., SEVERIN, F. F., BHALLA, N., SASSOON, I., HYMAN, A. A. & MURRAY, A. W. 1999. The conserved protein kinase Ipl1 regulates microtubule binding to kinetochores in budding yeast. *Genes Dev,* 13**,** 532-44.

BITTON, D. A., WOOD, V., SCUTT, P. J., GRALLERT, A., YATES, T., SMITH, D. L., HAGAN, I. M. & MILLER, C. J. 2011. Augmented annotation of the Schizosaccharomyces pombe genome reveals additional genes required for growth and viability. *Genetics,* 187**,** 1207-17.

BLOWER, M. D., SULLIVAN, B. A. & KARPEN, G. H. 2002. Conserved organization of centromeric chromatin in flies and humans. *Dev Cell,* 2**,** 319-30.

BOCK, L. J., PAGLIUCA, C., KOBAYASHI, N., GROVE, R. A., OKU, Y., SHRESTHA, K., ALFIERI, C., GOLFIERI, C., OLDANI, A., DAL MASCHIO, M., BERMEJO, R., HAZBUN, T. R., TANAKA, T. U. & DE WULF, P. 2012. Cnn1 inhibits the interactions between the KMN complexes of the yeast kinetochore. *Nat Cell Biol,* 14**,** 614-24.

BOLANOS-GARCIA, V. M. & BLUNDELL, T. L. 2011. BUB1 and BUBR1: multifaceted kinases of the cell cycle. *Trends Biochem Sci,* 36**,** 141-50.

BRADY, D. M. & HARDWICK, K. G. 2000. Complex formation between Mad1p, Bub1p and Bub3p is crucial for spindle checkpoint function. *Curr Biol,* 10**,** 675-8.

BRINKLEY, B. R. & STUBBLEFIELD, E. 1966. The fine structure of the kinetochore of a mammalian cell in vitro. *Chromosoma,* 19**,** 28-43.

BROUHARD, G. J., STEAR, J. H., NOETZEL, T. L., AL-BASSAM, J., KINOSHITA, K., HARRISON, S. C., HOWARD, J. & HYMAN, A. A. 2008. XMAP215 is a processive microtubule polymerase. *Cell,* 132**,** 79-88.

BURTON, J. L. & SOLOMON, M. J. 2007. Mad3p, a pseudosubstrate inhibitor of APCCdc20 in the spindle assembly checkpoint. *Genes Dev,* 21**,** 655-67.

CALDAS, G. V., DELUCA, K. F. & DELUCA, J. G. 2013. KNL1 facilitates phosphorylation of outer kinetochore proteins by promoting Aurora B kinase activity. *J Cell Biol,* 203**,** 957-969.

CARROLL, C. W., SILVA, M. C., GODEK, K. M., JANSEN, L. E. & STRAIGHT, A. F. 2009. Centromere assembly requires the direct recognition of CENP-A nucleosomes by CENP-N. *Nat Cell Biol,* 11**,** 896-902.

CASTILLO, A. R., MEEHL, J. B., MORGAN, G., SCHUTZ-GESCHWENDER, A. & WINEY, M. 2002. The yeast protein kinase Mps1p is required for assembly of the integral spindle pole body component Spc42p. *J Cell Biol,* 156**,** 453-65.

CHAN, Y. W., JEYAPRAKASH, A. A., NIGG, E. A. & SANTAMARIA, A. 2012. Aurora B controls kinetochore-microtubule attachments by inhibiting Ska complex-KMN network interaction. *J Cell Biol,* 196**,** 563-71.

CHAO, W. C., KULKARNI, K., ZHANG, Z., KONG, E. H. & BARFORD, D. 2012. Structure of the mitotic checkpoint complex. *Nature,* 484**,** 208-13.

CHEESEMAN, I. M. 2014. The Kinetochore. *Cold Spring Harb Perspect Biol,* 6.

CHEESEMAN, I. M., ANDERSON, S., JWA, M., GREEN, E. M., KANG, J., YATES, J. R., 3RD, CHAN, C. S., DRUBIN, D. G. & BARNES, G. 2002. Phospho-regulation of kinetochore-microtubule attachments by the Aurora kinase Ipl1p. *Cell,* 111**,** 163-72.

CHEESEMAN, I. M., CHAPPIE, J. S., WILSON-KUBALEK, E. M. & DESAI, A. 2006. The conserved KMN network constitutes the core microtubule-binding site of the kinetochore. *Cell,* 127**,** 983-997.

CHEESEMAN, I. M. & DESAI, A. 2008. Molecular architecture of the kinetochore-microtubule interface. *Nat Rev Mol Cell Biol,* 9**,** 33-46.

CHEESEMAN, I. M., NIESSEN, S., ANDERSON, S., HYNDMAN, F., YATES, J. R., 3RD, OEGEMA, K. & DESAI, A. 2004. A conserved protein network controls assembly of the outer kinetochore and its ability to sustain tension. *Genes Dev,* 18**,** 2255-68.

CHEN, R. H. 2004. Phosphorylation and activation of Bub1 on unattached chromosomes facilitate the spindle checkpoint. *EMBO J,* 23**,** 3113-21.

CHEN, R. H., BRADY, D. M., SMITH, D., MURRAY, A. W. & HARDWICK, K. G. 1999. The spindle checkpoint of budding yeast depends on a tight complex between the Mad1 and Mad2 proteins. *Mol Biol Cell,* 10**,** 2607-18.

CHEN, Y., RILEY, D. J., CHEN, P. L. & LEE, W. H. 1997. HEC, a novel nuclear protein rich in leucine heptad repeats specifically involved in mitosis. *Mol Cell Biol,* 17**,** 6049-56.

CHEN, Y., RILEY, D. J., ZHENG, L., CHEN, P. L. & LEE, W. H. 2002. Phosphorylation of the mitotic regulator protein Hec1 by Nek2 kinase is essential for faithful chromosome segregation. *J Biol Chem,* 277**,** 49408-16.

CIFERRI, C., DE LUCA, J., MONZANI, S., FERRARI, K. J., RISTIC, D., WYMAN, C., STARK, H., KILMARTIN, J., SALMON, E. D. & MUSACCHIO, A. 2005. Architecture of the human ndc80-hec1 complex, a critical constituent of the outer kinetochore. *J Biol Chem,* 280**,** 29088-95.

CIFERRI, C., PASQUALATO, S., SCREPANTI, E., VARETTI, G., SANTAGUIDA, S., DOS REIS, G., MAIOLICA, A., POLKA, J., DE LUCA, J. G., DE WULF, P., SALEK, M., RAPPSILBER, J., MOORES, C. A., SALMON, E. D. & MUSACCHIO, A. 2008. Implications for kinetochore-microtubule attachment from the structure of an engineered Ndc80 complex. *Cell,* 133**,** 427-439.

CLEVELAND, D. W., MAO, Y. & SULLIVAN, K. F. 2003. Centromeres and kinetochores: from epigenetics to mitotic checkpoint signaling. *Cell,* 112**,** 407-21.

COHEN-FIX, O., PETERS, J. M., KIRSCHNER, M. W. & KOSHLAND, D. 1996. Anaphase initiation in Saccharomyces cerevisiae is controlled by the APC-dependent degradation of the anaphase inhibitor Pds1p. *Genes Dev,* 10**,** 3081-93.

COLLIN, P., NASHCHEKINA, O., WALKER, R. & PINES, J. 2013. The spindle assembly checkpoint works like a rheostat rather than a toggle switch. *Nat Cell Biol,* 15**,** 1378-85.

COMINGS, D. E. & OKADA, T. A. 1971. Fine structure of kinetochore in Indian muntjac. *Exp Cell Res,* 67**,** 97-110.

COURTHEOUX, T., GAY, G., REYES, C., GOLDSTONE, S., GACHET, Y. & TOURNIER, S. 2007. Dynein participates in chromosome segregation in fission yeast. *Biol Cell,* 99**,** 627-37.

DAGA, R. R. & NURSE, P. 2008. Interphase microtubule bundles use global cell shape to guide spindle alignment in fission yeast. *J Cell Sci,* 121**,** 1973-80.

DAVIES, A. E. & KAPLAN, K. B. 2010. Hsp90-Sgt1 and Skp1 target human Mis12 complexes to ensure efficient formation of kinetochore-microtubule binding sites. *J Cell Biol,* 189**,** 261-74.

DE ANTONI, A., PEARSON, C. G., CIMINI, D., CANMAN, J. C., SALA, V., NEZI, L., MAPELLI, M., SIRONI, L., FARETTA, M., SALMON, E. D. & MUSACCHIO, A. 2005. The Mad1/Mad2 complex as a template for Mad2 activation in the spindle assembly checkpoint. *Curr Biol,* 15**,** 214-25.

DELUCA, J. G., GALL, W. E., CIFERRI, C., CIMINI, D., MUSACCHIO, A. & SALMON, E. D. 2006. Kinetochore microtubule dynamics and attachment stability are regulated by Hec1. *Cell,* 127**,** 969-82.

DELUCA, J. G., HOWELL, B. J., CANMAN, J. C., HICKEY, J. M., FANG, G. & SALMON, E. D. 2003. Nuf2 and Hec1 are required for retention of the checkpoint proteins Mad1 and Mad2 to kinetochores. *Curr Biol,* 13**,** 2103-9.

DELUCA, J. G. & MUSACCHIO, A. 2011. Structural organization of the kinetochore-microtubule interface. *Curr Opin Cell Biol*.

DELUCA, J. G. & MUSACCHIO, A. 2012. Structural organization of the kinetochore-microtubule interface. *Curr Opin Cell Biol,* 24**,** 48-56.

DESAI, A. & MITCHISON, T. J. 1997. Microtubule polymerization dynamics. *Annu Rev Cell Dev Biol,* 13**,** 83-117.

DESAI, A., RYBINA, S., MULLER-REICHERT, T., SHEVCHENKO, A., SHEVCHENKO, A., HYMAN, A. & OEGEMA, K. 2003. KNL-1 directs assembly of the microtubule-binding interface of the kinetochore in C. elegans. *Genes Dev,* 17**,** 2421-35.

DIAZ-RODRIGUEZ, E., SOTILLO, R., SCHVARTZMAN, J. M. & BENEZRA, R. 2008. Hec1 overexpression hyperactivates the mitotic checkpoint and induces tumor formation in vivo. *Proc Natl Acad Sci U S A,* 105**,** 16719-24.

DICK, A. E. & GERLICH, D. W. 2013. Kinetic framework of spindle assembly checkpoint signalling. *Nat Cell Biol,* 15**,** 1370-7.

DING, R., MCDONALD, K. L. & MCINTOSH, J. R. 1993. Three-dimensional reconstruction and analysis of mitotic spindles from the yeast, Schizosaccharomyces pombe. *J Cell Biol,* 120**,** 141-51.

DING, R., WEST, R. R., MORPHEW, D. M., OAKLEY, B. R. & MCINTOSH, J. R. 1997. The spindle pole body of Schizosaccharomyces pombe enters and leaves the nuclear envelope as the cell cycle proceeds. *Mol Biol Cell,* 8**,** 1461-79.

DOU, Z., LIU, X., WANG, W., ZHU, T., WANG, X., XU, L., ABRIEU, A., FU, C., HILL, D. L. & YAO, X. 2015. Dynamic localization of Mps1 kinase to kinetochores is essential for accurate spindle microtubule attachment. *Proc Natl Acad Sci U S A,* 112**,** E4546-E4555.

EARNSHAW, W. C. 2015. Discovering centromere proteins: from cold white hands to the A, B, C of CENPs. *Nat Rev Mol Cell Biol,* 16**,** 443-9.

EARNSHAW, W. C. & MIGEON, B. R. 1985. Three related centromere proteins are absent from the inactive centromere of a stable isodicentric chromosome. *Chromosoma,* 92**,** 290-6.

ESPERT, A., ULUOCAK, P., BASTOS, R. N., MANGAT, D., GRAAB, P. & GRUNEBERG, U. 2014. PP2A-B56 opposes Mps1 phosphorylation of Knl1 and thereby promotes spindle assembly checkpoint silencing. *J Cell Biol,* 206**,** 833-42.

ESPEUT, J., CHEERAMBATHUR, D. K., KRENNING, L., OEGEMA, K. & DESAI, A. 2012. Microtubule binding by KNL-1 contributes to spindle checkpoint silencing at the kinetochore. *J Cell Biol,* 196**,** 469-82.

ESSEX, A., DAMMERMANN, A., LEWELLYN, L., OEGEMA, K. & DESAI, A. 2009. Systematic analysis in Caenorhabditis elegans reveals that the spindle checkpoint is composed of two largely independent branches. *Mol Biol Cell,* 20**,** 1252-67.

FAMULSKI, J. K. & CHAN, G. K. 2007. Aurora B kinase-dependent recruitment of hZW10 and hROD to tensionless kinetochores. *Curr Biol,* 17**,** 2143-9.

FELSENSTEIN, J. 1989. Mathematics vs. Evolution: Mathematical Evolutionary Theory. *Science,* 246**,** 941-2.

FODDE, R., KUIPERS, J., ROSENBERG, C., SMITS, R., KIELMAN, M., GASPAR, C., VAN ES, J. H., BREUKEL, C., WIEGANT, J., GILES, R. H. & CLEVERS,

H. 2001. Mutations in the APC tumour suppressor gene cause chromosomal instability. *Nat Cell Biol,* 3**,** 433-8.

FOLEY, E. A. & KAPOOR, T. M. 2013. Microtubule attachment and spindle assembly checkpoint signalling at the kinetochore. *Nat Rev Mol Cell Biol,* 14**,** 25-37.

FORSBURG, S. L. & NURSE, P. 1991. Cell cycle regulation in the yeasts Saccharomyces cerevisiae and Schizosaccharomyces pombe. *Annu Rev Cell Biol,* 7**,** 227-56.

FOSTER, S. A. & MORGAN, D. O. 2012. The APC/C subunit Mnd2/Apc15 promotes Cdc20 autoubiquitination and spindle assembly checkpoint inactivation. *Mol Cell,* 47**,** 921-32.

FRASCHINI, R., BERETTA, A., LUCCHINI, G. & PIATTI, S. 2001. Role of the kinetochore protein Ndc10 in mitotic checkpoint activation in Saccharomyces cerevisiae. *Mol Genet Genomics,* 266**,** 115-25.

FU, C., WARD, J. J., LOIODICE, I., VELVE-CASQUILLAS, G., NEDELEC, F. J. & TRAN, P. T. 2009. Phospho-regulated interaction between kinesin-6 Klp9p and microtubule bundler Ase1p promotes spindle elongation. *Dev Cell,* 17**,** 257-67.

FUKAGAWA, T., MIKAMI, Y., NISHIHASHI, A., REGNIER, V., HARAGUCHI, T., HIRAOKA, Y., SUGATA, N., TODOKORO, K., BROWN, W. & IKEMURA, T. 2001. CENP-H, a constitutive centromere component, is required for centromere targeting of CENP-C in vertebrate cells. *EMBO J,* 20**,** 4603-17.

FULLER, B. G., LAMPSON, M. A., FOLEY, E. A., ROSASCO-NITCHER, S., LE, K. V., TOBELMANN, P., BRAUTIGAN, D. L., STUKENBERG, P. T. & KAPOOR, T. M. 2008. Midzone activation of aurora B in anaphase produces an intracellular phosphorylation gradient. *Nature,* 453**,** 1132-6.

GACHET, Y., TOURNIER, S., MILLAR, J. B. & HYAMS, J. S. 2001. A MAP kinase-dependent actin checkpoint ensures proper spindle orientation in fission yeast. *Nature,* 412**,** 352-5.

GACHET, Y., TOURNIER, S., MILLAR, J. B. & HYAMS, J. S. 2004. Mechanism controlling perpendicular alignment of the spindle to the axis of cell division in fission yeast. *EMBO J,* 23**,** 1289-300.

GARCIA, M. A., KOONRUGSA, N. & TODA, T. 2002. Spindle-kinetochore attachment requires the combined action of Kin I-like Klp5/6 and Alp14/Dis1-MAPs in fission yeast. *EMBO J,* 21**,** 6015-24.

GARCIA, M. A., VARDY, L., KOONRUGSA, N. & TODA, T. 2001. Fission yeast ch-TOG/XMAP215 homologue Alp14 connects mitotic spindles with the kinetochore and is a component of the Mad2-dependent spindle checkpoint. *EMBO J,* 20**,** 3389-401.

GASCOIGNE, K. E., TAKEUCHI, K., SUZUKI, A., HORI, T., FUKAGAWA, T. & CHEESEMAN, I. M. 2011. Induced ectopic kinetochore assembly bypasses the requirement for CENP-A nucleosomes. *Cell,* 145**,** 410-22.

GASSMANN, R., ESSEX, A., HU, J. S., MADDOX, P. S., MOTEGI, F., SUGIMOTO, A., O'ROURKE, S. M., BOWERMAN, B., MCLEOD, I., YATES, J. R., 3RD, OEGEMA, K., CHEESEMAN, I. M. & DESAI, A. 2008. A new mechanism controlling kinetochore-microtubule interactions revealed by comparison of two dynein-targeting components: SPDL-1 and the Rod/Zwilch/Zw10 complex. *Genes Dev,* 22**,** 2385-99.

GASSMANN, R., HOLLAND, A. J., VARMA, D., WAN, X., CIVRIL, F., CLEVELAND, D. W., OEGEMA, K., SALMON, E. D. & DESAI, A. 2010.

Removal of Spindly from microtubule-attached kinetochores controls spindle checkpoint silencing in human cells. *Genes Dev,* 24**,** 957-71.

GHONGANE, P., KAPANIDOU, M., ASGHAR, A., ELOWE, S. & BOLANOS-GARCIA, V. M. 2014. The dynamic protein Knl1 - a kinetochore rendezvous. *J Cell Sci,* 127**,** 3415-23.

GILLETT, E. S., ESPELIN, C. W. & SORGER, P. K. 2004. Spindle checkpoint proteins and chromosome-microtubule attachment in budding yeast. *J Cell Biol,* 164**,** 535-46.

GLOTZER, M. 2009. The 3Ms of central spindle assembly: microtubules, motors and MAPs. *Nat Rev Mol Cell Biol,* 10**,** 9-20.

GONEN, S., AKIYOSHI, B., IADANZA, M. G., SHI, D., DUGGAN, N., BIGGINS, S. & GONEN, T. 2012. The structure of purified kinetochores reveals multiple microtubule-attachment sites. *Nat Struct Mol Biol,* 19**,** 925-9.

GOSHIMA, G., SAITOH, S. & YANAGIDA, M. 1999. Proper metaphase spindle length is determined by centromere proteins Mis12 and Mis6 required for faithful chromosome segregation. *Genes Dev,* 13**,** 1664-77.

GOSHIMA, G. & YANAGIDA, M. 2000. Establishing biorientation occurs with precocious separation of the sister kinetochores, but not the arms, in the early spindle of budding yeast. *Cell,* 100**,** 619-33.

GRABSCH, H., TAKENO, S., PARSONS, W. J., POMJANSKI, N., BOECKING, A., GABBERT, H. E. & MUELLER, W. 2003. Overexpression of the mitotic checkpoint genes BUB1, BUBR1, and BUB3 in gastric cancer--association with tumour cell proliferation. *J Pathol,* 200**,** 16-22.

GRIFFIS, E. R., STUURMAN, N. & VALE, R. D. 2007. Spindly, a novel protein essential for silencing the spindle assembly checkpoint, recruits dynein to the kinetochore. *J Cell Biol,* 177**,** 1005-15.

GUIMARAES, G. J., DONG, Y., MCEWEN, B. F. & DELUCA, J. G. 2008. Kinetochore-microtubule attachment relies on the disordered N-terminal tail domain of Hec1. *Curr Biol,* 18**,** 1778-1784.

HABU, T., KIM, S. H., WEINSTEIN, J. & MATSUMOTO, T. 2002. Identification of a MAD2-binding protein, CMT2, and its role in mitosis. *EMBO J,* 21**,** 6419-28.

HAGAN, I. & YANAGIDA, M. 1990. Novel potential mitotic motor protein encoded by the fission yeast cut7+ gene. *Nature,* 347**,** 563-566.

HAGAN, I. & YANAGIDA, M. 1992. Kinesin-related cut7 protein associates with mitotic and meiotic spindles in fission yeast. *Nature,* 356**,** 74-6.

HAN, J. S., HOLLAND, A. J., FACHINETTI, D., KULUKIAN, A., CETIN, B. & CLEVELAND, D. W. 2013. Catalytic Assembly of the Mitotic Checkpoint Inhibitor BubR1-Cdc20 by a Mad2-Induced Functional Switch in Cdc20. *Mol Cell,* 51**,** 92-104.

HANAHAN, D. & WEINBERG, R. A. 2011. Hallmarks of cancer: the next generation. *Cell,* 144**,** 646-74.

HANKS, S., COLEMAN, K., REID, S., PLAJA, A., FIRTH, H., FITZPATRICK, D., KIDD, A., MEHES, K., NASH, R., ROBIN, N., SHANNON, N., TOLMIE, J., SWANSBURY, J., IRRTHUM, A., DOUGLAS, J. & RAHMAN, N. 2004. Constitutional aneuploidy and cancer predisposition caused by biallelic mutations in BUB1B. *Nat Genet,* 36**,** 1159-61.

HARDWICK, K. G., JOHNSTON, R. C., SMITH, D. L. & MURRAY, A. W. 2000. MAD3 encodes a novel component of the spindle checkpoint which interacts with Bub3p, Cdc20p, and Mad2p. *J Cell Biol,* 148**,** 871-82.

HARDWICK, K. G. & MURRAY, A. W. 1995. Mad1p, a phosphoprotein component of the spindle assembly checkpoint in budding yeast. *J Cell Biol,* 131**,** 709-20.

HARDWICK, K. G., WEISS, E., LUCA, F. C., WINEY, M. & MURRAY, A. W. 1996. Activation of the budding yeast spindle assembly checkpoint without mitotic spindle disruption. *Science,* 273**,** 953-6.

HARTWELL, L. H., CULOTTI, J., PRINGLE, J. R. & REID, B. J. 1974. Genetic control of the cell division cycle in yeast. *Science,* 183**,** 46-51.

HARTWELL, L. H., MORTIMER, R. K., CULOTTI, J. & CULOTTI, M. 1973. Genetic Control of the Cell Division Cycle in Yeast: V. Genetic Analysis of cdc Mutants. *Genetics,* 74**,** 267-86.

HARTWELL, L. H. & WEINERT, T. A. 1989. Checkpoints: controls that ensure the order of cell cycle events. *Science,* 246**,** 629-34.

HAYAMA, S., DAIGO, Y., KATO, T., ISHIKAWA, N., YAMABUKI, T., MIYAMOTO, M., ITO, T., TSUCHIYA, E., KONDO, S. & NAKAMURA, Y. 2006. Activation of CDCA1-KNTC2, members of centromere protein complex, involved in pulmonary carcinogenesis. *Cancer Res,* 66**,** 10339-48.

HAYASHI, A., DING, D. Q., TSUTSUMI, C., CHIKASHIGE, Y., MASUDA, H., HARAGUCHI, T. & HIRAOKA, Y. 2009. Localization of gene products using a chromosomally tagged GFP-fusion library in the fission yeast Schizosaccharomyces pombe. *Genes Cells,* 14**,** 217-25.

HE, X., PATTERSON, T. E. & SAZER, S. 1997. The Schizosaccharomyces pombe spindle checkpoint protein mad2p blocks anaphase and genetically interacts with the anaphase-promoting complex. *Proc Natl Acad Sci U S A,* 94**,** 7965-70.

HEINRICH, S., GEISSEN, E. M., KAMENZ, J., TRAUTMANN, S., WIDMER, C., DREWE, P., KNOP, M., RADDE, N., HASENAUER, J. & HAUF, S. 2013. Determinants of robustness in spindle assembly checkpoint signalling. *Nat Cell Biol,* 15**,** 1328-39.

HEINRICH, S., SEWART, K., WINDECKER, H., LANGEGGER, M., SCHMIDT, N., HUSTEDT, N. & HAUF, S. 2014. Mad1 contribution to spindle assembly checkpoint signalling goes beyond presenting Mad2 at kinetochores. *EMBO Rep,* 15**,** 291-8.

HEINRICH, S., WINDECKER, H., HUSTEDT, N. & HAUF, S. 2012. Mph1 kinetochore localization is crucial and upstream in the hierarchy of spindle assembly checkpoint protein recruitment to kinetochores. *J Cell Sci,* 125**,** 4720-4727.

HERNANDO, E., NAHLE, Z., JUAN, G., DIAZ-RODRIGUEZ, E., ALAMINOS, M., HEMANN, M., MICHEL, L., MITTAL, V., GERALD, W., BENEZRA, R., LOWE, S. W. & CORDON-CARDO, C. 2004. Rb inactivation promotes genomic instability by uncoupling cell cycle progression from mitotic control. *Nature,* 430**,** 797-802.

HEWITT, L., TIGHE, A., SANTAGUIDA, S., WHITE, A. M., JONES, C. D., MUSACCHIO, A., GREEN, S. & TAYLOR, S. S. 2010. Sustained Mps1 activity is required in mitosis to recruit O-Mad2 to the Mad1-C-Mad2 core complex. *J Cell Biol,* 190**,** 25-34.

HINSHAW, S. M. & HARRISON, S. C. 2013. An Iml3-Chl4 heterodimer links the core centromere to factors required for accurate chromosome segregation. *Cell Rep,* 5**,** 29-36.

HIRAOKA, Y., TODA, T. & YANAGIDA, M. 1984. The NDA3 gene of fission yeast encodes beta-tubulin: a cold-sensitive nda3 mutation reversibly blocks spindle formation and chromosome movement in mitosis. *Cell,* 39**,** 349-58.

HIRUMA, Y., SACRISTAN, C., PACHIS, S. T., ADAMOPOULOS, A., KUIJT, T., UBBINK, M., VON CASTELMUR, E., PERRAKIS, A. & KOPS, G. J. 2015. Competition between MPS1 and microtubules at kinetochores regulates spindle checkpoint signaling. *Science,* 348**,** 1264-1267.

HOLLAND, S., IOANNOU, D., HAINES, S. & BROWN, W. R. 2005. Comparison of Dam tagging and chromatin immunoprecipitation as tools for the identification of the binding sites for S. pombe CENP-C. *Chromosome Res,* 13**,** 73-83.

HOLLOWAY, S. L., GLOTZER, M., KING, R. W. & MURRAY, A. W. 1993. Anaphase is initiated by proteolysis rather than by the inactivation of maturation-promoting factor. *Cell,* 73**,** 1393-402.

HORI, T., HARAGUCHI, T., HIRAOKA, Y., KIMURA, H. & FUKAGAWA, T. 2003. Dynamic behavior of Nuf2-Hec1 complex that localizes to the centrosome and centromere and is essential for mitotic progression in vertebrate cells. *J Cell Sci,* 116**,** 3347-62.

HORI, T., OKADA, M., MAENAKA, K. & FUKAGAWA, T. 2008. CENP-O class proteins form a stable complex and are required for proper kinetochore function. *Mol Biol Cell,* 19**,** 843-54.

HORI, T., SHANG, W. H., TAKEUCHI, K. & FUKAGAWA, T. 2013. The CCAN recruits CENP-A to the centromere and forms the structural core for kinetochore assembly. *J Cell Biol,* 200**,** 45-60.

HORNUNG, P., MAIER, M., ALUSHIN, G. M., LANDER, G. C., NOGALES, E. & WESTERMANN, S. 2011. Molecular architecture and connectivity of the budding yeast Mtw1 kinetochore complex. *J Mol Biol,* 405**,** 548-59.

HOWE, M., MCDONALD, K. L., ALBERTSON, D. G. & MEYER, B. J. 2001. HIM-10 is required for kinetochore structure and function on Caenorhabditis elegans holocentric chromosomes. *J Cell Biol,* 153**,** 1227-38.

HOWELL, B. J., HOFFMAN, D. B., FANG, G., MURRAY, A. W. & SALMON, E. D. 2000. Visualization of Mad2 dynamics at kinetochores, along spindle fibers, and at spindle poles in living cells. *J Cell Biol,* 150**,** 1233-50.

HOWELL, B. J., MCEWEN, B. F., CANMAN, J. C., HOFFMAN, D. B., FARRAR, E. M., RIEDER, C. L. & SALMON, E. D. 2001. Cytoplasmic dynein/dynactin drives kinetochore protein transport to the spindle poles and has a role in mitotic spindle checkpoint inactivation. *J Cell Biol,* 155**,** 1159-72.

HOWELL, B. J., MOREE, B., FARRAR, E. M., STEWART, S., FANG, G. & SALMON, E. D. 2004. Spindle checkpoint protein dynamics at kinetochores in living cells. *Curr Biol,* 14**,** 953-64.

HOYT, M. A., TOTIS, L. & ROBERTS, B. T. 1991. S. cerevisiae genes required for cell cycle arrest in response to loss of microtubule function. *Cell,* 66**,** 507-17.

HSU, K. S. & TODA, T. 2011. Ndc80 internal loop interacts with Dis1/TOG to ensure proper kinetochore-spindle attachment in fission yeast. *Curr Biol,* 21**,** 214-220.

IOUK, T., KERSCHER, O., SCOTT, R. J., BASRAI, M. A. & WOZNIAK, R. W. 2002. The yeast nuclear pore complex functionally interacts with components of the spindle assembly checkpoint. *J Cell Biol,* 159**,** 807-19.

ITO, D., SAITO, Y. & MATSUMOTO, T. 2012. Centromere-tethered Mps1 pombe homolog (Mph1) kinase is a sufficient marker for recruitment of the spindle checkpoint protein Bub1, but not Mad1. *Proc Natl Acad Sci U S A,* 109**,** 209-214.

JAKOPEC, V., TOPOLSKI, B. & FLEIG, U. 2012. Sos7, an essential component of the conserved Schizosaccharomyces pombe Ndc80-MIND-Spc7 complex, identifies a new family of fungal kinetochore proteins. *Mol Cell Biol,* 32**,** 3308-20.

JELLUMA, N., BRENKMAN, A. B., VAN DEN BROEK, N. J., CRUIJSEN, C. W., VAN OSCH, M. H., LENS, S. M., MEDEMA, R. H. & KOPS, G. J. 2008. Mps1 phosphorylates Borealin to control Aurora B activity and chromosome alignment. *Cell,* 132**,** 233-46.

JELLUMA, N., DANSEN, T. B., SLIEDRECHT, T., KWIATKOWSKI, N. P. & KOPS, G. J. 2010. Release of Mps1 from kinetochores is crucial for timely anaphase onset. *J Cell Biol,* 191**,** 281-90.

JI, Z., GAO, H. & YU, H. 2015. CELL DIVISION CYCLE. Kinetochore attachment sensed by competitive Mps1 and microtubule binding to Ndc80C. *Science,* 348**,** 1260-1264.

JOKELAINEN, P. T. 1967. The ultrastructure and spatial organization of the metaphase kinetochore in mitotic rat cells. *J Ultrastruct Res,* 19**,** 19-44.

JONES, D. T., TAYLOR, W. R. & THORNTON, J. M. 1992. The rapid generation of mutation data matrices from protein sequences. *Comput Appl Biosci,* 8**,** 275-82.

KANBE, T., HIRAOKA, Y., TANAKA, K. & YANAGIDA, M. 1990. The transition of cells of the fission yeast beta-tubulin mutant nda3-311 as seen by freeze-substitution electron microscopy. Requirement of functional tubulin for spindle pole body duplication. *J Cell Sci,* 96 (Pt 2)**,** 275-82.

KANG, J., CHEN, Y., ZHAO, Y. & YU, H. 2007. Autophosphorylation-dependent activation of human Mps1 is required for the spindle checkpoint. *Proc Natl Acad Sci U S A,* 104**,** 20232-7.

KAPOOR, T. M., MAYER, T. U., COUGHLIN, M. L. & MITCHISON, T. J. 2000. Probing spindle assembly mechanisms with monastrol, a small molecule inhibitor of the mitotic kinesin, Eg5. *J Cell Biol,* 150**,** 975-88.

KARESS, R. 2005. Rod-Zw10-Zwilch: a key player in the spindle checkpoint. *Trends Cell Biol,* 15**,** 386-92.

KASUBOSKI, J. M., BADER, J. R., VAUGHAN, P. S., TAUHATA, S. B., WINDING, M., MORRISSEY, M. A., JOYCE, M. V., BOGGESS, W., VOS, L., CHAN, G. K., HINCHCLIFFE, E. H. & VAUGHAN, K. T. 2011. Zwint-1 is a novel Aurora B substrate required for the assembly of a dynein-binding platform on kinetochores. *Mol Biol Cell,* 22**,** 3318-30.

KAWASHIMA, S. A., TSUKAHARA, T., LANGEGGER, M., HAUF, S., KITAJIMA, T. S. & WATANABE, Y. 2007. Shugoshin enables tension-generating attachment of kinetochores by loading Aurora to centromeres. *Genes Dev,* 21**,** 420-35.

KAWASHIMA, S. A., YAMAGISHI, Y., HONDA, T., ISHIGURO, K. & WATANABE, Y. 2010a. Phosphorylation of H2A by Bub1 prevents chromosomal instability through localizing shugoshin. *Science,* 327**,** 172-7.

KAWASHIMA, S. A., YAMAGISHI, Y., HONDA, T., ISHIGURO, K. & WATANABE, Y. 2010b. Phosphorylation of H2A by Bub1 prevents chromosomal instability through localizing shugoshin. *Science,* 327**,** 172-177.

KEMMLER, S., STACH, M., KNAPP, M., ORTIZ, J., PFANNSTIEL, J., RUPPERT, T. & LECHNER, J. 2009. Mimicking Ndc80 phosphorylation triggers spindle assembly checkpoint signalling. *EMBO J,* 28**,** 1099-110.

KHODJAKOV, A., COLE, R. W., OAKLEY, B. R. & RIEDER, C. L. 2000. Centrosome-independent mitotic spindle formation in vertebrates. *Curr Biol,* 10**,** 59-67.

KIM, D. U., HAYLES, J., KIM, D., WOOD, V., PARK, H. O., WON, M., YOO, H. S., DUHIG, T., NAM, M., PALMER, G., HAN, S., JEFFERY, L., BAEK, S. T., LEE, H., SHIM, Y. S., LEE, M., KIM, L., HEO, K. S., NOH, E. J., LEE, A. R., JANG, Y. J., CHUNG, K. S., CHOI, S. J., PARK, J. Y., PARK, Y., KIM, H. M., PARK, S. K., PARK, H. J., KANG, E. J., KIM, H. B., KANG, H. S., PARK, H. M., KIM, K., SONG, K., SONG, K. B., NURSE, P. & HOE, K. L. 2010. Analysis of a genome-wide set of gene deletions in the fission yeast Schizosaccharomyces pombe. *Nat Biotechnol,* 28**,** 617-23.

KIM, S., SUN, H., TOMCHICK, D. R., YU, H. & LUO, X. 2012. Structure of human Mad1 C-terminal domain reveals its involvement in kinetochore targeting. *Proc Natl Acad Sci U S A,* 109**,** 6549-54.

KIM, S. & YU, H. 2015. Multiple assembly mechanisms anchor the KMN spindle checkpoint platform at human mitotic kinetochores. *J Cell Biol,* 208**,** 181-96.

KIM, S. H., LIN, D. P., MATSUMOTO, S., KITAZONO, A. & MATSUMOTO, T. 1998. Fission yeast Slp1: an effector of the Mad2-dependent spindle checkpoint. *Science,* 279**,** 1045-7.

KING, E. M., RACHIDI, N., MORRICE, N., HARDWICK, K. G. & STARK, M. J. 2007. Ipl1p-dependent phosphorylation of Mad3p is required for the spindle checkpoint response to lack of tension at kinetochores. *Genes Dev,* 21**,** 1163-8.

KING, R. W., PETERS, J. M., TUGENDREICH, S., ROLFE, M., HIETER, P. & KIRSCHNER, M. W. 1995. A 20S complex containing CDC27 and CDC16 catalyzes the mitosis-specific conjugation of ubiquitin to cyclin B. *Cell,* 81**,** 279-88.

KING, S. M., HYAMS, J. S. & LUBA, A. 1982. Absence of microtubule sliding and an analysis of spindle formation and elongation in isolated mitotic spindles from the yeast Saccharomyces cerevisiae. *J Cell Biol,* 94**,** 341-9.

KIYOMITSU, T., OBUSE, C. & YANAGIDA, M. 2007. Human Blinkin/AF15q14 is required for chromosome alignment and the mitotic checkpoint through direct interaction with Bub1 and BubR1. *Dev Cell,* 13**,** 663-76.

KLARE, K., WEIR, J. R., BASILICO, F., ZIMNIAK, T., MASSIMILIANO, L., LUDWIGS, N., HERZOG, F. & MUSACCHIO, A. 2015. CENP-C is a blueprint for constitutive centromere-associated network assembly within human kinetochores. *J Cell Biol,* 210**,** 11-22.

KLEBIG, C., KORINTH, D. & MERALDI, P. 2009. Bub1 regulates chromosome segregation in a kinetochore-independent manner. *J Cell Biol,* 185**,** 841-58.

KLINE, S. L., CHEESEMAN, I. M., HORI, T., FUKAGAWA, T. & DESAI, A. 2006. The human Mis12 complex is required for kinetochore assembly and proper chromosome segregation. *J Cell Biol,* 173**,** 9-17.

KOPS, G. J., WEAVER, B. A. & CLEVELAND, D. W. 2005. On the road to cancer: aneuploidy and the mitotic checkpoint. *Nat Rev Cancer,* 5**,** 773-85.

KRENN, V., OVERLACK, K., PRIMORAC, I., VAN GERWEN, S. & MUSACCHIO, A. 2014. KI motifs of human Knl1 enhance assembly of comprehensive spindle checkpoint complexes around MELT repeats. *Curr Biol,* 24**,** 29-39.

KRISSINEL, E. & HENRICK, K. 2007. Inference of macromolecular assemblies from crystalline state. *J Mol Biol,* 372**,** 774-97.

KRUSE, T., LARSEN, M. S., SEDGWICK, G. G., SIGURDSSON, J. O., STREICHER, W., OLSEN, J. V. & NILSSON, J. 2014. A direct role of Mad1 in the spindle assembly checkpoint beyond Mad2 kinetochore recruitment. *EMBO Rep,* 15**,** 282-90.

KRUSE, T., ZHANG, G., LARSEN, M. S., LISCHETTI, T., STREICHER, W., KRAGH NIELSEN, T., BJORN, S. P. & NILSSON, J. 2013. Direct binding between BubR1 and B56-PP2A phosphatase complexes regulate mitotic progression. *J Cell Sci,* 126**,** 1086-92.

KULUKIAN, A., HAN, J. S. & CLEVELAND, D. W. 2009. Unattached kinetochores catalyze production of an anaphase inhibitor that requires a Mad2 template to prime Cdc20 for BubR1 binding. *Dev Cell,* 16**,** 105-17.

LAMPERT, F., MIECK, C., ALUSHIN, G. M., NOGALES, E. & WESTERMANN, S. 2013. Molecular requirements for the formation of a kinetochore-microtubule interface by Dam1 and Ndc80 complexes. *J Cell Biol,* 200**,** 21-30.

LAMPSON, M. A. & CHEESEMAN, I. M. 2011. Sensing centromere tension: Aurora B and the regulation of kinetochore function. *Trends Cell Biol,* 21**,** 133-40.

LARA-GONZALEZ, P., WESTHORPE, F. G. & TAYLOR, S. S. 2012. The spindle assembly checkpoint. *Curr Biol,* 22**,** R966-R980.

LARKIN, M. A., BLACKSHIELDS, G., BROWN, N. P., CHENNA, R., MCGETTIGAN, P. A., MCWILLIAM, H., VALENTIN, F., WALLACE, I. M., WILM, A., LOPEZ, R., THOMPSON, J. D., GIBSON, T. J. & HIGGINS, D. G. 2007. Clustal W and Clustal X version 2.0. *Bioinformatics,* 23**,** 2947-8.

LARSEN, N. A., AL-BASSAM, J., WEI, R. R. & HARRISON, S. C. 2007. Structural analysis of Bub3 interactions in the mitotic spindle checkpoint. *Proc Natl Acad Sci U S A,* 104**,** 1201-6.

LEE, S., THEBAULT, P., FRESCHI, L., BEAUFILS, S., BLUNDELL, T. L., LANDRY, C. R., BOLANOS-GARCIA, V. M. & ELOWE, S. 2012. Characterization of spindle checkpoint kinase Mps1 reveals domain with functional and structural similarities to tetratricopeptide repeat motifs of Bub1 and BubR1 checkpoint kinases. *J Biol Chem,* 287**,** 5988-6001.

LESAGE, B., QIAN, J. & BOLLEN, M. 2011. Spindle checkpoint silencing: PP1 tips the balance. *Curr Biol,* 21**,** R898-903.

LETUNIC, I. & BORK, P. 2011. Interactive Tree Of Life v2: online annotation and display of phylogenetic trees made easy. *Nucleic Acids Res,* 39**,** W475-8.

LI, D., MORLEY, G., WHITAKER, M. & HUANG, J. Y. 2010. Recruitment of Cdc20 to the kinetochore requires BubR1 but not Mad2 in Drosophila melanogaster. *Mol Cell Biol,* 30**,** 3384-95.

LI, R. & MURRAY, A. W. 1991. Feedback control of mitosis in budding yeast. *Cell,* 66**,** 519-31.

LI, X. & NICKLAS, R. B. 1995. Mitotic forces control a cell-cycle checkpoint. *Nature,* 373**,** 630-2.

LIN, Z., JIA, L., TOMCHICK, D. R., LUO, X. & YU, H. 2014. Substrate-specific activation of the mitotic kinase Bub1 through intramolecular autophosphorylation and kinetochore targeting. *Structure,* 22**,** 1616-27.

LIU, D. & LAMPSON, M. A. 2009. Regulation of kinetochore-microtubule attachments by Aurora B kinase. *Biochem Soc Trans,* 37**,** 976-980.

LIU, D., VLEUGEL, M., BACKER, C. B., HORI, T., FUKAGAWA, T., CHEESEMAN, I. M. & LAMPSON, M. A. 2010. Regulated targeting of protein phosphatase 1 to the outer kinetochore by KNL1 opposes Aurora B kinase. *J Cell Biol,* 188**,** 809-820.

LIU, X., MCLEOD, I., ANDERSON, S., YATES, J. R., 3RD & HE, X. 2005. Molecular analysis of kinetochore architecture in fission yeast. *EMBO J,* 24**,** 2919-2930.

LOIODICE, I., STAUB, J., SETTY, T. G., NGUYEN, N. P., PAOLETTI, A. & TRAN, P. T. 2005. Ase1p organizes antiparallel microtubule arrays during interphase and mitosis in fission yeast. *Mol Biol Cell,* 16**,** 1756-68.

LONDON, N. & BIGGINS, S. 2014a. Mad1 kinetochore recruitment by Mps1-mediated phosphorylation of Bub1 signals the spindle checkpoint. *Genes Dev,* 28**,** 140-52.

LONDON, N. & BIGGINS, S. 2014b. Signalling dynamics in the spindle checkpoint response. *Nat Rev Mol Cell Biol,* 15**,** 736-47.

LONDON, N., CETO, S., RANISH, J. A. & BIGGINS, S. 2012. Phosphoregulation of Spc105 by Mps1 and PP1 regulates Bub1 localization to kinetochores. *Curr Biol,* 22**,** 900-6.

LUO, X., TANG, Z., RIZO, J. & YU, H. 2002. The Mad2 spindle checkpoint protein undergoes similar major conformational changes upon binding to either Mad1 or Cdc20. *Mol Cell,* 9**,** 59-71.

LUO, X., TANG, Z., XIA, G., WASSMANN, K., MATSUMOTO, T., RIZO, J. & YU, H. 2004. The Mad2 spindle checkpoint protein has two distinct natively folded states. *Nat Struct Mol Biol,* 11**,** 338-45.

MACIEJOWSKI, J., GEORGE, K. A., TERRET, M. E., ZHANG, C., SHOKAT, K. M. & JALLEPALLI, P. V. 2010. Mps1 directs the assembly of Cdc20 inhibitory complexes during interphase and mitosis to control M phase timing and spindle checkpoint signaling. *J Cell Biol,* 190**,** 89-100.

MADDOX, P. S., OEGEMA, K., DESAI, A. & CHEESEMAN, I. M. 2004. "Holo"er than thou: chromosome segregation and kinetochore function in C. elegans. *Chromosome Res,* 12**,** 641-53.

MALDONADO, M. & KAPOOR, T. M. 2011. Constitutive Mad1 targeting to kinetochores uncouples checkpoint signalling from chromosome biorientation. *Nat Cell Biol,* 13**,** 475-82.

MAPELLI, M. & MUSACCHIO, A. 2007. MAD contortions: conformational dimerization boosts spindle checkpoint signaling. *Curr Opin Struct Biol,* 17**,** 716-25.

MARESCA, T. J. & SALMON, E. D. 2010. Welcome to a new kind of tension: translating kinetochore mechanics into a wait-anaphase signal. *J Cell Sci,* 123**,** 825-35.

MARTIN-LLUESMA, S., STUCKE, V. M. & NIGG, E. A. 2002. Role of Hec1 in spindle checkpoint signaling and kinetochore recruitment of Mad1/Mad2. *Science,* 297**,** 2267-2270.

MASUMOTO, H., MASUKATA, H., MURO, Y., NOZAKI, N. & OKAZAKI, T. 1989. A human centromere antigen (CENP-B) interacts with a short specific sequence in alphoid DNA, a human centromeric satellite. *J Cell Biol,* 109**,** 1963-73.

MATSON, D. R., DEMIREL, P. B., STUKENBERG, P. T. & BURKE, D. J. 2012. A conserved role for COMA/CENP-H/I/N kinetochore proteins in the spindle checkpoint. *Genes Dev,* 26**,** 542-7.

MATSON, D. R. & STUKENBERG, P. T. 2014. CENP-I and Aurora B act as a molecular switch that ties RZZ/Mad1 recruitment to kinetochore attachment status. *J Cell Biol,* 205**,** 541-54.

MATSUO, Y., ASAKAWA, K., TODA, T. & KATAYAMA, S. 2006. A rapid method for protein extraction from fission yeast. *Biosci Biotechnol Biochem,* 70**,** 1992-4.

MATSUYAMA, A., ARAI, R., YASHIRODA, Y., SHIRAI, A., KAMATA, A., SEKIDO, S., KOBAYASHI, Y., HASHIMOTO, A., HAMAMOTO, M., HIRAOKA, Y., HORINOUCHI, S. & YOSHIDA, M. 2006. ORFeome cloning and global analysis of protein localization in the fission yeast Schizosaccharomyces pombe. *Nat Biotechnol,* 24**,** 841-7.

MATTISON, C. P., OLD, W. M., STEINER, E., HUNEYCUTT, B. J., RESING, K. A., AHN, N. G. & WINEY, M. 2007. Mps1 activation loop autophosphorylation enhances kinase activity. *J Biol Chem,* 282**,** 30553-61.

MAURE, J. F., KOMOTO, S., OKU, Y., MINO, A., PASQUALATO, S., NATSUME, K., CLAYTON, L., MUSACCHIO, A. & TANAKA, T. U. 2011. The Ndc80 loop region facilitates formation of kinetochore attachment to the dynamic microtubule plus end. *Curr Biol,* 21**,** 207-213.

MCCLELAND, M. L., GARDNER, R. D., KALLIO, M. J., DAUM, J. R., GORBSKY, G. J., BURKE, D. J. & STUKENBERG, P. T. 2003. The highly conserved Ndc80 complex is required for kinetochore assembly, chromosome congression, and spindle checkpoint activity. *Genes Dev,* 17**,** 101-14.

MCCLELLAND, S. E., BORUSU, S., AMARO, A. C., WINTER, J. R., BELWAL, M., MCAINSH, A. D. & MERALDI, P. 2007. The CENP-A NAC/CAD kinetochore complex controls chromosome congression and spindle bipolarity. *EMBO J,* 26**,** 5033-47.

MEADOWS, J. C., SHEPPERD, L. A., VANOOSTHUYSE, V., LANCASTER, T. C., SOCHAJ, A. M., BUTTRICK, G. J., HARDWICK, K. G. & MILLAR, J. B. 2011. Spindle checkpoint silencing requires association of PP1 to both Spc7 and kinesin-8 motors. *Dev Cell,* 20**,** 739-50.

MENG, Q. C., WANG, H. C., SONG, Z. L., SHAN, Z. Z., YUAN, Z., ZHENG, Q. & HUANG, X. Y. 2015. Overexpression of NDC80 is correlated with prognosis of pancreatic cancer and regulates cell proliferation. *Am J Cancer Res,* 5**,** 1730-40.

MERALDI, P., DRAVIAM, V. M. & SORGER, P. K. 2004. Timing and checkpoints in the regulation of mitotic progression. *Dev Cell,* 7**,** 45-60.

MERALDI, P., MCAINSH, A. D., RHEINBAY, E. & SORGER, P. K. 2006. Phylogenetic and structural analysis of centromeric DNA and kinetochore proteins. *Genome Biol,* 7**,** R23.

MILLBAND, D. N. & HARDWICK, K. G. 2002. Fission yeast Mad3p is required for Mad2p to inhibit the anaphase-promoting complex and localizes to kinetochores in a Bub1p-, Bub3p-, and Mph1p-dependent manner. *Mol Cell Biol,* 22**,** 2728-42.

MILLER, S. A., JOHNSON, M. L. & STUKENBERG, P. T. 2008. Kinetochore attachments require an interaction between unstructured tails on microtubules and Ndc80(Hec1). *Curr Biol,* 18**,** 1785-1791.

MIRANDA, J. J., DE WULF, P., SORGER, P. K. & HARRISON, S. C. 2005. The yeast DASH complex forms closed rings on microtubules. *Nat Struct Mol Biol,* 12**,** 138-43.

MITCHISON, T. & KIRSCHNER, M. 1984. Dynamic instability of microtubule growth. *Nature,* 312**,** 237-42.

MORENO, S., KLAR, A. & NURSE, P. 1991. Molecular genetic analysis of fission yeast Schizosaccharomyces pombe. *Methods Enzymol,* 194**,** 795-823.

MOYLE, M. W., KIM, T., HATTERSLEY, N., ESPEUT, J., CHEERAMBATHUR, D. K., OEGEMA, K. & DESAI, A. 2014. A Bub1-Mad1 interaction targets the Mad1-Mad2 complex to unattached kinetochores to initiate the spindle checkpoint. *J Cell Biol,* 204**,** 647-57.

MUSACCHIO, A. & SALMON, E. D. 2007. The spindle-assembly checkpoint in space and time. *Nat Rev Mol Cell Biol,* 8**,** 379-393.

NABETANI, A., KOUJIN, T., TSUTSUMI, C., HARAGUCHI, T. & HIRAOKA, Y. 2001. A conserved protein, Nuf2, is implicated in connecting the centromere to the spindle during chromosome segregation: a link between the kinetochore function and the spindle checkpoint. *Chromosoma,* 110**,** 322-34.

NIJENHUIS, W., VALLARDI, G., TEIXEIRA, A., KOPS, G. J. & SAURIN, A. T. 2014. Negative feedback at kinetochores underlies a responsive spindle checkpoint signal. *Nat Cell Biol*.

NIJENHUIS, W., VON CASTELMUR, E., LITTLER, D., DE MARCO, V., TROMER, E., VLEUGEL, M., VAN OSCH, M. H., SNEL, B., PERRAKIS, A. & KOPS, G. J. 2013. A TPR domain-containing N-terminal module of MPS1 is required for its kinetochore localization by Aurora B. *J Cell Biol,* 201**,** 217-231.

NILSSON, J., YEKEZARE, M., MINSHULL, J. & PINES, J. 2008. The APC/C maintains the spindle assembly checkpoint by targeting Cdc20 for destruction. *Nat Cell Biol,* 10**,** 1411-20.

NISHIHASHI, A., HARAGUCHI, T., HIRAOKA, Y., IKEMURA, T., REGNIER, V., DODSON, H., EARNSHAW, W. C. & FUKAGAWA, T. 2002. CENP-I is essential for centromere function in vertebrate cells. *Dev Cell,* 2**,** 463-76.

NISHINO, T., TAKEUCHI, K., GASCOIGNE, K. E., SUZUKI, A., HORI, T., OYAMA, T., MORIKAWA, K., CHEESEMAN, I. M. & FUKAGAWA, T. 2012. CENP-T-W-S-X forms a unique centromeric chromatin structure with a histone-like fold. *Cell,* 148**,** 487-501.

NOGALES, E. 1999. A structural view of microtubule dynamics. *Cell Mol Life Sci,* 56**,** 133-42.

NOGALES, E., WOLF, S. G. & DOWNING, K. H. 1998. Structure of the alpha beta tubulin dimer by electron crystallography. *Nature,* 391**,** 199-203.

NURSE, P. 2000. A long twentieth century of the cell cycle and beyond. *Cell,* 100**,** 71-8.

NURSE, P., MASUI, Y. & HARTWELL, L. 1998. Understanding the cell cycle. *Nat Med,* 4**,** 1103-6.

OBUSE, C., IWASAKI, O., KIYOMITSU, T., GOSHIMA, G., TOYODA, Y. & YANAGIDA, M. 2004. A conserved Mis12 centromere complex is linked to heterochromatic HP1 and outer kinetochore protein Zwint-1. *Nat Cell Biol,* 6**,** 1135-41.

OKADA, M., CHEESEMAN, I. M., HORI, T., OKAWA, K., MCLEOD, I. X., YATES, J. R., 3RD, DESAI, A. & FUKAGAWA, T. 2006. The CENP-H-I complex is required for the efficient incorporation of newly synthesized CENP-A into centromeres. *Nat Cell Biol,* 8**,** 446-57.

OKADA, N., TODA, T., YAMAMOTO, M. & SATO, M. 2014. CDK-dependent phosphorylation of Alp7-Alp14 (TACC-TOG) promotes its nuclear accumulation and spindle microtubule assembly. *Mol Biol Cell,* 25**,** 1969-82.

OLESEN, S. H., THYKJAER, T. & ORNTOFT, T. F. 2001. Mitotic checkpoint genes hBUB1, hBUB1B, hBUB3 and TTK in human bladder cancer, screening for mutations and loss of heterozygosity. *Carcinogenesis,* 22**,** 813-5.

OLIFERENKO, S. & BALASUBRAMANIAN, M. K. 2002. Astral microtubules monitor metaphase spindle alignment in fission yeast. *Nat Cell Biol,* 4**,** 816-20.

OSBORNE, M. A., SCHLENSTEDT, G., JINKS, T. & SILVER, P. A. 1994. Nuf2, a spindle pole body-associated protein required for nuclear division in yeast. *J Cell Biol,* 125**,** 853-66.

PAGLIUCA, C., DRAVIAM, V. M., MARCO, E., SORGER, P. K. & DE WULF, P. 2009. Roles for the conserved spc105p/kre28p complex in kinetochore-microtubule binding and the spindle assembly checkpoint. *PLoS One,* 4**,** e7640.

PALFRAMAN, W. J., MEEHL, J. B., JASPERSEN, S. L., WINEY, M. & MURRAY, A. W. 2006. Anaphase inactivation of the spindle checkpoint. *Science,* 313**,** 680-4.

PERPELESCU, M. & FUKAGAWA, T. 2011. The ABCs of CENPs. *Chromosoma,* 120**,** 425-46.

PETROVIC, A., PASQUALATO, S., DUBE, P., KRENN, V., SANTAGUIDA, S., CITTARO, D., MONZANI, S., MASSIMILIANO, L., KELLER, J., TARRICONE, A., MAIOLICA, A., STARK, H. & MUSACCHIO, A. 2010. The MIS12 complex is a protein interaction hub for outer kinetochore assembly. *J Cell Biol,* 190**,** 835-52.

PFARR, C. M., COUE, M., GRISSOM, P. M., HAYS, T. S., PORTER, M. E. & MCINTOSH, J. R. 1990. Cytoplasmic dynein is localized to kinetochores during mitosis. *Nature,* 345**,** 263-5.

PIDOUX, A. L. & ALLSHIRE, R. C. 2004. Kinetochore and heterochromatin domains of the fission yeast centromere. *Chromosome Res,* 12**,** 521-34.

PINES, J. & RIEDER, C. L. 2001. Re-staging mitosis: a contemporary view of mitotic progression. *Nat Cell Biol,* 3**,** E3-6.

PINSKY, B. A., NELSON, C. R. & BIGGINS, S. 2009. Protein phosphatase 1 regulates exit from the spindle checkpoint in budding yeast. *Curr Biol,* 19**,** 1182-7.

PRIMORAC, I. & MUSACCHIO, A. 2013. Panta rhei: the APC/C at steady state. *J Cell Biol,* 201**,** 177-89.

RADCLIFFE, P., HIRATA, D., CHILDS, D., VARDY, L. & TODA, T. 1998. Identification of novel temperature-sensitive lethal alleles in essential beta-tubulin and nonessential alpha 2-tubulin genes as fission yeast polarity mutants. *Mol Biol Cell,* 9**,** 1757-1771.

RHIND, N., CHEN, Z., YASSOUR, M., THOMPSON, D. A., HAAS, B. J., HABIB, N., WAPINSKI, I., ROY, S., LIN, M. F., HEIMAN, D. I., YOUNG, S. K., FURUYA, K., GUO, Y., PIDOUX, A., CHEN, H. M., ROBBERTSE, B., GOLDBERG, J. M., AOKI, K., BAYNE, E. H., BERLIN, A. M., DESJARDINS, C. A., DOBBS, E., DUKAJ, L., FAN, L., FITZGERALD, M. G.,

FRENCH, C., GUJJA, S., HANSEN, K., KEIFENHEIM, D., LEVIN, J. Z., MOSHER, R. A., MULLER, C. A., PFIFFNER, J., PRIEST, M., RUSS, C., SMIALOWSKA, A., SWOBODA, P., SYKES, S. M., VAUGHN, M., VENGROVA, S., YODER, R., ZENG, Q., ALLSHIRE, R., BAULCOMBE, D., BIRREN, B. W., BROWN, W., EKWALL, K., KELLIS, M., LEATHERWOOD, J., LEVIN, H., MARGALIT, H., MARTIENSSEN, R., NIEDUSZYNSKI, C. A., SPATAFORA, J. W., FRIEDMAN, N., DALGAARD, J. Z., BAUMANN, P., NIKI, H., REGEV, A. & NUSBAUM, C. 2011. Comparative functional genomics of the fission yeasts. *Science,* 332**,** 930-6.

RHIND, N. & RUSSELL, P. 2012. Signaling pathways that regulate cell division. *Cold Spring Harb Perspect Biol,* 4.

RIEDER, C. L. 1981. The structure of the cold-stable kinetochore fiber in metaphase PtK1 cells. *Chromosoma,* 84**,** 145-58.

RIEDER, C. L., COLE, R. W., KHODJAKOV, A. & SLUDER, G. 1995. The checkpoint delaying anaphase in response to chromosome monoorientation is mediated by an inhibitory signal produced by unattached kinetochores. *J Cell Biol,* 130**,** 941-8.

ROBERTS, B. T., FARR, K. A. & HOYT, M. A. 1994. The Saccharomyces cerevisiae checkpoint gene BUB1 encodes a novel protein kinase. *Mol Cell Biol,* 14**,** 8282-91.

RODRIGUEZ-BRAVO, V., MACIEJOWSKI, J., CORONA, J., BUCH, H. K., COLLIN, P., KANEMAKI, M. T., SHAH, J. V. & JALLEPALLI, P. V. 2014. Nuclear pores protect genome integrity by assembling a premitotic and Mad1-dependent anaphase inhibitor. *Cell,* 156**,** 1017-31.

ROSENBERG, J. S., CROSS, F. R. & FUNABIKI, H. 2011. KNL1/Spc105 recruits PP1 to silence the spindle assembly checkpoint. *Curr Biol,* 21**,** 942-7.

ROUT, M. P. & KILMARTIN, J. V. 1990. Components of the yeast spindle and spindle pole body. *J Cell Biol,* 111**,** 1913-27.

RUCHAUD, S., CARMENA, M. & EARNSHAW, W. C. 2007. Chromosomal passengers: conducting cell division. *Nat Rev Mol Cell Biol,* 8**,** 798-812.

SANTAGUIDA, S., TIGHE, A., D'ALISE, A. M., TAYLOR, S. S. & MUSACCHIO, A. 2010. Dissecting the role of MPS1 in chromosome biorientation and the spindle checkpoint through the small molecule inhibitor reversine. *J Cell Biol,* 190**,** 73-87.

SANTAGUIDA, S., VERNIERI, C., VILLA, F., CILIBERTO, A. & MUSACCHIO, A. 2011. Evidence that Aurora B is implicated in spindle checkpoint signalling independently of error correction. *EMBO J,* 30**,** 1508-1519.

SATO, M. & TODA, T. 2007. Alp7/TACC is a crucial target in Ran-GTPase-dependent spindle formation in fission yeast. *Nature,* 447**,** 334-7.

SATO, M. & TODA, T. 2010. Space shuttling in the cell: nucleocytoplasmic transport and microtubule organization during the cell cycle. *Nucleus,* 1**,** 231-6.

SAUNDERS, M., FITZGERALD-HAYES, M. & BLOOM, K. 1988. Chromatin structure of altered yeast centromeres. *Proc Natl Acad Sci U S A,* 85**,** 175-9.

SAURIN, A. T., VAN DER WAAL, M. S., MEDEMA, R. H., LENS, S. M. & KOPS, G. J. 2011. Aurora B potentiates Mps1 activation to ensure rapid checkpoint establishment at the onset of mitosis. *Nat Commun,* 2**,** 316.

SAWIN, K. E. & NURSE, P. 1998. Regulation of cell polarity by microtubules in fission yeast. *J Cell Biol,* 142**,** 457-71.

SCHITTENHELM, R. B., CHALECKIS, R. & LEHNER, C. F. 2009. Intrakinetochore localization and essential functional domains of Drosophila Spc105. *EMBO J,* 28**,** 2374-86.

SCHMIDT, J. C., ARTHANARI, H., BOESZOERMENYI, A., DASHKEVICH, N. M., WILSON-KUBALEK, E. M., MONNIER, N., MARKUS, M., OBERER, M., MILLIGAN, R. A., BATHE, M., WAGNER, G., GRISHCHUK, E. L. & CHEESEMAN, I. M. 2012. The kinetochore-bound Ska1 complex tracks depolymerizing microtubules and binds to curved protofilaments. *Dev Cell,* 23**,** 968-80.

SCHWEIZER, N., FERRAS, C., KERN, D. M., LOGARINHO, E., CHEESEMAN, I. M. & MAIATO, H. 2013. Spindle assembly checkpoint robustness requires Tpr-mediated regulation of Mad1/Mad2 proteostasis. *J Cell Biol,* 203**,** 883-93.

SCREPANTI, E., DE ANTONI, A., ALUSHIN, G. M., PETROVIC, A., MELIS, T., NOGALES, E. & MUSACCHIO, A. 2011. Direct binding of Cenp-C to the Mis12 complex joins the inner and outer kinetochore. *Curr Biol,* 21**,** 391-8.

SCZANIECKA, M., FEOKTISTOVA, A., MAY, K. M., CHEN, J. S., BLYTH, J., GOULD, K. L. & HARDWICK, K. G. 2008. The spindle checkpoint functions of Mad3 and Mad2 depend on a Mad3 KEN box-mediated interaction with Cdc20-anaphase-promoting complex (APC/C). *J Biol Chem,* 283**,** 23039-47.

SEELEY, T. W., WANG, L. & ZHEN, J. Y. 1999. Phosphorylation of human MAD1 by the BUB1 kinase in vitro. *Biochem Biophys Res Commun,* 257**,** 589-95.

SHAH, J. V., BOTVINICK, E., BONDAY, Z., FURNARI, F., BERNS, M. & CLEVELAND, D. W. 2004. Dynamics of centromere and kinetochore proteins; implications for checkpoint signaling and silencing. *Curr Biol,* 14**,** 942-52.

SHEPPERD, L. A., MEADOWS, J. C., SOCHAJ, A. M., LANCASTER, T. C., ZOU, J., BUTTRICK, G. J., RAPPSILBER, J., HARDWICK, K. G. & MILLAR, J. B. 2012. Phosphodependent recruitment of Bub1 and Bub3 to Spc7/KNL1 by Mph1 kinase maintains the spindle checkpoint. *Curr Biol,* 22**,** 891-9.

SHIN, H. J., BAEK, K. H., JEON, A. H., PARK, M. T., LEE, S. J., KANG, C. M., LEE, H. S., YOO, S. H., CHUNG, D. H., SUNG, Y. C., MCKEON, F. & LEE, C. W. 2003. Dual roles of human BubR1, a mitotic checkpoint kinase, in the monitoring of chromosomal instability. *Cancer Cell,* 4**,** 483-97.

SIRONI, L., MAPELLI, M., KNAPP, S., DE ANTONI, A., JEANG, K. T. & MUSACCHIO, A. 2002. Crystal structure of the tetrameric Mad1-Mad2 core complex: implications of a 'safety belt' binding mechanism for the spindle checkpoint. *EMBO J,* 21**,** 2496-506.

SIRONI, L., MELIXETIAN, M., FARETTA, M., PROSPERINI, E., HELIN, K. & MUSACCHIO, A. 2001. Mad2 binding to Mad1 and Cdc20, rather than oligomerization, is required for the spindle checkpoint. *EMBO J,* 20**,** 6371-82.

SOTILLO, R., HERNANDO, E., DIAZ-RODRIGUEZ, E., TERUYA-FELDSTEIN, J., CORDON-CARDO, C., LOWE, S. W. & BENEZRA, R. 2007. Mad2 overexpression promotes aneuploidy and tumorigenesis in mice. *Cancer Cell,* 11**,** 9-23.

SPIREK, M., BENKO, Z., CARNECKA, M., RUMPF, C., CIPAK, L., BATOVA, M., MAROVA, I., NAM, M., KIM, D. U., PARK, H. O., HAYLES, J., HOE, K. L., NURSE, P. & GREGAN, J. 2010. S. pombe genome deletion project: an update. *Cell Cycle,* 9**,** 2399-402.

STEINER, F. A. & HENIKOFF, S. 2015. Diversity in the organization of centromeric chromatin. *Curr Opin Genet Dev,* 31**,** 28-35.

SUIJKERBUIJK, S. J., VLEUGEL, M., TEIXEIRA, A. & KOPS, G. J. 2012. Integration of kinase and phosphatase activities by BUBR1 ensures formation of stable kinetochore-microtubule attachments. *Dev Cell,* 23**,** 745-55.

SUNDIN, L. J., GUIMARAES, G. J. & DELUCA, J. G. 2011. The NDC80 complex proteins Nuf2 and Hec1 make distinct contributions to kinetochore-microtubule attachment in mitosis. *Mol Biol Cell,* 22**,** 759-68.

SUZUKI, A., HORI, T., NISHINO, T., USUKURA, J., MIYAGI, A., MORIKAWA, K. & FUKAGAWA, T. 2011. Spindle microtubules generate tension-dependent changes in the distribution of inner kinetochore proteins. *J Cell Biol,* 193**,** 125-40.

TAKAHASHI, K., YAMADA, H. & YANAGIDA, M. 1994. Fission yeast minichromosome loss mutants mis cause lethal aneuploidy and replication abnormality. *Mol Biol Cell,* 5**,** 1145-58.

TAKEUCHI, K. & FUKAGAWA, T. 2012. Molecular architecture of vertebrate kinetochores. *Exp Cell Res,* 318**,** 1367-74.

TANG, N. H., TAKADA, H., HSU, K. S. & TODA, T. 2013. The internal loop of fission yeast Ndc80 binds Alp7/TACC-Alp14/TOG and ensures proper chromosome attachment. *Mol Biol Cell,* 24**,** 1122-1133.

TANG, N. H. & TODA, T. 2015a. Alp7/TACC recruits kinesin-8-PP1 to the Ndc80 kinetochore protein for timely mitotic progression and chromosome movement. *J Cell Sci,* 128**,** 354-363.

TANG, N. H. & TODA, T. 2015b. MAPping the Ndc80 loop in cancer: A possible link between Ndc80/Hec1 overproduction and cancer formation. *Bioessays,* 37**,** 248-256.

TANGE, Y. & NIWA, O. 2008. Schizosaccharomyces pombe Bub3 is dispensable for mitotic arrest following perturbed spindle formation. *Genetics,* 179**,** 785-92.

THEBAULT, P., CHIRGADZE, D. Y., DOU, Z., BLUNDELL, T. L., ELOWE, S. & BOLANOS-GARCIA, V. M. 2012. Structural and functional insights into the role of the N-terminal Mps1 TPR domain in the SAC (spindle assembly checkpoint). *Biochem J,* 448**,** 321-8.

TIEN, J. F., FONG, K. K., UMBREIT, N. T., PAYEN, C., ZELTER, A., ASBURY, C. L., DUNHAM, M. J. & DAVIS, T. N. 2013. Coupling unbiased mutagenesis to high-throughput DNA sequencing uncovers functional domains in the Ndc80 kinetochore protein of Saccharomyces cerevisiae. *Genetics,* 195**,** 159-70.

TIEN, J. F., UMBREIT, N. T., GESTAUT, D. R., FRANCK, A. D., COOPER, J., WORDEMAN, L., GONEN, T., ASBURY, C. L. & DAVIS, T. N. 2010. Cooperation of the Dam1 and Ndc80 kinetochore complexes enhances microtubule coupling and is regulated by aurora B. *J Cell Biol,* 189**,** 713-23.

TOOLEY, J. & STUKENBERG, P. T. 2011. The Ndc80 complex: integrating the kinetochore's many movements. *Chromosome Res,* 19**,** 377-391.

TOOLEY, J. G., MILLER, S. A. & STUKENBERG, P. T. 2011. The Ndc80 complex uses a tripartite attachment point to couple microtubule depolymerization to chromosome movement. *Mol Biol Cell,* 22**,** 1217-26.

TOURNIER, S., GACHET, Y., BUCK, V., HYAMS, J. S. & MILLAR, J. B. 2004. Disruption of astral microtubule contact with the cell cortex activates a Bub1,

Bub3, and Mad3-dependent checkpoint in fission yeast. *Mol Biol Cell,* 15**,** 3345-56.

UHLEN, M., OKSVOLD, P., FAGERBERG, L., LUNDBERG, E., JONASSON, K., FORSBERG, M., ZWAHLEN, M., KAMPF, C., WESTER, K., HOBER, S., WERNERUS, H., BJORLING, L. & PONTEN, F. 2010. Towards a knowledge-based Human Protein Atlas. *Nat Biotechnol,* 28**,** 1248-50.

UMBREIT, N. T., GESTAUT, D. R., TIEN, J. F., VOLLMAR, B. S., GONEN, T., ASBURY, C. L. & DAVIS, T. N. 2012. The Ndc80 kinetochore complex directly modulates microtubule dynamics. *Proc Natl Acad Sci U S A,* 109**,** 16113-8.

UMESONO, K., HIRAOKA, Y., TODA, T. & YANAGIDA, M. 1983a. Visualization of chromosomes in mitotically arrested cells of the fission yeast Schizosaccharomyces pombe. *Curr Genet,* 7**,** 123-8.

UMESONO, K., TODA, T., HAYASHI, S. & YANAGIDA, M. 1983b. Cell division cycle genes nda2 and nda3 of the fission yeast Schizosaccharomyces pombe control microtubular organization and sensitivity to anti-mitotic benzimidazole compounds. *J Mol Biol,* 168**,** 271-84.

UZUNOVA, K., DYE, B. T., SCHUTZ, H., LADURNER, R., PETZOLD, G., TOYODA, Y., JARVIS, M. A., BROWN, N. G., POSER, I., NOVATCHKOVA, M., MECHTLER, K., HYMAN, A. A., STARK, H., SCHULMAN, B. A. & PETERS, J. M. 2012. APC15 mediates CDC20 autoubiquitylation by APC/C(MCC) and disassembly of the mitotic checkpoint complex. *Nat Struct Mol Biol,* 19**,** 1116-23.

VAN HOOSER, A. A., OUSPENSKI, II, GREGSON, H. C., STARR, D. A., YEN, T. J., GOLDBERG, M. L., YOKOMORI, K., EARNSHAW, W. C., SULLIVAN, K. F. & BRINKLEY, B. R. 2001. Specification of kinetochore-forming chromatin by the histone H3 variant CENP-A. *J Cell Sci,* 114**,** 3529-42.

VANOOSTHUYSE, V. & HARDWICK, K. G. 2009. A novel protein phosphatase 1-dependent spindle checkpoint silencing mechanism. *Curr Biol,* 19**,** 1176-81.

VARMA, D., CHANDRASEKARAN, S., SUNDIN, L. J., REIDY, K. T., WAN, X., CHASSE, D. A., NEVIS, K. R., DELUCA, J. G., SALMON, E. D. & COOK, J. G. 2012a. Recruitment of the human Cdt1 replication licensing protein by the loop domain of Hec1 is required for stable kinetochore-microtubule attachment. *Nat Cell Biol*.

VARMA, D., CHANDRASEKARAN, S., SUNDIN, L. J., REIDY, K. T., WAN, X., CHASSE, D. A., NEVIS, K. R., DELUCA, J. G., SALMON, E. D. & COOK, J. G. 2012b. Recruitment of the human Cdt1 replication licensing protein by the loop domain of Hec1 is required for stable kinetochore-microtubule attachment. *Nat Cell Biol,* 14**,** 593-603.

VARMA, D., WAN, X., CHEERAMBATHUR, D., GASSMANN, R., SUZUKI, A., LAWRIMORE, J., DESAI, A. & SALMON, E. D. 2013. Spindle assembly checkpoint proteins are positioned close to core microtubule attachment sites at kinetochores. *J Cell Biol,* 202**,** 735-46.

VLEUGEL, M., TROMER, E., OMERZU, M., GROENEWOLD, V., NIJENHUIS, W., SNEL, B. & KOPS, G. J. 2013. Arrayed BUB recruitment modules in the kinetochore scaffold KNL1 promote accurate chromosome segregation. *J Cell Biol,* 203**,** 943-55.

WALKER, G. M. 1982. Cell cycle specificity of certain antimicrotubular drugs in Schizosaccharomyces pombe. *J Gen Microbiol,* 128**,** 61-71.

WAN, X., O'QUINN, R. P., PIERCE, H. L., JOGLEKAR, A. P., GALL, W. E., DELUCA, J. G., CARROLL, C. W., LIU, S. T., YEN, T. J., MCEWEN, B. F., STUKENBERG, P. T., DESAI, A. & SALMON, E. D. 2009. Protein architecture of the human kinetochore microtubule attachment site. *Cell,* 137**,** 672-84.

WANG, E., BALLISTER, E. R. & LAMPSON, M. A. 2011. Aurora B dynamics at centromeres create a diffusion-based phosphorylation gradient. *J Cell Biol,* 194**,** 539-49.

WANG, H. W., LONG, S., CIFERRI, C., WESTERMANN, S., DRUBIN, D., BARNES, G. & NOGALES, E. 2008. Architecture and flexibility of the yeast Ndc80 kinetochore complex. *J Mol Biol,* 383**,** 894-903.

WANG, R. H., YU, H. & DENG, C. X. 2004. A requirement for breast-cancer-associated gene 1 (BRCA1) in the spindle checkpoint. *Proc Natl Acad Sci U S A,* 101**,** 17108-13.

WANG, Y., JIN, F., HIGGINS, R. & MCKNIGHT, K. 2014. The current view for the silencing of the spindle assembly checkpoint. *Cell Cycle,* 13**,** 1694-701.

WARREN, C. D., BRADY, D. M., JOHNSTON, R. C., HANNA, J. S., HARDWICK, K. G. & SPENCER, F. A. 2002. Distinct chromosome segregation roles for spindle checkpoint proteins. *Mol Biol Cell,* 13**,** 3029-41.

WEI, R., NGO, B., WU, G. & LEE, W. H. 2011. Phosphorylation of the Ndc80 complex protein, HEC1, by Nek2 kinase modulates chromosome alignment and signaling of the spindle assembly checkpoint. *Mol Biol Cell,* 22**,** 3584-94.

WEI, R. R., SORGER, P. K. & HARRISON, S. C. 2005. Molecular organization of the Ndc80 complex, an essential kinetochore component. *Proc Natl Acad Sci U S A,* 102**,** 5363-7.

WELBURN, J. P., VLEUGEL, M., LIU, D., YATES, J. R., 3RD, LAMPSON, M. A., FUKAGAWA, T. & CHEESEMAN, I. M. 2010. Aurora B phosphorylates spatially distinct targets to differentially regulate the kinetochore-microtubule interface. *Mol Cell,* 38**,** 383-92.

WEST, R. R., VAISBERG, E. V., DING, R., NURSE, P. & MCINTOSH, J. R. 1998. cut11(+): A gene required for cell cycle-dependent spindle pole body anchoring in the nuclear envelope and bipolar spindle formation in Schizosaccharomyces pombe. *Mol Biol Cell,* 9**,** 2839-55.

WESTERMANN, S., AVILA-SAKAR, A., WANG, H. W., NIEDERSTRASSER, H., WONG, J., DRUBIN, D. G., NOGALES, E. & BARNES, G. 2005. Formation of a dynamic kinetochore- microtubule interface through assembly of the Dam1 ring complex. *Mol Cell,* 17**,** 277-90.

WESTERMANN, S., CHEESEMAN, I. M., ANDERSON, S., YATES, J. R., 3RD, DRUBIN, D. G. & BARNES, G. 2003. Architecture of the budding yeast kinetochore reveals a conserved molecular core. *J Cell Biol,* 163**,** 215-22.

WESTHORPE, F. G. & STRAIGHT, A. F. 2013. Functions of the centromere and kinetochore in chromosome segregation. *Curr Opin Cell Biol,* 25**,** 334-40.

WESTHORPE, F. G., TIGHE, A., LARA-GONZALEZ, P. & TAYLOR, S. S. 2011. p31comet-mediated extraction of Mad2 from the MCC promotes efficient mitotic exit. *J Cell Sci,* 124**,** 3905-16.

WIGGE, P. A., JENSEN, O. N., HOLMES, S., SOUES, S., MANN, M. & KILMARTIN, J. V. 1998. Analysis of the Saccharomyces spindle pole by matrix-assisted laser desorption/ionization (MALDI) mass spectrometry. *J Cell Biol,* 141**,** 967-77.

WIGGE, P. A. & KILMARTIN, J. V. 2001. The Ndc80p complex from Saccharomyces cerevisiae contains conserved centromere components and has a function in chromosome segregation. *J Cell Biol,* 152**,** 349-60.

WILLIAMS, B., LEUNG, G., MAIATO, H., WONG, A., LI, Z., WILLIAMS, E. V., KIRKPATRICK, C., AQUADRO, C. F., RIEDER, C. L. & GOLDBERG, M. L. 2007. Mitch a rapidly evolving component of the Ndc80 kinetochore complex required for correct chromosome segregation in Drosophila. *J Cell Sci,* 120**,** 3522-33.

WILSON-KUBALEK, E. M., CHEESEMAN, I. M., YOSHIOKA, C., DESAI, A. & MILLIGAN, R. A. 2008. Orientation and structure of the Ndc80 complex on the microtubule lattice. *J Cell Biol,* 182**,** 1055-61.

WINDECKER, H., LANGEGGER, M., HEINRICH, S. & HAUF, S. 2009. Bub1 and Bub3 promote the conversion from monopolar to bipolar chromosome attachment independently of shugoshin. *EMBO Rep,* 10**,** 1022-8.

WINEY, M., GOETSCH, L., BAUM, P. & BYERS, B. 1991. MPS1 and MPS2: novel yeast genes defining distinct steps of spindle pole body duplication. *J Cell Biol,* 114**,** 745-54.

WINEY, M., MAMAY, C. L., O'TOOLE, E. T., MASTRONARDE, D. N., GIDDINGS, T. H., JR., MCDONALD, K. L. & MCINTOSH, J. R. 1995. Three-dimensional ultrastructural analysis of the Saccharomyces cerevisiae mitotic spindle. *J Cell Biol,* 129**,** 1601-15.

WOOD, V., GWILLIAM, R., RAJANDREAM, M. A., LYNE, M., LYNE, R., STEWART, A., SGOUROS, J., PEAT, N., HAYLES, J., BAKER, S., BASHAM, D., BOWMAN, S., BROOKS, K., BROWN, D., BROWN, S., CHILLINGWORTH, T., CHURCHER, C., COLLINS, M., CONNOR, R., CRONIN, A., DAVIS, P., FELTWELL, T., FRASER, A., GENTLES, S., GOBLE, A., HAMLIN, N., HARRIS, D., HIDALGO, J., HODGSON, G., HOLROYD, S., HORNSBY, T., HOWARTH, S., HUCKLE, E. J., HUNT, S., JAGELS, K., JAMES, K., JONES, L., JONES, M., LEATHER, S., MCDONALD, S., MCLEAN, J., MOONEY, P., MOULE, S., MUNGALL, K., MURPHY, L., NIBLETT, D., ODELL, C., OLIVER, K., O'NEIL, S., PEARSON, D., QUAIL, M. A., RABBINOWITSCH, E., RUTHERFORD, K., RUTTER, S., SAUNDERS, D., SEEGER, K., SHARP, S., SKELTON, J., SIMMONDS, M., SQUARES, R., SQUARES, S., STEVENS, K., TAYLOR, K., TAYLOR, R. G., TIVEY, A., WALSH, S., WARREN, T., WHITEHEAD, S., WOODWARD, J., VOLCKAERT, G., AERT, R., ROBBEN, J., GRYMONPREZ, B., WELTJENS, I., VANSTREELS, E., RIEGER, M., SCHAFER, M., MULLER-AUER, S., GABEL, C., FUCHS, M., DUSTERHOFT, A., FRITZC, C., HOLZER, E., MOESTL, D., HILBERT, H., BORZYM, K., LANGER, I., BECK, A., LEHRACH, H., REINHARDT, R., POHL, T. M., EGER, P., ZIMMERMANN, W., WEDLER, H., WAMBUTT, R., PURNELLE, B., GOFFEAU, A., CADIEU, E., DREANO, S., GLOUX, S., et al. 2002. The genome sequence of Schizosaccharomyces pombe. *Nature,* 415**,** 871-80.

YAMAGISHI, Y., HONDA, T., TANNO, Y. & WATANABE, Y. 2010. Two histone marks establish the inner centromere and chromosome bi-orientation. *Science,* 330**,** 239-43.

YAMAGISHI, Y., SAKUNO, T., GOTO, Y. & WATANABE, Y. 2014. Kinetochore composition and its function: lessons from yeasts. *FEMS Microbiol Rev,* 38**,** 185-200.

YAMAGISHI, Y., YANG, C. H., TANNO, Y. & WATANABE, Y. 2012. MPS1/Mph1 phosphorylates the kinetochore protein KNL1/Spc7 to recruit SAC components. *Nat Cell Biol,* 14**,** 746-752.

ZAYTSEV, A. V., MICK, J. E., MASLENNIKOV, E., NIKASHIN, B., DELUCA, J. G. & GRISHCHUK, E. L. 2015. Multisite phosphorylation of the NDC80 complex gradually tunes its microtubule-binding affinity. *Mol Biol Cell,* 26**,** 1829-1844.

ZHANG, G., KELSTRUP, C. D., HU, X. W., KAAS HANSEN, M. J., SINGLETON, M. R., OLSEN, J. V. & NILSSON, J. 2012. The Ndc80 internal loop is required for recruitment of the Ska complex to establish end-on microtubule attachment to kinetochores. *J Cell Sci,* 125**,** 3243-53.

ZHANG, G., LISCHETTI, T., HAYWARD, D. G. & NILSSON, J. 2015. Distinct domains in Bub1 localize RZZ and BubR1 to kinetochores to regulate the checkpoint. *Nat Commun,* 6**,** 7162.

ZHANG, G., LISCHETTI, T. & NILSSON, J. 2014. A minimal number of MELT repeats supports all the functions of KNL1 in chromosome segregation. *J Cell Sci,* 127**,** 871-84.

ZHU, C., ZHAO, J., BIBIKOVA, M., LEVERSON, J. D., BOSSY-WETZEL, E., FAN, J. B., ABRAHAM, R. T. & JIANG, W. 2005. Functional analysis of human microtubule-based motor proteins, the kinesins and dyneins, in mitosis/cytokinesis using RNA interference. *Mol Biol Cell,* 16**,** 3187-99.

ZHU, T., DOU, Z., QIN, B., JIN, C., WANG, X., XU, L., WANG, Z., ZHU, L., LIU, F., GAO, X., KE, Y., WANG, Z., AIKHIONBARE, F., FU, C., DING, X. & YAO, X. 2013. Phosphorylation of microtubule-binding protein Hec1 by mitotic kinase Aurora B specifies spindle checkpoint kinase Mps1 signaling at the kinetochore. *J Biol Chem,* 288**,** 36149-36159.

ZICH, J. & HARDWICK, K. G. 2010. Getting down to the phosphorylated 'nuts and bolts' of spindle checkpoint signalling. *Trends Biochem Sci,* 35**,** 18-27.

ZICH, J., SOCHAJ, A. M., SYRED, H. M., MILNE, L., COOK, A. G., OHKURA, H., RAPPSILBER, J. & HARDWICK, K. G. 2012. Kinase activity of fission yeast mph1 is required for mad2 and mad3 to stably bind the anaphase promoting complex. *Curr Biol,* 22**,** 296-301.

ZIMMERMAN, S., DAGA, R. R. & CHANG, F. 2004. Intra-nuclear microtubules and a mitotic spindle orientation checkpoint. *Nat Cell Biol,* 6**,** 1245-6.